SALT TECTONICS OF THE ABENAKI GRABEN AND CENTRAL SABLE SUBBASIN: INSIGHTS FROM REGIONAL SEISMIC INTERPRETATION AND 4D SCALED PHYSICAL EXPERIMENTS

by

Clarke Campbell

Submitted in partial fulfillment of the requirements
for the degree of Master of Science

at

Dalhousie University
Halifax, Nova Scotia
August 2010

DALHOUSIE UNIVERSITY
DEPARTMENT OF EARTH SCIENCES

The undersigned hereby certify that they have read and recommend to the Faculty of Graduate Studies for acceptance of a thesis entitled "**SALT TECTONICS OF THE ABENAKI GRABEN AND CENTRAL SABLE SUBBASIN: INSIGHTS FROM REGIONAL SEISMIC INTERPRETATION AND 4D SCALED PHYSICAL EXPERIMENTS**" by Clarke Campbell in partial fulfillment of the requirements for the degree of Master of Science.

Dated: August 6th, 2010

Supervisor: _____

Co-Supervisor: _____

External Examiner: _____

Department Reader: _____

Department Chair:

DALHOUSIE UNIVERSITY

DATE: August 6th, 2010

AUTHOR: Clarke Campbell

TITLE: Salt Tectonics of the Abenaki Graben and Central Sable Subbasin: Insights from Regional Seismic Interpretation and 4D Scaled Physical Experiments

DEPARTMENT OR SCHOOL: Department of Earth Sciences

DEGREE: M.Sc. CONVOCATION: October YEAR: 2010

Permission is herewith granted to Dalhousie University to circulate and to have copied for non-commercial purposes, at its discretion, the above title upon the request of individuals or institutions.

Signature of Author

TABLE OF CONTENTS

LIST OF FIGURES

LIST OF TABLES

ABSTRACT

The tectono-stratigraphic evolution of the Abenaki graben and central Sable Subbasin of the north-central Scotian margin has been highly influenced by salt deformation. Shimeld (2004) has identified five salt subprovinces defined by varying salt structural styles across the margin. Although it has been hypothesized these varying structural styles are the result of complex salt basin morphologies and variable Mesozoic post-rift sedimentation patterns, there is still a lack of understanding of how these first order controlling factors specifically controlled the tectono-stratigraphic evolution across the margin. Disappointing petroleum exploration results from the last round of deepwater drilling supports the further need to investigate how variable salt basin morphologies, and depositional rates and patterns controlled salt deformation as well as the evolution of the margin.

The purpose of this project is to integrate regional 2D seismic reflection data including the ION-GXT NovaSPAN dataset, with 4D scaled physical experiments to better understand the tectono-stratigraphic evolution of the Abenaki Graben and central Sable Subbasin. The study area is located in Shimeld's salt Subprovince III that comprises an extensive salt tongue-canopy system that has spread upwards of 80 km on the secondary detachment level. Seismic interpretation indicates an original salt basin characterized by a landward tapering wedge representing the Abenaki Graben, an intermediate high referred to as the North Sable High (NSH), and a symmetric graben with basin step representing the Sable Subbasin. The geometry of the salt basin floor is composed of rifted basement blocks and syn-rift fill that was originally been infilled with upwards of 2 km of Argo salt.

Scaled 4D physical experiments simulating the study area indicate the presence of 4 kinematic domains from the shelf to slope including a: *(1) Salt Weld and Pillow, (2) Normal Fault and Reactive Diapir, (3) Passive Diapir and Expulsion Rollover*, and *(4) Contractional Salt and Allochthonous Salt-Tongue Canop*y domain. Experiment results indicate early deposition focused in the Abenaki Graben, later shifting across the NSH into the Sable sub-basin as increased sediment supply and progradation occurred from the Late Jurassic to Early Cretaceous. Experiment evolutions replicated diapir and canopy evolutions with early-inflated salt complexes in the downdip contractional domain focused at changes in the basin-floor and original salt thickness. The inflated salt complexes later evolved into passive diapirs and eventual extensive salt tongue-canopy systems during subsequent sediment progradation.

Derived kinematic concepts from the physical experiments successfully explain the regional structural and related depocentre evolution of the margin form the early post-rift stage to the modern margin. Understanding the tectono-stratigraphic evolution, from early salt mobilization to late stage salt tongue-canopy formation, aids in developing new concepts for reservoir distribution and trap formation for the Abenaki Graben and Sable Subbasin area.

ACKNOWLEDGEMENTS

I would first like to thank my supervisor Dr. Juergen Adam for the wealth of knowledge he has contributed to my understanding of basin dynamics, salt tectonics, and physical modeling for numerous years at Dalhousie University. I am extremely appreciative for the discussions, encouragement, patience and feedback I have received from him during my time here. Dr. Mladen Nedimovic has also been very helpful here for stepping in as a co-supervisor for my thesis. I would like to thank Dr. Djordje Grujic for introducing me to structural geology as an undergrad. I would also like to thank Dr. Grant Wach for contributing to my development as a petroleum geologist over the years, a career I plan to pursue. Special thanks go out to my fellow MSc. students Jonathan Cribb and Cody MacDonald form the Salt Dynamics Group. We have become great friends and have had great discussions through the durations of our projects. The 2, 4 and 6 am sieving shifts would have been impossible without them.

I have also had great support outside of school during this project and would like to thank the great friends and family who helped me through my time here at Dalhousie. I would especially like to thank Mike Giles, Shawn Goss, Eric Negulic, and the "neighbours" Pete and Taryn for all the great times during this degree. It was great to be surrounded by such amazing people. My parents deserve many thanks for being there every step of the way and I am indebted to them for everything they've done for me through university.

Finally, my research would not have been possible without the generous donation of the Ion GXT NovaSPAN dataset (Menno Dinkelmann) and financial support from the Pengrowth-Nova Scotia Petroleum Innovation Grant, ACOA/AIF, CFI, NSERC and PRAC. The Canada Nova Scotian Offshore Petroleum Board also deserves thanks for providing public seismic reflection datasets.

CHAPTER 1: Introduction

The Scotian Basin is located offshore Nova Scotia (Figure 1.1) on the Atlantic continental margin (Scotian margin). The basin is comprised of a series of rifted interconnected Mesozoic sub-basins formed from the break-up of Pangaea. As these sub-basins formed, sedimentation was initiated leading to continental and marine sediment deposits, including up to 2 km of salt, infilling the rift systems (Wade and MacLean 1990). Following rifting, the rift basin became a passive margin with up to 16 – 18 km of sediments deposited from the Jurassic to today. Early deposition within the basin caused passive downbuilding of sediments from the Early Jurassic to Late Cretaceous into the Argo salt, resulting in salt-withdrawal basins and welding in the modern day shelf, and passive diapirism and a large salt tongue-canopy system within the modern day slope and abyssal plain.

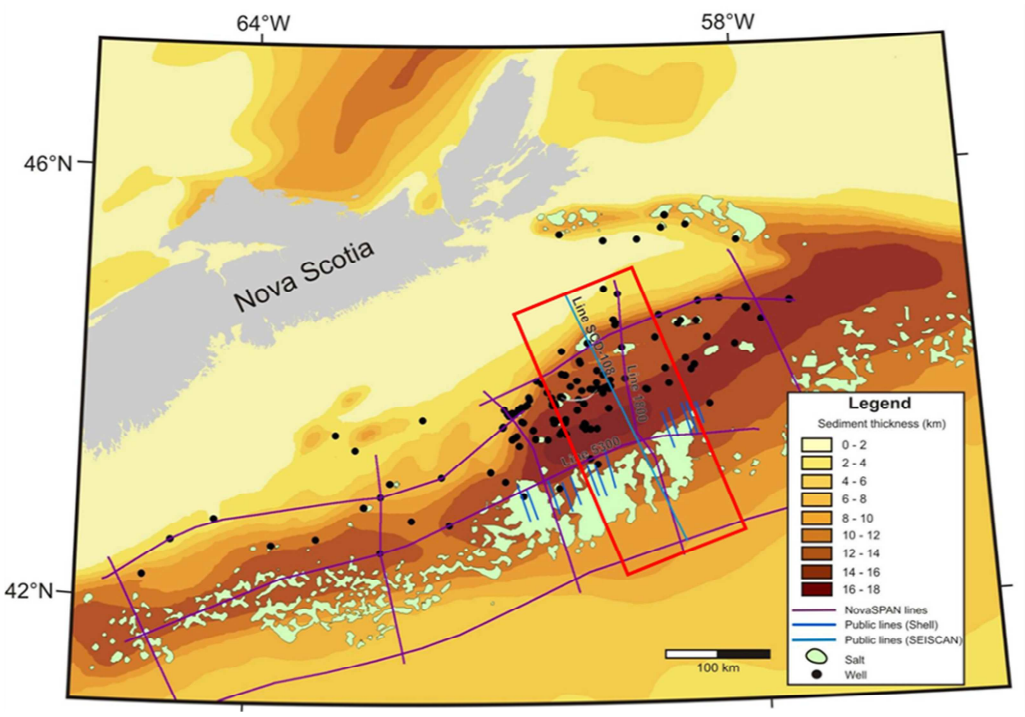

Figure 1.1 Map of the Scotian margin indicating the study area for the project. Map also includes the location of the various seismic lines for the study.

For this study, interpretation of available 2D seismic data combined with optically monitored 4D physical experiments is used to aid in understanding the salt tectonic evolution of the Abenaki Graben and central Sable Subbasin. Specifically, the study investigates the roles of first order parameters on the evolution of this area of the basin including:

1. Salt basin geometry
2. Original salt thickness
3. Sedimentation patterns and rates

Project motivation

Disappointing results from recent exploration activity on the Scotian Margin illustrate the need for a better understanding of the tectono-stratigraphic evolution of the Scotian Basin. Improving constraints on the framework of the evolution requires an in-depth analysis of the interplay between salt tectonic processes and sediment input on both the overall basin and individual subbasin scales. This thesis work will investigate the effects of salt basement topography, original salt thickness, and sediment input played in the evolution of the Abenaki Graben and central Sable Subbasin, offshore north-central Nova Scotia. A regional-scale subbasin analysis using seismic data and mechanically constrained experiments will contribute to the understanding of the evolution of deformation from the shelf and slope to deep basin. Analogue experiments will simulate coupled salt tectonic processes and depocentre migration in the Abenaki Graben and central Sable sub-basin. Mechanically constrained salt tectonic concepts and seismic interpretation templates deduced from the experiments should aid further seismic

interpretation of the Abenaki Graben and central Sable sub-basin area and unravel its tectono-stratigraphic evolution.

Hypotheses

The three hypotheses to be tested by this study are:

1. Changes in salt thickness due to a variable original salt basin geometry have heavily controlled salt mobilization and deformation styles for the study area;
2. The basement step within the Sable Subbasin was responsible for localized inflation as sediments prograded during the Late Jurassic and Early Cretaceous; and
3. Reduced sedimentation in the late Early Cretaceous following major progradational phase allowed the spreading of salt and evolution of the salt tongue-canopy system within salt Subprovince III.

Objectives

The objective of this study is to investigate tectono-stratigraphic evolution of the Abenaki Graben and central Sable Subbasin by integrating regional 2D seismic data and 4D scaled physical experiments. Specific objectives include:

1. Investigating the depositional history and depocentre evolution from the Middle Jurassic to Late Cretaceous for the Abenaki Graben and central Sable sub-basin.
2. Running 4D physical experiments using constraints from interpretation of regional 2D seismic data including original salt basin morphology, salt thickness, and sedimentation patterns and rates to investigate the roles these parameters had on the salt tectonic evolution of the Abenaki Graben and central Sable Subbasin;

3. Analysing the mechanics, kinematics and timing of the salt tectonic processes in the region using concepts derived from the experiments to improve seismic interpretation of the region.

CHAPTER 2: Salt tectonics overview

2.1 Formation of salt basins

Salt basins occur either in rift basins, along passive margins or to a lesser extent in collisional settings such as in the Alpine/Himalayan system (e.g. Rowan 2005). In rifted continental margins, salt deposition mainly occurs during the main late syn-rift to early post rift phase of the basin evolution (Figure 2.1; Jackson and Vendeville 1994). Salt accumulates in these basins due to repeated evaporation events of saline waters.

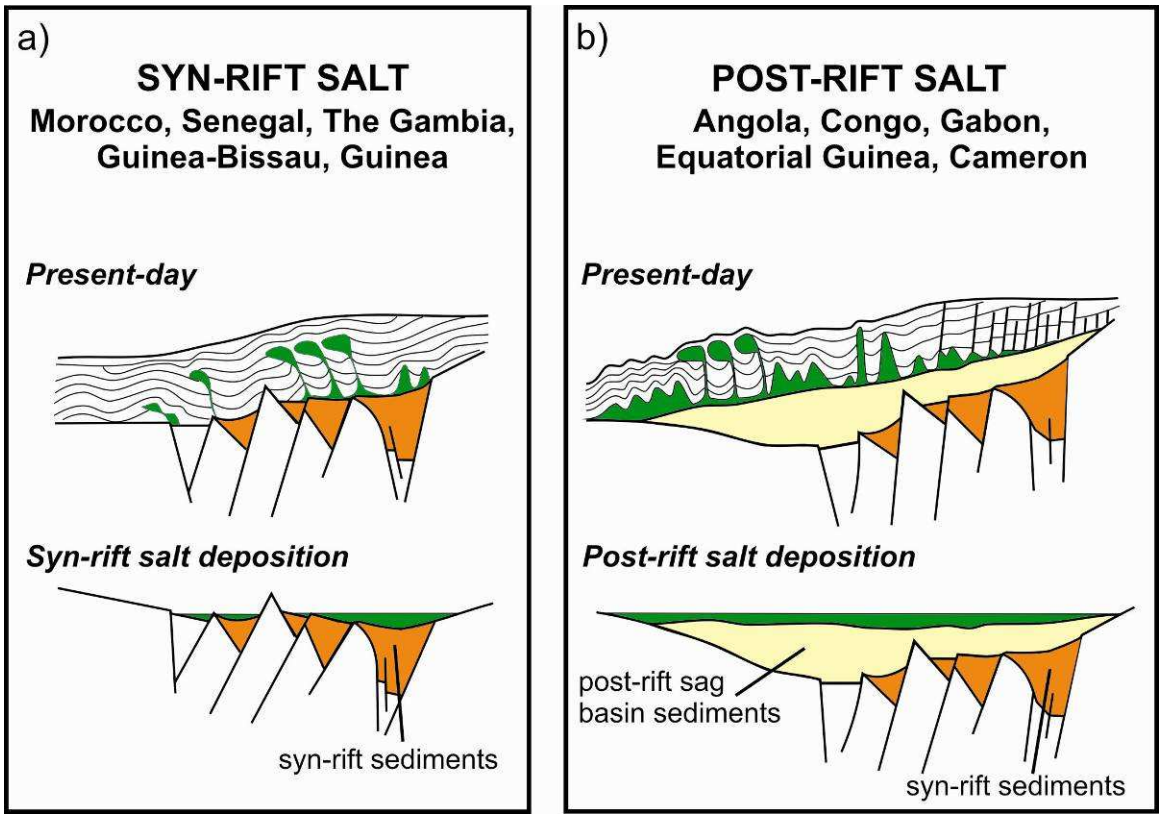

Figure 2.1 Cross-sectional evolution of salt structures on an idealized passive margin, in a) syn-rift and b) post-rift settings (Modified from Tari et al. 2003). Important to note is the variation in salt thickness caused by the basement across the syn-rift salt basin. The effects of basement structure become greatly subdued in the case of post-rift salt as it is blanketed by thick syn-rift and sag basin sediments.

During the rifting process, extension of the continental crust results in a series of grabens and half grabens that create depositional lows on the soon to be formed margin.

Typically during rifting, high heat flow in the rifted basin causes crustal uplift and erosion of rift shoulders leading to deposition of non-marine syn-rift clastics (Rowan 2005). As the basin begins to cool and subside it transitions from terrestrial deposition to shallow marine incursion. In a warm and arid climate, evaporates are deposited in this terrestrial to shallow marine environment (Rowan, 2005). Repeated marine ingression evaporation cycles may result in the cumulative deposition of several kilometres of evaporites.

The influence of the rift basin geometry on the evolution of the future passive margin varies with the timing of salt deposition in relation to the rift stage, e.g. main or late syn-rift, early post rift phase.

1. Syn-rift and inter-rift salt deposits are strongly influenced by rift basin geometries (Figure 2.1a). As salt deposits fill the remaining accommodation space of rift grabens and half grabens, extensive salt basins are created with variable thickness (Rowan 2005).
2. In the post-rift phase the effects of the rift basement geometry on salt deposited is often subdued or negligible due to the infilling of the accommodation space created by grabens and half-grabens with syn-rift and early post-rift sediments (Figure 2.1b).

2.2 Salt deformation mechanics

The deformation behavior of viscous salt successions differs significantly from that of typical brittle sedimentary strata because of its distinctive strength and density properties. Under pressure and tension salt becomes much weaker than other lithologies (e.g. Rowan 2005). The strength of brittle sedimentary rocks increases linearly with depth whereas salt is very weak strength and its strength is mainly constant with

increasing depth (Figure 2.2). This low strength causes salt layers to act as a preferred detachment surface and faults in the brittle sedimentary overburden sole out into the salt layer (e.g. Rowan 2005).

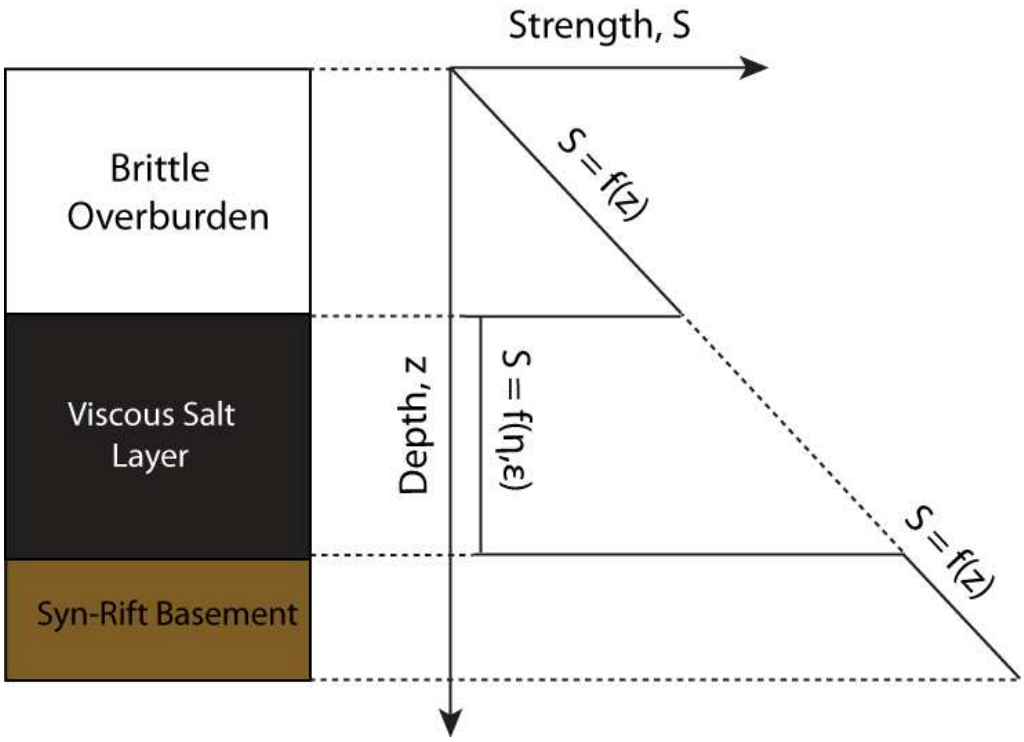

Figure 2.2 The general strengths of brittle overburden sediments and salt as a function of depth (Jackson and Vendeville 1994). Unlike the brittle overburden salt maintains little to no strength with depth. This property is why salt acts as a detachment surface to the brittle overburden sediments.

Due to its low yield strength, salt deforms similar to a viscous fluid under pressure. In a salt source layer under gravitational loading by sediment overburden, basinward salt flow is achieved through a combination of Poiseuille channel flow (Figure 2.3b) and Couette shear flow (Figure 2.3c). Poiseuille flow within salt is initiated by differential sedimentary loading and the passive down-building of overburden sediments (Gemmer et al. 2004; Turcotte & Schubert 1982). Couette flow is caused by the extension and translation of overburden (Gemmer et al. 2004). In a system affected by a large differential overburden thickness or low overburden strength, Poiseuille flow will

drive the lateral flow of the viscous material causing thinning of the viscous material beneath the overburden (Gemmer et al. 2004). If the overburden reaches its yield limit and becomes unstable, failure in the system will occur. This failure results in extension and translation on top of the salt detachment inducing Couette shear flow in the viscous salt (Gemmer et al. 2004).

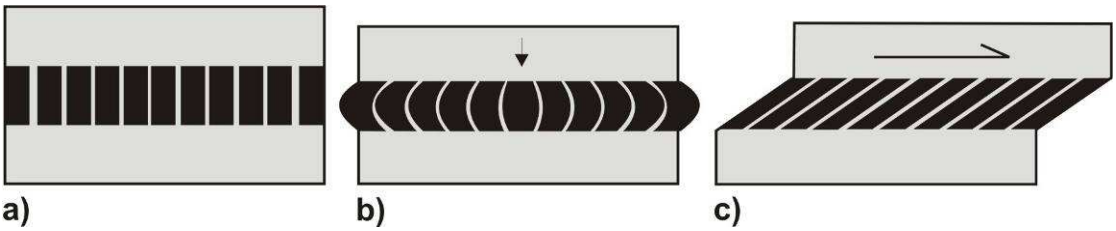

Figure 2.3 Flow types for viscous materials beginning with: a) the initial undeformed viscous material before initial flow takes place; b) Poiseuille or channel flow created as the overburden loading induces lateral flow with the highest velocity of flow in the center of the viscous layer; and c) Couette or shear flow created as the overburden is sheared and translated with the highest velocities along the shearing boundary (Modified from Rowan 2005).

The second factor that controls the deformation behavior of salt is density. Unlike most sedimentary strata, salt's density of 2.2 g/cm^3 decreases slightly with depth due to thermal expansion (e.g. Rowan 2005). This unique property makes salt denser than its surrounding sedimentary strata at the surface but less dense at depths below 1000 – 1500 m (Figure 2.4; e.g. Rowan 2005). Earlier studies in the 20th century modeled both salt and overburden deformation with fluid behavior and assumed that the density contrast was the driver of salt tectonics, i.e. less dense salt pushed through the denser overburden until reaching neutral buoyancy (e.g. Nettleton 1934). Buoyancy has been proven to be only a secondary effect in situations where the overburden is thin and weak enough to push through. Since the late 20th century it is generally accepted that salt only reacts passively to the deforming overburden (Vendeville and Jackson 1995). More recent studies (e.g. Jackson and Vendeville 1994; Rowan 2005; Vendeville 2005) observe that

while salt acts as a fluid material during geological processes, the sedimentary overburden behaves dominantly as a brittle material. The modern studies describe how differential loading, thin-skinned extension, and the influence of sedimentation rates influence the geometry of passive diapirs and extrusions (Jackson 1995).

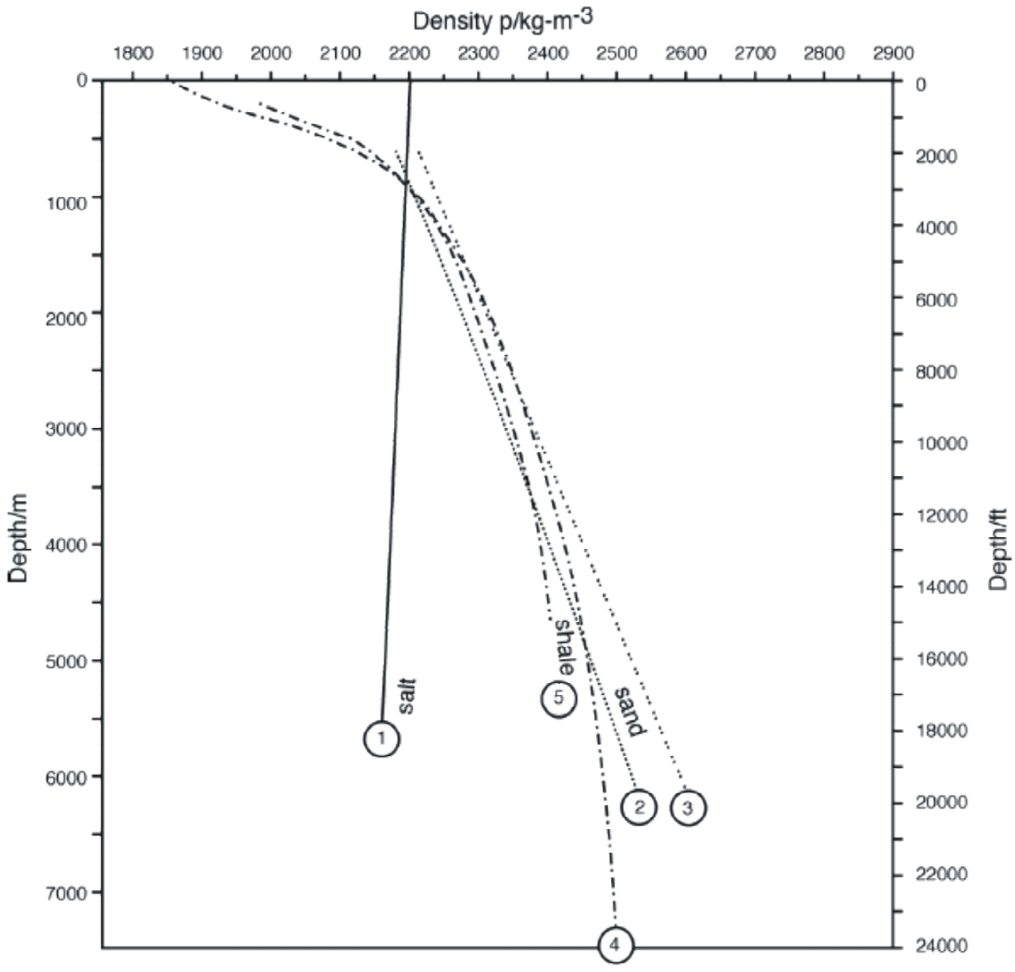

Figure 2.4 Relationship between densities through depth for various lithologies (Jackson and Talbot, 1986). Unlike most lithologies, density of salt decreases slightly with depth.

Vendeville and Jackson (1992) have discussed how a strong brittle overburden will minimize the effects of density contrast and impede salt from rising and piercing through the surface (Figure 2.5). They found that the major factor controlling salt mobilization is

differential loading on both regional and local scales. Vendeville and Jackson (1995) showed:

1. An underlying diapir typically forms under an unimpeded overburden block regardless of density ratio, and its position either below or above a datum surface if it is less or more dense than the fluid.
2. Not all fluid ridges (reactive diapirs) can rise due to vertical restrictions imposed by friction or overburden shear strength. Also, not all thin overburden roofs over a fluid of constant thickness can be pierced since the strength of the overburden must be overcome by the pressure of upwelling salt.
3. A thin roof of strong overburden above a fluid of constant thickness is inherently unstable, regardless of density ratio. If the strength of a locally thin roof is overcome, the fluid and its overburden will eventually rise. The forces from pressurized fluid under a trough are always larger than those in an open fluid column (i.e. passive diapir), such that P_2 is greater than P_1.

Vendeville and Jackson (1995) found that any force exerted on the salt causes it to adjust in such a way that it does not drive extension or contraction in a system; rather it passively flows into existing space. The study concluded that the following factors are needed for salt flow to occur:

1) Must be an open path to a near-surface salt body;
2) The overburden must be thin and weak enough for the differential fluid pressure to overcome its strength, which will deform the thin overburden;
3) Salt does not drive salt tectonics; it only reacts passively to external forces.

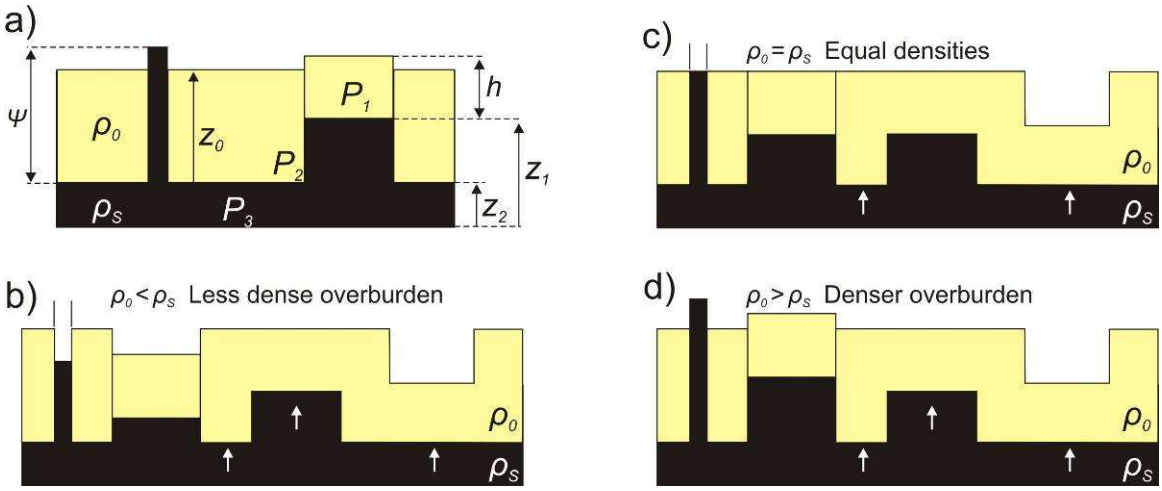

Figure 2.5 Pressurized distribution in a pressurized fluid (black) overlain by a rigid overburden (yellow). a) ρ_0 and ρ_s refer to the densities of the overburden and fluid (salt), respectively; *z* values are elevations above the pressure datum at the base of the fluid layer; h is the reduced (to 50%) thickness of the overburden above the fluid; *P* values are fluid pressures at the points indicated; Ψ is the pressure head of the fluid layer; white arrows in other sections show relative movement of the overburden if it subsequently faults. (b, c, d) Pressures and equilibrium levels for less dense, equally dense, and denser overburden, respectively (Modified from Vendeville and Jackson 1991).

2.3 Salt tectonics at passive margins

Thin-skinned salt tectonics on passive margins such as the Scotian Margin is triggered by sedimentary differential loading (Figure 2.6; e.g. Jackson and Vendeville 1994; Krezsek *et al.* 2007; Ge *et al.* 1997). The progradation of delta and shelf systems along the continental margin causes differential loading (Gemmer et al. 2004; Ge *et al.* 1997). Differential loading creates a pressure difference in the visco-plastic salt substratum inducing seaward salt flow, down-slope gravitational spreading and extensional failure of the overburden (Figure 2.6; Krezsek *et al.* 2007; Jackson 1995; Gemmer et al. 2004). Up-dip extension on the shelf is accommodated by down-dip contraction in the lower slope (Figure 2.6; e.g. Worrall and Snelson 1989; Ge *et al.* 1997; Krezsek *et al.* 2007). Sediment loading and progradation over a very thick, visco-plastic

substratum, cause sediment subsidence and lateral expulsion to be the dominant method of deformation in the system (Ge *et al.* 1997).

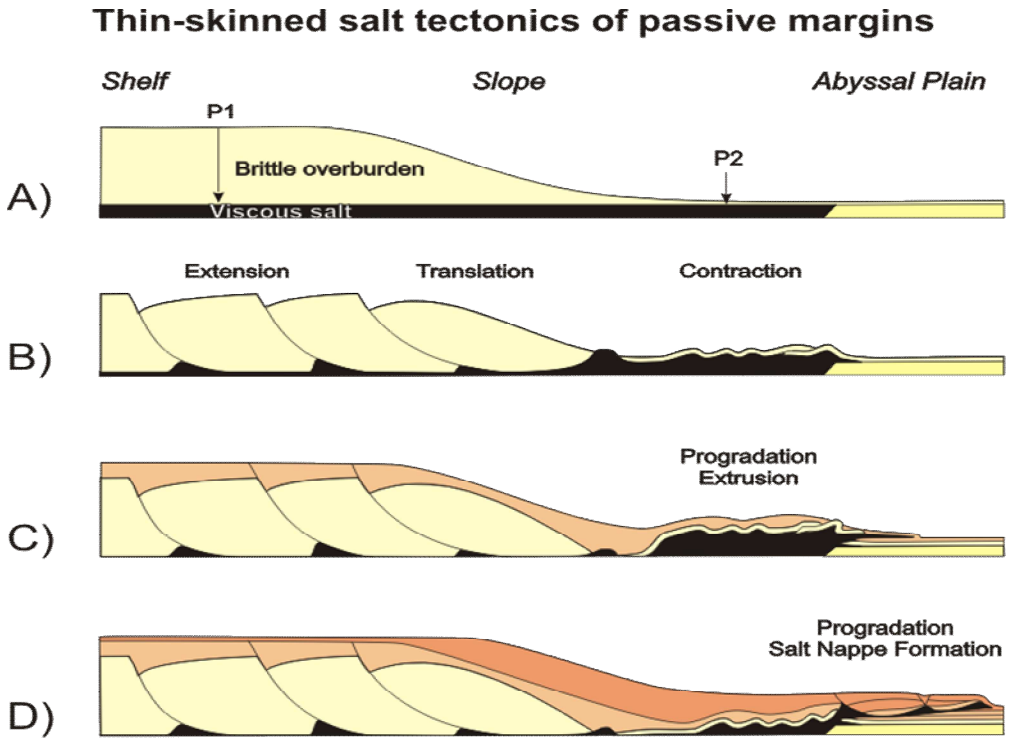

Figure 2.6 Schematic cross-section of a passive margin with a brittle sedimentary wedge overlying a viscous salt layer. A) Pressures P1 and P2 are induced by the differential load of the sedimentary wedge. B) Early stage of deformation with basinward salt mobilisation originating kinematic segmentation in up-dip proximal extension, central translation and distal contraction domain. C) Intermediate stage: Prograding sediments initiate initial extrusion of salt out of the autochthonous salt basin. D) Late stage deformation is focussed outboard of the autochthonous basin and is confined to the allochthonous region (Adam et al., 2008).

Gravitational failure of the sedimentary overburden at passive margins occurs through a combination of gravity gliding and gravity spreading (Figure 2.7; Gemmer et al. 2004). Gravity gliding results as the sedimentary overburden moves down a sloping detachment mainly without internal deformation, while gravity spreading occurs as the overburden vertically collapses and laterally spreads under its own weight (Vendeville 2005).

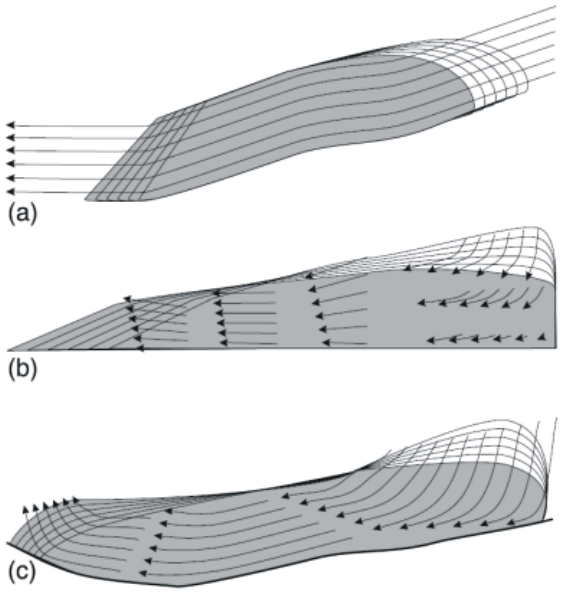

Figure 2.7 Schematic of gravity driven salt deformation including: a) gravity gliding as a rigid block slides down a sloped detachment; b) gravity spreading as a rock mass distorts under its own weight by vertical collapse and lateral spreading; and c) a combination of both styles of deformation. The final stage of deformation is represented by the grey shaded areas with arrows indicating vectors of material deformation (Rowan et al., 2004).

2.4 Glossary of salt tectonic terminology

Salt and related fault structures associated with salt tectonics give insight into the structural evolution of salt basins. These individual structures occur under certain conditions relating to sedimentation rates, erosion histories and original salt thickness. Appendix A provides an overview of commonly occurring salt tectonic structures.

2.5 Previous concepts derived by the Dalhousie Salt Dynamics Group

Previous 4D scaled physical experiments implemented by the Salt Dynamics Group of Dalhousie University provided new insights into understanding the evolution of passive margins affected by thin-skinned salt deformation (Krezsek et al. 2007; Adam et al. 2008; Campbell 2007; MacDonald 2007). Previous physical experiment series have studied first-order parameters of passive margin salt basin evolution that include:

1) Syn-rift salt basin geometry
2) Original salt thickness
3) Sedimentation rates and patterns

2.5.1 Syn-rift salt basin geometry and original salt thickness

Physical experiments completed by Ge et al. (1997) compared the evolutions of prograding sediments over a tabular pre-kinematic salt layer and a basin with basement steps to understand the general influence of basin architecture (Figure 2.8). These experiments used silica sand to represent brittle overburden and silicone putty to simulate salt.

In the tabular salt experiments, salt expelled basinward of the prograding wedge and became evenly inflated, forming a distal, sediment-starved plateau. All brittle deformation in the overburden was concentrated in the distal region of the wedges and formed three seaward-migrating domains including an expulsion rollover, a rollover syncline, and a progressively steepening landward-oriented limb of a salt-cored monocline.

Experiments with basement steps evolved similarly to the tabular salt experiments in the early stages but major differences occurred in the middle and late structural evolutions of the experiments. Seaward flow of salt became restricted at the basement steps resulting in broad inflation in the form of salt-cored anticlines as progradation overcame seaward salt movement. Aggrading distal sediments effectively pinned the position of salt-cored anticlines by hindering basinward propagation. The anticlines then became sites of active, and then passive diapirs, which fed allochthonous salt tongues and canopies.

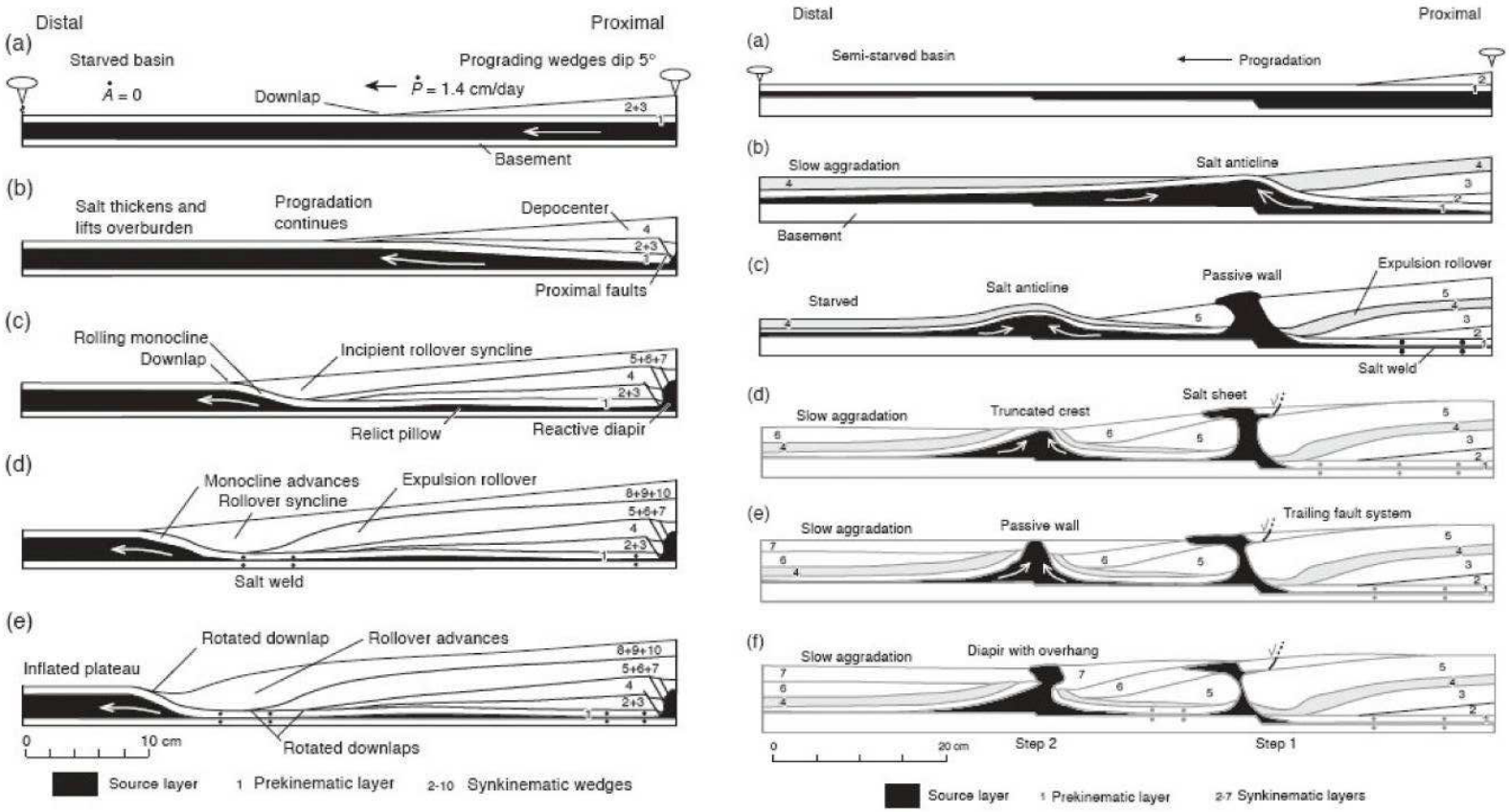

Figure 2.8 Comparison between tabular basin (left) and a setup with landward dipping steps (right) experiments. In the tabular basin, silicone is withdrawn from its autochthonous position with little to no restrictions. Sand downbuilds into the distally inflated silicone, creating a large monocline or expulsion rollover. With the experiment with basin steps basin, silicone inflation becomes localized at each change in silicone thickness, resulting in silicone-cored anticlines. These anticlines then evolve into passive diapirs, which may feed allochthonous silicone canopy systems. After Ge et al. (1997).

Analogue experiments completed by Campbell (2007) and MacDonald (2007) further investigated the role of syn-rift salt basin geometries as a main controlling factor of structural styles in the salt-tectonic evolution of passive margins. The experiments studied four generic salt basin configurations with scaled model sedimentation patterns comparable to those during the Jurassic to Cretaceous evolution of the Scotian Margin. The simplified basin configurations are shown in figure 2.9 and included a:

1) Symmetric graben
2) Half graben wedge
3) Symmetric graben with basement fault step
4) Symmetric graben with intermediate basement horst

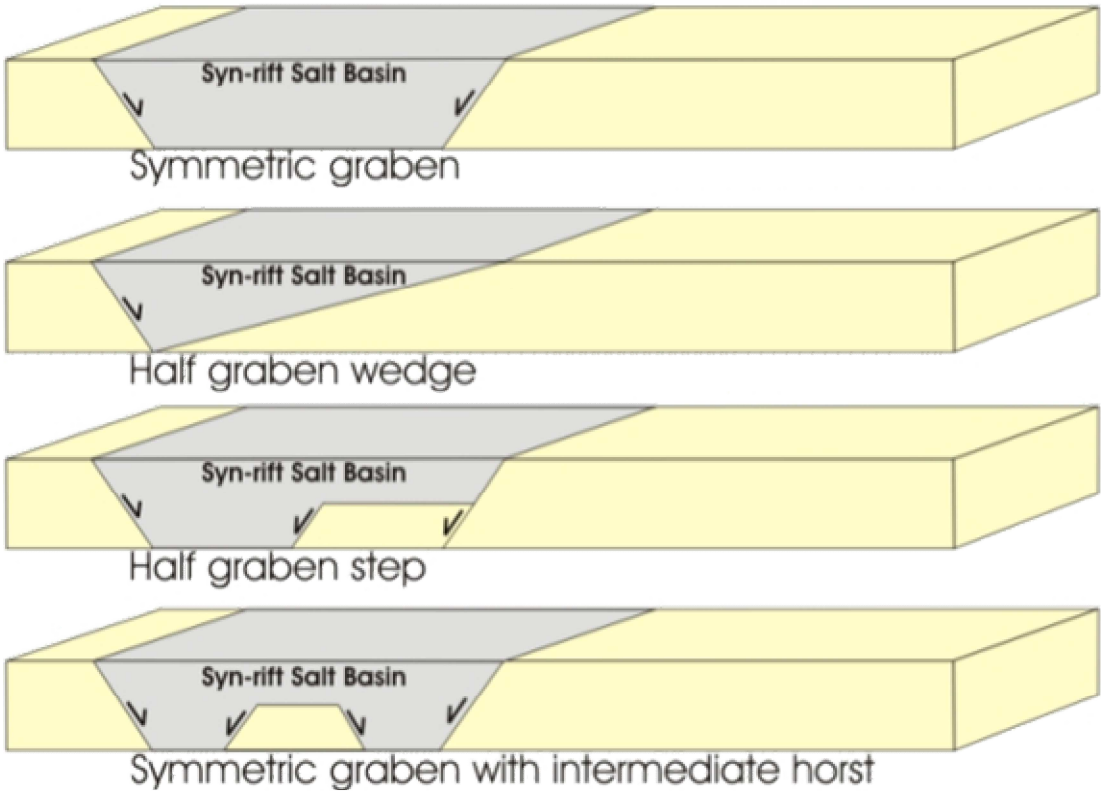

Figure 2.9 Schematic of the four salt basin geometries tested by Campbell (2007); and MacDonald (2007). The geometries include a symmetric graben, half graben wedge, half graben step and symmetric graben with intermediate horst.

These varying salt basin morphologies strongly controlled the structural evolution and depositional history of the individual experiments leading to distinctive salt tectonic structures and basin architectures (Figure 2.10). The symmetric graben, and symmetric graben with intermediate horst experiments, efficiently inflated and then evacuated silicone into the allochthonous region. The half graben wedge, and symmetric graben with basement fault step experiments, each evolved with mid basin inflation as the basin thinned and slowed the seaward migration of silicone until later stages where prograding sediments drove the silicone quickly out of the basin. The following section summarises the **early**, **intermediate** and **late** stages of the four experiments (Figure 2.11).

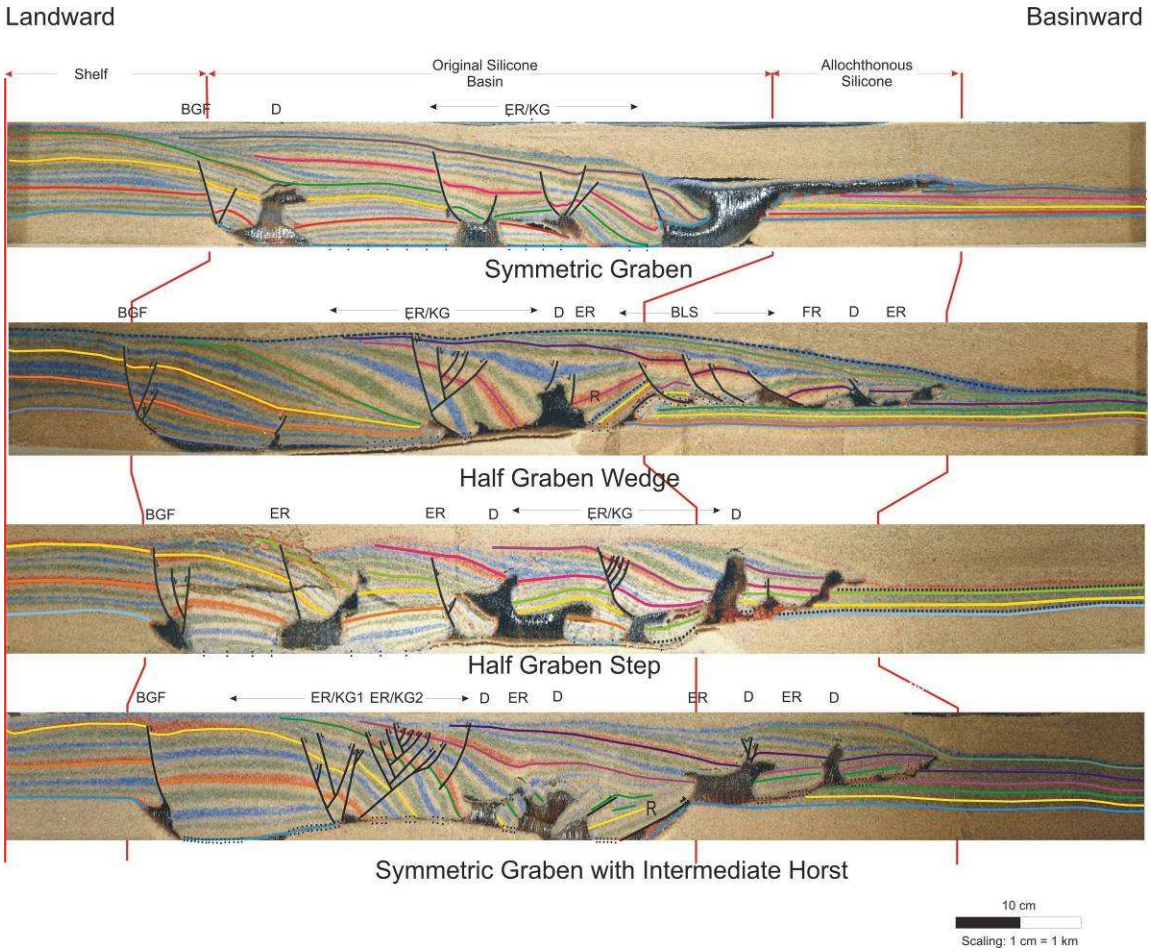

Figure 2.10 Center cross-sections of analogue experiments with varying salt basin geometries. Observed structures include: basinward listric growth faults (BGF), diapirs (D), expulsion rollovers (ER), keystone grabens (KG) (Campbell, 2007; MacDonald 2007).

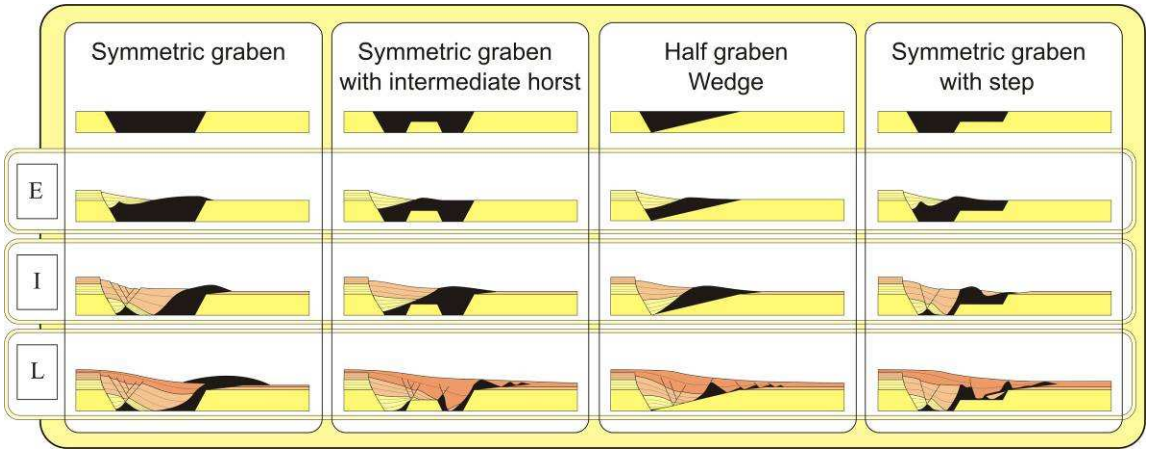

Figure 2.11 Schematic evolutions of analogue experiments including the early (E), intermediate (I) and late (L) stages of model evolution. Black indicates silicone putty, yellow aggrading sediments and orange prograding sediments (Modified from Campbell 2007 and MacDonald 2007).

The **early stage** is comparable to the early post-rift stage of salt basin evolution. The early stages of the experiments are characterised by differential loading of early post-rift sediments that initiate salt mobilization and proximal subsidence (E; Figure 2.11). The deformation of the brittle overburden begins with basinward dipping growth faults located above the edge of the landward rift shoulder. As sediments passively downbuild in the landward portion of the silicone basin, silicone is evacuate basinward forming an inflated silicone massif in the distal basin.

The **intermediate stage** of the experiment represents the main post-rift stage of basin development. The sediments continue downbuilding until silicone is evacuated. The base of sediments eventually touches the bottom of the basin and a regional weld forms beneath the landward salt basin (I; Figure 2.11). Landward regional weld formation results in basinward migration of depocentres as sediments begin to prograde into the deeper basin.

The **late stage** is the late post-rift stage of the basin evolution. This stage is characterised by further welding in seaward direction as progradation continues and

deformation becomes focused in the deep basin (L; Figure 2.11). During this stage the development of major allochthonous silicone nappes and tongues occur. Subsequently, sedimentation and deformation becomes focused on the secondary salt levels of these allochthonous structures.

The main conclusions developed from the experiment results of Campbell (2007) and MacDonald (2007) were:

1) The dominant mechanism for the initial salt mobilization in rift basins with thick initial salt deposits (≥2 km) is Poiseuille (channel) flow resulting from sedimentary loading and passive downbuilding of early salt withdrawal basins. This mechanism is observed to favour passive diapirism and associated expulsion rollover structures as opposed to extensive basinward dipping listric growth faulting.
2) Initial landward salt withdrawal and the location of seaward inflated salt depend mainly on the salt thickness controlled by basin floor geometry, rather than the geometry or angle of the basinward rift shoulder.
3) The timing and extent of allochthonous salt nappe advancement are dependent on the efficiency of early salt evacuation of the landward original salt basin and continued sedimentation and progradation on top of the inflated salt.

2.5.2 Sedimentation rates and patterns

Early experiments completed by the Salt Dynamics Group investigated the role sedimentation patterns and rates play in the formation of salt structures. Experiments simulated low, high and variable sedimentation rates.

For high sedimentation experiments, 5 mm thick sand layers were sieved onto the "salt basin" over hour intervals simulating a very high sedimentation rate of 1600 m/ma to represent rapid aggradation and progradation of a wedge of sediments (Figure 2.12). During these experiments depressions and active grabens were completely infilled. For the low sedimentation experiments, 2.5 mm thick sand layers were sieved over two hour intervals simulating a sedimentation rate of 420 m/ma. Unlike the high sedimentation experiments, active grabens were not filled completely (Figure 2.12).

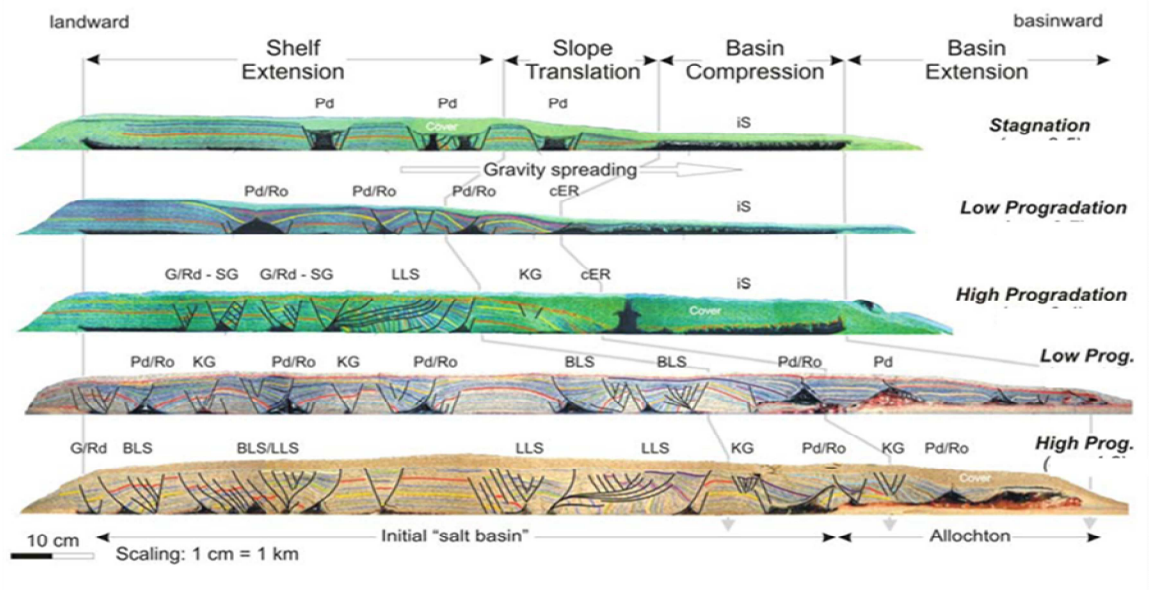

Figure 2.12 Structures observed in cross-sections of analogue experiments with varying sedimentation rates and basin slope. Structures observed include: graben systems and associated reactive diapirism (G/Rd), landward / basinward dipping listric fault/rollover systems (LLS/BLS), passive diapirism and associated symmetric rollovers (Pd, Pd/Ro), keystone grabens (KG), inflated silicone (iS), and compressional expulsion rollover (cER) (Krezsek et al. 2007).

These experiments have generated similar complex salt and fault structures to those observed in seismic profiles along passive margins. Structures included salt-withdrawal basins, landward and seaward dipping growth fault and rollover structures, expulsion rollovers, reactive, passive and active diapirs, canopies, as well as salt-cored folds, thrusts and allochthonous "salt" sheets. The experiments show similar kinematic segmentation (e.g. extensional, translational, and contractional domain) of a typical passive margin sedimentary wedge detached on a regional décollement, such as salt, during gravity spreading (Chapter 2.2).

The experiments with variable sedimentation rates demonstrate that the structural evolution of fault and "salt" structures is controlled by the coupled strain and sedimentation rates. With low sedimentation rates, the reactive diapirs beneath the grabens developed into passive diapirs that pierced the graben centers and formed extensive canopy systems. With high sedimentation rates, the early grabens evolved into growth fault rollover systems. The temporal evolution of extensional structures and associated diapirs with relation to sedimentation rates is summarized in Figure 2.13.

Comparable to the natural prototype, differential loading governs the stresses in the experiments and controls the individual strain histories of fault structures. This is observed by the characteristic succession of structural styles in the different types of experiments.

1. Very low sedimentation rates encourage reactive diapir rise leading to passive diapirs and canopy development in unstable shelf-slope transition and deepwater slope.
2. Low sedimentation rates create long lasting symmetric passive diapir/rollover systems and basinward growth fault/rollover systems.

3. High sedimentation rates create basinward growth fault/rollover systems that transition into landward growth fault/rollover systems with asymmetric salt rollers.

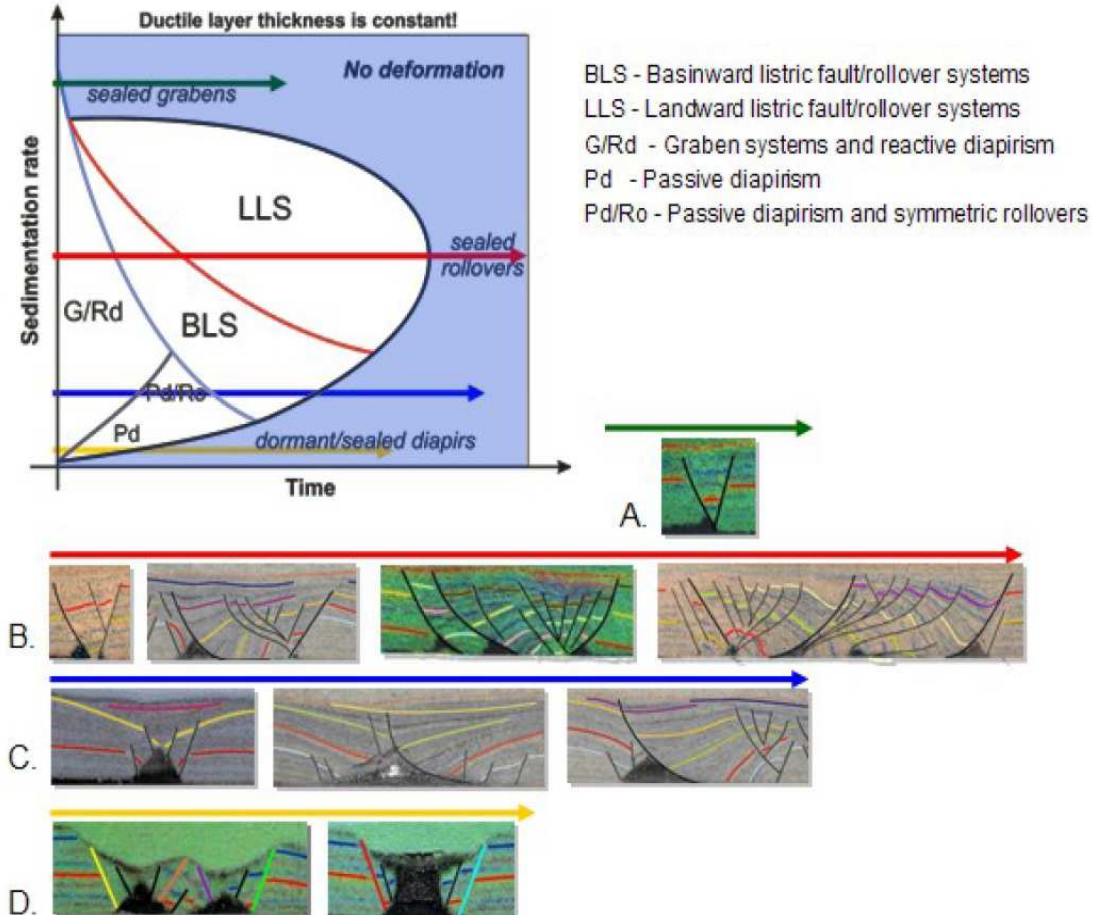

Figure 2.13 Temporal relationship between sedimentation (strain) rate and evolution of extensional salt-related structures in scaled analogue experiments (Figure 20). Ductile layer thickness 10 mm (= 1000 m in nature), x-axis total time 50 hours (= 15 my), sedimentation rates (y-axis): high 5 mm/h (= 1600 m/my), low 1.25 mm/h (= 420 m/my). A – D: Characteristic succession of fault and diapir structures; A – very high, B – high, C – low, and D. stagnant sedimentation (Kreszek et al. 2007).

CHAPTER 3: Overview of the Scotian Margin

3.1 Evolution of the Scotian margin

The Scotian Margin, located offshore Nova Scotia, is part of the rifted continental margin of Eastern Canada and stretches 1200 km from the eastern part of the Georges Bank in the southwest to the northwestern portion of the Grand Banks in the northeast (Figure 3.1; Wade and MacLean 1990). Wade and MacLean (ibid) have described the Scotian Basin as an accreted wedge of Mesozoic-Cenozoic sediments deposited on the eastern flank of the Appalachian orogen.

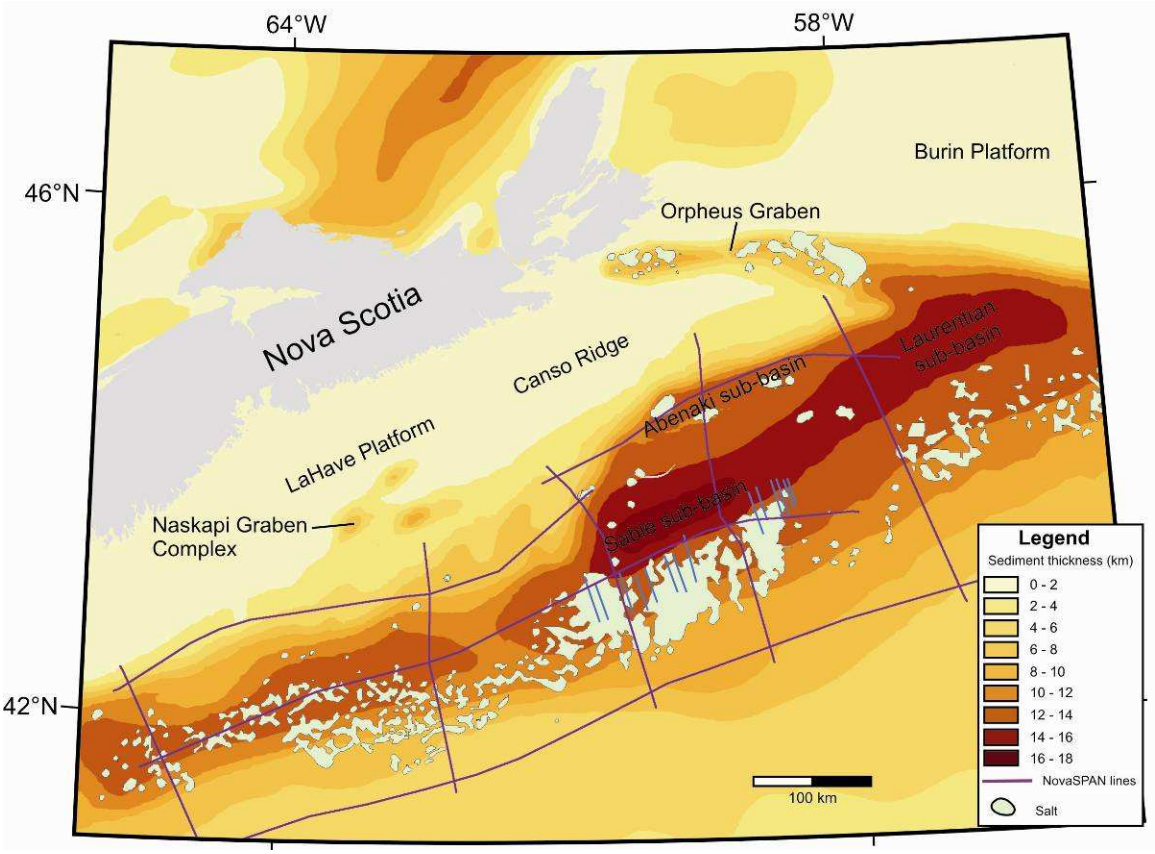

Figure 3.1 Continental shelf and slope of the Scotian Margin, offshore Nova Scotia with Mesozoic sediment thickness shown as color isobaths. The positions of the sub-basins of the Scotian Basin are also indicated. Shallow salt is indicated in light green.

Rifting along the Scotian margin occurred from the Middle Triassic to Early Jurassic during the break-up of Pangaea (e.g. Keen and Beaumont 1990; Louden 2002; Funck *et al.* 2004; Wu et al. 2006). Rifting was later followed by Jurassic seafloor spreading (Klitgord and Schouten 1986). During rifting the basin developed into a number of NE-SW trending interconnected sub-basins defined by syn-rift graben structures and related depocentres (Figure 3.1; Jansa and Wade 1975; Wade and MacLean 1990).

3.2 Crustal structure

The Scotian margin is characterized by a transition from a volcanic margin in the south to a non-volcanic margin in the north (Keen and Potter 1995; Funck et al. 2004; Wu et al. 2006). A strong, linear magnetic anomaly (~300 nT) known as the East Coast Magnetic Anomaly (ECMA) is well developed along the eastern US seaboard and the southern Scotian margin near Georges Bank (Figure 3.2; Wu et al. ibid). Keen and Potter (ibid) have identified seaward-dipping reflection (SDR) sequences on deep marine seismic reflection profiles from the southern Scotian margin coincident with the high-amplitude ECMA. SDR sequences occurring in basement and thick underplated igneous rocks in the lower part of the thinned continental crust and initial oceanic crust are characteristic of volcanic margins such as the US East Coast (e.g. Talwani and Abreu 2000; Wu et al. ibid). The ECMA weakens and disappears within the northern Scotian margin near Sable Island. No SDR sequences are observed in the northern Scotian margin. This is characteristic of non-volcanic rifted margins, such as the Iberia-Galicia Bank, (Keen and Potter ibid; Funck et al. ibid).

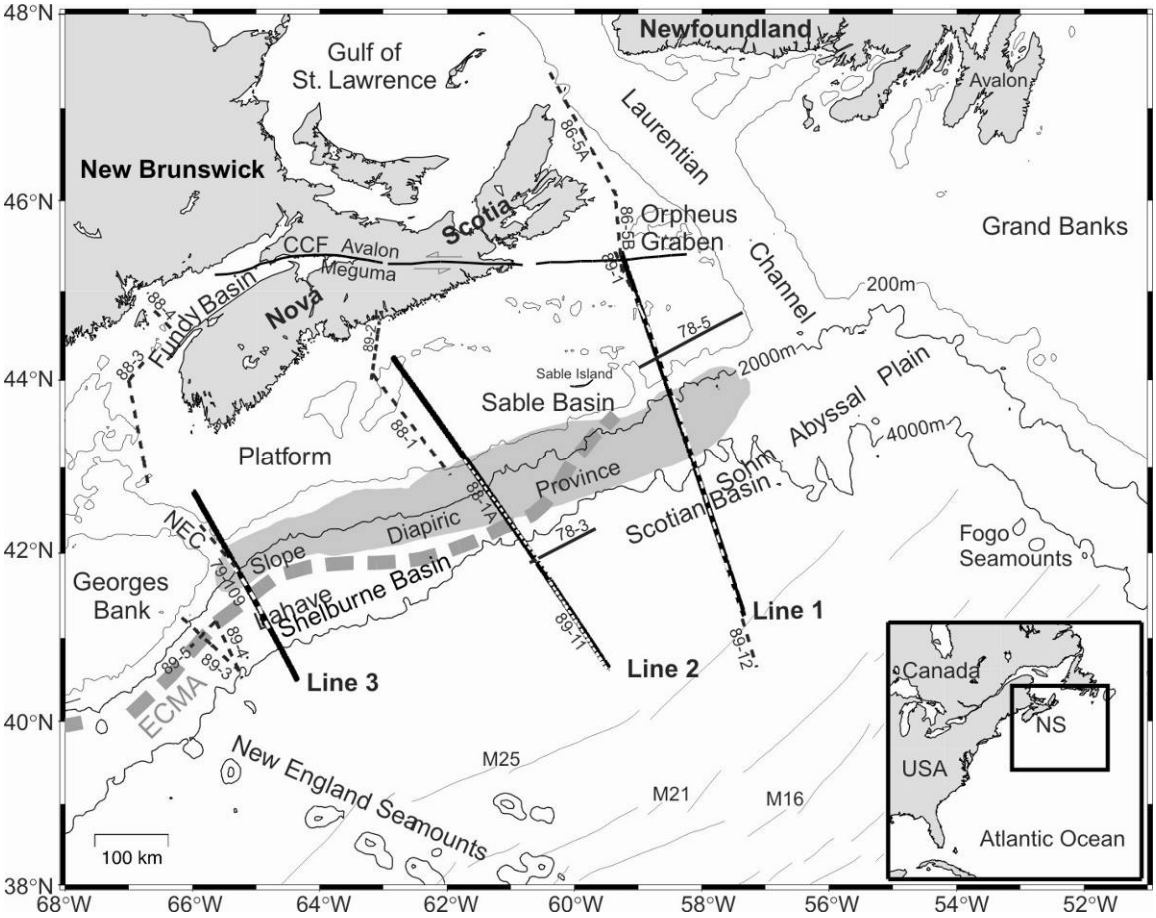

Figure 3.2 Location map of the Nova Scotia margin (Modified from Wu et al. 2006). Refraction seismic lines of the SMART experiment marked by bold solid lines. Bathymetric contours from the National Geophysical Data Center (1988). East Coast Magnetic Anomaly (ECMA) after Keen & Potter 1995. Shaded area indicates the location of the Jurassic salt of the Slope Diapiric Province (after MacLean 1991). Magnetic lineations (Klitgord & Schouten 1986). Earlier seismic refraction lines 78-3, 5 (Keen & Cordsen 1981). Relevant MCS reflection lines in the study area are shown as dashed lines: lines 86-5A, 5B (Marillier *et al.* 1989); lines 88-1, 1A (Keen *et al.* 1991b), lines 88-2, 3, 4 (Keen *et al.* 1991), lines 79-109, 89-11 and 89-12 (unpublished data by the German Federal Agency of Natural Resources and Geosciences, BGR), lines 89-3, 4, 5 (Keen & Potter 1995a); line 89-1 (Keen & Potter 1995b). Abbreviations are NS, Nova Scotia; NEC, Northeast Channel, and Cobequid Chedabucto fault (CCF).

Velocity modeling by Funck et al. (2004) and Wu et al. (2006) on the northern segment of the margin indicate a non-volcanic character for both the northern and central portions of the margin based on characteristic velocities indicating the presence of serpentenized mantle (Figure 3.3). However, they observed in the portions, differences in the continental extension phase and the transition to seafloor spreading. The ocean-

continent-transition (OCT) zone in the central margin is interpreted to have a partially serpentinized upper mantle (PSM) layer overlain by a highly faulted continental crust in the northwest, and oceanic crust in the southeast. In comparison, the OCT zone in the northern margin contains a 70 km wide upper layer of exhumed and highly serpentinized mantle (HSM) overlying the PSM layer. Differences between the thickness of the OCT also exists between the two sections where in the central margin it is observed to be only 4 km thick and in the northern margin is 5 – 7 km thick. Both differences indicate that during break-up, limited magma was generated across the central margin while no melt was generated across the northern margin (Wu et al. 2006).

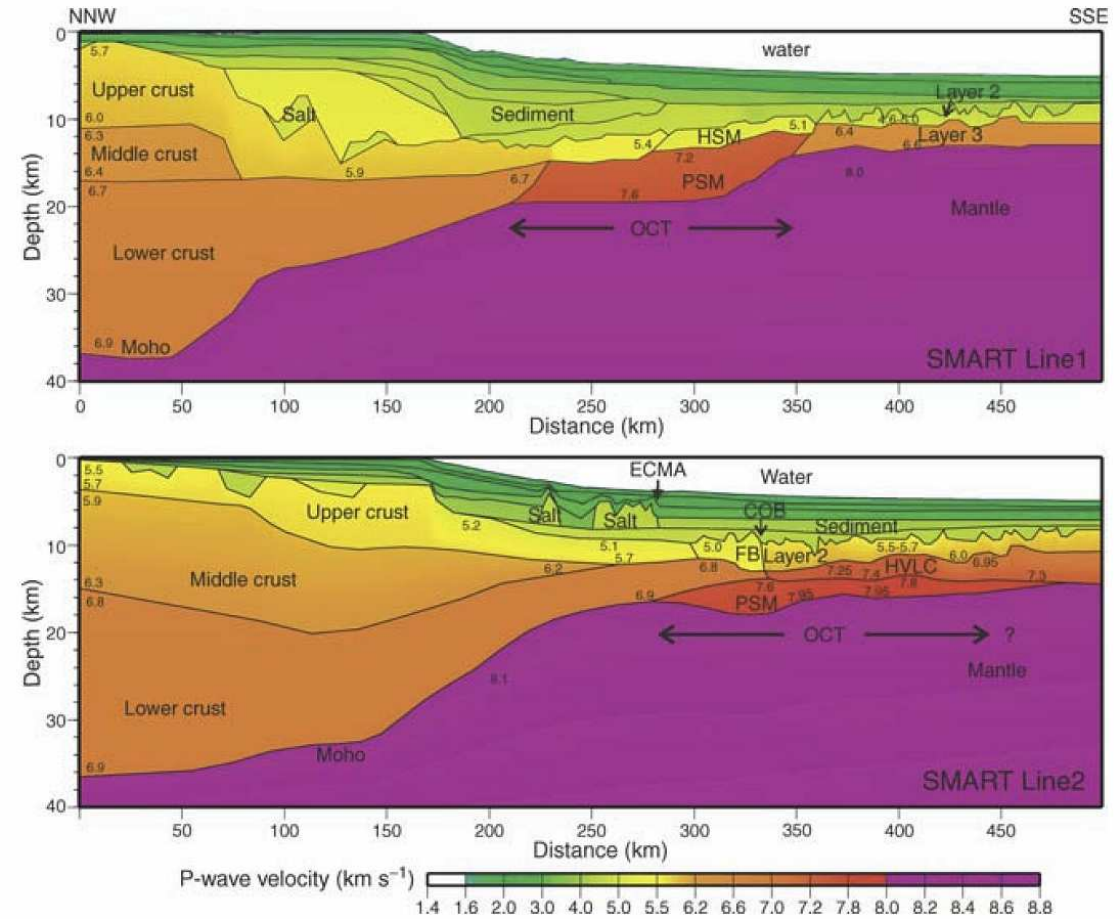

Figure 3.3 A comparison of velocity models along Line 1 of the northern margin (upper panel, Funck *et al.* 2004) and Line 2 of the central margin (lower panel, Wu et al. 2006). *P*-wave velocities are indicated by a color scale and numbers in sections (in km s^{-1}). Abbreviation: HSM, exhumed and highly serpentinized upper mantle. Location of lines shown in figure 3.2.

Modeling by Wu et al. (2006) also indicates that continental crustal thinning in the central margin was initially gradual along the outer continental shelf, followed by a much faster thinning along the continental slope and into the ocean basin. Within the northern margin, (e.g. Sable, Abenaki, and Laurentian Subbasins) thick sedimentary successions accumulated in response to drastic thinning of continental crust from the onset of rifting, followed by a gradual thinning to the ocean basin (Wu et al. 2006). Abrupt crustal thinning across the north-central margin gave rise to rapid subsidence and formation of the deep Sable Subbasin seawards of the hinge line (Wu et al. 2006).

3.3 Rift basin architecture

The Scotian Basin is flanked to the north by more stable platforms known as the Lahave Platform and Canso Ridge forming the weakly deformed NW continental rift shoulder. Regional data suggests the initial Scotian Basin was probably a northeast-trending complex of grabens variably filled with Late Triassic red beds and salt (Figure 3.4; Wade and MacLean 1990). A prominent Early Jurassic (post-breakup) basement hinge trends northeasterly along the flank of the basin. This hinge zone consists of a series of normal faults and flexures across which the depth to basement increases rapidly from approximately 4 km on the platforms to 10 km or more in the subbasins (Wade and MacLean ibid). The hinge developed after rifting and is believed to be related to crustal downwarp resulting from processes associated with initial seafloor spreading and sediment loading (Wade and MacLean ibid). Complex rifted basement structures trending northeast occur southeast of the hinge zone but are often difficult to detect in seismic data due to their depth and because thick sediments blanket the structures. The presence of these basement structures, however, may be inferred from associated salt

structures as well as from faulting in the overlying sediments. The early rift structures initiated as a result of sinistral trans-tensional forces within a broad zone to the south of the Acadian suture. Thus, the bounding extensional faults of the Mesozoic Scotian Basin hinge zone are likely reactivated Paleozoic faults (Ratcliffe et al. 1986).

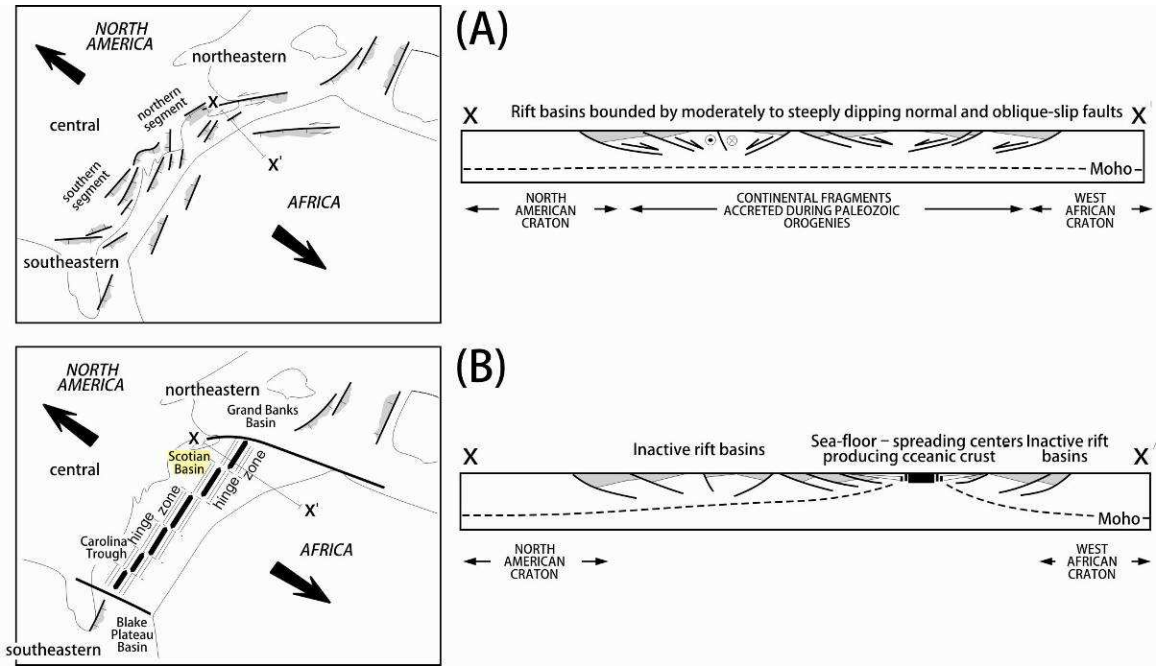

Figure 3.4 Schematic map and cross-sectional views of the two-stage model for the evolution of the passive continental margin of eastern North America: (A) rifting during the Middle Triassic to Early Jurassic, and (B) drifting beginning during the Early to Middle Jurassic and continuing today (modified from Withjack et al. 1998).

3.4 Salt Tectonic Subprovinces

Early studies have identified extensive diapirism in the slope of the Scotian Basin defined as the Slope Diapiric Province (e.g. Jansa and Wade 1975; Wade and MacLean 1990). More recently, Kidston *et al.* (2002, 2007) and Shimeld (2004) used modern regional TGS-NOPEC seismic data to map the regional salt tectonic structures of the Scotian Basin. They respectively subdivided the Slope Diapiric Province into distinctive salt tectonic subprovinces based on the distinctive salt deformation styles and

depositional environments (Figure 3.5). Shimeld (ibid) suggests the diverse salt structural styles in the provinces were controlled by basement morphology and variations in sedimentation history and defined five subprovinces:

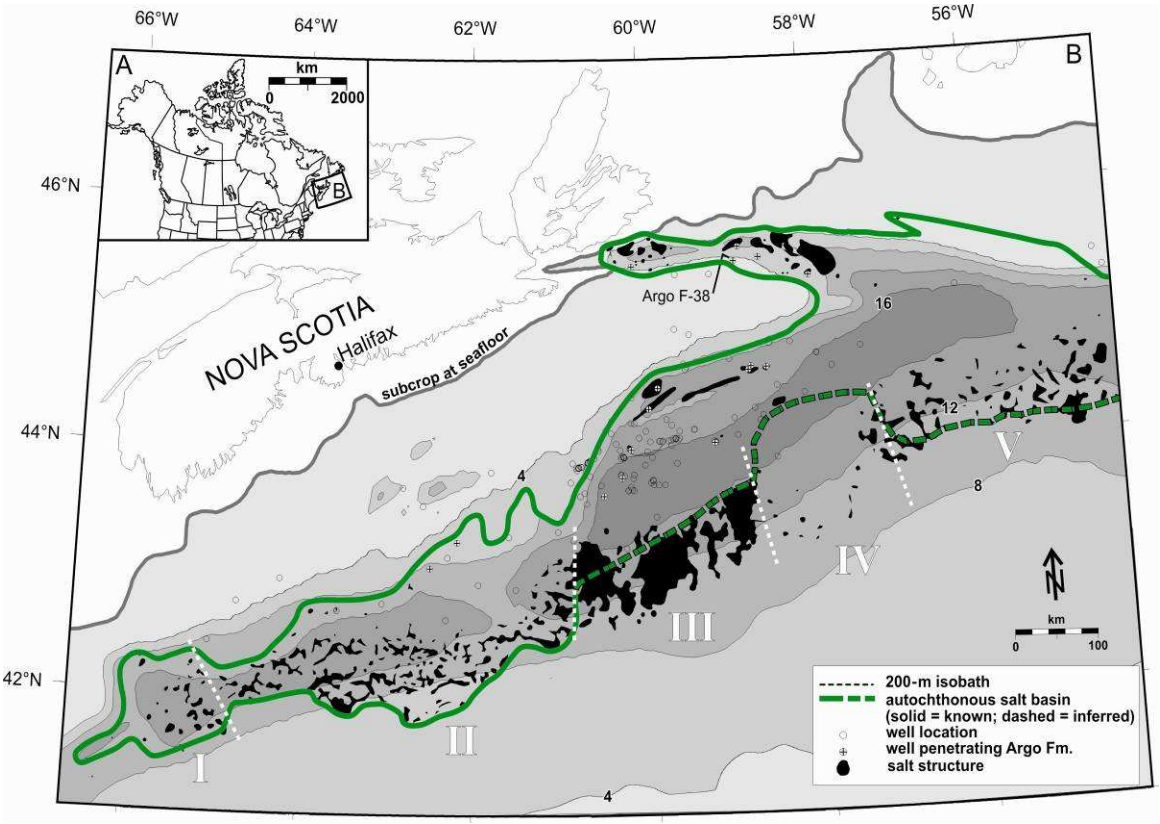

Figure 3.5 Map of the Scotian Margin with shaded areas showing the total thickness (in kilometers) of Triassic to Neogene sediments (modified from Wade, 2000) and the location of shallow salt structures mapped by Shimeld (2004). Most of the salt structures, shown as black polygons, lie beyond the 200-m (660-ft) isobath. White dashed lines indicate the boundaries between the five salt tectonic subprovinces defined by Shimeld (2004) and are shown in Roman numerals (Modified from Ings and Shimeld 2006).

1) Subprovince I

Subprovince I occurs on the south-western limit of the Scotian margin offshore near Georges Bank (Figure 3.5) and is characterized by the presence of elongated salt walls and diapirs recording passive growth from Jurassic to the Cretaceous. Observed strata concordant with diapir crests above the latest Cretaceous Wyandot Formation suggests source depletion caused by a shutdown of the salt system by this time.

Allochthonous salt canopy systems averaging 15-20 km in width occur outboard of the autochthonous salt basin. These canopy systems overlie Middle Jurassic and older sediments.

2) Subprovince II

Subprovince II occurs adjacent to Subprovince I on the central-western Scotian margin (Figure 3.5). It is characterized by the presence of linear salt walls aligned with the edges of the late Abenaki carbonate platform. In the western portion of the subprovince, mushroom to tongue shaped diapirs occur and transition to vertical diapirs and seaward-oriented salt nappe systems in the east.

3) Subprovince III

Subprovince III is located on the central Scotian margin (Figure 3.5) and is characterized by extensive salt tongue canopies overlying lower Cretaceous and older sediments. These tongue canopies extend 80 to 100 km basinward and have associated overburden Late Cretaceous sediments showing a variety of extensional syn-kinematic structures. These extensive tongue canopy systems coupled with a lack of autochthonous salt structures indicates significant salt withdrawal and seaward translation in Subprovince III. Middle Jurassic to Early Cretaceous progradation of the Sable delta most likely drove this salt system.

4) Subprovince IV

Subprovince IV is characterized by a lack of diapirism in the shelf area and virtually no diapirs beneath the shelf break (Figure 3.5). Beneath the upper slope of the

modern margin are salt nappes with basinward dipping listric rollover systems developed in the sediment overburden (Shimeld, 2004). A defining feature of Subprovince IV is the presence of an up to 4.5 km thick and laterally extensive basinward-dipping listric fault rollover system of Middle to Upper Jurassic age sediments. This succession is referred to as the Banquereau synkinematic wedge (BSW).

5) Subprovince V

Salt structures in Subprovince IV are observed to have complex 3D morphologies (Figure 3.5). Structures include allochthonous salt tongues with thick post-Jurassic sedimentary cover. The structures were influenced by significant extension during the Cretaceous and later contraction during the latest Cretaceous through Neogene (Shimeld 2004). Diapirs in the slope have overburden cover as thin as 100 m.

3.5 Stratigraphy of the North-Central Scotian Margin

The stratigraphy of the Scotian margin has been documented in numerous studies (e.g. Jansea and Wade 1975; Wade and MacLean 1990; Piper et al. 2004; Cummings et al. 2006) using available seismic reflection and well data. The stratigraphy in the Scotian Shelf is well defined but due to a lack of data available on the slope the deepwater stratigraphy of the Scotian margin is less constrained (Figure 3.6).

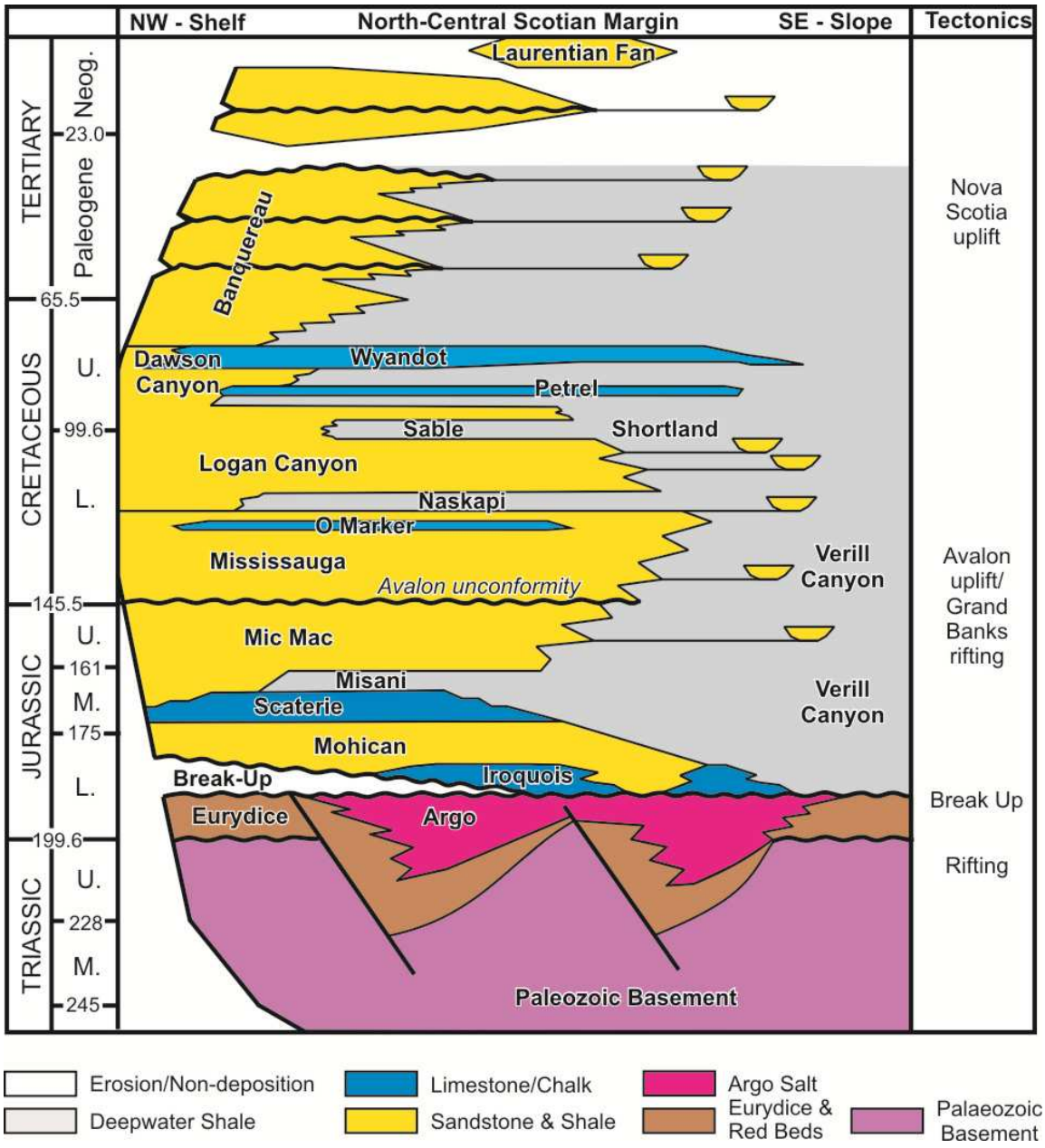

Figure 3.6 Generalized stratigraphy for the north-central Scotian margin (modified from Wade and MacLean 1990; Kidston *et al.* 2002; 2007; Adam *in prep.*).

3.5.1 Basement

The Mesozoic sedimentary rocks of the Scotian Basin overlie a crystalline basement complex except in the Burin Platform where they are locally deposited on upper Paleozoic sedimentary strata (Figure 3.1; Wade and MacLean 1990). The basement rocks

of the Scotian Shelf consist of Paleozoic metasedimentary rocks of the Meguma Terrane with some granitic plutons (Wade and MacLean 1992).

3.5.2 Syn-rift stratigraphy

During the Triassic, the rifting phase of continental breakup resulted in the formation of a complex of north-easterly trending horsts and grabens that are underlying the Mesozoic Scotian Basin (Wade and MacLean 1990). As grabens formed they created localized accommodation zones for thick fluvial and lacustrine red clastic sediments referred to as the Eurydice Formation (Figure 3.6; Jansa and Wade 1975; Wade and MacLean ibid). These sediments were deposited under seasonally arid conditions and were overlain and interfingered with evaporites of the Argo Formation in many of the deeper grabens of the rift basin (Figure 3.6; Wade and MacLean ibid). The Argo consists of a series of massive beds of coarse crystalline salt separated by zones of red shale. A deficiency of anhydrite in the evaporite sequences occurs within the Argo suggesting the salt precipitated from brines already depleted of carbonate and sulphate minerals (Jansa et al. 1980; Wade and MacLean ibid). Deposition of the syn-rift salt ceased abruptly in the Early Jurassic as rifting ended as indicated by the creation of a breakup unconformity observed on the LaHave Platform and the Canso Ridge (Wade and MacLean ibid).

3.5.3 Post-rift stratigraphy

In the post-rift stage, the Argo and Eurydice formations were unconformably overlain locally by shallow marine dolomitic rocks of the Iroquois Formation (Figure 3.6). Elsewhere in the basin they are overlain by the continental orogenic clastics of the Mohican Formation (Figure 3.6; Wade and MacLean 1990). Mohican sandstones and

shales were deposited into actively subsiding sub-basins adjacent to the hinge zone forming a very thick lower to middle Jurassic molasse sequence. Seismic data indicates that the formation can be more than 4 km thick south of the Abenaki Graben hinge zone and as much as 5.5 km thick over the syn-rift sequences beneath the eastern Scotian Shelf (Wade and MacLean ibid). The Mohican thins greatly at the hinge zone and either pinches out against or is truncated by the post-Jurassic Avalon Unconformity (Wade and MacLean ibid).

Within the Abenaki Graben, the Mohican Formation is conformably overlain by thin limestone beds of the Scaterie Member and Abenaki Formation. Elsewhere, it is overlain by a thick, predominantly clastic sequence known as the Mic Mac Formation (Figure 3.6). Within the Scotian Basin, the Mic Mac and its equivalents - the Abenaki carbonates to the south, Mohawk to the north and the distal deepwater Verrill Canyon Formation - span the late-Middle and Late Jurassic (Figure 3.6; Wade and MacLean 1990). The clastics formed broad alluvial plains and the Abenaki formed an extensive carbonate succession (Figure 3.7). Thicknesses for the interbedded sandstones and shales of the Mic Mac are as great as 6 km in the Laurentian Subbasin and 4 to 5 km southeast of Sable Island (Wade and MacLean ibid). Moving seaward, Mic Mac coarse clastics transition into marine shales of the equivalent Jurassic Verrill Canyon Formation (Figure 3.6; Wade and MacLean ibid).

During the latest Jurassic, the eastern margin of Canada was affected by the breakup of Iberia from North America. The margin south of Newfoundland was the most impacted by uplift, deformation and extensive erosion of Jurassic and older strata. The uplift has lead to a westward shift in depocentres from the Laurentian to the Sable

Subbasin. The breakup unconformity created by this event is referred to as the Avalon Unconformity.

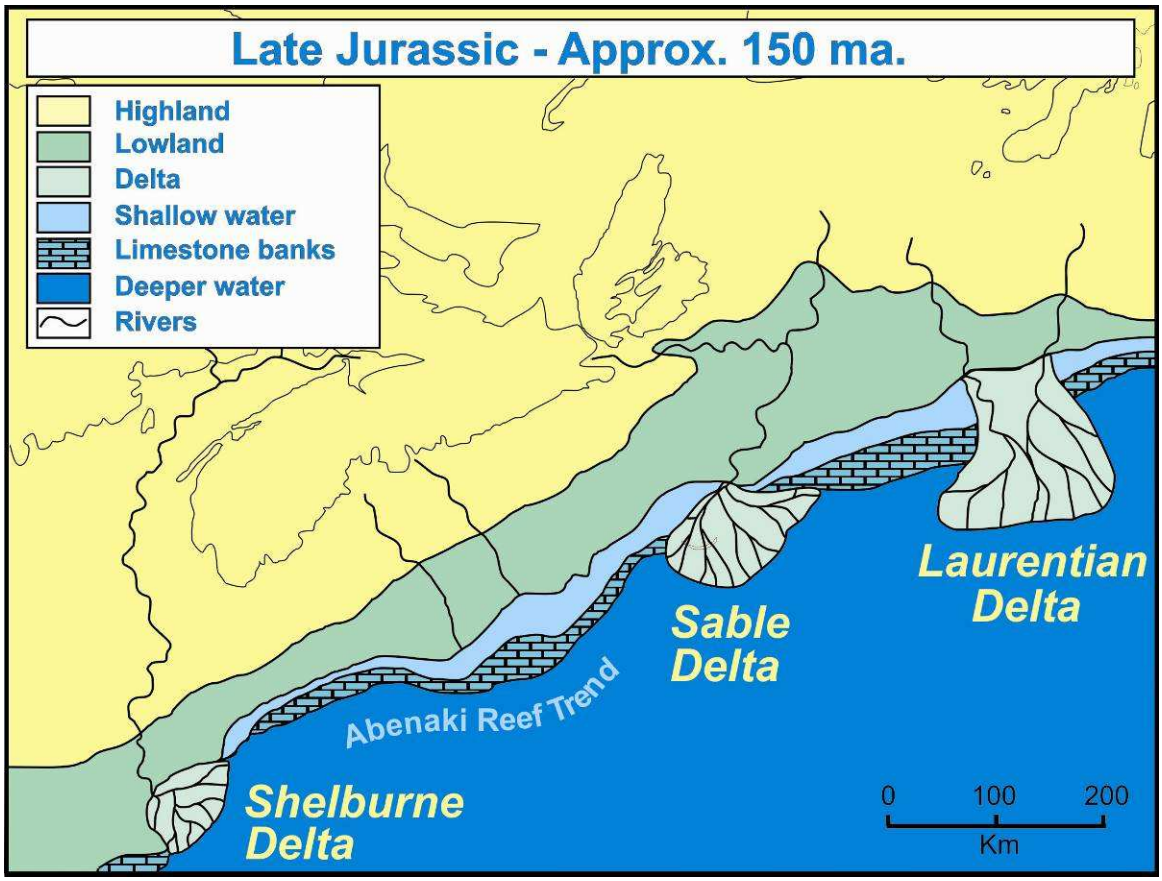

Figure 3.7 Paleogeography and paleo-delta sediment transport along the Scotian margin during the Late Jurassic (Modified after John Wade, GSC).

The Cretaceous Missisauga Formation overlies the MicMac Formation and is widespread throughout the Scotian Basin (Figure 3.6; Figure 3.8). Across the LaHave and Burin platforms as well as the Canso Ridge it is less than 1000 m thick and is composed mostly of sandstone in the northeastern basin (Wade and MacLean 1990). In the Sable Subbasin, the total estimated thickness is more than 3 km containing 30-50% coarse-grain siliclastics. Within the upper Missisauga is a series of thin Barremian age limestone beds referred to as the "O" (oolitic) Marker. As with the Mic Mac, the

Missisauga Formation grades basinward into deepwater sequences of the laterally equivalent Verrill Canyon Formation (Figure 3.6).

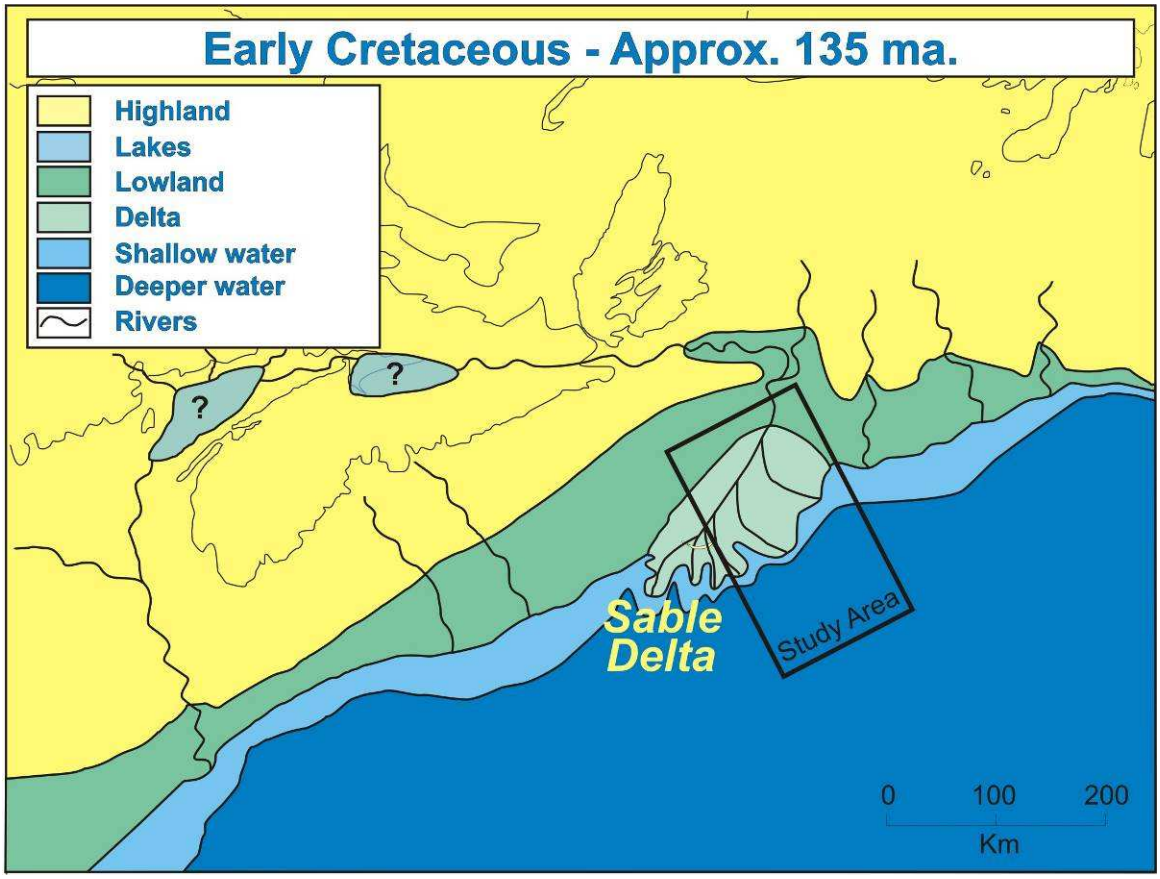

Figure 3.8 Paleogeography and paleo-delta sediment transport along the Scotian margin during the Cretaceous (Modified after John Wade, GSC).

The Early to early-Late Cretaceous Logan Canyon Formation conformably overlies the Missisauga Formation (Figure 3.6). It is an upward-fining fluvial-marine succession with a broad distribution and a maximum estimated thickness of approximately 2.5 km (Wade and MacLean 1990). Its distal turbidite/shale equivalent is known as the Shortland Shale (Wade and MacLean ibid).

Overlying the Logan Canyon Formation is a Late Cretaceous transgressive unit known as the Dawson Canyon Formation (Figure 3.6). The Dawson Canyon is composed of marine shales, chalks and minor limestones which were deposited across the Scotian Basin (Wade and MacLean 1990). The formation varies in thickness from more than 700 m in the South Whale Subbasin and parts of the Scotian Shelf in the east, to approximately 200 m on the Canso Ridge and approximately 100 m in the more sediment starved outer Sable Subbasin (Wade and MacLean ibid).

The Wyandot Formation overlies the Logan Canyon and is composed of chalks, chalky mudstones, marls and minor limestones (Figure 3.6; Wade and MacLean 1990). The thickness of this latest Cretaceous unit ranges from less than 50 m in the Sable Island area to approximately 400 m in the southeastern part of the Scotian Shelf but is missing over extensive portions of the basin due to later Tertiary erosion (Wade and MacLean ibid). Along the outer shelf and slope, the top of the Wyandot is often marked by an unconformity which is overlain by younger sediments (Wade and MacLean ibid).

The remaining successions of the Scotian Margin between the top Wyandot and the top Cenozoic are grouped within the Banquereau Formation (Figure 3.6; Wade and MacLean 1990). It is a coarsening-upward siliclastic succession, predominantly Tertiary in age and consists of a series of downlapping or prograding sequences (Wade and MacLean ibid). Thicknesses of the Banquereau Formation range from a zero edge along the basin margin to more than 4 km beneath the Scotian Slope (Wade and MacLean ibid).

CHAPTER 4: Seismic Data

4.1 Seismic data for the Abenaki Graben and Sable Subbasin region

This thesis relies on interpretation of regional seismic data to better understand the tectono-stratigraphic evolution of the Abenaki Graben and central Sable Subbasin area of the Scotian margin. The following section describes the seismic dataset available for the study area and the interpretation results with particular focus on salt structures, related depositional systems in the Abenaki Graben and its deepwater extension, and what are the derived first order characteristics and parameters for the experiment setup.

4.1.1 Seismic database

The interpretation of the margin's basin structure and stratigraphy relies mainly on the recently acquired high resolution 2D ION GXT NovaSPAN seismic survey (Figure 4.1). Acquired in 2004, the NovaSPAN dataset consists of 3,300 km of depth migrated regional lines (285 km Line 1800) including five lines extending out from the shelf to the distal abyssal plain as well as three strike lines that image the margin parallel variations of the basin. The survey includes a 17 second record time and large 9,000 meter offsets that generate better imaging of the underlying crustal architecture of the rift-related horsts and graben structures. These offsets allow for imaging of up to 20 km depth on the lines. Line resolution is aided by advanced processing techniques (e.g. Kirchhoff pre-stack depth migration, free-surface multiple elimination) to create better imaging at depth.

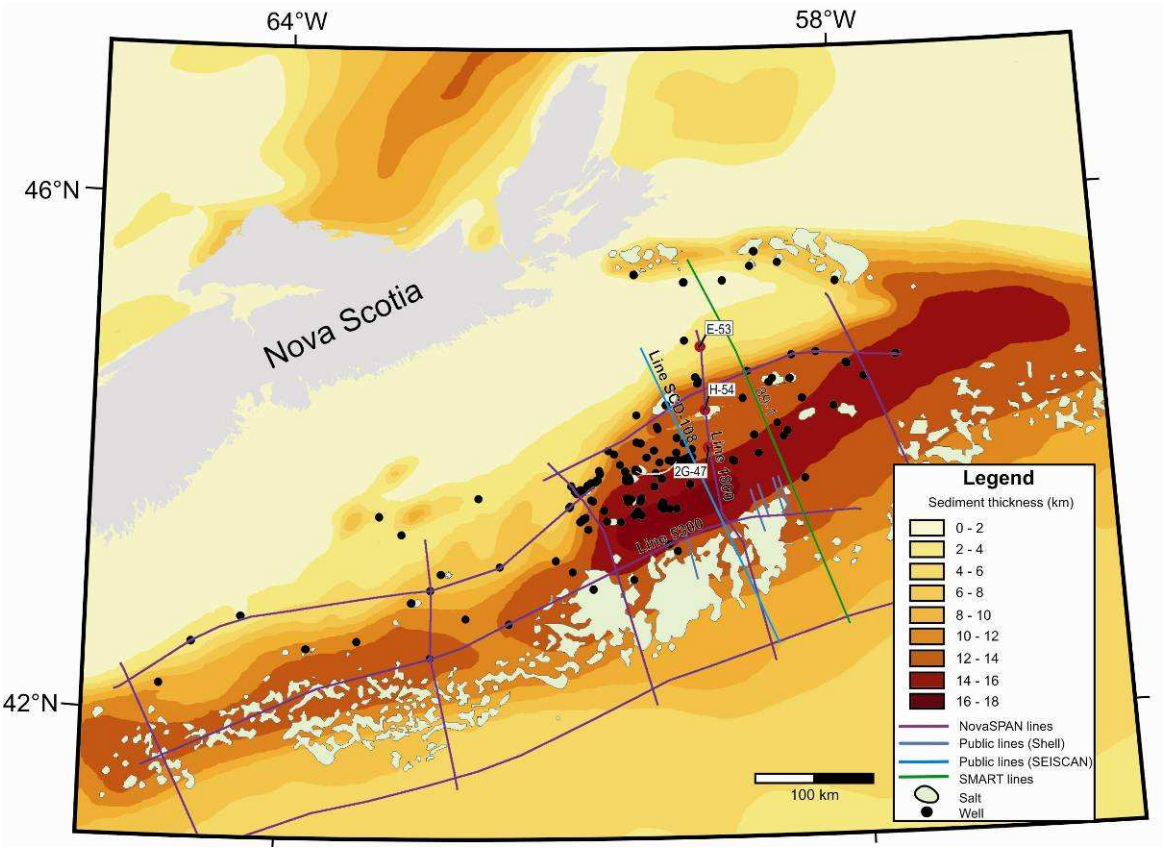

Figure 4.1 Map of the Scotian margin indicating the location of the various seismic lines for the study. The sediment thickness is taken from the GSC BASIN database. To observe the public Shell lines, please refer to Appendix B.

GXT Line 1800 of the NovaSPAN dataset provides the basis for interpretation of the salt basin morphology, stratigraphy and salt structures across the Abenaki Graben and central Sable Subbasin region (Figure 4.2; large scale section found in Appendix B on CD). Three wells are crossed by Line 1800 along the shelf (Wyandot E-53, Missisauga H-54 and the Bluenose 2G-47; Figure 4.2). Well data were retrieved from the GSC BASIN database to allow for age control and obtain thicknesses of major depositional events (http://basin.gsca.nrcan.gc.ca/index_e.php). Due to the lack of well control in the deepwater slope, correlation was aided by using published seismic reflectors from the slope into the deepwater (Wade 1978; Ewing and Radinowitz 1984; Swift 1985; Ebinger

and Tucholke 1988), as well as implementing concepts of seismic stratigraphy and tectono-stratigraphic concepts developed from this project.

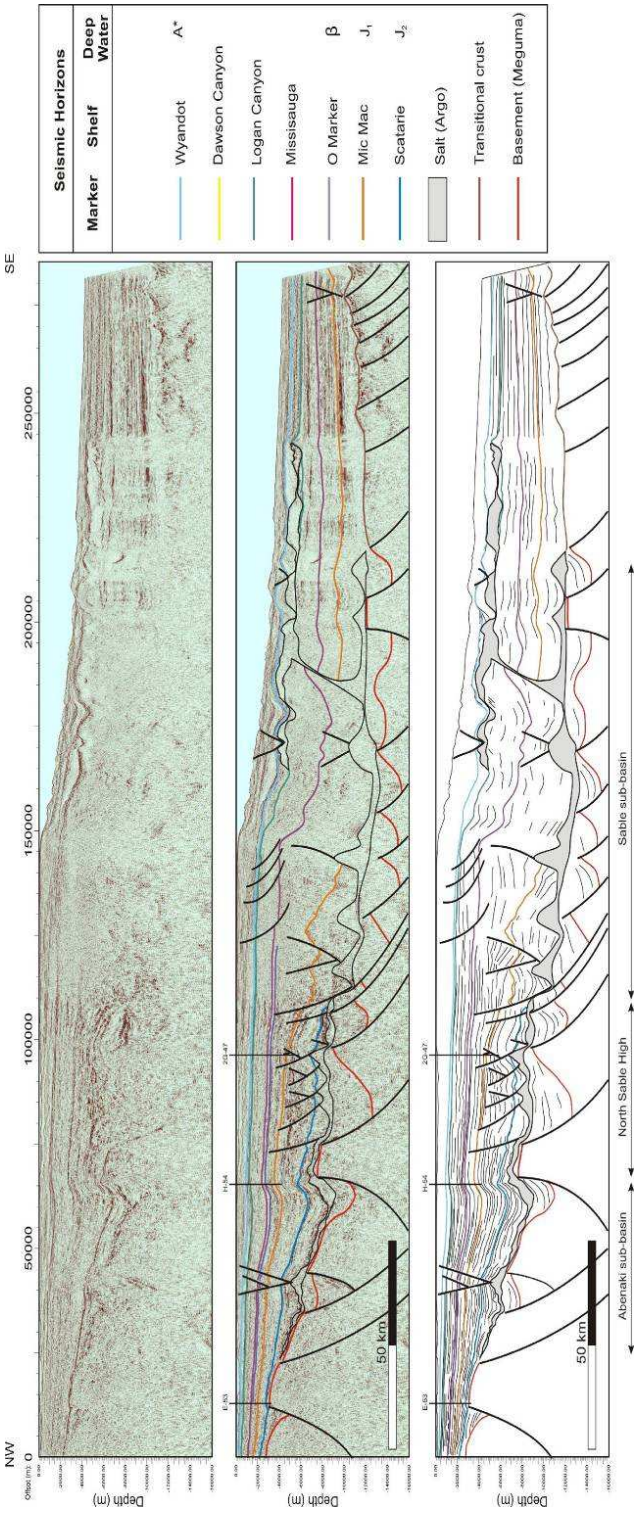

Figure 4.2 Line 1800 interpreted with the aid of the E-53, H-54 and 2G-47 wells as seen in figure 4.1. Lower panel shows major dip domains interpreted from the seismic to aid in the deepwater interpretation. Refer to figure 4.1 for line location (Refer to Appendix B on CD for larger section).

Public domain 2D profiles also provide an important component to understanding the study area. These profiles often do not cover the regional extent, depth or resolution (Figure 4.3) of the NovaSPAN lines. However, they can be useful to better understand the lateral extent and variability of shallow salt structures in the slope area of the margin (Appendix C). The public lines also give clues into the continuation of basement structures across the margin. GSC Lithoprobe Line 89-1 occurs approximately 50 km to the east of Line 1800 and images the subsurface well, but indicates a basin morphology more closely resembling NovaSPAN Line 2000 to the east (Figure 4.4; Cribb, in prep.) as the margin appears faulted and not flexed as discussed for Line 1800 later in this chapter. The transition between the western Laurentian Subbasin and the Central Sable Subbasin as imaged by these lines thus marks a drastic change in rift basin morphology.

To compliment the seismic database, a GIS database is used by the Salt Dynamic Group to correlate additional data across seismic data gaps to further evaluate the complexities of the basin (i.e. sediment distribution, basin architecture, paleo-depositional maps). The database includes seismic line positions correlated with well locations, satellite bouger and free-air anomalies, satellite magnetic anomalies, sediment thickness (Figure 4.1), and present day shallow salt distribution acquired from the GSC MIRAGE database, GSC BASIN database and Louden *et al.* (2004). Depositional maps by MacLean (1991) are included in the database for a better understanding of the history of sediment distribution across the margin. Examples of these maps can be found in Appendix D.

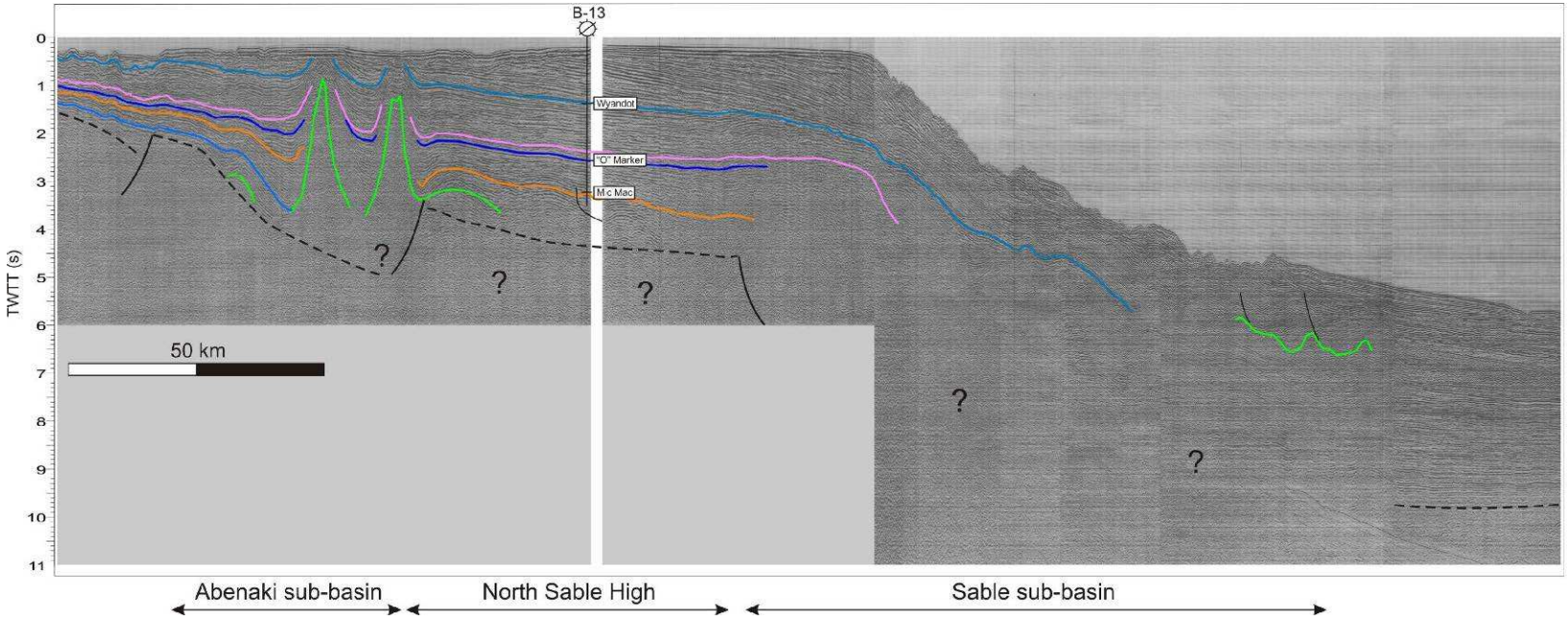

Figure 4.3 Line SCD-108 shot in 1972 by Seiscan Delta. Interpretation of the publically available seismic data becomes difficult to impossible to interpret at depth due to small streamer offsets during acquisition. Refer to figure 4.1 for line location.

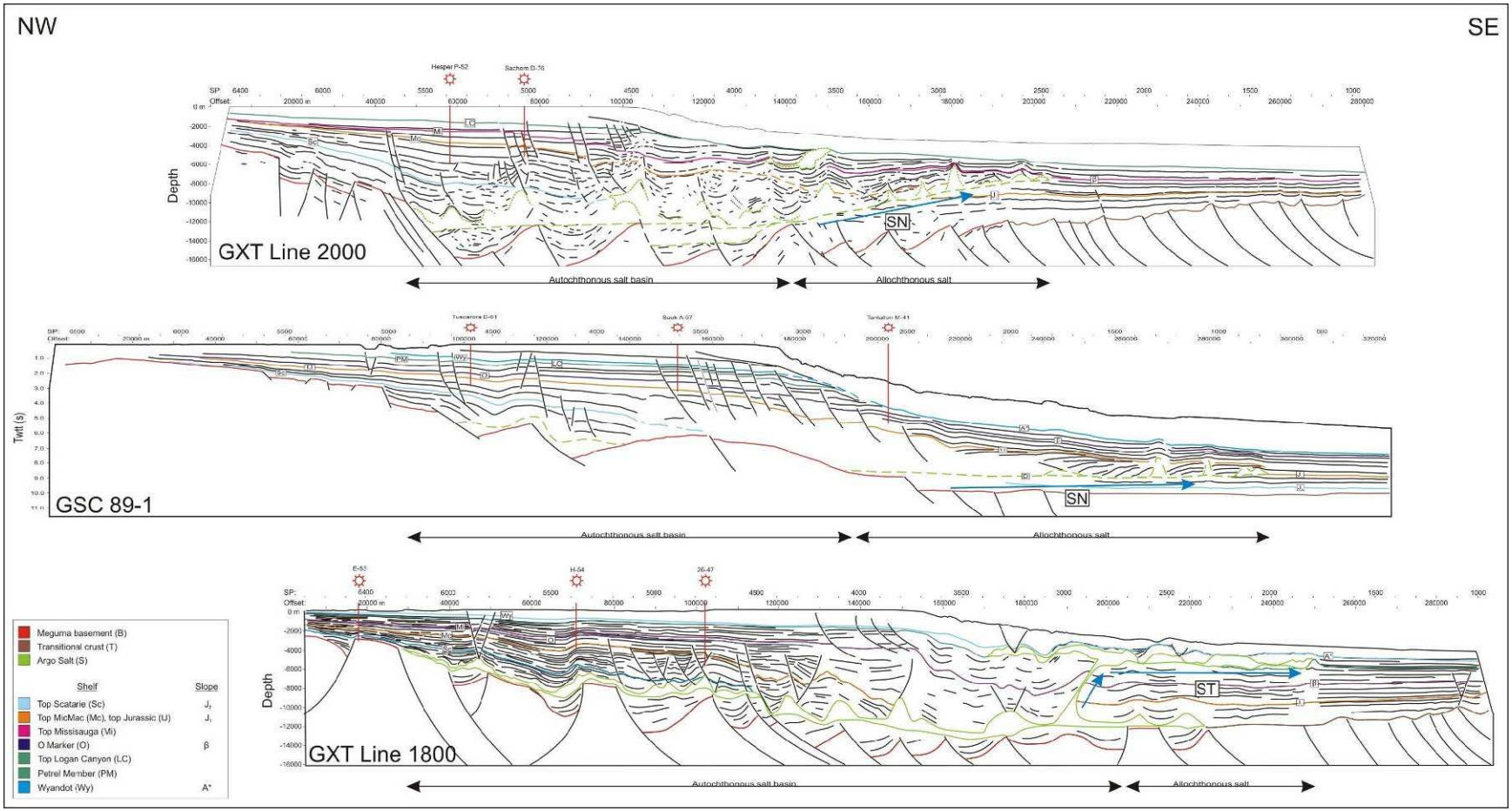

Figure 4.4 Comparison between ION-GXT Line 1800, and ION-GXT Line 2000 and GSC Lithoprobe Line 89-1. Both lines 2000 and 89-1 display similar ramp basin geometries with resulting salt nappe (SN) systems. These differ from the step geometry interpreted in Line 1800 which resulted in the creation of a salt tongue system (ST). For line locations please refer to Figure 4.1 and 4.13.

4.1.2 Workflow

Interpretation of the 2D seismic data is carried out on the SMT Kingdom Suite® seismic software. Data within the SMT Kingdom Suite project includes the ION-GXT NovaSPAN dataset with velocity profiles, and publicly available seismic profiles. Interpretation of stratigraphic horizons was completed to facilitate time correlations across the seismic profiles and defining the major depositional events (Figure 4.5). Stratigraphic picks interpreted are indicated in Figure 4.3 and include: 1) top basement (Palaeozoic); (2) top syn-rift 3) top salt (Early Jurassic); 4) top Scaterie (Middle Jurassic); 5) top Mic Mac (Late Jurassic); 6) O Marker (Early Cretaceous; 7) top Missisauga (Early Cretaceous); 8) top Logan Canyon (Late Cretaceous); 9) top Dawson Canyon (Late Cretaceous); 10) top Wyandot (Late Cretaceous). As mentioned in the previous section, interpretation of horizons on the seismic profiles relies on well data retrieved from the NRCan BASIN Database. To retain consistency, data from the wells is based on the interpretations of Wade and Maclean (1993). The Wyandot E-53 well gives the most complete stratigraphic record in reaching the Palaeozoic basement, while the Missisauga H-54 and the Bluenose 2G-47 wells both reach the Late Jurassic Mic Mac interval.

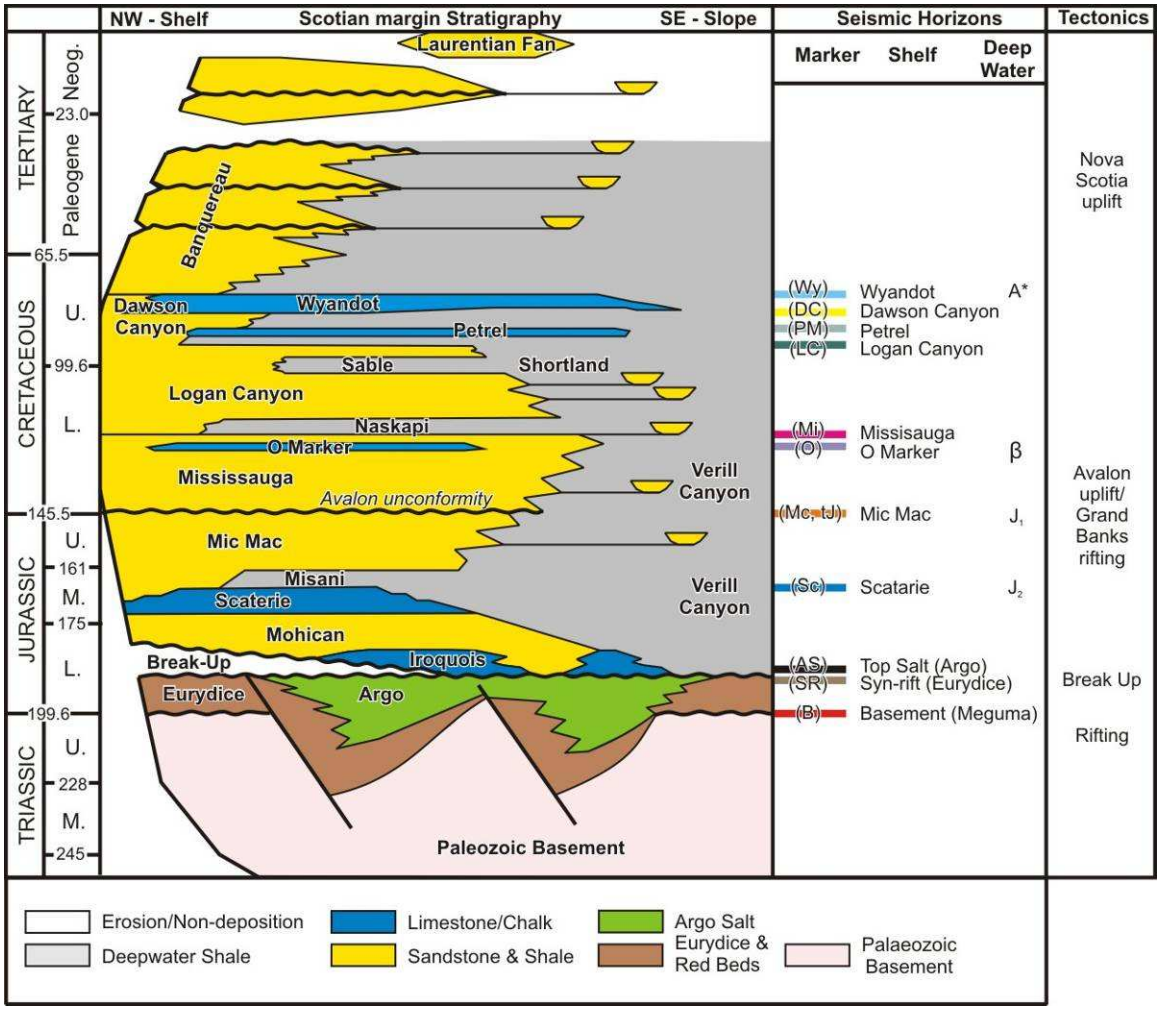

Figure 4.5 Stratigraphic chart of the Scotian margin indicating the horizons picked for the study (modified from Adam et. al (in prep).

4.2 Subbasin architecture of ION-GXT Line 1800

The crustal basement along the shelf and proximal basin of the ION-GXT Line 1800 is confirmed to be Meguma Terrane as it was penetrated by the Wyandot E-53 well (Figure 4.6). Seismic reflection of the Meguma slates and quartzites result in semi-coherent reflections making the distinct boundary between stratified sediments and basement somewhat difficult to interpret. Interpretation of the crustal structure is therefore aided by recognizing fault patterns as well as fan-shaped syn-rift fill patterns above rotated basement fault blocks (Figure 4.7).

Rift Shoulder (Shelf)

The basement top beneath the modern day shelf and along the stable Canso Ridge Platform shows minor deformation and consists of slightly rotated fault blocks with up to 1.5 km of normal displacement with grabens infilled by syn-rift sediments (Figure 4.7). The basement depth of the rift shoulder increases gently from approximately 2.5 km in the northeast to 4 km towards the hinge zone. Basement reflections show some continuity within the Meguma basement but signal strength does slightly decrease from the above stratified sediments making basement easy to recognize (Figure 4.6).

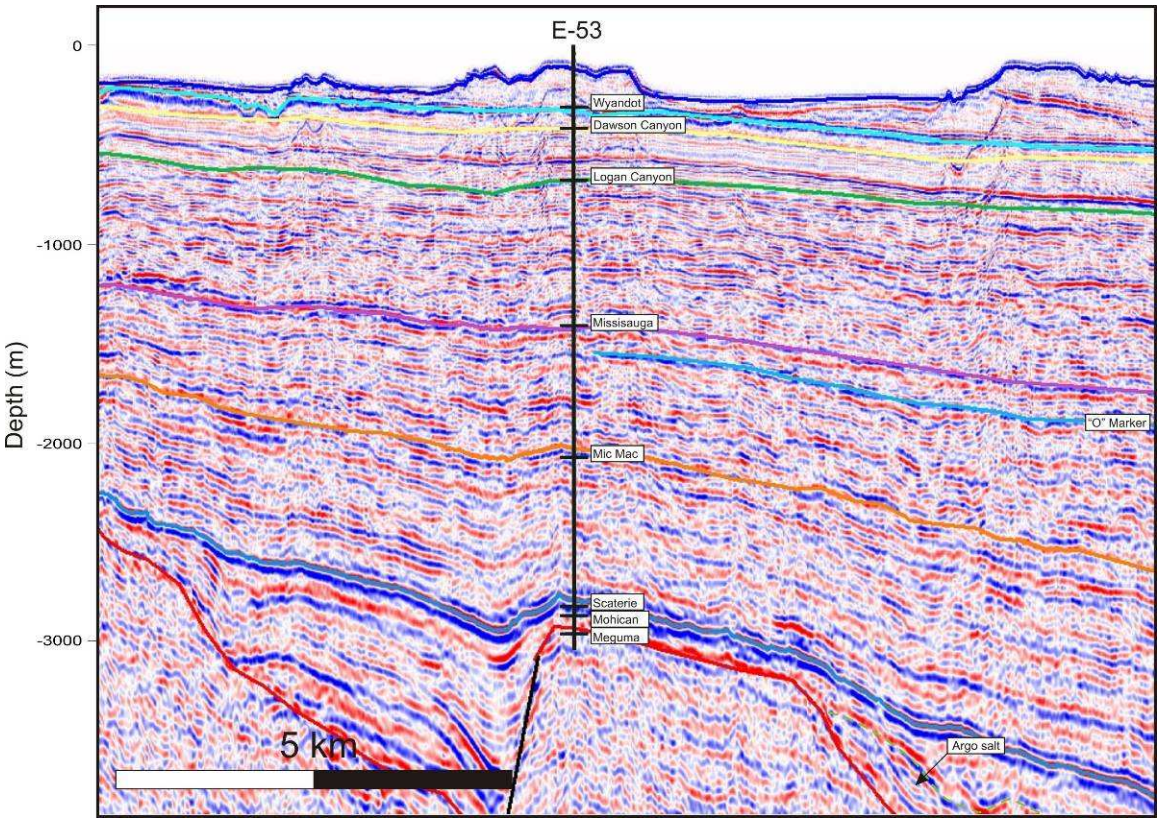

Figure 4.6 Segment of ION-GXT Line 1800 demonstrating the seismic characteristics for each interpreted formation. The well shown is Wyandot E-53.

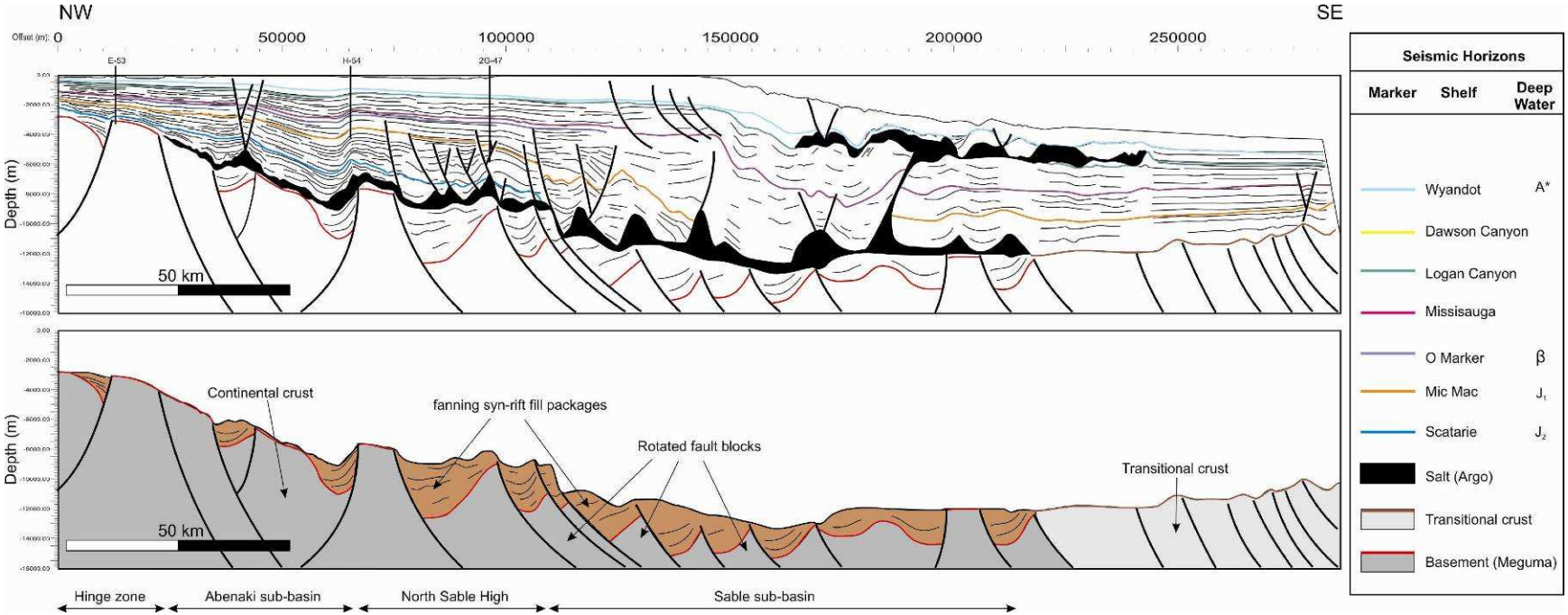

Figure 4.7 Interpretation of the crustal structure and syn-rift fill for Line 1800

Rift Margin (Hinge Zone)

Along the hinge zone, extensional faults with minor offsets are observed in the proximal rift basin (Figure 4.7). Deep-seated seaward-dipping basement faults are interpreted from high angle reflectors that extend beyond the seismic sections deep into the crust (over 12 km). However, the gentle slope of the basement top from the stable Canso Ridge platform (e.g. rift shoulder) into the rift basin supports interpretation that the hinge zone in the Abenaki area is represented by a large crustal flexure (Figure 4.2; Figure 4.7) rather than a pronounced border fault system as observed in the Laurentian Subbasin. Basement depth increases from the landward hinge limit from 4 km over the stable platform to 7 km into what is referred to as the Abenaki Graben. This differs to the east as observed from GSC Line 89-1 and ION-GXT line 2000 as the faulted hinge zone is more prominent in the generally wedge-shaped salt basin (Figure 4.4).

Abenaki Graben (Proximal basin)

Subsidence controlled by flexure of the hinge zone, as well as rift-related basement faulting, formed a small subbasin which is flanked seaward by a basement horst (North-Sable High; Figure 4.2; Figure 4.7). The half graben with wedge-shaped basin fill represents the asymmetric Abenaki Graben and includes up to 4 km of syn-rift sediments deposited as adjacent basement blocks rotated to create accommodation space. The proximal Abenaki Graben marks the landward limit of salt deposition within the area as evidenced by a buried diapir as well as numerous salt pillows. The subbasin is approximately 45 km wide and extends from the stable platform to the prominent basement horst block. The horst block marks the landward edge of what is referred to as

the North Sable High and extends approximately 130 km on the shelf parallel to the margin edge (Figure 4.8; Wade and MacLean 1990).

Figure 4.8 Regional geological cross section A-A' across the Scotian shelf and slope (modified form Wade and MacLean 1990).

North Sable High

Seaward of the Abenaki Graben and separating it from the Sable Subbasin to the southeast is the prominent North Sable High located at approximately 8 km depth and consists of a series of elevated horsts and grabens filled with syn-rift sediments (Figure 4.4). A large symmetric horst block approximately 7 km wide marks the landward limit of the high and is followed by a series of rotated fault blocks. Syn-rift sediments observed within the grabens display fanning seismic reflection patterns and are up to 4 km thick (Figure 4.2; Figure 4.7). This high is approximately 60 km wide along Line 1800 and seismic data infers it extends approximately 130 km on the shelf parallel to the margin, tapering out at its limits.

Sable Subbasin (Distal basin)

Seaward of the North Sable High, the basement steps down approximately 4 km through a series of predominately seaward-dipping listric faults (Figure 4.2; Figure 4.7). The deepest portion of the basement floor is interpreted to be approximately 13 km below present day sea level. The seismic imaging of this portion of the basin is disrupted largely due to its depth as well as the geometry of the slope and overlying salt sheets. Fanning syn-rift reflection patterns infer the general geometry of the basin floor (Figure 4.2; Figure 4.7). As with the other areas within the basin, the fanning syn-rift packages are separated by rotated basement blocks. The completely to partially-filled asymmetric rift half grabens are bounded by seaward dipping listric rift faults, and form the main structural element in the central rift basin. The post-rift salt basin floor appears quite flat for approximately 60 km until the appearance of a step feature created by a fault block

and syn-rift fill geometry of the distal Sable Subbasin (Figure 4.2; Figure 4.7). This basin step extends approximately for 35 km to where the salt basin finally ends.

Deepwater abyssal plain

Seaward of the distal salt basin, changes in seismic response of the basement indicates a change from continental to transitional crust (Figure 4.2; Figure 4.7). ION-GXT Line 1800 includes approximately 65 km of transitional crust located ~12 km below sea level (Figure 4.2; Figure 4.7). As observed by Funck et. al. (2004) and discussed in Chapter 3, the transitional crust appears as strong, chaotic and non-parallel reflectors with seaward dipping listric faults that can be mapped revealing a spacing of approximately 10 km. The top of the transitional crust is highly irregular due to the slight rotation of the fault blocks. They are overlain by strong parallel reflections indicating deepwater sediments (Figure 4.2).

4.3 Seismic Stratigraphy

The seismic stratigraphy is described for each formation based on its internal seismic characteristics. The genetic reflection packages for each are described in the following section based on observations in ION-GXT Line 1800 and aided by general descriptions highlighted by Wade and MacLean (1990).

Basement rocks

Unlike typical crystalline crustal basement, coherent reflectors can be observed within the metasediments of the Meguma Terrane continental crust (Figure 4.6). As noted earlier, weaker parallel seismic reflectors within the Meguma slates and quartzites

contrast with the more coherent reflections of the overlying continental clastics and allow the top basement to be mapped. Within the basin, the basement consists as a series of rotated fault blocks (Figure 4.7).

Beneath the base of the continental slope, a change in seismic response is observed that marks the transition from continental to transitional oceanic crust (Figure 4.9). The seismic response in the transitional crust appears as strong, chaotic and non-parallel reflectors differing from the more coherent Meguma reflection response. The distinct response makes the top of the transitional crust easily to interpret as it differs greatly from the stacked parallel reflectors from the overlying deepwater clastics. Like the seismic response from the continental crust, steeply dipping seismic reflectors allow deep crustal faults to be mapped (Figure 4.2).

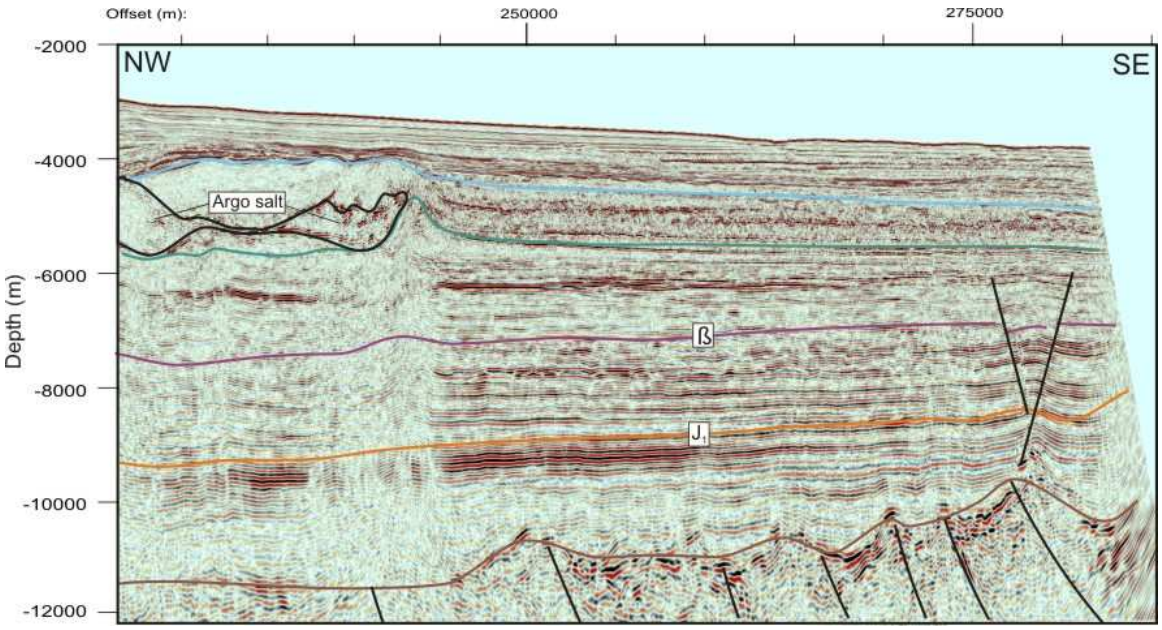

Figure 4.9 Deepwater segment of ION-GXT Line 1800 demonstrating the seismic characteristics for each interpreted formation. Refer to figure 4.1 for line location.

Eurydice and Argo Formations (Middle Triassic – Early Jurassic)

Strong parallel and rotated reflectors define the characteristic growth strata of the Eurydice red beds and indicate where the salt beds are thin and make up a small component of the total section. The Argo Formation displays classic examples of reflection-free diapiric structures and related features (Figure 4.2). Thick salt beds in the section produce few coherent internal reflectors and are susceptible to mobilization and diapirism (Figure 4.2). Strong amplitude reflectors are due to a significant impedance contrast at the top of the salt that can be observed in areas of where salt is near the surface.

Mohican Formation (Early – Middle Jurassic)

The coarse fluvial clastic sediments and shales of the Mohican Formation thin over basement highs and are represented by strong sub-parallel reflections indicating an increased content of limestone or siltstone (Figure 4.6; Wade and MacLean 1990). As the formation thickens into grabens, the internal reflectors weaken and are less continuous (Figure 4.2). Strata infilling the grabens onlap the sides and produce parallel and sub-parallel seismic reflections of various amplitudes.

Abenaki Formation/Scaterie Member (Middle Jurassic)

The seismic response from the Scaterie Member carbonates is identified as a strong reflector in the shelf but is marked by the seaward shale-out into the Verill Canyon formation (Figure 4.2; Figure 4.6). The strong reflector at the top of the member can be easily correlated from the Wyandot E-53 well (Figure 4.6) across the shelf into the proximal Sable Subbasin. The associated strong basal reflection is due to the velocity

contrast between the underlying Misaine shales and Mohican clastics. The reflector dips gently into the Abenaki Graben and up onto the North Sable High where it is broken up by a series of listric faults with small (~200 m) offsets (Figure 4.2). The reflector appears to terminate as it onlaps onto a small salt pillow at the edge of the North Sable High.

Mic Mac Formation (Middle – Late Jurassic)

The Mic Mac Formation is the deepest formation penetrated by all the wells along the shelf including Wyandot E-53, Missisauga H-54 and Bluenose 2G-47, which allows for more confident correlation across the section (Figure 4.2). The seismic response along the shelf from the formation's alluvial plain facies appear as semi-continuous, parallel reflections likely from shales with variable thickness interbeds of sandstones and siltstones (Figure 4.6). In the deepwater portion of the section, the seismic reflections become discontinuous and weak as the sandstones and limestones of the Mic Mac Fm. transition into the marine shales of the lateral equivalent Jurassic Verrill Canyon Formation (Figure 4.9). Similar to the Scaterie Member, the top Mic Mac reflector dips gently into the Abenaki Graben and then onto the North Sable High (Figure 4.2). Listric faulting affects internal reflectors but little to no offset occurs along the top reflector (Figure 4.2). The reflector continues into the Sable Subbasin where it is interpreted to terminate at a diapir (Figure 4.2). Interpretation in this area is more difficult as this is where the Mic Mac transitions into the Verill Canyon shales, but internal semi-continuous dipping reflectors sufggest continued seaward progradation (Figure 4.2).

Missisauga Formation (Late Jurassic – Early Cretaceous)

Along the shelf, the interbedded sandstones and siltstones of the Missisauga Formation is tested by the three wells. The formation is characterized by continuous parallel and sub-parallel reflectors that are generally weak (Figure 4.2; Figure 4.6). Like the top Scaterie and Mic Mac seismic markers, the top Missisauga reflector gently dips into the Abenaki Graben and up onto the North Sable High (Figure 4.2). Listric faults in the shelf, with small offsets, appear to sole out within the Missisauga. The top reflector appears fairly flat until its dip rapidly increases at the approximate edge of the modern day shelf break in the Sable Subbasin (Figure 4.2). As it transitions into the distal shales of the Verrill Canyon Formation, the reflector appears to onlap the edge of the salt feeder of the large salt tongue feature (Figure 4.2; Figure 4.9).

The "O" Marker reflection represents a series of thin oolitic to skeletal and sandy limestone beds that occur in the upper part of the Missisauga Formation (Figure 4.2; Wade and MacLean 1990). This reflection is an excellent regional seismic marker horizon that is often used to map the top of the Missisauga formation (Figure 4.6). This strong reflector parallels the trend of the formation top but ends abruptly just seaward of the North Sable High (Figure 4.2).

Verrill Canyon Formation (Middle Jurassic – Early Cretaceous)

As mentioned in the previous sections, there are no distinctive seismic reflections in the distal, deepwater Verrill Canyon Formation shales that form the central basin time-equivalent of the Mic Mac and Missisauga formations. Its occurrence is interpreted where gradual weakening of the discontinuous, semi-parallel reflectors, within the distal parts of the Missisauga Formation, are observed and give way to a zone with no coherent

or continuous reflectors (Figure 4.9). Interpretation is aided by dip domain maps from sparse coherent reflectors within the formation to correlate with the tops of the concurrent Mic Mac and Missisauga formations (Figure 4.7).

Beneath the abyssal plain, the formation is characterized by a sequence of strong parallel to sub-parallel reflectors interpreted as shales with interbedded siltstones and sandstones (Figure 4.9). The stacked reflectors are undeformed and are approximately 6 km thick.

Logan Canyon Formation (Early – Late Cretaceous)

On the shelf, the seismic response from the interbedded coarse clastics and shales of the Logan Canyon Formation is characterized as a series of sub-parallel, fairly continuous reflections that lose their strength seaward towards the Sable Subbasin (Figure 4.6). The formation is fairly flat-lying across the Abenaki Graben and over the North Sable High, and dips from a depth of 2 to 3 km at the point of the modern day shelf break (Figure 4.2). The formation continues into the Sable Subbasin where it onlaps onto the major salt canopies (Figure 4.2). The seismic characteristics of the formation remain fairly consistent as it transitions into the distal equivalent Shortland shales indicating interbedded coarse clastics within the formation (Figure 4.9).

Dawson Canyon and Wyandot Formations (Late Cretaceous)

The top of the Dawson Canyon Formation appears on seismic profiles as a relatively strong and clean reflection (Figure 4.6). Below this event is a zone of weak but continuous reflectors that thin and downlap to the south onto the Petrel Member reflection. The Petrel Member limestone generates a strong regional marker over the

shelf (Figure 4.2). The seismic expression varies in thickness and deteriorates as the limestone interval thins, though broadens into two reflectors where the Petrel Member is thickest (Figure 4.2).

Also of Late Cretaceous age is the Wyandot Formation, which was deposited conformably above the Dawson Canyon Formation. The Wyandot marine marls and chalky mudstones appear on seismic profiles as several strong events but more commonly produces one strong and clean reflection throughout the section (Figure 4.6).

Banquereau Formation (Late Cretaceous – Present)

The mudstones, sandstones and thin chalks of the Banquereau Formation are represented on seismic by very strong, continuous reflection packages (Figure 4.6). The packages represent an overall seaward progradational event (Figure 4.2). As most of the salt-related evolution of the margin ceased during this time, this portion of the seismic is not discussed in detail in this thesis.

4.4 Salt and fault structures

Most of the salt and fault structures observed in ION-GXT Line 1800 that evolved since the Middle Jurassic are no longer active and were terminated by prograding sedimentation during the Tertiary. Presently, minor faulting indicates salt deformation is active but restricted to the deepwater areas above the allochthonous salt tongue. The following section describes the division of the observed salt and fault structures into autochthonous and allochthonous structures. Labelled salt structures are presented in Figures 4.10 and 4.11.

4.4.1 Autochthonous salt

The autochthonous salt structures refer to those features that developed within the Abenaki Graben and Sable Subbasin, as well as over the North Sable High that separates the two subbasins. The obvious lack of salt structures in the autochthonous salt basin, particularly in the younger strata, indicates a very efficient seaward evacuation of salt during the early post-rift stage that eventually fed the allochthonous salt tongue canopy system.

Abenaki Graben

Within the Abenaki Graben, sediments were downbuilding onto the original salt layer and after complete salt evacuation finally were welded to the salt basin floor. The sediments thicken into the deepest portion of the seaward basin (Figure 4.10). Remnants of the initial salt deposits in the Abenaki Graben include numerous salt pillows as well as a small 1.5 km high reactive diapir (D1) that is located in the center of the sub-basin (Figure 4.10). Crestal faulting occurs in the Tertiary Banquereau strata indicating the diapir fall throughout the Mesozoic and into the Cenozoic.

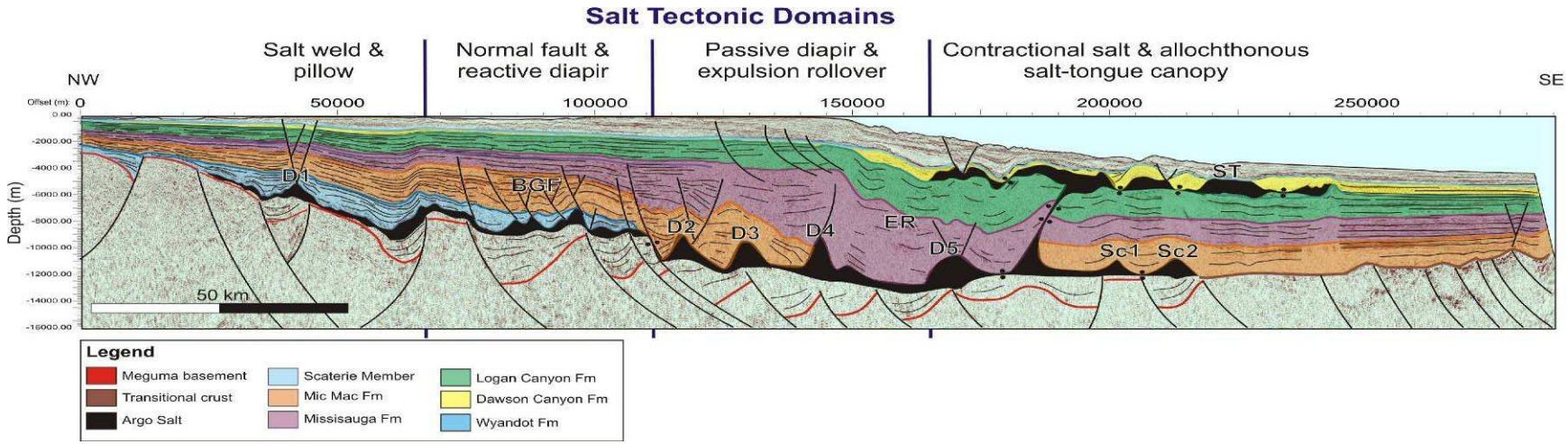

Figure 4.10 ION-GXT Line 1800 with major structural features including diapirs (D), basinward dipping growth faults (BGF), expulsion rollovers (ER), and a salt tongue (ST). The section has also been divided into 4 distinct salt tectonic domains based on the present day structures.

North Sable High

The North Sable High is dominated by a basinward-dipping listric growth fault system (BGF) that developed mainly in the Late Jurassic (Mic Mac Formation, Figure 4.10). The faults are spaced approximately 7 km apart and appear to have ceased activity by Early Missisauga time likely due to welding of the overlying strata to the Meguma basement and Eurydice red beds. Landward-dipping reflectors indicate rotation of the overlying strata. Reactive diapirs (e.g. salt rollers) are observed over the high as salt was trapped within the foot walls of the listric faults.

Sable Subbasin

A large, regional expulsion rollover (ER) within the Sable Subbasin is manifested by the growth strata in the Late Jurassic MicMac, Early Cretaceous Missisauga, and Early Cretaceous Logan Canyon formations (Figure 4.10). Growth strata of the rollover anticline are welded to the underlying basin floor, and buried at the base of the structure are trapped reactive diapirs. The triangular-shaped diapirs (D2, D3, D4, and D5) are all approximately 3 km thick (Figure 4.10). Crestal faults above the D2, D4 and D5 diapirs extend into the Early Cretaceous Missisauga Formation and indicate salt deformation occurred in these diapirs ceased by that time (Figure 4.10). Seaward of diapir D5 is a large feeder and allochthonous salt tongue with associated late salt deformation and mini basin formation on the secondary salt level. Vertical welding of the feeder system and the steeply dipping onlap structures of the Cretaceous Mississauga overburden indicates the feeder was likely formed by late-stage contraction. Two 2 km thick salt walls, forming the core of detachment folds Sc1 and Sc2, occur seaward of the feeder. Folded overlying Late Jurassic and Early Cretaceous sediments indicate the timing of the salt-cored fold

structures (Figure 4.10). Aggrading deepwater pelagic sediments following Early Cretaceous deposition caused the structures to shutdown during Logan Canyon time (Figure 4.10). The aggrading deepwater succession prevented the salt from evacuating out of the distal termination of the autochthonous basin.

4.4.2 Allochthonous salt

The main allochthonous salt feature that occurs in ION-GXT Line 1800 is an extensive salt tongue (ST, Fig. 4.10). The salt tongue (ST) extends approximately 70 km along the line and ranges in thickness from 2 km to 0 km where Tertiary welding occurred at the allochthonous salt tongue level. This feature is part of the Salt Province III canopy system and is imaged clearly in Line 1800 (Figure 4.11). Further evidence for the extent of the canopy system can also be found in public seismic lines to the east and west of Line 1800, but their resolution is greatly reduced (Appendix B). The high velocity contrast between the shallow salt tongue, its shallow position and the salt's transparent seismic signature together permit grater resolution of underlying strata and make interpretation much easier than the deeper salt structures in the central Sable Subbasin (Figure 4.2; Figure 4.9). The tongue on Line 1800 has spread both landward and basinward from the main feeder system. The landward canopy could also have originated from suturing of salt tongues fed from other diapirs out of the line of section. The base of the salt tongue overlies the Early Cretaceous Logan Canyon Formation, indicating that spreading of the tongue in the Early Cretaceous occurred as a marine transgression reduced sedimentation in the area.

Numerous salt and salt-related fault structures can be observed at the secondary salt level in the overlying Late Cretaceous Dawson Canyon Formation throughout the

extent of the salt tongue. Minibasins are frequent and appear to have been the main depositional structures that formed during the spreading of the salt canopies. In some instances, the minibasins later developed into turtle structures after welding in the canopy center. This is evident from fanning reflection packages that thicken and roll into the salt. These turtle structures are observed above the tongue where rolling of strata occurred both landward and basinward as salt expelled (Figure. 4.11).

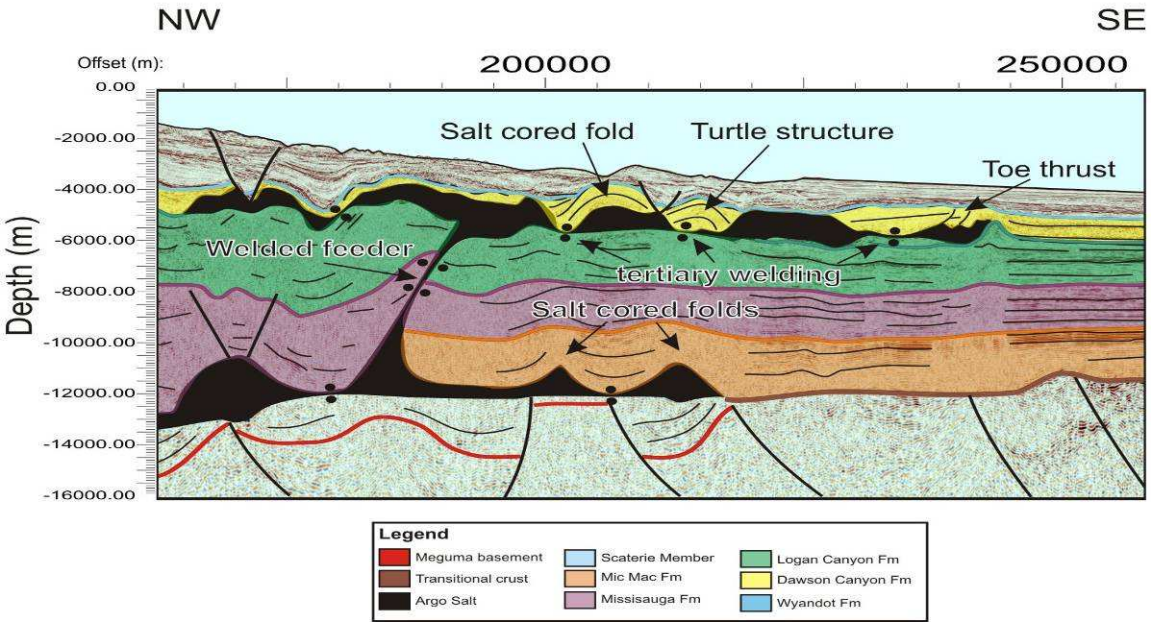

Figure 4.11 Labelled deepwater salt structures observed in Line 1800.

Sediment loading and downbuilding of minibasins lead to welding along the base of the salt tongue (Figure 4.11). Between the welded minibasins, remnant salt pillows and diapirs became trapped. Crestal faulting occurs above some salt pillows extending into Tertiary Banquereau strata (Figure 4.11), and in some instances, can be observed extending to the seafloor, indicating minor salt deformation is ongoing (Figure 4.11). This active deformation indicates salt mobilization out of plane of section, as the salt appears trapped by welding landward and seaward along the line.

Contraction observed at the seaward limit of the salt tongue has been accommodated by buckle folding of the overlying Late Cretaceous Dawson Canyon Formation. The wavelength of these folds is approximately 1 km, with an amplitude of approximately 0.5 km. The folds are preserved as the Tertiary Banquereau sediments blanketed and effectively shut down salt mobilization on the canopy.

4.5 Kinematic segmentation of salt structures

The differing salt structure styles observed in the seismic sections across the Abenaki Graben and central Sable Subbasin area can be divided into four major kinematic salt tectonic domains from the shelf to deepwater abyssal plain (Figure 4.10):

1. Salt weld and pillow domain;
2. Normal fault and reactive diapir domain;
3. Passive diapir and expulsion rollover domain;
4. Contractional salt and allochthonous salt tongue-canopy domain.

Salt weld and pillow domain

In the seismic data, the salt weld and pillow domain encompass the Abenaki Graben (Figure 4.10). It extends approximately 50 km from the hinge zone to the basinward limit of the Abenaki Graben in Line 1800. The domain is characterized by small salt pillows and remnant salt in the Abenaki Graben. Major deformation of Early to Middle Jurassic successions above the salt structures indicate the structures of this domain developed in the early post-rift stage of the basin evolution as sediment downbuilding and seaward salt withdrawal occurred.

Normal fault and reactive diapir domain

The normal fault and reactive diapir domain is located above the NSH and separates the Abenaki and Sable Subbasins and associated salt structures (Figure 4.10). The domain is characterized by triangular, reactive salt diapirs trapped in the footwalls of basinward-dipping normal faults across the 50 km extent of the NSH. The salt structures primarily developed during the Lower to Middle Jurassic with minor deformation occurring early in the Lower Cretaceous as deformation over the NSH ceased.

Passive diapir and expulsion rollover domain

The passive diapir and expulsion rollover domain occurs within the Sable Subbasin and extends 75 km from the landward limit of the basin to the basin floor step within the central Sable Subbasin (Figure 4.10). The domain is characterized by several extensional diapirs and a large expulsion rollover system. Deformation of Middle Jurassic to Upper Cretaceous sediment packages indicates the long lived evolution of the rollover system as sediments prograded and downbuilt onto the landward limit of an inflated salt massif.

Contractional salt and allochthonous salt tongue-canopy domain

In Line 1800, the allochthonous salt tongue-canopy domain consists of an extensive, approximately 80 km long salt tongue-canopy system that extends more than 25 km seaward of the original salt basin (Figure 4.10). As previously discussed in Section 4.4.2, vertical welds of the original feeder system and steeply dipping onlap structures of Cretaceous Mississauga sediments indicate that the feeder was likely squeezed by late-stage contraction. This contraction would have aided in evacuating salt

onto the seafloor and thus further feeding the spreading canopy system. Interpretation of the deepwater seismic reflection pattern indicates that the salt tongue system has spread over Lower Cretaceous sediments, with major deformation occurring in the Upper Cretaceous. Minibasins and turtle structures occur above the extensive salt tongues.

4.6 Depocentre Evolution

Depositional patterns of the Abenaki Graben and central Sable Subbasin areas were highly influenced by salt mobilization and salt withdrawal. The main depocentres of each formation were inferred from thickness variations within interpreted seismic data (Figure 4.12). With this interpretation, the depocentre evolution can be divided into three major phases, including: 1) Early post-rift basin formation, 2) Intermediate post-rift (early-drift) basin formation, and 3) Late post-rift (drift) basin formation.

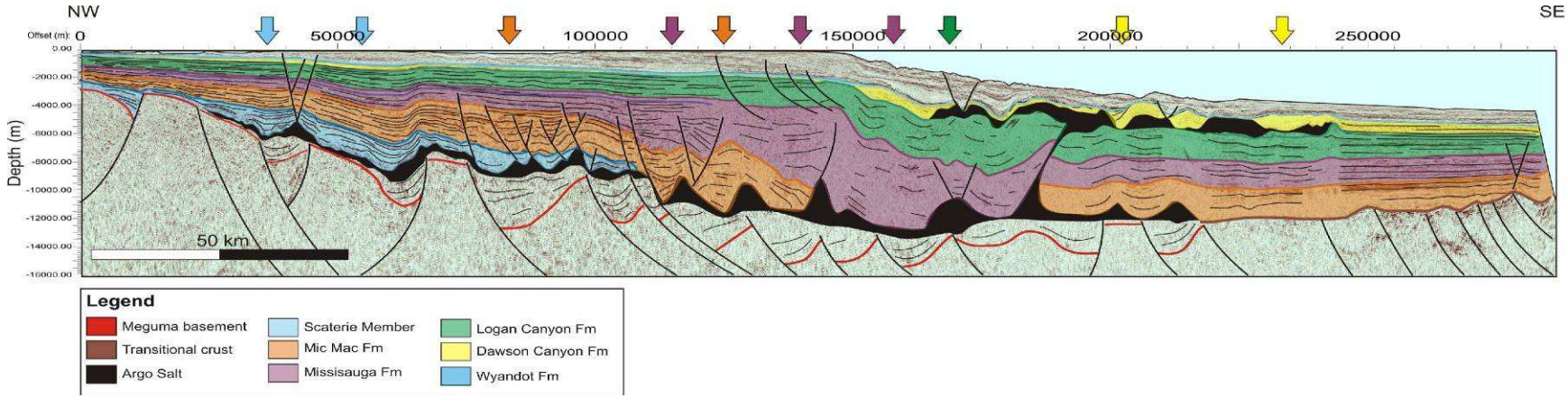

Figure 4.12 ION-GXT Line 1800 with arrows marking the main depocentres for each of the formations.

Early post-rift basin formation (Early - Middle Jurassic)

Deposition of the Early Jurassic Mohican sediments and Middle Jurassic Scaterie Member carbonates into the proximal Abenaki Graben marks the initial post-rift sediment pulse into the salt basin. The distribution of the sediments indicates widespread deposition extending from the shelf approximately 100 km seaward across the hinge zone into the Abenaki Graben and onto the North Sable High (NSH). The wide deposition indicates the North Sable High did not block sediment transport during this time (Figure 4.12). The sediment fill is thickest (~2 km) within the Abenaki Graben indicating it was a major basin depocentre in the Early-Middle Jurassic (Figure 4.12). Loading of these sediments caused initial salt withdrawal in the Abenaki Graben that in turn created more accommodation space in the subbasin and controlled subsequent sediment deposition.

Intermediate post-rift basin formation (Middle Jurassic – Early Cretaceous)

Sediments of the Mic Mac Formation indicate continuous deposition in the Abenaki Graben and over the North Sable High during the Middle – Late Cretaceous (Figure 4.12). The Mic Mac thickens across the hinge zone into the proximal Sable Subbasin reflecting the first major sediment progradation phase of the Sable delta (Figure 4.12). The Sable Subbasin was the main depocentre and the formation thickens from approximately 0.5 km over the hinge to approximately 6 km in the basin center (Figure 4.12). Interpretation of ION-GXT Line 1800 indicates the thick Middle Jurassic to Early Cretaceous sediment package in the basin was deposited along the subsiding flanks of seaward-translating diapirs. Thus, during the later stages of Mic Mac deposition and delta progradation, increased sediment input in the Sable Subbasin eventually loaded and

evacuated the salt in the proximal parts of the basin. Salt withdrawal and basinward inflation likely controlled sediment deposition.

In the Missisauga Formation, the same progradational trend continues as sediments were deposited across the Abenaki Graben and North Sable High, and then into the Sable Subbasin (Figure 4.12). With ongoing sediment progradation, a depocentre shift of approximately 30 km basinward occurred as sediments were deposited outboard of the proximal Sable Subbasin into the central portion of the basin. As with the Mic Mac, the Missisauga continually thickens from 0.5 km thick in the hinge area to 7 km in the central Sable Subbasin making this the regional depocentre during the Late Jurassic to Early Cretaceous (Figure 4.12). Mississauga sediments subsequently welded to the Sable Subbasin floor in the central basin.

Late post-rift basin formation (Early Cretaceous – Late Cretaceous)

From the Early to Late Cretaceous, the onset of a marine transgression led to a reduction of sediment input into the distal basin. The deposition of the Logan Canyon Formation marked the beginning of the late post-rift stage of basin formation for the area (Figure 4.12). Deposition during this time occurred mostly within the Sable Subbasin just seaward of the earlier Missisauga Formation depocentre (Figure 4.12). Within the subbasin depocentre, the Logan Canyon reaches a maximum thickness of approximately 4 km (Figure 4.12). The slight seaward shift of the depocentre at this time, despite the onset of a transgression, is most likely due to salt withdrawal and expulsion that lead in truth to the emplacement of the extensive salt tongue canopy system observed within the seismic profiles (Figure 4.12).

Following deposition of the Logan Canyon, sediments of the Late Cretaceous Dawson Canyon Formation thinly drape over the salt tongue canopy system. Deposition of this formation mainly occurs in this part of the Sable Subbasin as loading over the tongue created various mini-basins that trapped sediments as salt extruded basinward (Figure 4.12).

4.7 Regional variations of basement architecture

Variable rifting processes along the margin has resulted in variations of the rift basin geometry along the strike of the Scotian Margin including the Abenaki Graben and central Sable Subbasin. These observed variations in the basement architecture are aided by work completed by Cribb (*in prep.*) on ION-GXT Line 2000 and MacDonald (*in prep.*) on Line 1600, as well as previously completed basement maps from Tari *et al.* (2003), Olsen (1977) and the GSC Mirage Database (Figure 4.13).

Abenaki Graben

Seismic data, as well as sediment thickness maps of the Scotian margin, indicate that the Abenaki Graben is characterised by an overall lenticular shape as it pinches out southwest and northeast of ION-GXT line 1800 (Figure 4.13). The sub-basin extends approximately 210 km along strike, and appears to represent a landward-tapering wedge shape as interpreted in Line 1800. The sub-basin is limited by the Canso Ridge to the northwest and the North Sable High to the southeast (Figure 4.13).

North Sable High

The major basement high (North Sable High), which marks the distal edge of the Abenaki Graben, is a prominent basement feature consisting of a symmetric horst block with smaller asymmetric horst blocks along the strike of the margin in the study area (Figure 4.13). The landward limit of the high follows the general trend of the curved distal limit of the Abenaki Graben. The high appears to be less pronounced and eventually absent in the southwest and northeast ION-GXT dip lines 1600 & 2000 (Cribb in *prep.*, MacDonald *in prep*.; Figure 4.13). This occurs as the asymmetric horst blocks become less pronounced to the southwest and northeast of Line 1800.

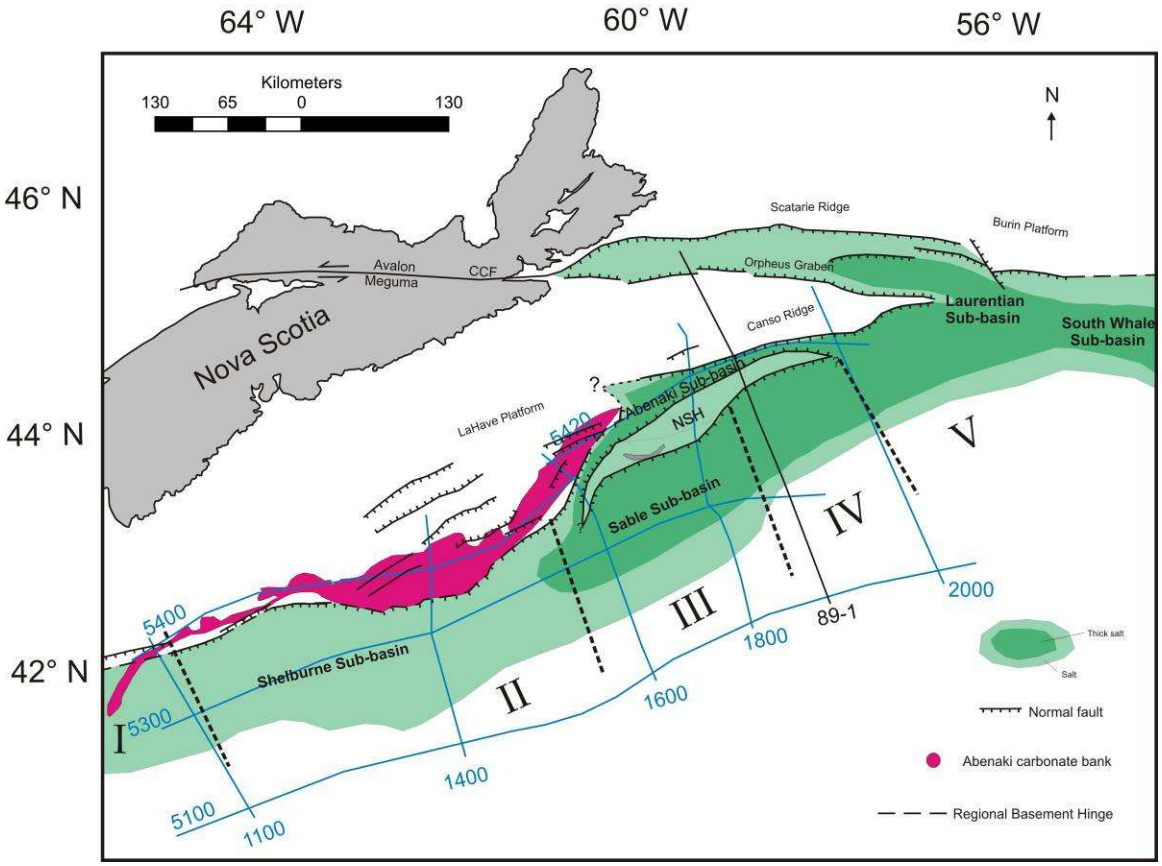

Figure 4.13 Map of the Scotian margin indicating the interpreted position of the original Early Jurassic salt basin including major structural elements.

Sable Subbasin

The Sable Subbasin is much larger and broader than the restricted Abenaki Graben (Figure 4.13). In the seismic section, the basin architecture is often difficult to interpret due to acoustic shadowing caused by the extensive salt tongue canopy system. However, sediment thickness maps of the area seem to indicate a fairly consistent shape across the study area filled with 12 – 14 km of sediment (Figure 4.1; Figure 4.13).

4.8 Derived analogue model constraints

Regional interpretation of the geological and geophysical data of the Abenaki Graben and central Sable Subbasin provided the constraints for the setup and parameters of analogue experiments simulating the basin evolution of the study area. Key parameters for the experiment setup and run are salt basin floor morphology, sediment input and original salt thickness. Where seismic and other geological data coverage is limited, the derived concepts from previous analogue experiments are used to aid interpretation of the basin evolution. The following section describes the major constraints derived for the setup and construction of scaled analogue experiments simulating the post-rift evolution of the salt structures and first-order depositional features of the central Sable Subbasin.

4.8.1 Original salt basin floor geometry and salt thickness

Seismic interpretation of ION-GXT Line 1800 infers an approximately 220 km wide autochthonous salt basin stretching from the hinge zone across the Abenaki Graben to the distal edge of the Sable Subbasin. Complexities within the architecture of the original salt basin are reflected by the configuration of underlying horsts and grabens with varying syn-rift fill. For experiment constraints, the first-order salt basin architecture is

represented by a landward-thinning wedge representing the Abenaki Graben followed by an intermediate high and a symmetric basin with a further seaward basement step representing the Sable Subbasin (Figure 4.14). The intermediate high represents the North Sable High (Wade and MacLean 1990). Although difficult to view in seismic due to acoustic shadowing by the salt tongue, the basement step is inferred from the location of the feeder of the allochthonous tongue canopy system. Modelling concepts developed by Campbell (2007) and MacDonald (2007) as well as modelling results from Ge et al. (1997) indicate that initial salt flow will be restricted across the basement step causing mid basin salt inflation. Distal aggradation will effectively pin the inflated salt until it actively pierces the crest and flows passively.

After the definition of the initial salt basin architecture, assumptions of the thickness of the original salt layer were inferred. Within the Abenaki Graben, welded sediments in the deepest basin area were restored to a horizontal position indicating approximately 1.5 km of initial salt (Figure 4.15). The highly extensional regime consisting of numerous listric faults and reactive diapirs located over the North Sable High, is consistent with previous experiment results with initial thin ($\leq$ 0.5 km) salt (Campbell 2007; MacDonald 2007; Krezsek et al. 2007). In the Sable Subbasin, passive downbuilding structures such as salt withdrawal basins between diapirs occur as the overall sediment packages dip steeply seaward. The sediments represent a large, gradually basinward-dipping expulsion rollover that dips into the main feeder of the allochthonous tongue. Previous analogue experiments indicate that these structures are representative of a relatively thick (2 km) initial salt deposit (Campbell ibid; MacDonald ibid; Krezsek et al. ibid). The initial salt deposited over the basement step is interpreted to be approximately 1 km based on diapirs occurring above the basement step that also

indicate a passive system. Due to limitations of the strain monitoring system for the field of view in large-scale experiments, the initial salt basin length is reduced from 200 km to 80 km (80 cm) maintaining the ratio with the internal basin architecture.

Two experiment setups were implemented for this project based on seismic interpretation. The observed results from Experiment 1 show a prominent basinward-dipping expulsion rollover system across the North Sable High differing from the presence of a basinward dipping listric growth fault system interpreted in the ION-GXT Line 1800. Previous work by Campbell (2007) and MacDonald (2007) attribute these differing structural patterns to slight variances in salt thickness. Both structural styles are associated with thin salt (≤1.5 km) but differences associated between the experiment and natural prototype indicate a reduction in original salt over the intermediate high. Thus, for Experiment 2, the North Sable High is modified from 1 km thick to 1.5 km thick with 0.5 km of original salt in place of the high (Figure 4.14). The new experiment setup maintains the same geometry as Experiment 1 with slight modifications to the proximal half-graben representing the Abenaki Graben, which is now 15 cm long with the thickest portion of the graben reduced from 2 cm to 1.5 cm silicone to achieve results closer to those observed in the natural prototype. Improved interpretation of the North Sable High also showed the structure extended slightly further SE, as previously interpreted Scatarie sediments were reinterpreted as fanning syn-rift sediments (Figure 4.16).

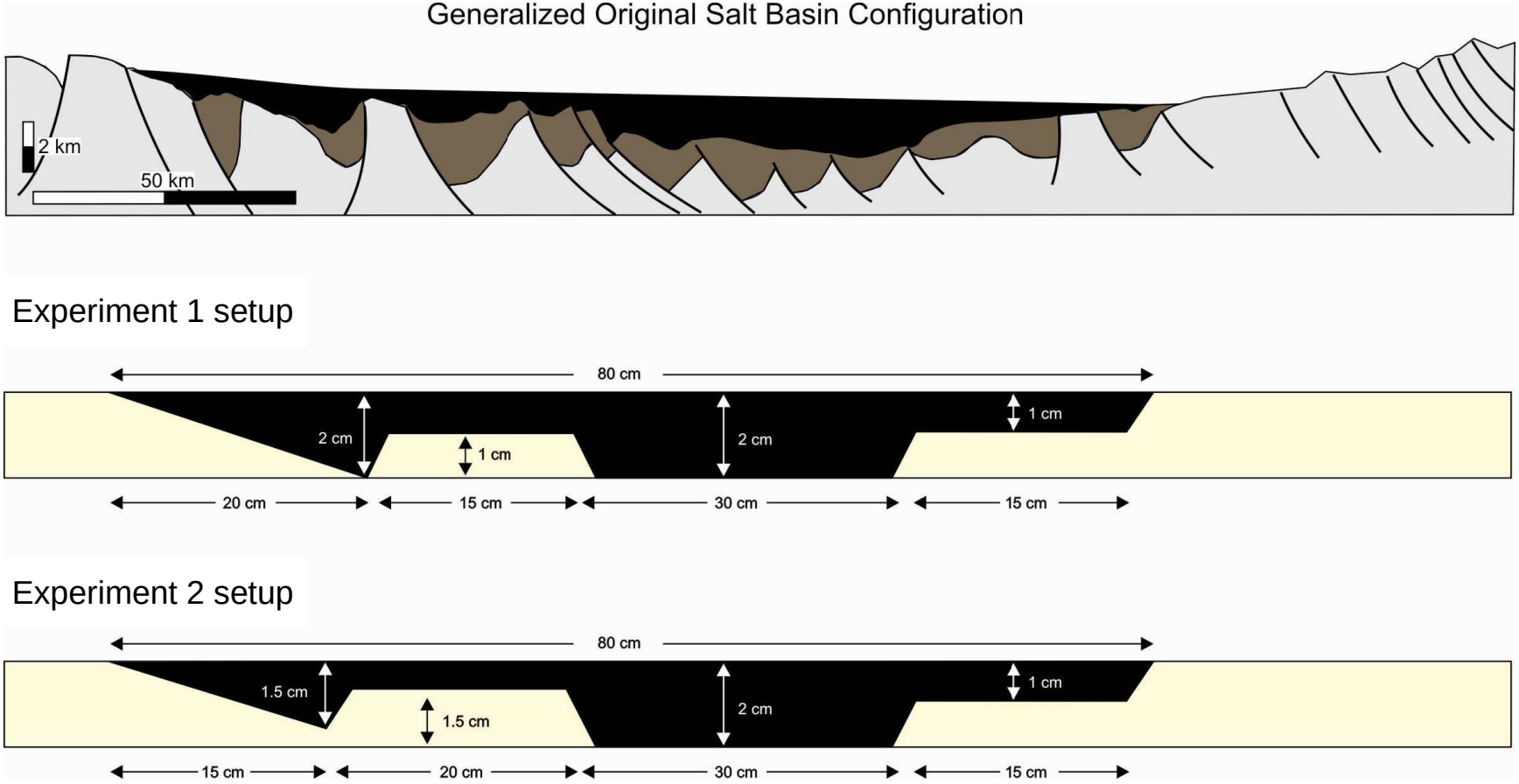

Figure 4.14 Generalized original salt basin configuration including potential physical experiment setups.

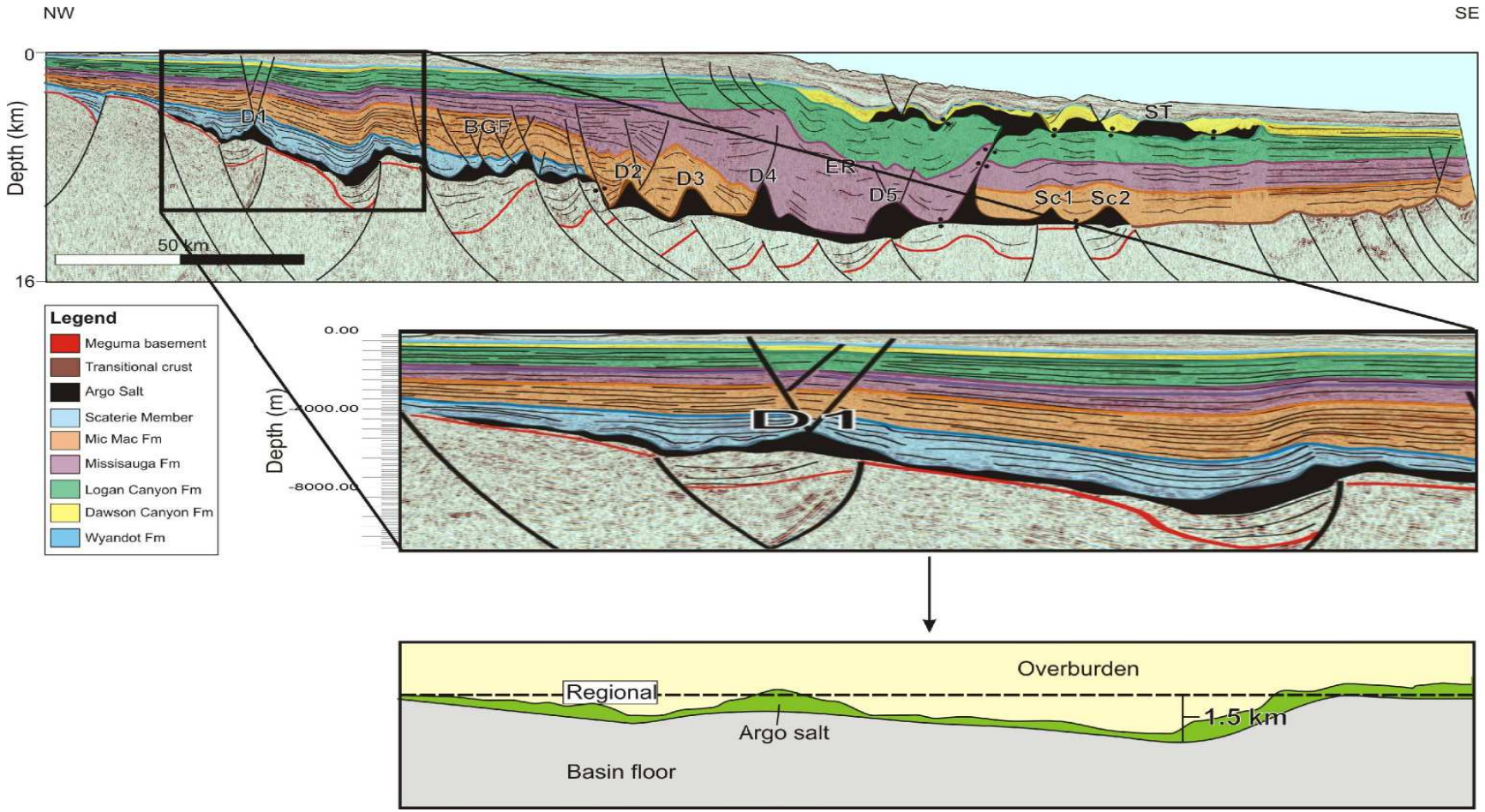

Figure 4.15 Restoration of downbuilt overburden sediments to approximate thickness of original salt within the Abenaki sub-basin.

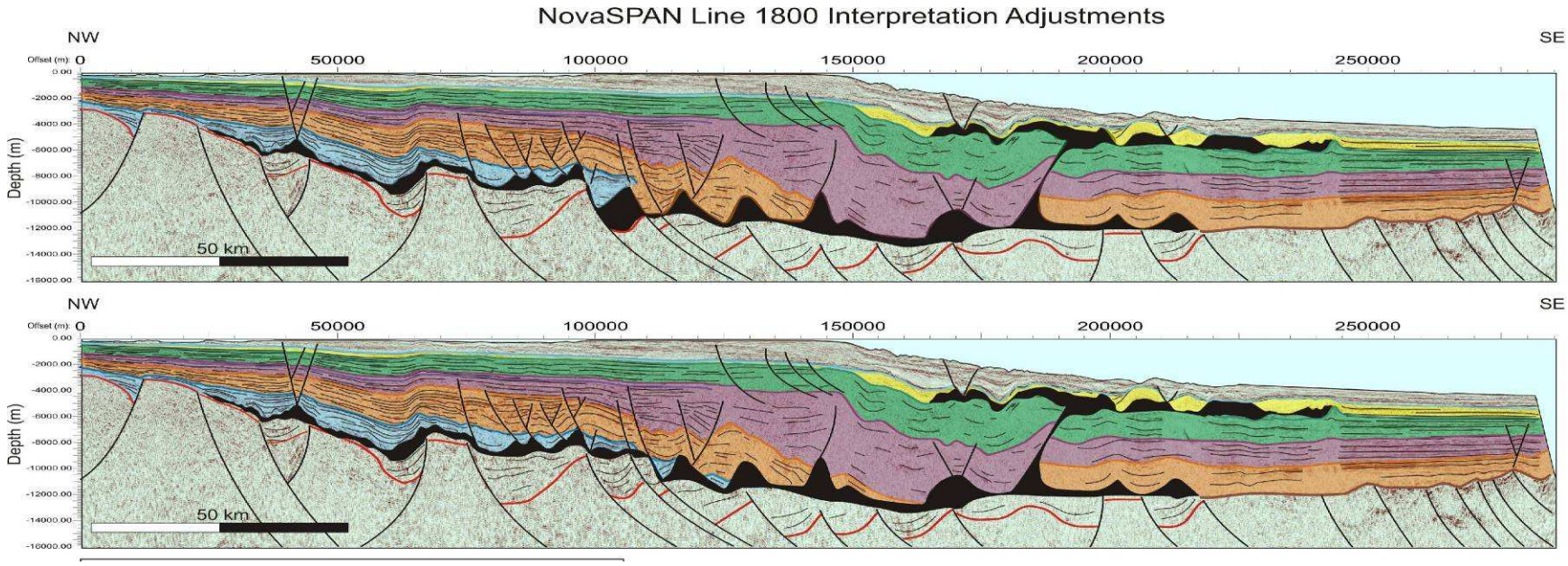

Figure 4.16 Interpretation adjustments to Line 1800 based on experiment results and improved basin interpretation.

4.8.2 Post-salt sediment input

Sedimentation rates for the study area were calculated from line 1800 based on the average thickness for each formation and their deepwater equivalents (Table 4.1). Compaction rates are factored into the calculation for the sediment input during deposition of each formation using curves for the average density of sedimentary units with increasing depth. Specifically, the average depth of each formation is calculated to estimate a percentage of compaction (Table 4.1). Without consideration of the compaction factor, the sediment input and sedimentation rates, especially for the early post-rift formations would be systematically underestimated. Once calculated, these averaged sedimentation rates represent five main depositional units for salt tectonics history of the area. These depositional units include the:

1) Scaterie/Mohican (Early Jurassic – Middle Jurassic);
2) Mic Mac (Middle Jurassic – Late Jurassic);
3) Missisauga (Early Cretaceous);
4) Logan Canyon (Early to Late Cretaceous);
5) Dawson Canyon (Late Cretaceous)

	Scatarie/Mohican	Mic Mac	Missisauga	Logan Canyon	Dawson Canyon
Time interval	25 Ma	16.4 Ma	23 Ma	28.4 Ma	19.2 Ma
Avg thickness	1025 m	1880 m	1980 m	1850 m	850 m
Avg sedimentation rate	40 m/Ma	115 m/Ma	86 m/Ma	65 m/Ma	45 m/Ma
Avg depth	7000 m	5500 m	4000 m	2600 m	2000 m
Avg density	2600 kg/m^3	2500 kg/m^3	2400 kg/m^3	2300 kg/m^3	2200 kg/m^3
Surface density	2150 kg/m^3	2150 kg/m^3	2150 kg/m^3	2150 kg/m^3	2150 kg/m^3
Decompaction factor	20%	15%	10%	7%	5%
Sed. Rate	50 m/Ma	130 m/Ma	95 m/Ma	70 m/Ma	50 m/Ma

Table 4.1 Derived decompacted sedimentation rates for each formation of the Abenaki and central Sable Subbasin area. Derived from ION-GXT Line 1800.

It is important to note that by simplifying the depositional history of the study area to the first-order parameters of the five depositional units, transitions and fluctuations induced by variations of supply and sea level within each formation are not considered. These depositional units also include their deepwater equivalents. However, these generalized sedimentation rates are viable as the purposes of the analog experiments are to understand the coupling between varying sedimentation patterns and rates with the overall salt-tectonic evolution of the basin.

Calculations from Line 1800 indicate a very low initial sediment input into the basin for the Scatarie/Mohican depositional unit from the Early – Middle Jurassic. The decompacted sedimentation rate for the area is calculated to be approximately 48 m/Ma. Sedimentation at this time appears to have been restricted to the Abenaki Graben and onto the North Sable High.

The major sediment input occurred during the deposition of the Mic Mac from the Middle – Late Jurassic. In the Scotian Basin, the Abenaki / North Sable High area became the main depositional region for the prograding Sable delta, and sedimentation rates would be greater underestimated. The decompacted sedimentation rate during this interval was calculated to have increased to approximately 130 m/Ma (Table 4.1). During this time, the major depocentre shifted into the Sable Subbasin with upwards of 4,000 m of sediments deposited. This progradation continued into the Early Cretaceous with the deposition of the Missisauga Formation at a decompacted rate of approximately 95 m/Ma (Table 4.1).

From the Early – Late Cretaceous, a major marine transgression occurred causing a reduction in deltaic sedimentation and decrease in sedimentation in this area (Wade and MacLean 1990). At this time, the sedimentation rate decreased during deposition of the

Logan Canyon Formation (70 m/Ma), and the Dawson Canyon Formation (45 m/Ma, Table 4.1).

Chapter 5: 4D Abenaki Graben and Central Sable Subbasin Physical Experiments

5.1 Analogue modeling overview

Analogue experiments are an effective and useful method to investigate salt tectonic processes through lab-scaled experiments. Analogue experiments use sand to represent brittle sedimentary overburden and silicone rubbers for salt. Over the past two decades, analogue modeling studies have greatly improved our understanding of passive margin salt tectonics (eg. Jackson and Talbot 1986; Cobbold et al. 1989; Talbot 1992; Jackson and Talbot 1994; Koyi et al. 1995; Ge et al. 1997; Vendeville 2005). Despite these advances, very few studies have addressed basin-scale salt tectonic processes from the extensional shelf domain to the deep basin contractional domain (Vendeville 2005; Fort et al. 2004). Other experiments fail to include appropriate model time scales or sedimentation procedures to simulate realistically the sediment input of the natural prototype.

The Dalhousie Salt Dynamics Group has developed a new generation of physical experiments that address both basin-scale salt tectonic processes and include appropriate model time scales. The physical experiments are constrained by geological data and seismic interpretation results. Using these constraints, the experiments are able to include realistic variable sedimentation rates and depositional patterns to simulate the entire salt basin evolution from the early post-rift stage to the modern margin. Simulating the complete basin evolution from early to late stages allows for an investigation of how first order controls (i.e. salt basin morphology, sedimentation rates and patterns, salt thickness) influence tectono-stratigraphic passive margin evolution.

The 3D surface evolution and deformation of experiments is monitored by two high resolution, charge-coupled device cameras (CCD) with stereoscopic setup (Adam et

al. 2005; Figure 5.1). Time series images are analysed by Digital Image Correlation techniques (DIC) to enable the computation of the 3D displacement data with sub-millimetre accuracy and to fully quantify small and large-scale deformation in the experiment.

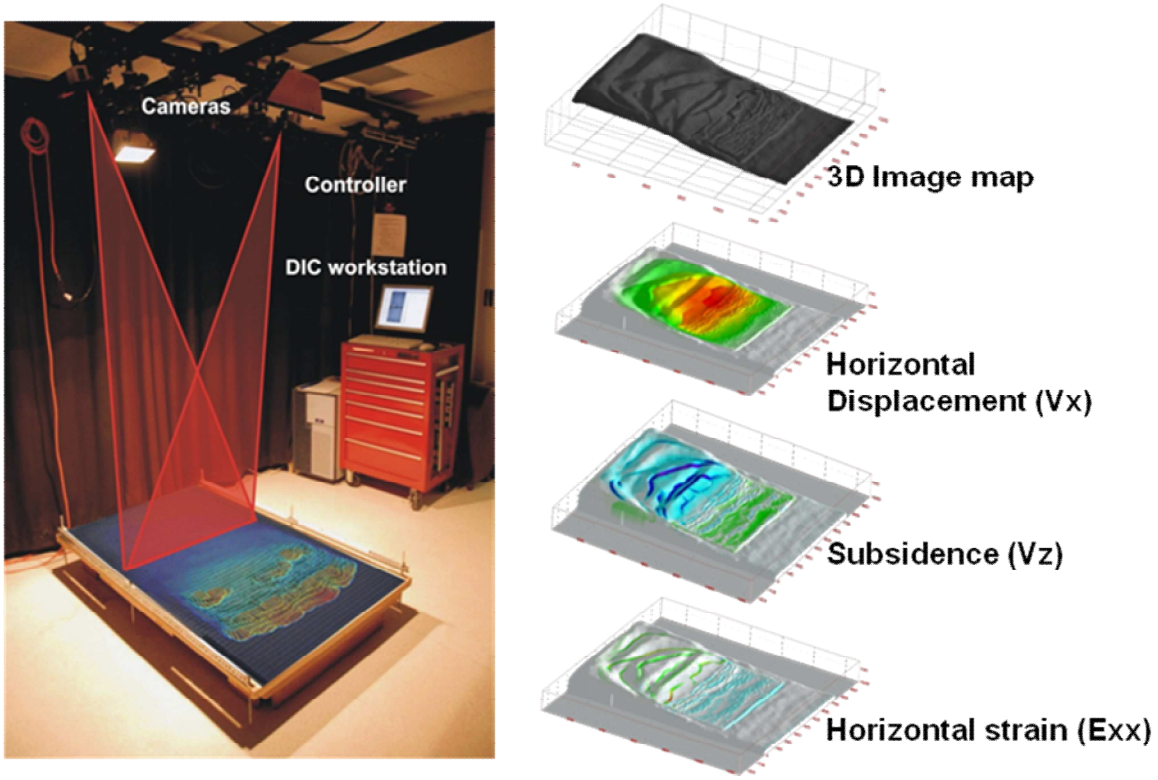

Figure 5.1 The experiment setup with stereoscopic DIC monitoring system including two high resolution CCD cameras. Derived displacement data is shown as a vector grid on experiment surface. To the right of the experiment are examples of 3D DIC experiment data including 3D surface image, horizontal strain, horizontal displacement, and vertical displacement data of early experiment stage (Adam et al., 2009)

5.2 Objectives of physical experiments for the study

The objective of the physical experiments in this study was to aid in understanding the linked salt tectonic evolution across the Abenaki Graben and central Sable Subbasin. The experiments were setup to simulate the first-order basin characteristics including basin architecture and sediment input. The experiments

investigate the relation of structures and depocentres, depocentre migration, as well as key stages in basin evolution. The results from these experiments provide mechanically constrained concepts for salt structure correlations and paleogeographic reconstructions for the Abenaki and central Sable Subbasin area.

By developing mechanically constrained templates to support structural interpretation and regional correlations, uncertainties can be reduced in understanding the basin evolution and may aid in current and future petroleum exploration efforts in the basin. Specifically, results from these experiments can be used to solve questions related to the evolution of the Abenaki Graben and central Sable Subbasin including:

1) The tectono-stratigraphic framework of the two subbasins.
2) The presence of the North Sable High and its role during the salt basin evolution.
3) The controls on the position and emplacement of the salt tongue-canopy system in salt Subprovince III (after Shimeld 2004).

5.3 Analogue materials and experiment scaling

For the analogue experiments, sifted silica sand and silicone rubber (Polydimethylsiloxane - PDMS) are used to simulate brittle deformation of sedimentary rocks and the viscous flow of salt sediments under gravitational loading respectively. For purposes of structural interpretation and stratigraphic correlation of completed experiment sections, alternating layers of coloured silica sand were used. Both the sifted silica sand and silicone elastomer materials have known material properties that are required to understand how each material scales to nature (Table 5.1).

Variables used in equations (1), (2), (3), (4)					
l_{model}	$l_{prototype}$	p_{model}	$p_{prototype}$	η_{model}	$\eta_{prototype}$
0.10 m	1000 m	1.6 g cm^{-3}	2.3 g cm^{-3}	1 x 10^{4} Pa s	2 x 10^{18} Pa s

Table 5.1 Values for variables used to calculate scaling factors.

Scaling for the experiments of the Dalhousie Salt Dynamics Group has been detailed in Krezsek *et al.* (2007) and Adam et al. (2008). Our experiments are scaled to allow for a qualitative as well as quantitative comparison of the model geometries, kinematics and dynamics to the natural prototype (Hubbert 1937; Ramberg 1981; Weijermars *et al.*1993; Brun 1999; Costa & Vendeville 2002).

The geometric scaling factor l^* for our models is 1 x 10^{-5} and is derived from similarities in cohesion, density of sand and sedimentary rocks as well as gravitational acceleration (Lallemand et al. 1994). From these calculations, 1 cm in the model represents 1 km in the natural prototype. In order to calculate the time scaling factor t^*, the stress ratio σ^* must first be calculated. The stress ratio σ^* is constrained by the geometric scaling factor l^*, the density ratio p^* and gravity ratio g^*. The density ratio p^* ($p_{model}/p_{prototype}$) is 0.7 while the gravity ratio g^* is 1 since gravitational acceleration is equal in both the model and the natural prototype. From these values, the stress ratio σ^* equals:

$$\begin{aligned} \sigma^* &= l^* \text{ x } p^* \text{ x } g^* \\ &= (l_{model}/l_{prototype}) \text{ x } (p_{model}/p_{prototype}) \\ &= 7 \text{ x } 10^{-6} \end{aligned} \qquad (5.1)$$

The next step in calculating the time scaling factor is to determine the strain ratio ε^*, which is calculated using the stress ratio σ^* and the viscosity ratio η^* ($\eta_{model}/\ \eta_{prototype}$). From these values, the strain ratio ε^* equals:

$$\varepsilon^* = \sigma^* / \eta^* = 1.4 \times 10^{9} \quad (5.2)$$

Since the time scaling factor t^* is inversely proportional to the strain ratio ε^*, the time scaling factor is:

$$t^* = 1/ \varepsilon^* \approx 7.2 \times 10^{-10} \quad (5.3)$$

This time scale describes the relation between a subaerial experiment and subaerial sedimentary wedge deforming by gravity spreading on a weak salt layer. However, a passive margin sedimentary wedge is submerged where the buttressing effect of the seawater on the submarine slope is creating a horizontal force opposing the differential gravitational forces further stabilising the sedimentary wedge (Gemmer et al. 2005). Numerical experiments of the Dalhousie Geodynamics Group comparing numerical models of passive margin sedimentary wedges deforming under subaerial and submerged conditions, have demonstrated that the affect of water load in a passive margin setting is slowing the evolution of the system by a factor of 2 (Dalhousie Geodynamics Group, pers. comm.). Since all our experiments are dry experiments, this factor must be calculated into the time scaling factor to account for water load, giving a new time scaling factor t^*_{new} equalling:

$$t^*_{new} = (7.2 \times 10^{-10})/2 = 3.6 \times 10^{-10} \quad (5.4)$$

With this new time scale factor, one hour in the experiments equals approximately 300 000 years in the natural prototype.

The density ratio between sand and silicone in the experiments is greater than that of the natural prototype, which leads to higher buoyancy forces in the silicone than expected in the salt sediments. However, this effect is mitigated by the realization that salt structures in passive margin, thin-skinned extensional systems develop passively due to overburden deformation rather than actively pushing through overburden driven by buoyancy forces (Vendeville & Jackson 1992). Additionally, Hudec et al. (2009) indicated that in systems with temporal migration of minibasin depocentres, differential loading, not density contrast, is the primary mechanism controlling subsidence.

5.4 Experimental procedures

The 3D analogue experiments were performed on a 120 cm x 90 cm horizontal rig (Figures 5.1, 5.2, and Figure 5.3). The basin margins and post-rift salt basin architecture is built using silica sand. Silicone putty is placed within the constructed basin and allowed to spread until a flat layer across the basin is achieved. Both the basin geometry and original salt thickness are constrained from seismic interpretation.

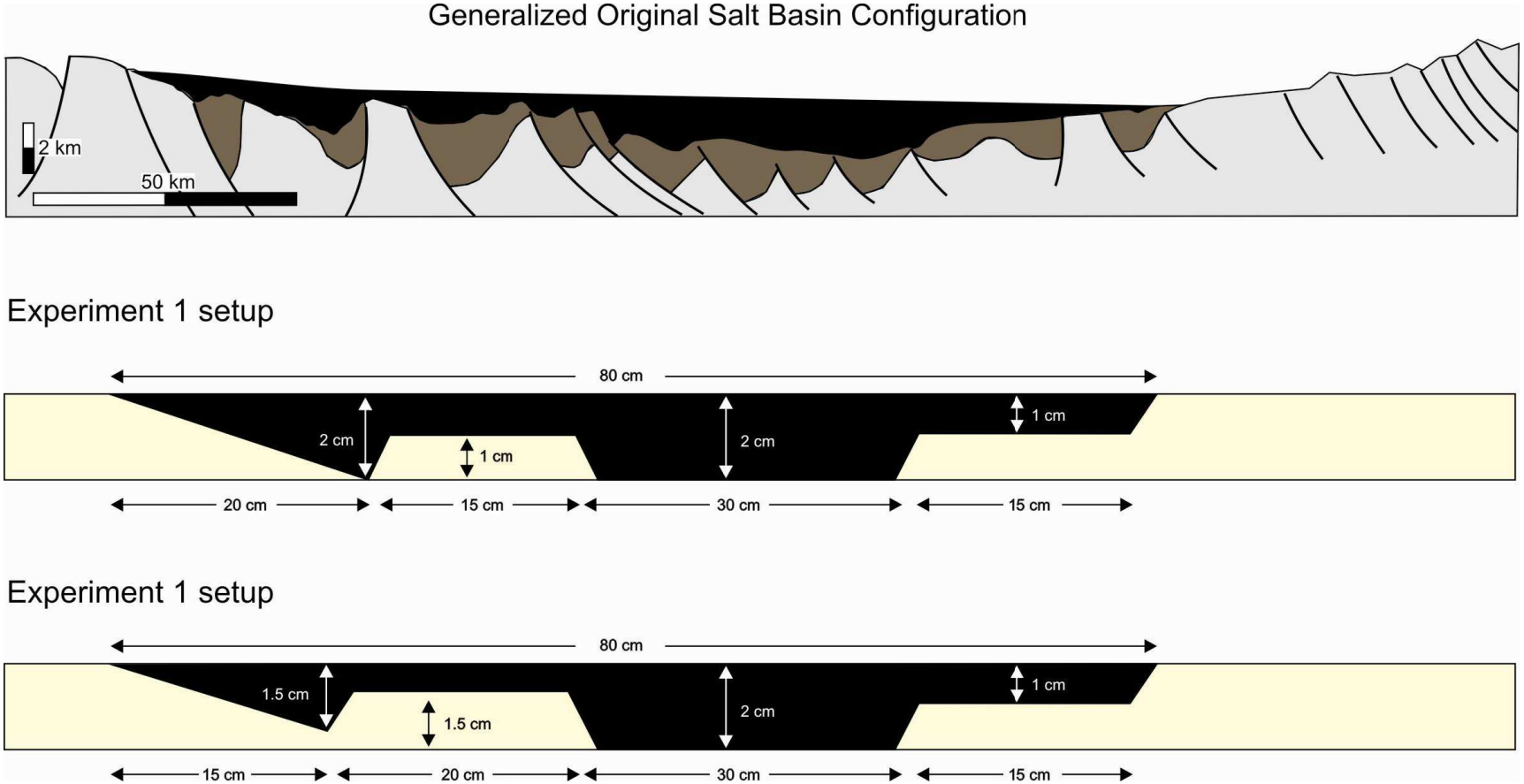

Figure 5.2 Salt basin geometry of the Abenaki and Central Sable basins deduced from ION-GXT Line 1800 and the derived experiment setups.

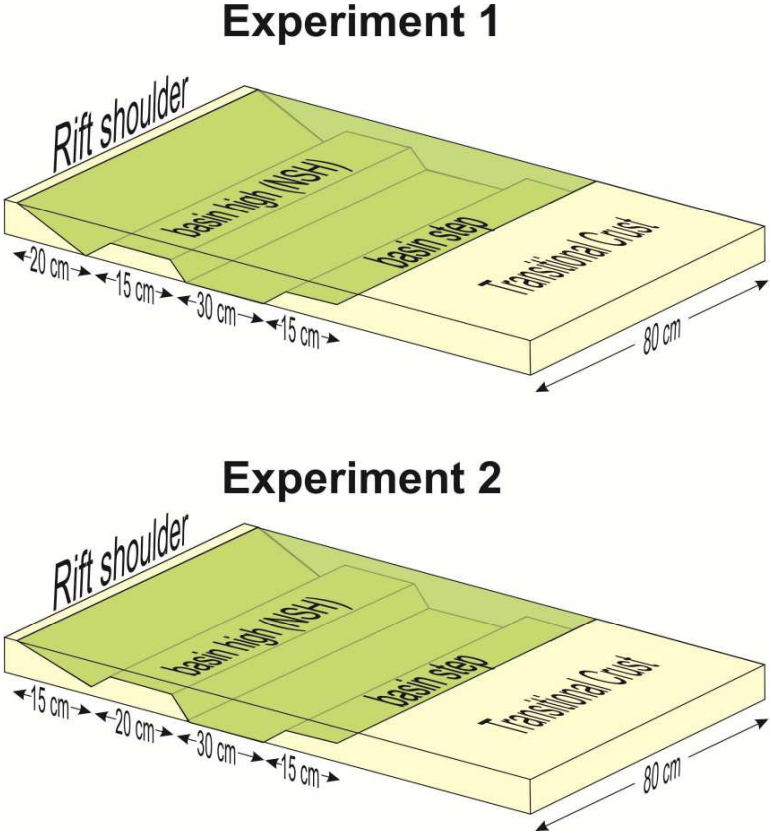

Figure 5.3 Geometry of experiments 1 and 2 deduced from ION-GXT Line 1800.

5.4.1 Sedimentation

During the experiments, sand layers are sieved manually onto the pre-experiment layer to simulate a passive margin sedimentary wedge aggrading and prograding over the post-rift salt basin (Figure 5.4). The sand layers are sieved at precisely defined time intervals with specific volumes and thicknesses scaled to the sedimentation rates and volumes of the natural prototype as deduced from the seismic and geological data. During sieving, a height adjustable rail guide system is used to ensure sand is distributed evenly across the wedge. The sieving procedure provides homogeneous mechanical conditions in the sand layer (Lohrmann et al. 2003; Adam et al. 2005) and also allows for interaction between the structural evolution of the model surface, sedimentation rates and

patterns (Adam et al. 2008). Sieving manually allows for topographic features to control the transportation of sediments from the shelf to the slope as is the case in the natural prototype.

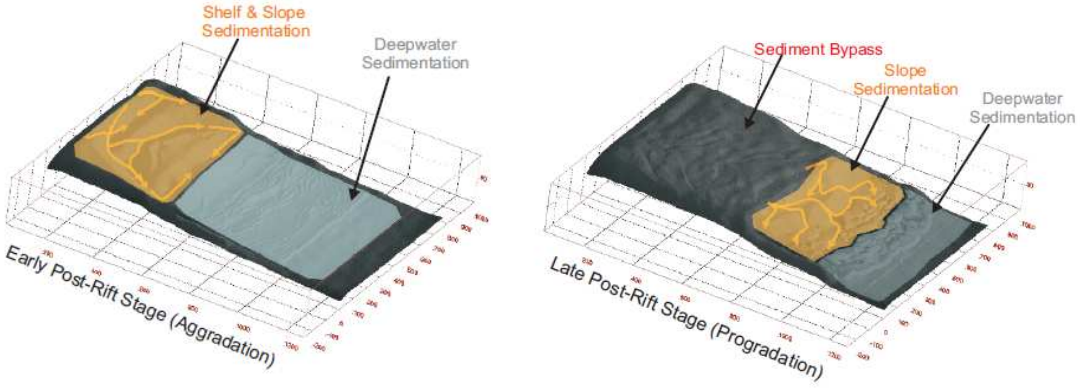

Figure 5.4 Sedimentation procedure for the 4D analogue experiments. During the early post-rift stage sediments are aggraded on the shelf to a height of 4 cm (4km). During the late post-rift stage sediments bypass the shelf and prograde onto the slope. Orange overlays indicate the highest sediment input and the arrows indicate sediment fairways defined by the dynamic topography of the experiment surface. Grey overlays indicate small amounts of deepwater pelagic sediment deposition.

The early aggradation phase of the experiments simulates the initial restricted sedimentation in the shelf area during the early post-rift relative sea level rise. Aggradation is simulated by building the shelf wedge to a predetermined total thickness of 4 cm through the incremental sieving of sand layers at four and eight hour intervals for the first six days (Figure 5.4; Table 5.2; Table 5.3). As silicone evacuates from the shelf area and sediments weld in the landward part of the basin, the progradation phase across the slope area of the experiment is initiated (Figure 5.4) and continued for the duration of the experiments (~14 days). The progradation phase simulates the basinward depocentre migration with little or no sedimentation occurring in the shelf as indicated by the seismic data.

				Seismic		Experiment		Abenaki and central Sable sub-basin		
Age (Ma)	Age			Formation	Duration	Hours	Days	Sed. rate	Model sed. Rate	
	CRETACEOUS	EARLY	Aptian	Logan Canyon Formation	7.2 Ma	240	10	50 m/Ma	1.5 mm/4h	Progradation
						236				
						232				
						228				
						224				
						220				
						216	9			
125			Barremian	Mississauga Formation	23 Ma	212		95 m/Ma	2.0 mm/4h	
						208				
						204				
			Hauterivian			200				
						196				
						192	8			
						188				
						184				
135			Valangian			180				
						176				
						172				
						168	7			
			Berriasian			164				
						160				
						156				
						152				
						148				
						144	6			
146						140				
						136				
	JURASSIC	LATE	Tithonian	Mic Mac / Abenaki Formation	17 Ma	132		130 m/Ma	2.5 mm/4h	
						128				
						124				
						120	5			
			Kimmerid.			116				
155						112				
						108				
						104				
			Oxfordian			100				Aggradation
						96	4			
						92				
						88				
161			Call/Bath.			84				
						80				
		MIDDLE	Bajocian	Mohican and Scatarie Formations	25 Ma	76		50 m/Ma	1.5 mm/8h	
						72	3			
						68				
						64				
			Alalenian			60				
						56				
						52				
						48	2			
176						44				
			Toarc			40				
						36				
						32				
						28				
		EARLY	Pliensbach			24	1			
						20				
						16				
						12				
			Sinem.			8				
						4				
195						0				

Table 5.2 Sedimentation rates for Experiment 1.

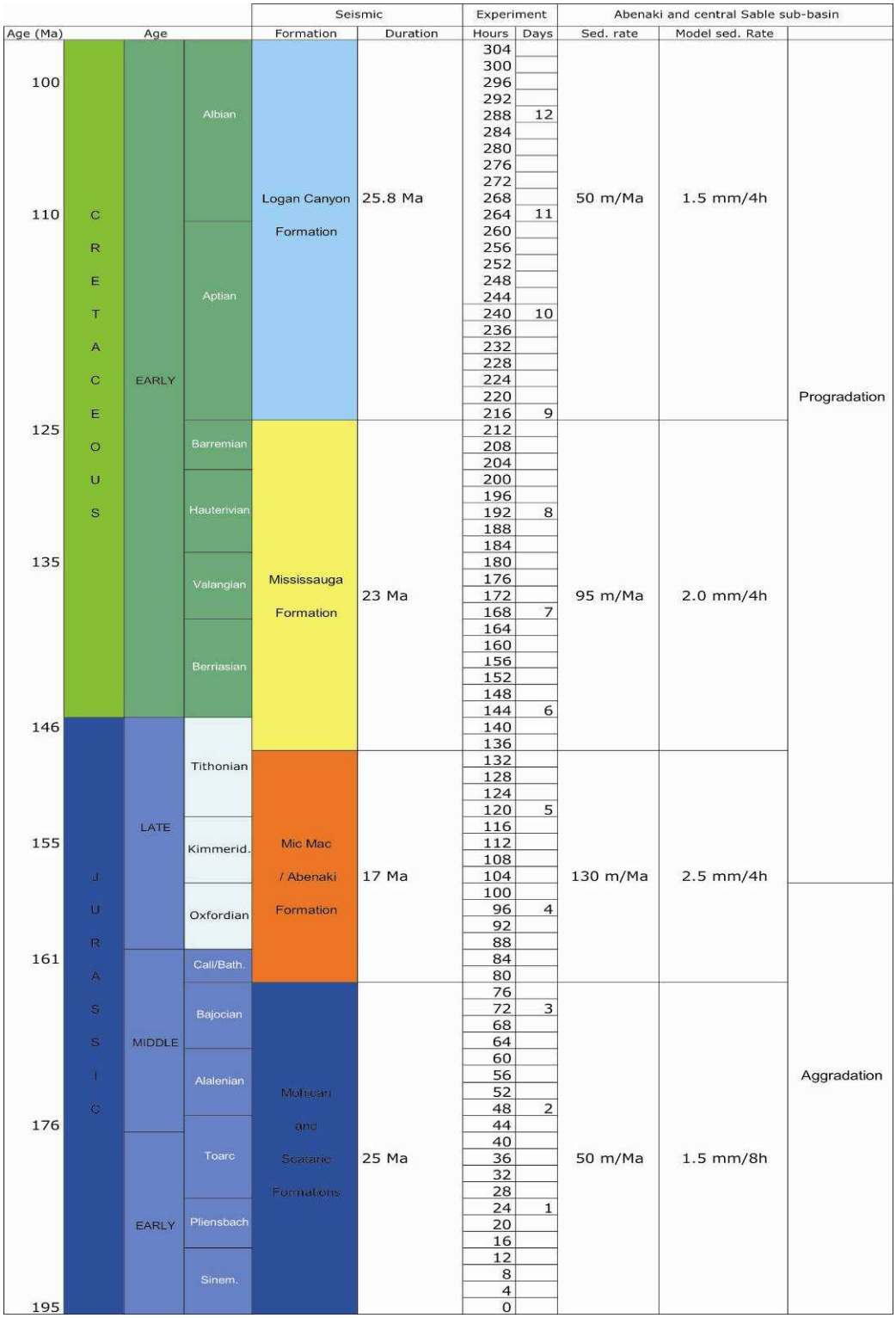

Table 5.3 Sedimentation rates for Experiment 2.

5.4.2 Optical Strain Monitoring

The incremental and total 3D surface deformation of each experiment was monitored using two computer controlled high-resolution charge-coupled device cameras (CCD) with stereoscopic setup (Figure 5.1). Stereo images of the experiment surface were taken at 10 minute intervals and processed, analysed and cross-correlated with Digital Image Correlation (DIC) software (Strain Master, LaVision©) adapted for analogue experiments by Adam et al. (2005). The software allows the incremental 3D displacement vector field to be calculated from successive images with sub-millimetre accuracy. The calculated 3D incremental displacement vector field allows for further experiment analysis including incremental and finite horizontal displacement (v_x), subsidence (v_z) and horizontal strain (e_{xx}). This high-resolution 3D displacement (DIC) data provides accurate information regarding fault kinematics, silicone mobilization, as well as coupled depositional systems during the basin evolution of scaled experiments. Salt tectonics concepts and basin interactions derived from the scaled experiments are used to better understand the mechanics, timing, and coupling of salt-tectonic processes in nature.

5.4.3 Experiment Sectioning

Upon the completion of each experiment, the table was covered with sand and sprayed with water to protect the experiment surface and essentially freeze it from further movement. The experiments were cut into cross sections at 5 cm spacing from shelf to slope (Figure 5.5). Each section is photographed using a high resolution digital camera and structurally interpreted to analyse the styles and lateral variations of silicone and fault structures as well as related depositional structures. Interpreted model cross-sections are

sequentially restored to better understand the structural evolution of the experiment using standard salt restoration techniques (Rowan 1993). The time-series data deduced from the DIC allows for constraints of surface heights, fault kinematics and silicone mobilization at each time step of the restoration.

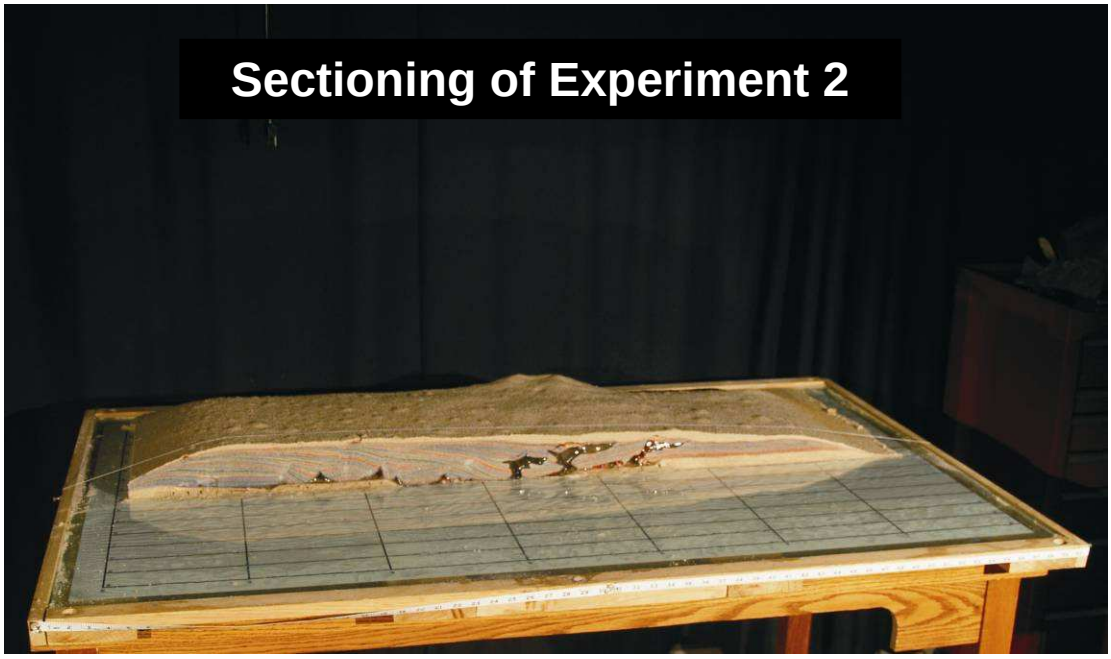

Figure 5.5 Sectioning of the completed experiment 2 on base plate.

5.5 4D Physical Experiment 1

To better understand the tectono-stratigraphic evolution of the Abenaki and central Sable region, Experiment 1 was setup and constrained by the interpretation of NovaSPAN Line 1800 as discussed earlier in Chapter 4 (Figure 5.3). This first physical experiment was developed to 1) test the influence of the salt basin geometry consisting of a landward tapering wedge, intermediate high and symmetric graben with basement step and 2) test the effects of sedimentation rates and patterns derived from preliminary interpretation of the seismic data on the basin's evolution.

5.5.1 Experiment 1 setup

The salt basin geometry of Experiment 1 consists of a proximal landward-tapering wedge, intermediate high and distal symmetric graben with basement step (Experiment 1; Figure 5.2; Figure 5.3). To accommodate the limits of the field of view from the stereoscopic setup, the basin configuration along with internal features was proportionally reduced in size In the experiments, the width and proportions of the salt basins are scaled with a length scaling factor of $l^*_{Salt\ Basin} = 0.4\text{x}10^5$ to fit within field of view of the DIC camera system. The sediment volumes for the experiments are scaled down accordingly to represent a comparable depositional input in relation to the salt basin volume. Downscaling of approx. 60% of horizontal dimensions is within range of geometric scaling factor ($l^* = 10^5$) and vertical geometric dimensions controlling stresses acting in the experiment remain unchanged. Vertical dimensions are not affected and are scaled with l^* to assure proper dynamic scaling of force, stress & strain rates in the experiment. This is acceptable because the experiment's role is to test the influence of prominent basin structures and not to specifically recreate the natural prototype basin.

From the interpretation of ION-GXT Line 1800, the proximal half-graben representing the Abenaki Graben is approximately 45 km long in nature but is reduced to 20 cm in the experiment corresponding to 20 km in reality. The intermediate high representing the North Sable High is approximately 40 km but is reduced to 15 cm in the experiment corresponding to 15 km in nature. The distal symmetric graben with a basement step representing the central Sable Subbasin is approximately 100 km wide with the step occurring approximately 70 km across the basin in reality but is reduced to 45 cm with the step occurring 30 cm across the basin. These new values correspond to 45 km in

nature with the step occurring at the 30 km mark. Overall, the basin has been reduced from a total length of 185 km to a length corresponding to 80 km in nature for the experiment. As for the original salt thickness, the thickest portions are 2 km, occurring in the deepest portion of the wedge in the Abenaki Graben and the central Sable Subbasin, and 1 km over the intermediate North Sable High and across the Sable Subbasin step.

The sedimentation rates for Experiments 1 and 2 are scaled from the averaged sedimentation rates derived from GXT line 1800 and indicated on Table 4.1 in Chapter 4. Table 5.1 lists the scaled sedimentation rates, patterns and duration for Experiment 1.

5.5.2 Results from Experiment 1

The following section highlights the results from Experiment 1. Upon completion, the experiment was sectioned every 5 cm from shelf to slope, photographed and interpreted. A representative section from the experiment was also sequentially restored to gain insight into the evolution of structures as well as the entire basin evolution. Experiment 1 ran over a 10 day period for a total of 240 hours and simulated 72.0 Ma of post-rift evolution from the Early Jurassic to the mid-Early Cretaceous of the Abenaki Graben and central Sable Subbasin.

Structural overview

Structures from three representative cross-sections (55 cm, 35 cm, 15 cm) of the completed experiment are presented in Figure 5.6. The complete set of experiment cross-sections, illustrated in 5 cm intervals in the shelf-slope direction, is detailed in Appendix E on the CD. Silicone-withdrawal basins are indicated on the sections representing the seaward-propagating sediment succession. Although the overall structural style across

the dip-sections remains the same, along-strike variations of individual structures and localized depocentres occur from section to section. These variances in structures are attributed to local feedback mechanism between deposition, silicone flow, and dynamic topography given the absence of along-strike changes in basin morphology. Boundary effects also attribute to minor differences, as silicone mobilization is somewhat slowed at the edges of the basin leading to slight variances in the placement of structures. These boundary effects are acceptable as salt basins in nature are not infinite and similar effects occur.

The landward margin of the silicone basin is marked by primary welding occurring as silicone evacuated from the landward tapering wedge. Within the tapering wedge, salt rollers (Sr1, Sr2, Sr3) formed as growth faults evolved in the early stage of silicone evacuation and sediments rolled and subsided into the proximal basin. Much of the silicone was evacuated beneath the wedge, with minor amounts trapped as sediments welded to the landward edge of the "basement" high.

A diapir (D1) appears in the central sections, trapped as silicone extruded onto the intermediate high and become overrun by sedimentation. Across the experiment high, a prominent basinward-dipping expulsion rollover system and associated keystone faulting (Er2a/KG) are the dominant structural styles. Here, the beds are near vertical and welded to the high as a result of the beds having rotated and subsided into the landward flank of diapir (D2). Boundary effects can be observed in D2 as it occurs over the high in sections close the experiment edges, whereas it has translated into the seaward main basin in the central sections.

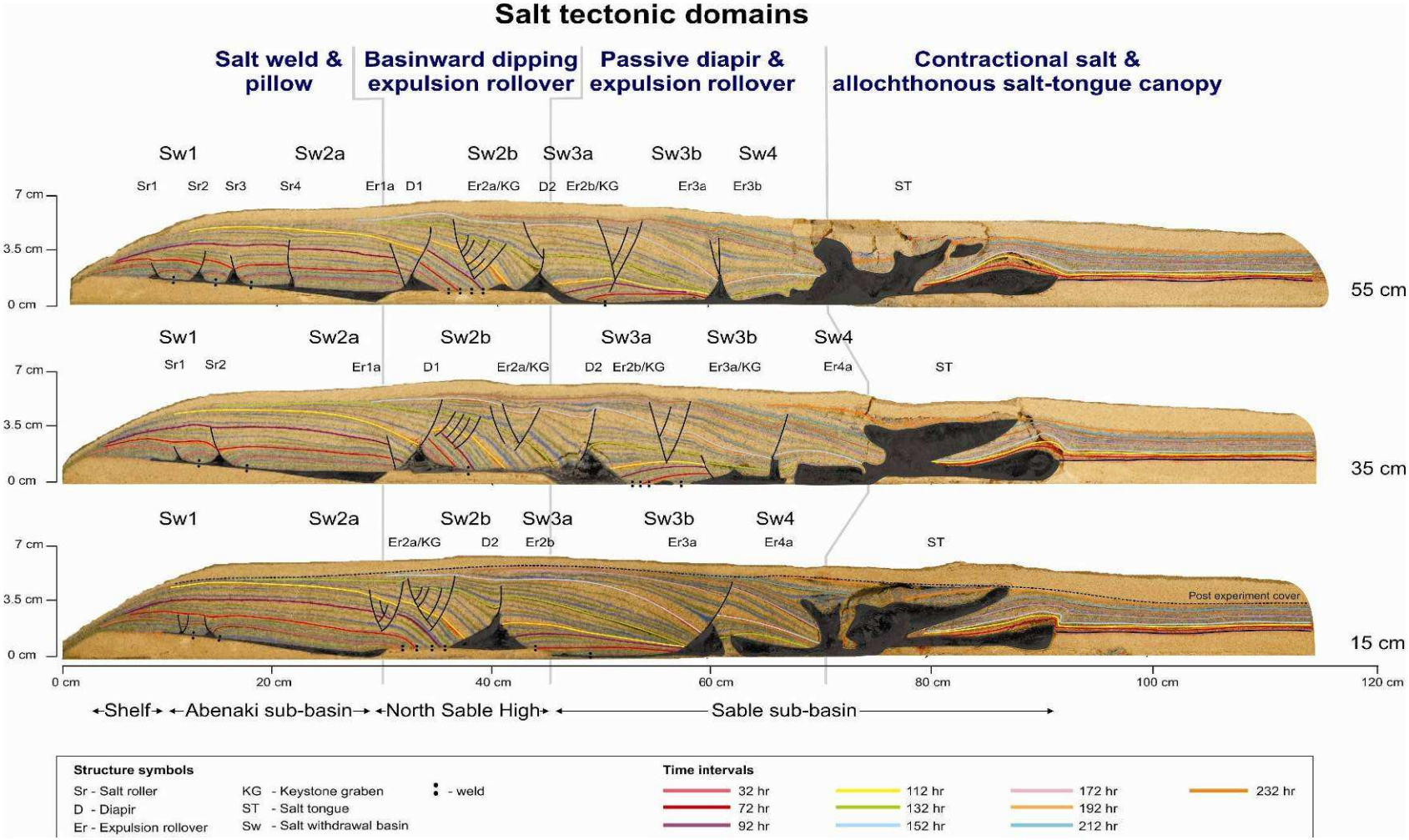

Figure 5.6 Three representative cross-sections from the Abenaki Graben and central Sable Subbasin Experiment 1. Coloured horizons illustrate the final placement of different timed sedimentation intervals (hours). Black overlays cover transparent silicone. Salt withdrawal basins are labelled for sections (Sw) but these depocentres were not active throughout basin evolution. Refer to Figure 5.9 to see the evolution of depocentres.

Within the symmetric basin with basement step, a landward-dipping expulsion rollover system (Er2b/KG in Fig. 5.6) formed adjacent to the basinward flank of diapir D2. Sediments deposited seaward of D2, from 48 - 156 hr, formed a landward-dipping expulsion rollover system (Er3a/KG) with keystone faulting in the landward flank of diapir D2 (in ER2a/KG). Close to the basement step, another basinward-dipping expulsion rollover (Er4a) occurs against the feeder system for the salt tongue-canopy system (ST). The salt tongues-canopy system makes up the dominant allochthonous salt structures that are present across the experiment cross-sections and occur as a series of salt tongues coalesced to form salt tongue-canopies. The salt tongue extends up to 15 cm long in some sections. Pelagic sedimentation effectively pinned the salt feeder system for the salt tongue-canopy system from translating into the distal edge of the basin. Silicone over the basement step at the basin's distal edge is inflated but was also effectively trapped by pelagic sedimentation.

Experiment 1 basin evolution

The evolution of Experiment 1 is documented in two time-space diagrams (Figure 5.7; Figure 5.8) as well as 3D experiment images with strain data (Figure 5.9; Figure 5.10). Time-series 3D surface elevation and strain data also allowed for a representative experiment section (35 cm) to be sequentially restored over specific intervals using mechanically derived concepts (Figure 5.11).

The time-space diagrams present the spatial and temporal evolution of silicone structures and associated depositional systems. The diagrams are created by tracking the position of structural and depositional elements from the time-series data as well as the strain data along the 35 cm shelf-slope transect and plotted along the x-axis. Once

completed over 24 hour intervals, the temporal evolution of these structures was plotted along the y-axis (Figure 5.7; Figure 5.8).

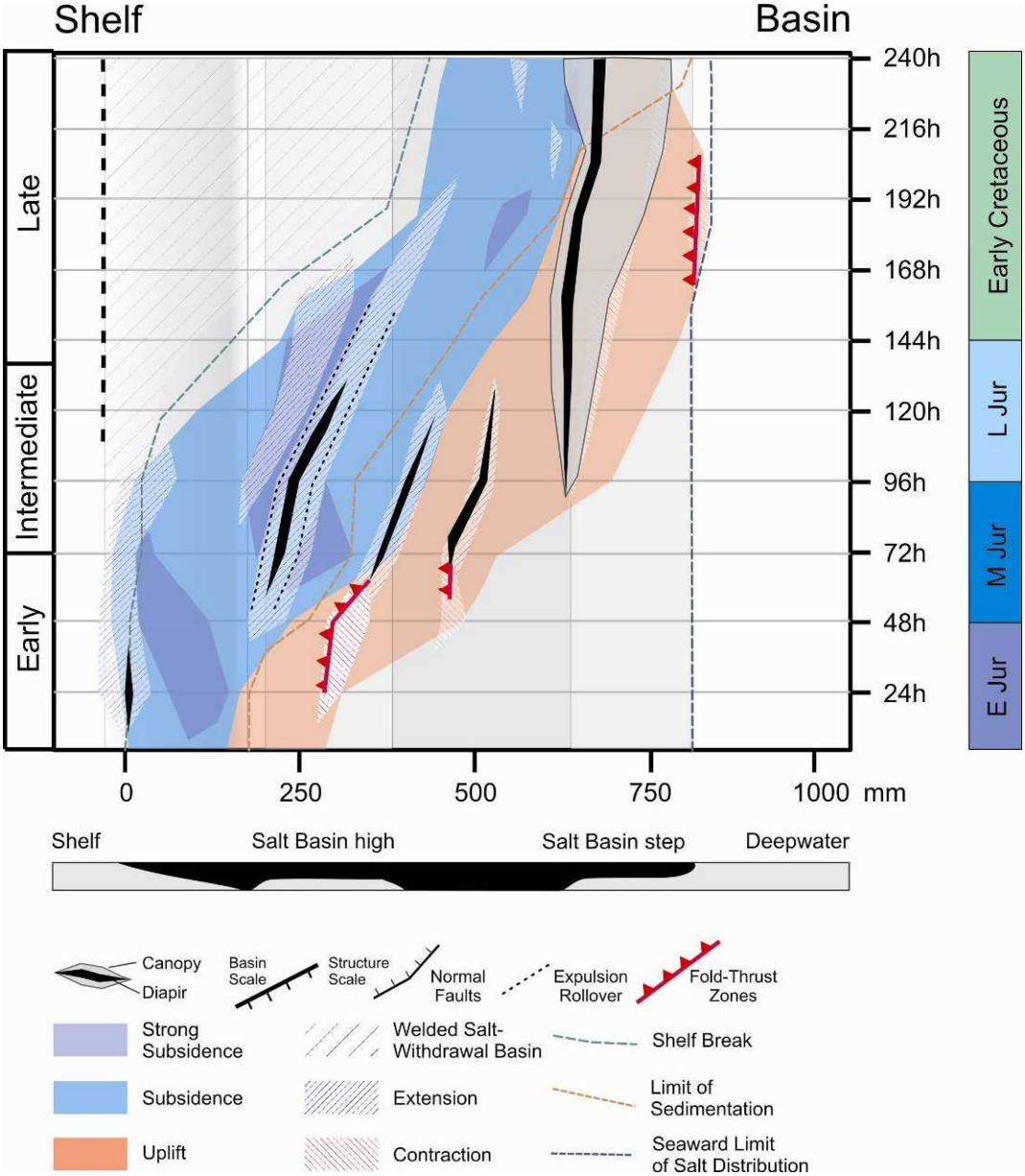

Figure 5.7 Spatial and temporal diagram of Experiment 1 illustrating the evolution of salt tectonics structures and associated depositional systems deduced from time-series images and DIC strain analysis. The diagram illustrates vertical displacement and horizontal strain of a center cross-section (35 cm) during the experiment evolution. The position of structural and depositional elements in a shelf-to-deep basin transect are plotted along the x-axis. The variation in the x position of elements was done over 24 hour intervals, shown on the y-axis.

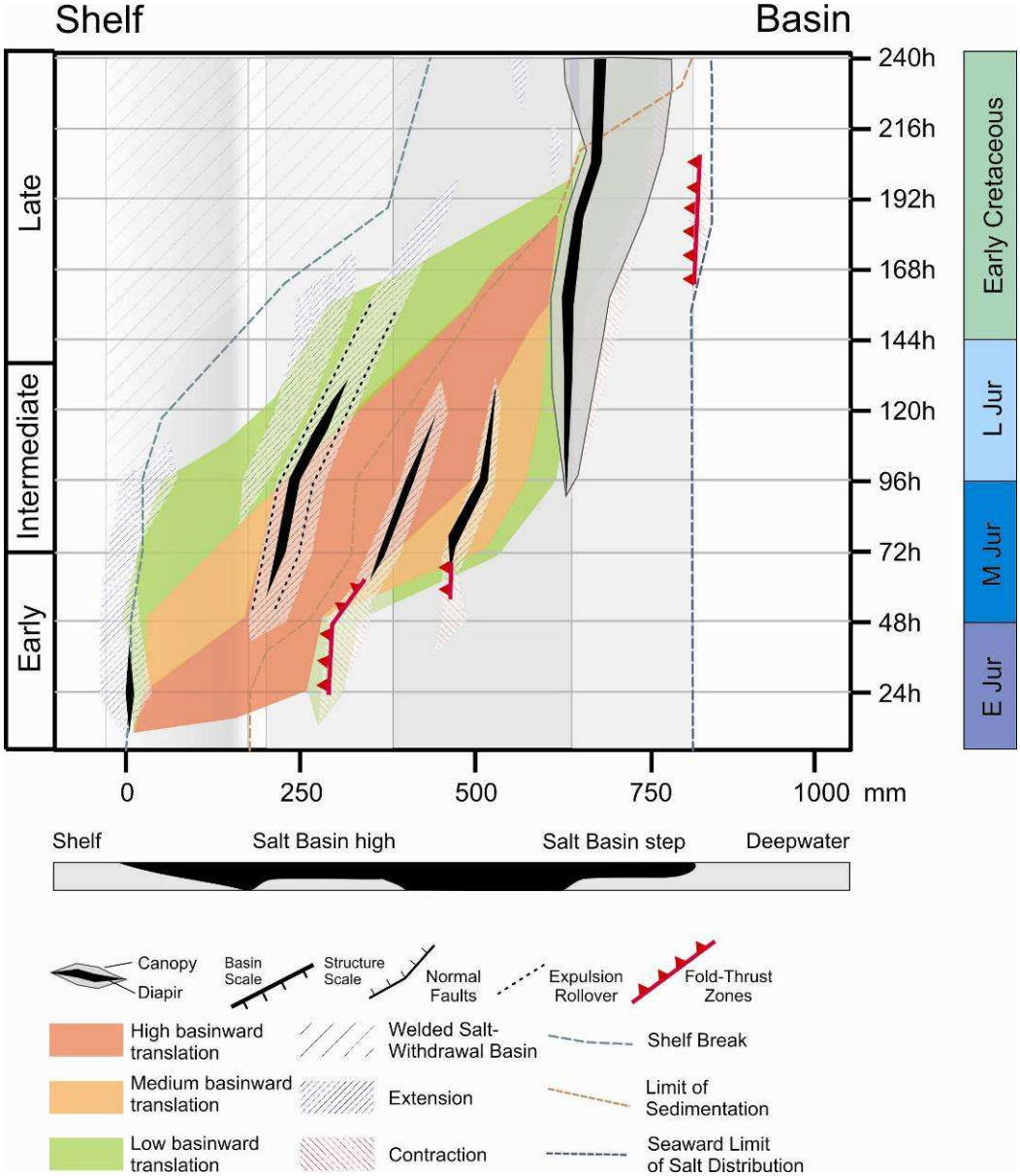

Figure 5.8 Spatial and temporal diagram of Experiment 1 illustrating the evolution of salt tectonics structures and associated depositional systems deduced from time-series images and DIC strain analysis. The diagram illustrates horizontal displacement and horizontal strain of a center cross-section (35 cm) during the experiment evolution. The position of structural and depositional elements in a shelf-to-deep basin transect are plotted along the x-axis. The variation in the x position of elements was done over 24 hour intervals, shown on the y-axis.

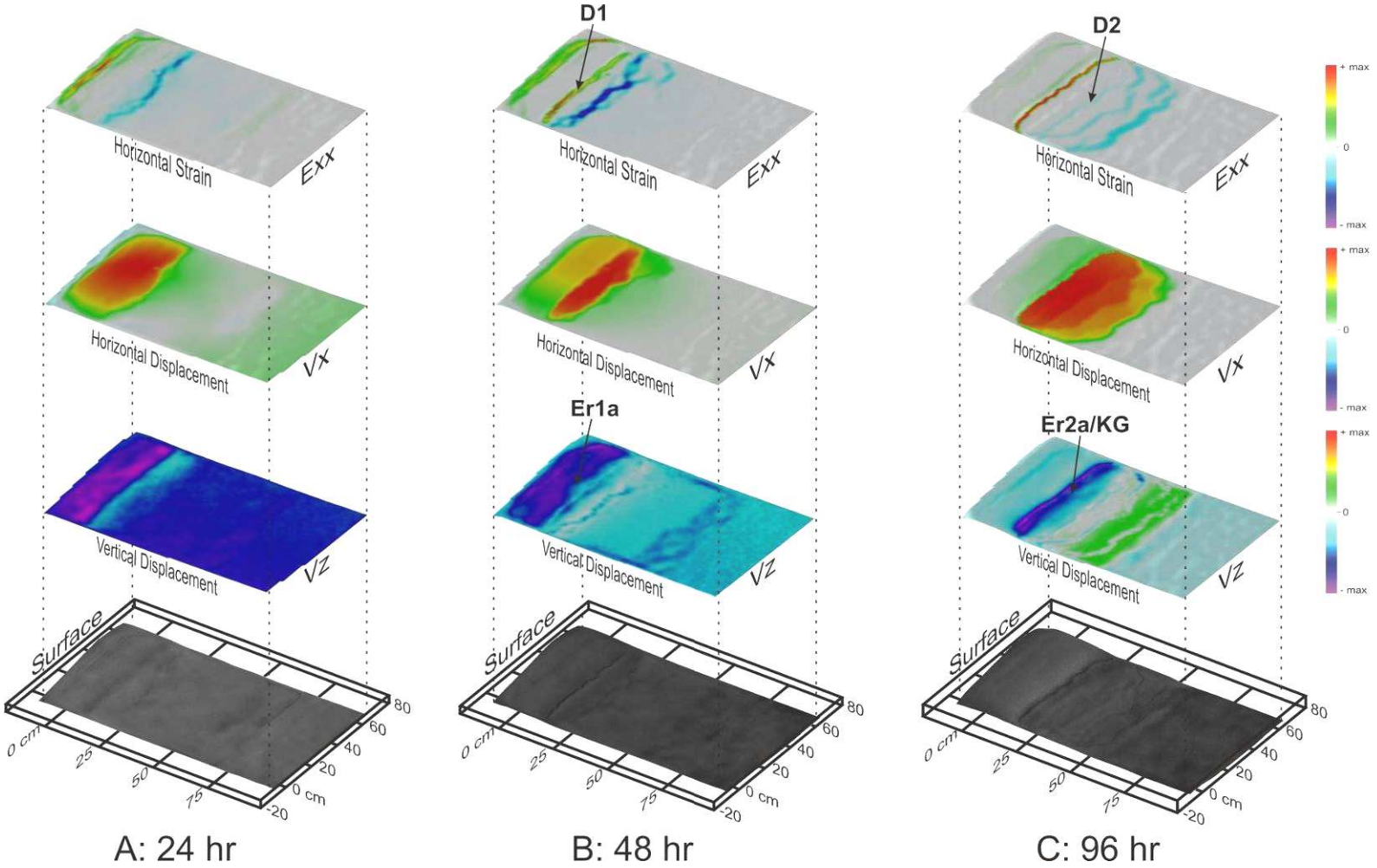

Figure 5.9 Temporal evolution of Experiment 1 simulating the salt basin evolution of the Abenaki and central Sable sub-basin from 0 – 96 hr. The experiment evolution is visualized in 24 hr and 48 hr intervals. The 3D surface intervals include overlays of horizontal strain (Exx), horizontal displacement (Vx), vertical displacement data (Vz). Incremental strain and displacement components obtained by 3D DIC monitoring are summarized for the previous 24/48 hour interval and overlain on the model surface to visualize deformation trends for each interval. Abbreviations: D = Diapir; Er = Expulsion rollover; KG = Keystone Graben.

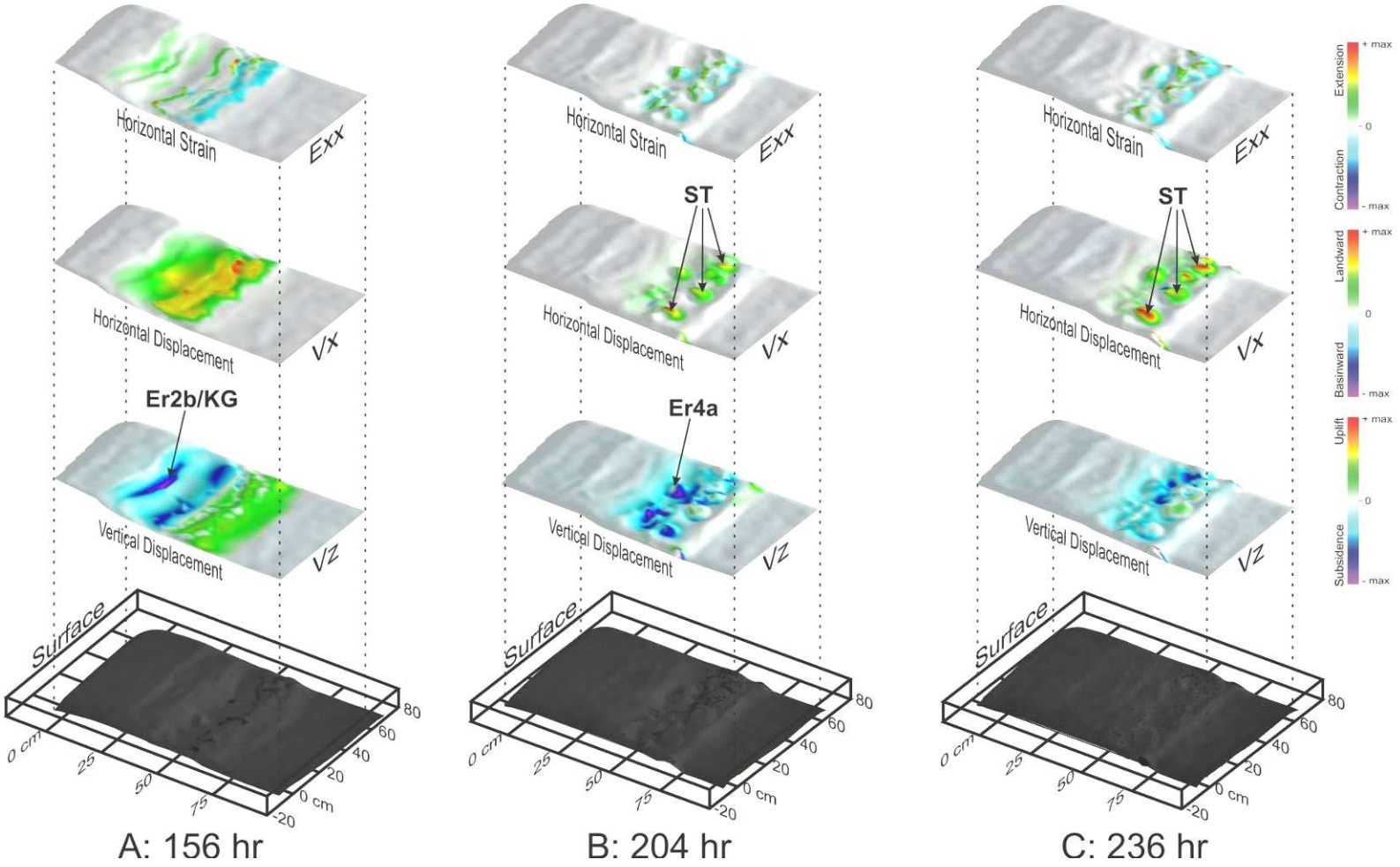

Figure 5.10 Temporal evolution Experiment 1 simulating the salt basin evolution of the Abenaki and central Sable sub-basin from 156 - 236 hr. The experiment evolution is visualized in 48 hour intervals. The 3D surface intervals include overlays of horizontal strain (Exx), horizontal displacement (Vx), vertical displacement data (Vz). Incremental strain and displacement components obtained by 3D DIC monitoring are summarized for the previous 48 hour interval and overlain on the model surface to visualize deformation trends for each interval. . Abbreviations: D = Diapir; Er = Expulsion rollover; KG = Keystone Graben.

The 3D images illustrate the experiment evolution over 24 hour intervals and also include displacement and strain overlays (Figure 5.9; Figure 5.10). The overlays visualize active deformation including horizontal strain (Exx), horizontal displacement (Vx), and vertical displacement (Vz). The horizontal strain overlays record extension (e.g. diapirs, faults) represented in warm colors and contraction (e.g. folds, thrusts) represented in cold colors. The horizontal displacement overlays record translation and spreading of the sedimentary wedge with seaward translation represented in warm colors and landward translation represented in cold colors. The vertical displacement overlays record uplift (folds, rising diapirs) represented in warm colors and subsidence (grabens, withdrawal basins) represented in cold colors.

The evolution of Experiment 1 can be divided into three major kinematic stages: early, intermediate and late stage.

Early stage (0 – 72 hr)

The early stage (0 – 72 hr) is defined by silicone evacuation from the landward tapering wedge. The development of salt rollers in the proximal subbasin occurred at this time as well as the inflation of silicone over the intermediate North Sable High. Complex contractional deformation including folds and silicone cored thrusts between diapirs and inflated silicone massifs record the interplay between gravity driven extensional processes and early, downdip silicone inflation.

The extensional domain during this stage was characterized by silicone rollers and normal faulting related to sediment downbuilding within the landward tapering wedge (Figure 5.7). The maximum subsidence during this stage was influenced by the basin topography and focused in the basinward portion of the landward tapering wedge (Figure

5.7). As sediments rotated asymmetrically seaward and silicone evacuated, a seaward-dipping expulsion rollover formed. Diapir D1 formed seaward of the expulsion rollover and evolved onto the intermediate North Sable High (Figure 5.9). Seaward-directed, high translation of sediments initially occurred on the basinward flanks of the silicone rollers within the landward tapering wedge, and later formed basinward of D1 resulting in an early rafted package of sediments (Figure 5.8). This package also marked a transition from extensional to contractional domains.

The early landward extension of the sedimentary wedge was balanced by contraction and silicone inflation over the intermediate high. Initial silicone-cored thrusts eventually evolved into a passive diapir D2 (Figure 5.7). Fold belts formed within the inflated silicone over the intermediate high. These fold belts accommodate much of the contraction and slow silicone advancement into the symmetric basin with the intermediate step representing the Sable Subbasin.

Intermediate stage (72 – 136 hr)

The intermediate stage (72 – 136 hr) is defined by the basinward migration of depocentres across the high and into the Sable Subbasin, represented here by the symmetric graben with an intermediate basement step. A diapir developed and migrated across the high with an associated expulsion rollover. Within the proximal Sable Subbasin, two diapirs developed and migrated basinward. Strong inflation and uplift in the distal region of the autochthonous silicone basin leading to a passive diapir forming above the basement step. The seaward migration of depocentres coincided with silicone withdrawal within the Sable Subbasin and initial welding in the Abenaki Graben.

The extensional domain during this interval was marked by passive diapirism over the intermediate high. Basinward of D1, the rafted package of sediments continued to translate seaward into the Sable Subbasin as silicone evacuated into the subbasin (Figure 5.9). Diapirs D2 and D3 began to evolve passively in the proximal Sable Subbasin. As sediments prograded and downbuilt into the subbasin, the inflated silicone massif migrated to above the basin step accommodated by salt cored folds (Figure 5.9).

Late stage (136 – 236 hr)

The late stage (136 – 236 hr) is defined by the progradation of the sedimentary wedge into the deep basin and continued passive diapir development onto the step until the creation of the silicone tongue-canopy system. This stage is characterized by deformation being confined to the Sable Subbasin with sedimentation patterns heavily controlled by allochthonous silicone tongues.

The extensional domain during this stage consisted of keystone grabens (Figure 5.6; Figure 5.8) as sediments rolled basinward into the Sable Subbasin and into the inflated silicone massif (Er4a; Figure 5.10). Silicone from the salt-cored fold flowed out as large silicone tongues (ST; Figure 5.10) as sediments prograded basinward. Contraction occurred in the deep basin accommodated by silicone-cored folding that moved to the seaward limit of the basin.

Sequential section restoration for Experiment 1

Figure 5.11 shows the sequential restoration of a representative shelf-slope cross-section (35 cm). Balancing assumes plane-strain deformation and is applied to a constant area, vertical shear method (Hoosak 1995; Rowan 1993; Rowan and Kligfield 1989). The

cross-section was restored over specific time intervals and referenced to topographic surface profiles deduced from the 3D digital elevation models for each restoration step (Figure 5.9; Figure 5.10; Figure 5.11). To further aid in restoration, other time series data, including horizontal strain, vertical displacement and horizontal displacement were used (Figure 5.9; Figure 5.10). Horizontal strain data identified active faulting and diapirs, vertical displacement data allowed for correlation of depocentres and areas of silicone inflation, and horizontal translation identified basinward translating sediment packages. The balanced sections constrained by the 3D displacement and strain data permitted a quantitative analysis of the complex salt and fault systems.

24 hours - Initial post-salt sedimentation and early basin development

Initial sedimentation during this time was confined to the landward tapering wedge (LTW) initiating early silicone withdrawal from the proximal basin. Two small passive diapirs later transitioning to silicone roller systems (Sr1, Sr2) as sedimentation overran the diapers. They developed close the landward limit of the silicone basin as passive downbuilding of early sediments continued in the proximal graben (24 hr; Figure 5.11). Subsiding sediments and silicone withdrawal led to the creation of two main depocentres (Sw1; Sw2) at this time separated by Sr2. Minor inflation of silicone over the mid-basin high also occurred during this time, as sediments downbuilt and evacuated silicone onto the high.

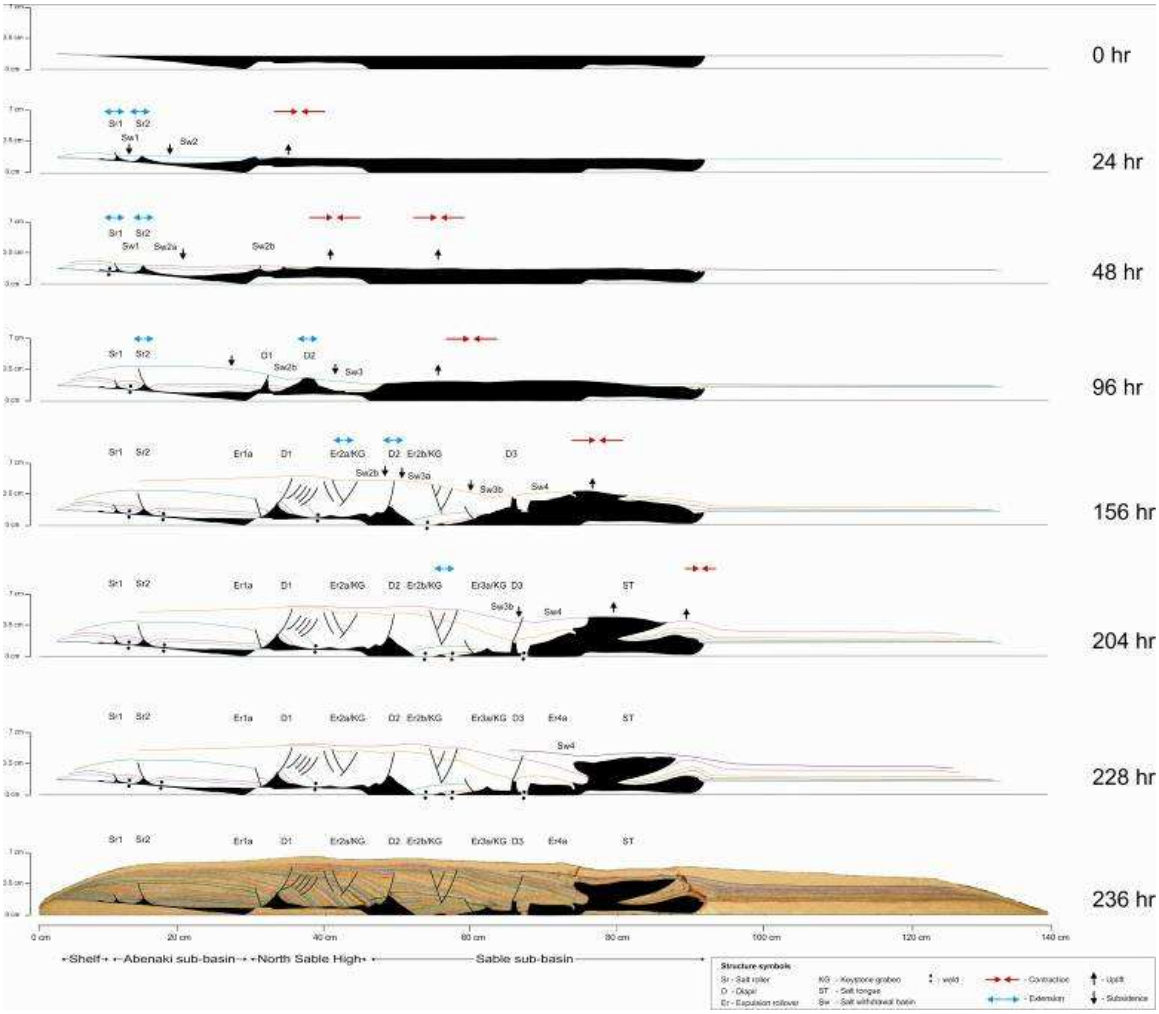

Figure 5.11 Sequential restoration of the central (35 cm) cross-section of Experiment 1 based on topographic profiles of model surface and incremental DIC strain and displacement data (Appendix B). Early model evolution is restored for 24 hour periods, while later model evolution restores horizons approximately 48 hours. Active and subsiding salt withdrawal basins are labelled Sw. Silicone structures are black and include diapirs (D), rollers (Sr), expulsion rollovers (Er), keystone grabens (KG) and silicone tongues (ST) (Larger restoration found in Appendix E on CD).

48 hours – Aggradation and continued subsidence within tapering wedge

Continued subsidence caused by silicone evacuation facilitated the continued evolution of Sr1 and Sr2 and sediment rotation along the fault plane (B – Figure 5.9; Figure 5.11). Just seaward of the reactive diapir (D1), a small landward-dipping expulsion rollover (Er1b) has developed along its basinward flank due to strong localized extension associated with the development of D1 (B - Figure 5.9). Slight translation of

the main depocentre (Sw2 – Figure 5.9) and high translation of silicone onto the high (B – Figure 5.9) also occurred during this time. Sediments also begin to be deposited onto the basement high, and updip extension was balanced by contraction and minor uplift over the high (B – Figure 5.9).

96 hours – Initial welding and diapir formation over baasement high

Initial welding occurred within the landward tapering wedge (LTW) representing the Abenaki Graben by the 96 hour mark, as sediments along the Sr1 rotated and subsided to the basin floor. The sediment loading within the LTW allowed the silicone to continue expulsion onto the high and into the distal basin. Over the high, diapirs D1 and D2 developed passively with a salt withdrawal basin (Sw2b), created between the diapirs. Over the high, approximately 6 cm of translation occurred, as a package of sediments (Sw3) prograded to the edge of the high concurrent with diapir (D2) growing passively on the high (Figure 5.11). Within the distal basin, silicone inflation took place mostly in front of the distal basin step, manifested as a series of contractional fold belts created as silicone evacuated from the proximal basin and basement high into the distal basin. This inflation before the basement step also permitted deepwater pelagic sedimentation in the distal silicone basin, above the step and out onto the experimental distal plain (C – Figure 5.9; Figure 5.11).

156 hours – Progradation of the sedimentary wedge and expulsion rollover/keystone graben formation in the distal symmetric graben with basin step

As sediments prograded and silicone evacuated from over the high and out into the distal basin, expulsion rollover Er2a further developed with sediments rotating to the

near vertical (Figure 5.11). A keystone graben system associated with the rotating sediments (Er2a/KG) also evolved as salt evacuated from the basin high (Figure 5.11). The rotating sediments pushed D2 into the distal basin and also allowed for the translation of basinward successions. These sediments also rotated along the basinward flank of D2 until welding to the basin floor (Er2b/KG). Inflated silicone within the experiment was now confined to a small portion of the basin associated with the basin step (A – Figure 5.10). The interaction between the basin step and deepwater pelagic sedimentation effectively pinned the inflated silicone to this position.

204 hours – Initial development of allochthonous salt tongue

Welding within the distal basin continues with sediments downbuilding to the basin floor as silicone evacuates and extrudes as an allochthonous silicone tongue (ST) (B – Figure 5.10; Figure 5.11). As the welding occurs, silicone also becomes trapped, creating silicone pillows. Deep basin pelagic sediments along the basinward flank of the ST feeder begin to subside as the ST advances basinward (Figure 5.11).

236 hours – Continued salt tongue development and system shutdown

By 236 hours, the ST continues to grow as the strata on the landward flank rolls into the feeder (Er4a; Figure 5.11). Deep basin pelagic sediments deposited by the 204 hr mark, and located on the basinward portion of the ST feeder, also continue to subside as the ST flows basinward.

5.6 4D Physical Experiment 2

Using the results from Experiment 1, Experiment 2 implemented minor variable adjustments to further constrain the setup and achieve a model closer to the natural prototype (Experiment 2; Figure 5.3). Primarily, minor adjustments to the basin geometry were applied to Experiment 1 based on slightly varying structural styles resulting from the previous experiment and nature.

5.6.1 Experiment 2 setup

Observed results from Experiment 1 show a prominent basinward-dipping expulsion rollover system across the North Sable High, differing from the presence of a basinward-dipping listric growth fault system interpreted in the ION-GXT Line 1800. Campbell (2007) and MacDonald (2007) attribute the differing structural patterns to slight variances in salt thickness. Both structural styles are associated with thin salt (<1.5 km) but differences associated between the experiment and natural prototype indicate a reduction in original salt over the intermediate high. Thus, for Experiment 2, the North Sable High is modified from 1 km to 1.5 km high, with 0.5 km of original salt in place on the high. The new experiment setup maintains the same geometry as Experiment 1, with slight modifications to the proximal half-graben representing the Abenaki Graben that is now 15 cm long, with the deepest portion of the graben reduced from 2 cm to 1.5 cm of silicone. The intermediate high representing the North Sable high is modified to 20 cm in length, and as mentioned above, the original silicone in place over the high is reduced to 0.5 cm.

5.6.2 Results from Experiment 2

The following section highlights the results from Experiment 2. After completion, the experiment was sectioned longitudinally from shelf to slope and interpreted every 5 cm. A representative section from the experiment was also sequentially restored to gain insight into the evolution of structures as well as the entire basin evolution. Experiment 2 ran over a 14 day span for a total of 304 hours and simulated 91.2 Ma of post-rift evolution from the Early Jurassic to the late-Early Cretaceous of the Abenaki Graben and central Sable Subbasin.

Structural overview of Experiment 2

Structures from three representative cross-sections (60 cm, 35 cm, 10 cm) of the completed experiment are presented in Figure 5.13. The complete set of experiment cross-sections sliced every 5 cm in the shelf-slope direction can be found on the CD in Appendix E. As with Experiment 1, variances in individual structures and localized depocentres occur from section to section, but the overall, structural style across the sections remains the same. These variances in structures are attributed to local variations in deposition associated with subsidence rates and silicone flow, considering no change in basin morphology and little change in sedimentation patterns along-strike.

Similar to Experiment 1, the landward margin of the silicone basin is marked by primary welding occurring as silicone evacuated from the landward tapering wedge. Within the tapering wedge, a small silicone rollover (Sr1) forms, resulting from subsiding sediments as silicone evacuated from the wedge onto the high. Very little silicone

remains as it is almost completely evacuated out of the wedge with minor amounts trapped as sediments welded to the edge of the experiment high.

A diapir (D1) appears in the sections, trapped as inflated silicone extruded onto the intermediate high and overrun by sedimentation. D1 is flanked on each side by two rollover systems (Er1a/KG, Er1b/KG). Basinward of Er1b/KG, minor rotation in the strata occurred (Er2a/KG) as the silicone evacuated into the distal basin. It is important to note that the high is not dominated by an expulsion rollover system as observed in Experiment 1, and instead, extension is accommodated by minor rollover systems and listric faulting.

Within the symmetric basin with the basement step, a landward-dipping expulsion rollover system (Er2b/KG) occurs that is associated with the basinward flank of remnant salt. As distal sediments from this rollover system rotated and created a basinward-dipping expulsion rollover system (Er3a/KG), a large pseudo-turtle structure developed with keystone faulting. The silicone tongue-canopy system is the dominant allochthonous silicone that extends across the experiment cross-sections as a series of silicone tongues that coalesced to form canopies. The silicone tongues (ST) are as long as 15 cm in some sections. Pelagic sedimentation eventually pinned most of the silicone feeders from translating to the distal edge of the basin. The feeders are located where silicone inflated before the basin step and eventually transitioned over the high. This led to a ST system developing just before, at, and after the basement step as inflated siliconereached the surface of the sediments.

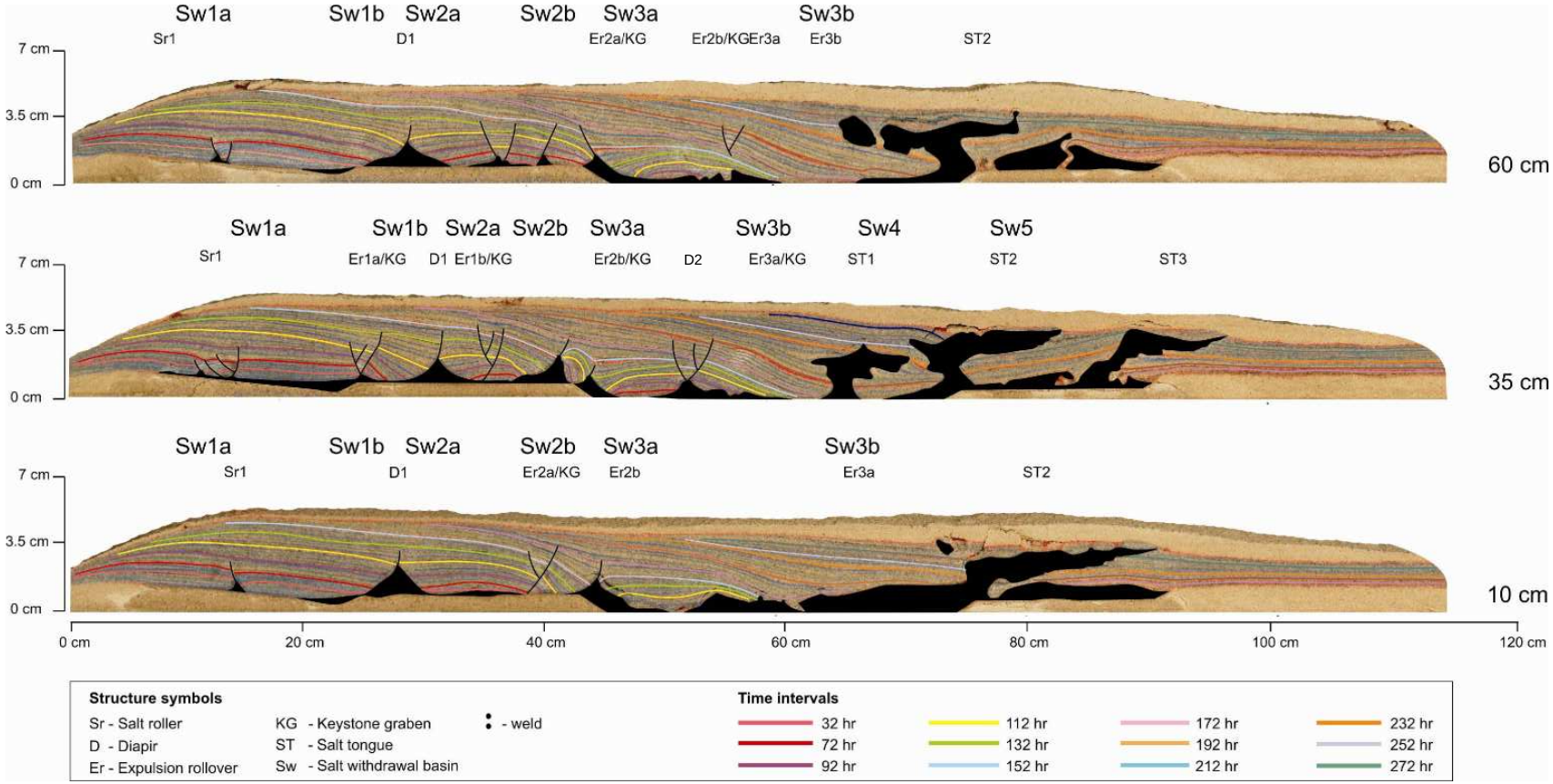

Figure 5.12 Three representative cross-sections from the Abenaki and central Sable Subbasin Experiment 2. Coloured horizons illustrate the final placement of different timed sedimentation intervals (hours). Black overlays cover transparent silicone. Salt withdrawal basins are labelled for sections (Sw) but these depocentres were not active throughout basin evolution. Refer to Figure 5.15 to see the evolution of depocentres.

Experiment 2 basin evolution

The evolution of Experiment 2 is documented in two time-space diagrams (Figure 5.13; Figure 5.14) as well as 3D experiment images with strain data (Figure 5.15; Figure 5.16). Time-series 3D surface elevation and strain data also allowed for a representative experiment section (35 cm) to be sequentially restored over specific intervals using mechanically-derived concepts (Figure 5.17). As implemented in the Experiment 1, the time-space diagrams present the spatial and temporal evolution of silicone structures and associated depositional systems along the 35 cm shelf-slope transect for Experiment 2. Refer to the Experiment 1 basin evolution section for methodology.

As with Experiment 1, 3D experiment images are used to illustrate the experiment evolution over 24 hour intervals and also include displacement and strain overlays (Figure 5.15; Figure 5.16). The overlays visualize active deformation including horizontal strain (Exx), horizontal displacement (Vx), and vertical displacement (Vz). The following section divides Experiment 2 into three major kinematic stages; early, intermediate and late.

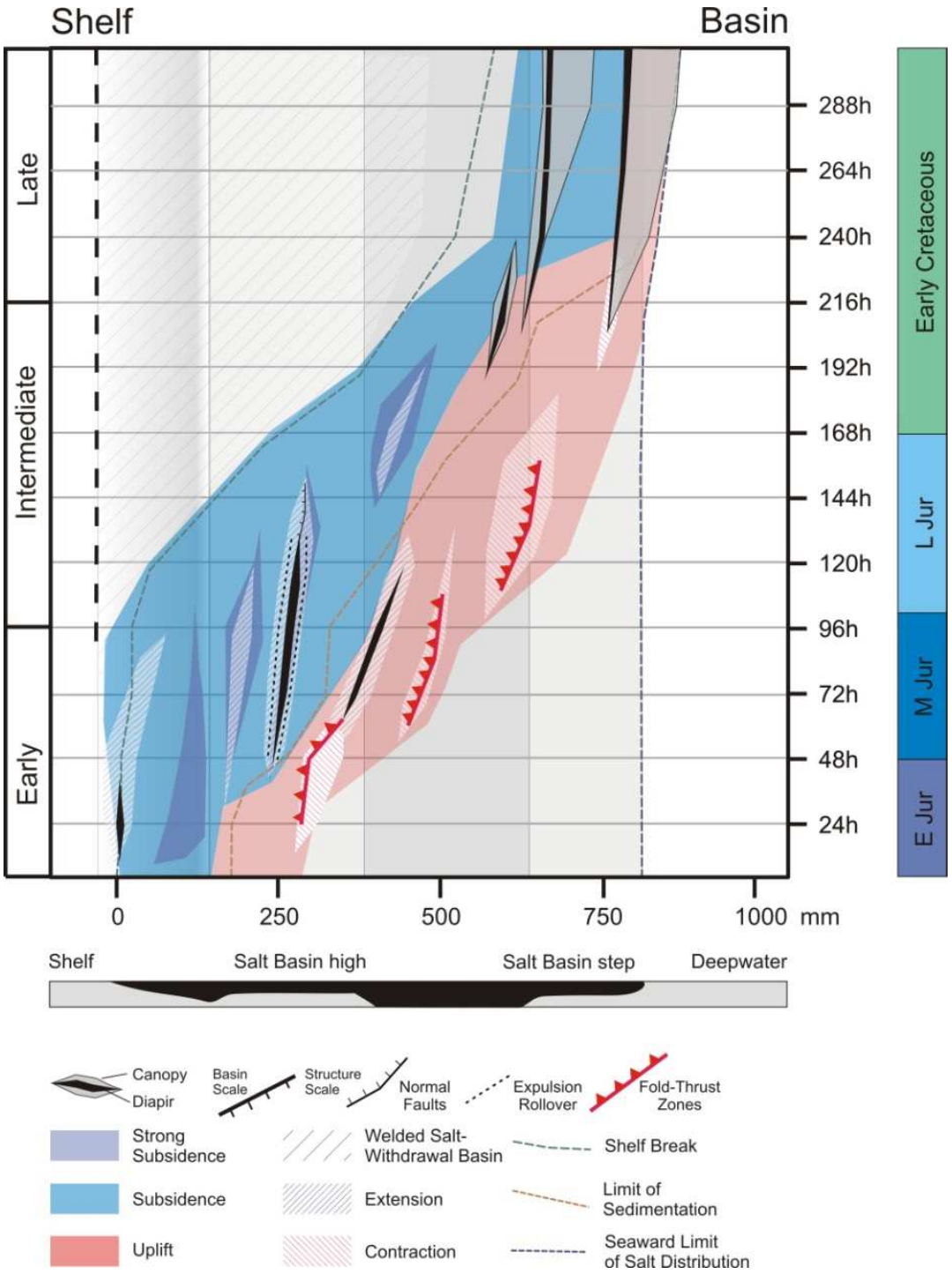

Figure 5.13 Spatial and temporal diagram of Experiment 2 illustrating the evolution of salt tectonics structures and associated depositional systems deduced from time-series images and DIC strain analysis. The diagram illustrates vertical displacement and horizontal strain of a center cross-section (35 cm) during the experiment evolution. The position of structural and depositional elements in a shelf-to-deep basin transect are plotted along the x-axis. The variation in the x position of elements was done over 24 hour intervals, shown on the y-axis.

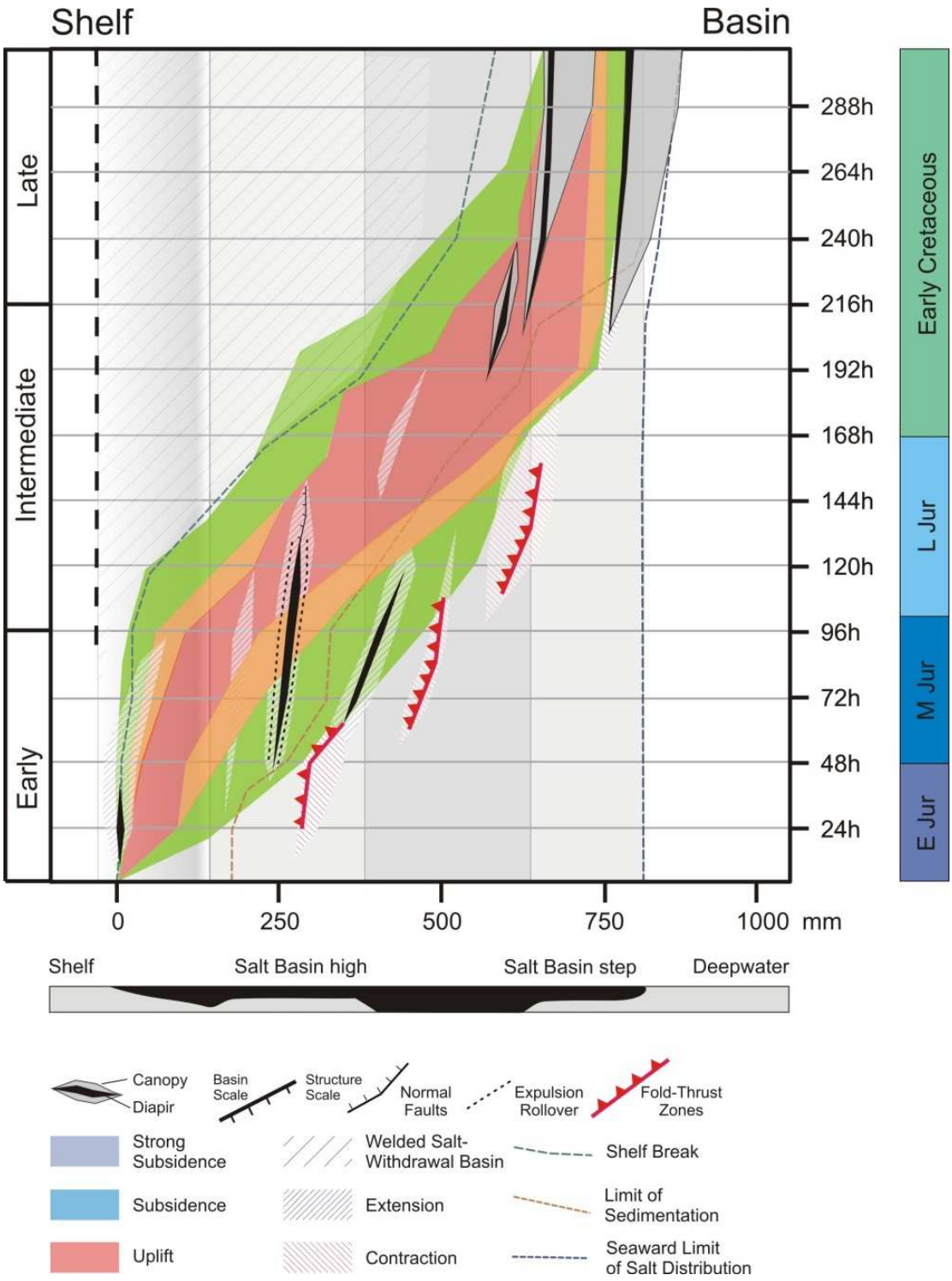

Figure 5.14 Spatial and temporal diagram of Experiment 2 illustrating the evolution of salt tectonics structures and associated depositional systems deduced from time-series images and DIC strain analysis. The diagram illustrates horizontal displacement and horizontal strain of a center cross-section (35 cm) during the experiment evolution. The position of structural and depositional elements in a shelf-to-deep basin transect are plotted along the x-axis. The variation in the x position of elements was done over 24 hour intervals, shown on the y-axis.

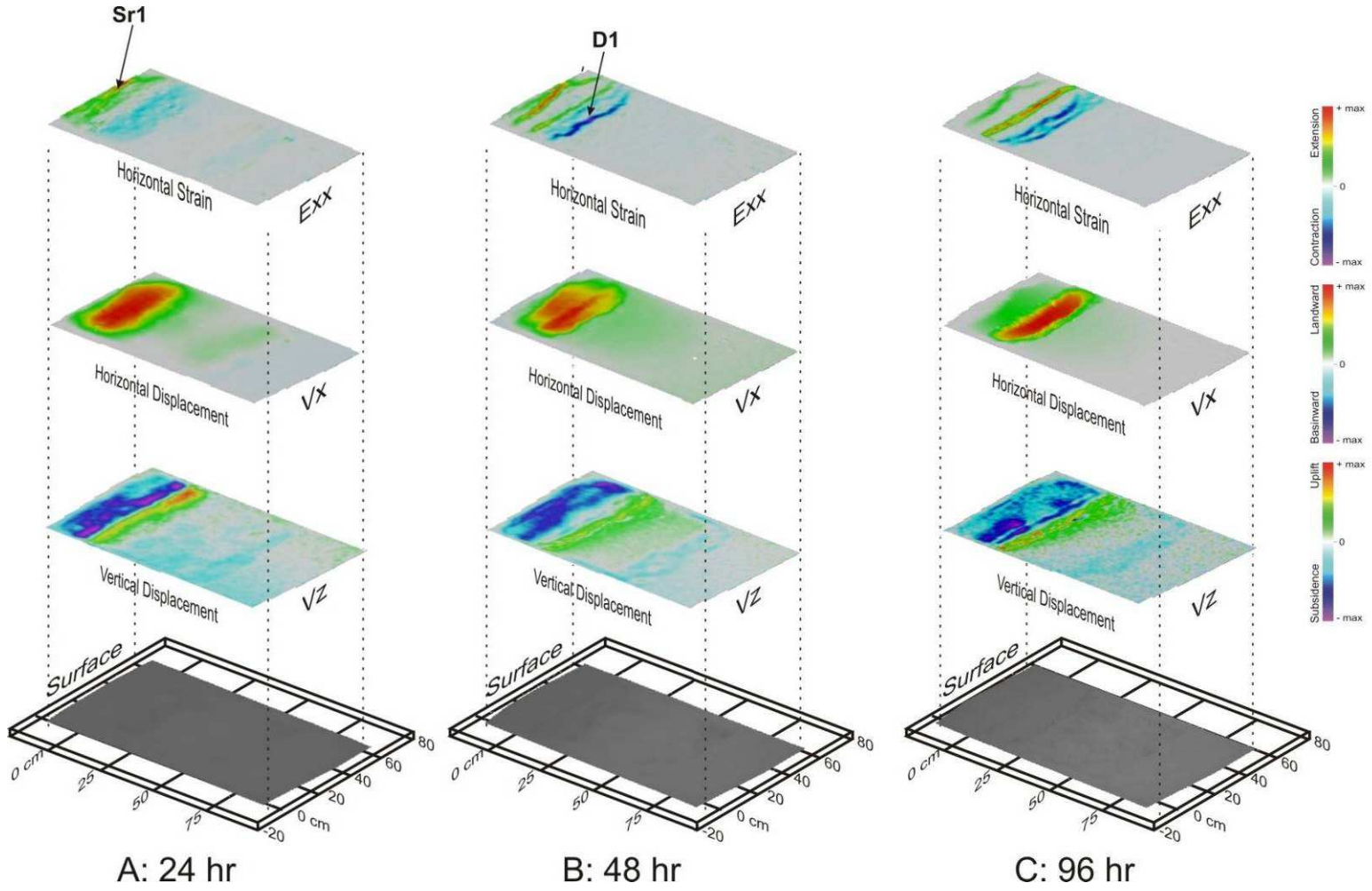

Figure 5.15 Temporal evolution of the experiment 2 simulating the salt basin evolution of the Abenaki and central Sable sub-basin from 0 – 96 hr. The experiment evolution is visualized in 24 hr and 48 hr intervals. The 3D surface intervals include overlays of horizontal strain (Exx), horizontal displacement (Vx), vertical displacement data (Vz). Incremental strain and displacement components obtained by 3D DIC monitoring are summarized for the previous 24/48 hour interval and overlain on the model surface to visualize deformation trends for each interval. Abbreviations: Sr = Silicone roller; D = Diapir.

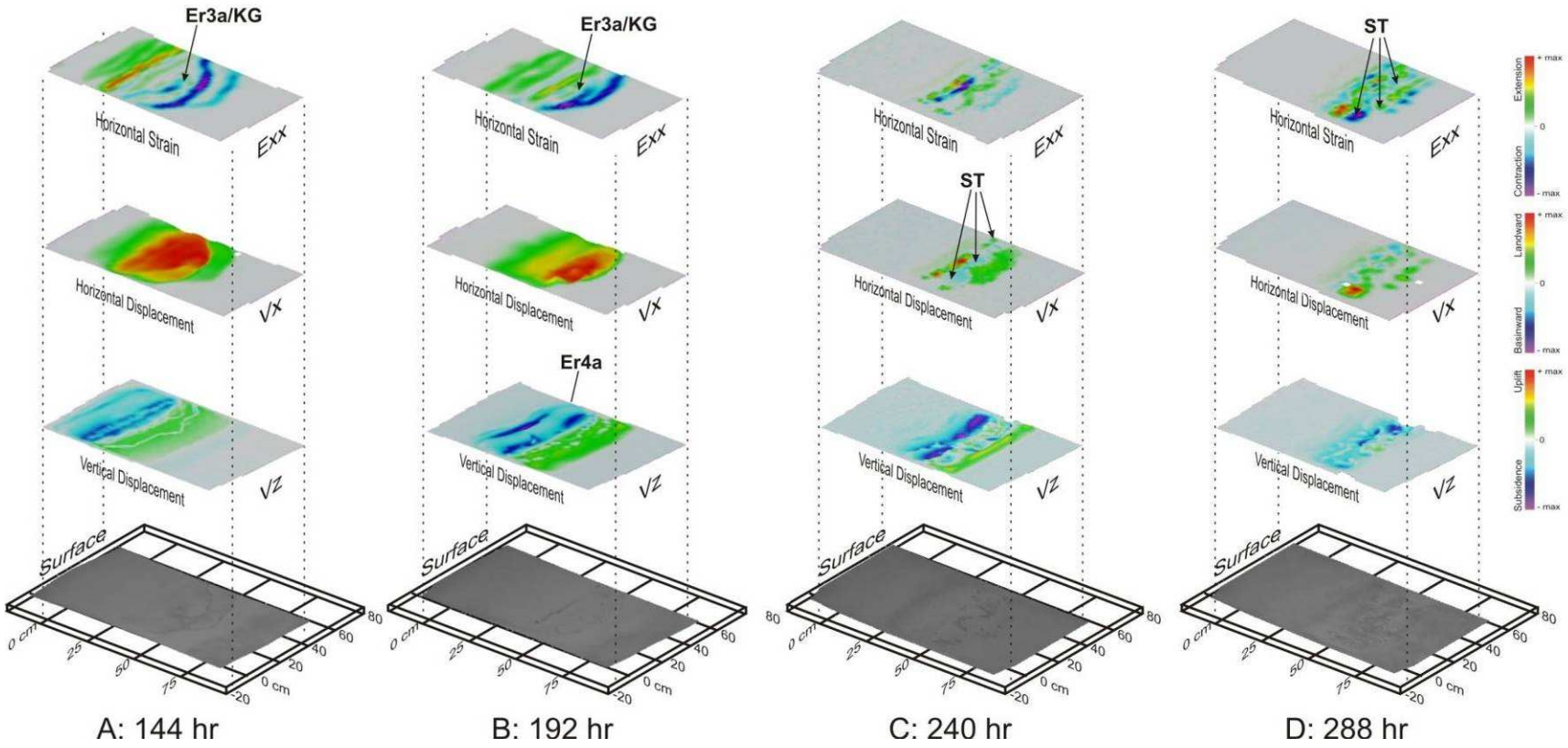

Figure 5.16 Temporal evolution of the experiment 2 simulating the salt basin evolution of the Abenaki and central Sable sub-basin from 144 - 288 hr. The experiment evolution is visualized in 48 hour intervals. The 3D surface intervals include overlays of horizontal strain (Exx), horizontal displacement (Vx), vertical displacement data (Vz). Incremental strain and displacement components obtained by 3D DIC monitoring are summarized for the previous 48 hour interval and overlain on the model surface to visualize deformation trends for each interval. Abbreviations: Er = Expulsion rollover; KG = Keystone graben; ST = Silicone tongue

Early stage (0 – 96 hr)

The early stage (0 – 96 hr) is defined by silicone evacuation from the landward tapering wedge. Silicone rollers in the proximal subbasin developed at this time as well as the inflation of silicone over the intermediate North Sable High (Sr1; Figure 5.15). Complex contractional deformation including folds, silicone-cored thrusts between diapers, and inflated silicone massifs recorded the interplay between gravity driven extensional processes and early, down-dip silicone inflation (Figure 5.13).

The extensional domain during this stage was characterized by salt rollers and normal faulting related to sediment downbuilding within the landward-tapering wedge (Figure 5.13). Maximum subsidence during this stage was influenced by basin topography and focused in the basinward portion of the landward-tapering wedge (Figure 5.13; Figure 5.15). As sediments rotated asymmetrically seaward due to silicone evacuation, a seaward-dipping expulsion rollover formed. Diapir D1 formed seaward of the expulsion rollover and evolved onto intermediate North Sable High (D1; Figure 5.15). Seaward translation of sediments initiated on the basinward flanks of the silicone rollers within the landward tapering wedge, and later over the high as silicone evacuated in the Sable Subbasin (Figure 5.14; Figure 5.15). This package also marked a transition from extensional to contractional domains (Figure 5.13; Figure 5.15).

The early landward extension of the sedimentary wedge was balanced by contraction and silicone inflation over the intermediate high. Initial silicone-cored thrusts eventually evolved into passive diapir D2 (Figure 5.13). Fold belts formed within the inflated silicone over the intermediate high. These fold belts accommodate much of the contraction, slowing silicone advancement into the symmetric basin with the intermediate step representing the Sable Subbasin.

Intermediate stage (96 – 216 hr)

The intermediate stage (96 – 216 hr) is defined by the basinward migration of depocentres across the high and into the Sable Subbasin represented by the symmetric graben with an intermediate basement step (Figure 5.14). A diapir developed and migrated across the high as translation and downbuilding of sediments occurred (D1; Figure 5.15). Within the proximal Sable Subbasin, strong inflation and uplift in the distal region of the autochthonous silicone basin created a passive diapir occurring above the basement step (Figure 5.13). The seaward migration of depocentres coincided with silicone withdrawal within the Sable Subbasin and initial welding in the proximal Abenaki Graben.

The extensional domain during this interval was marked by passive diapirism over the intermediate high. Basinward of D1, the rafted package of sediments continued to translate seaward into the Sable Subbasin as silicone evacuated into the basin (Figure 5.9). Diapirs D2 and D3 evolved passively in the proximal part of the basin. As sediments prograded and downbuilt into the basin, the inflated silicone massif migrated to and above the basin step, being accommodated by silicone-cored folds (Figure 5.9).

Late stage (216 – 304 hr)

The late stage (216 – 304 hr) is defined by progradation of the sedimentary wedge into the deep basin, and continued passive diapir development onto the step until the creation of the silicone tongue-canopy system (Figure 5.13; Figure 5.14). This stage is characterized by deformation being confined to the Sable Subbasin and sedimentation patterns heavily controlled by allochthonous silicone tongues (ST; Figure 5.16).

The extensional domain during this stage was confined to the Sable Subbasin as sediments rolled basinward into the basin and onto the inflated silicone massif (Er3a; Figure 5.16). As sediments prograded basinward, silicone from the silicone-cored fold flowed out as large silicone tongues (ST; Figure 5.16). Mild contraction took place in the deep basin accommodated by silicone-cored folding that moved to the seaward limit of the basin (Figure 5.16).

Sequential section restoration for Experiment 2

Figure 5.17 displays the sequential restoration of a representative shelf-slope Experiment 2 cross-section (35 cm). The cross-section was restored over 24 hr and 48 hr time intervals and, as with Experiment 1, referenced to topographic surface profiles deduced from the 3D digital elevation models for each restoration step (Figure 5.15; Figure 5.16). Horizontal strain, vertical displacement and horizontal displacement were all used to aid in the restoration of Experiment 2 (Figure 5.13; Figure 5.14).

24 hours - Initial post-salt sedimentation and early basin development

Sedimentation was initially confined to the Abenaki Graben (represented by the landward tapering wedge (LTW)) that started early silicone withdrawal from the proximal basin. A salt roller system (Sr1) developed close to the landward limit of the silicone basin via passive downbuilding of early sediments in the proximal graben (24 hr; Figure 5.17). Subsiding sediments and silicone withdrawal created a single depocentre (Sw1) (24 hr; Figure 5.17). Concurrently, minor inflation of silicone over the mid-basin high took place as sediments downbuilt and evacuated silicone onto the high.

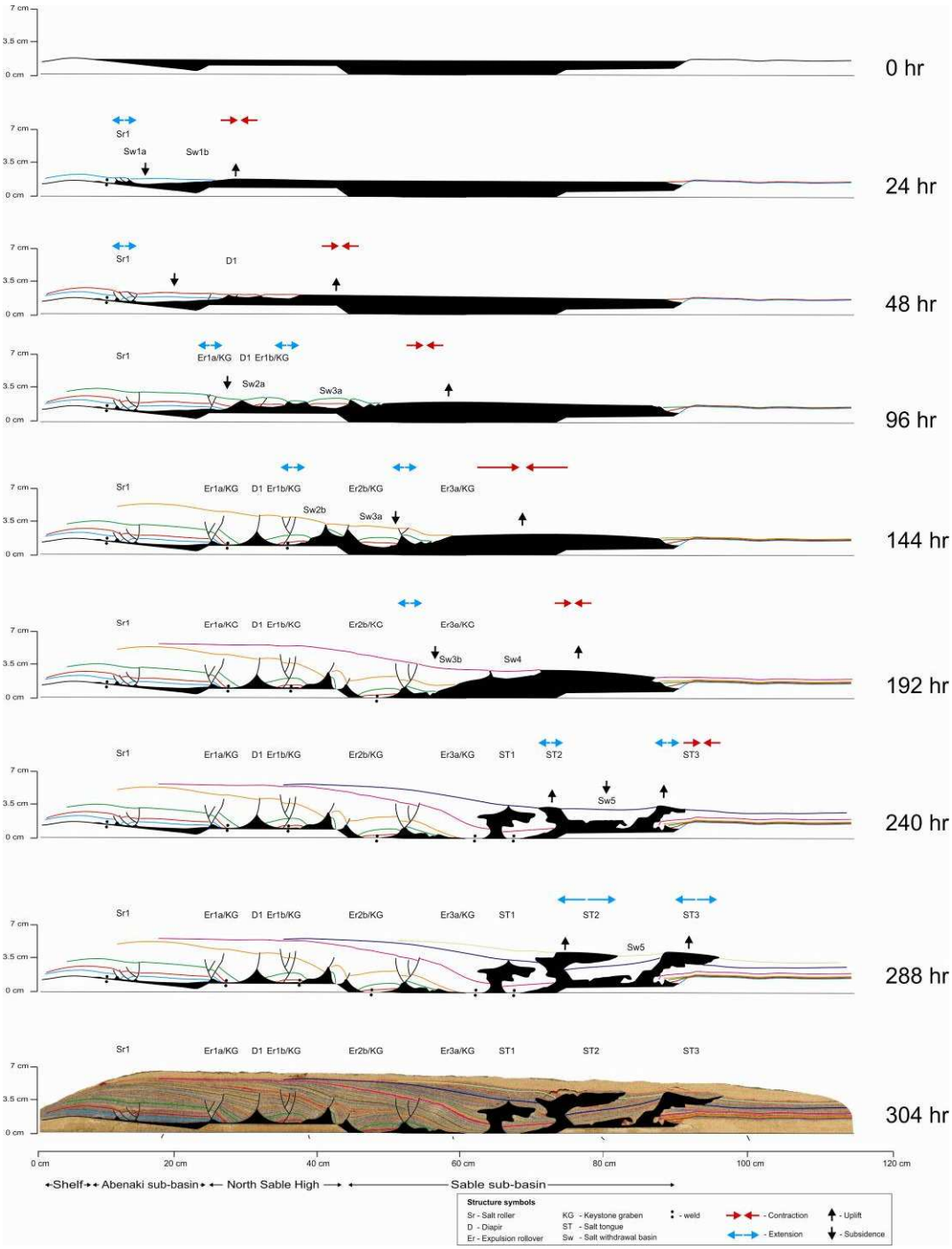

Figure 5.17 Sequential restoration of the central (35 cm) cross-section of Experiment 2 based on topographic profiles of model surface and incremental DIC strain and displacement data (Appendix B). Early model evolution is restored for 24 hour periods, while later model evolution restores horizons approximately 48 hours. Active and subsiding salt withdrawal basins are labelled Sw. Silicone structures are black and include diapirs (D), rollers (Sr), expulsion rollovers (Er), keystone grabens (KG) and silicone tongues (ST) (Larger restoration found in Appendix E on CD).

48 hours – Aggradation and continued subsidence within tapering wedge

Deposition of sediments continued facilitating the silicone to evacuate from the LTW onto the basin high. Sediments also began to deposit over the high as silicone later evacuated basinward. At the proximal edge of the basin, Sr1 continued to develop as sediments rotated along the fault planes (48 hr; Figure 5.17). Strong localized extension over the high permitted the development of D1 (48 hr; Figure 5.17) with concurrent high translation of silicone onto the high. Updip extension was balanced by contraction and minor uplift within the Sable Subbasin (48 hr; Figure 5.17).

96 hours – Initial welding and diapir formation over basin high

Initial welding took place within the landward tapering wedge (LTW) representing the Abenaki Graben by the 96 hour mark, as sediments along the Sr1 rotated and subsided to the basin floor (96 hr; Figure 5.17). This loading within the LTW allowed silicone to continue expulsion onto the high and into the distal basin. Over the high, diapir D1 grew passively as expulsion rollovers developed along the diapir flanks (Er1a/KG, Er1b/KG). Approximately 4 cm of translation occurred over the high, as a package of sediments (Sw3a) was “piggy-backed” to the edge of the high as the silicone migrated across the high into the Sable Subbasin (Figure 5.17). As the silicone evacuated from the proximal basin and basement high into the distal basin, silicone inflation was observed largely in front of the distal basin step as a series of contractional fold belts.

144 hours – Progradation of the sedimentary wedge and expulsion rollover/keystone graben formation in the distal symmetric graben with basin step

As sediments prograded and silicone evacuated from over the high into the distal basin, subsiding sediments over the high were welded to its top (144 hr; Figure 5.17). Sw3a continued to translate and subside into the Sable Subbasin as sediment progradation continued. A large basinward-dipping expulsion rollover system with an associated keystone graben system (Er3a/KG) began to evolve at this time within the subbasin (144 hr; Figure 5.17). The rotating and subsiding sediments continued to drive seaward migration of silicone with the main inflation occurring in front of the basin step. The basin step effectively pinned the inflated silicone in this position during this time.

192 hours – Initial welding and continued evolution of the expulsion rollover/keystone graben system formation in the distal symmetric graben with basin step

During this time, deformation was now focussed within the Sable Subbasin. Sediment package Sw3a subsided and welded to the basin floor (192 hr; Figure 5.17). The large expulsion rollover system (Er3a/KG) continued to evolve as sediment rotated and subsided into the flank of the inlated silicone (192 hr; Figure 5.17). The rotating and subsiding sediments continued to drive seaward migration of silicone, with inflation mainly occurring over the basin step.

240 hours – Initial development of allochthonous salt tongues

Welding within the distal basin continued as sediments downbuilt to the basin floor. Er3a/KG continued to evolve as this time as sediment rotated into the landward flank of the inflated silicone (240 hr; Figure 5.17). As the silicone withdrawal basin (Sw4) translated basinward and subsided, a silicone tongue (ST1) developed along the

experiment surface. The tongue shutdown as sediments along its flanks welded and sedimentation overran the seaward spreading tongue (240 hr; Figure 5.17). A package of sediments (Sw5) subsided over the basin step and two silicone tongues began to develop. ST2 began to spread landward as sediments rotated and subsided into it landward flank. ST3 spread seaward as the silicone extruded onto the surface.

288 hours – Continued salt tongue development and system shutdown

By 288 hours, ST2 and ST3 both spread seaward as the strata along the flank continued to subside (288 hr; Figure 5.17). Subsiding sediments along the flanks of the feeders extruded silicone along the experiment surface until the system shutdown.

5.7 Comparison between experiments 1 and 2

Differences in the salt tectonic evolutions between experiment 1 and 2 are primarily attributed to a slight adjustment in the initial basin morphology. A prominent feature along the mid-basin high in Experiment 1 was the extensive basinward dipping expulsion rollover system (Er2a/KG). As in nature with salt, the thin silicone over the high (1 km) does favour high extension but along the ION GXT Line 1800 transect, this extension was accommodated by a basinward-dipping growth fault system and not an expulsion rollover system as observed in the experiment. As observed in earlier experiments, this difference in evolution can be attributed to a slight change in salt (silicone) thickness (Krezsek et. al 2007). Specifically, slightly thinner salt (silicone) will favour a basinward-dipping growth fault system as opposed to an expulsion rollover system. Silicone evacuated from the proximal landward tapering wedge onto the high during the initial experiment evolution effectively favoured the evolution of the rollover

system (Er2a/KG). Besides this discrepancy, the experiment succeeded in evolving very similarly to the natural prototype as observed in Line 1800 including the extensive allochthonous salt-tongue canopy system.

In order to try and produce an experiment more closely related to the natural prototype, minor adjustments in the initial basin morphology were implemented for Experiment 2. The mid-basin high was changed from a thickness of 1 cm to 1.5cm thus leaving only 0.5 cm of silicone over the high for the initial setup. This adjustment influenced the evolution of the experiment by creating listric faulting over the high as sediment prograded into the distal basin as observed in the Line 1800 instead of the extensive rollover system created during Experiment 1.

5.8 Comparison between experiments and nature

The results both experiments reveal strong similarities to nature as observed in ION-GXT line 1800 from the early-post rift sediment input and downbuilding, to the late-post rift salt tongue canopy system. The types and location of structures also show good correlation when comparing the experiments to nature. Despite clear similarities between the experiments and nature, differences do occur and are important to include. The 35 cm section slice from Experiment 1 and the 35 cm section from Experiment 2 are used to compare these similarities and differences to nature represented by Line 1800.

5.8.1 Similarities between the experiments and nature

The following section compares the similar structures observed in the natural prototype with structures observed in the sections from Experiment 1 and 2 from the landward margin to the deepwater region.

Initial silicone withdrawal basin

As observed within the Early – Middle Jurassic Mohican Formation and Scatarie Member (Abenaki Formation) in the NovaSPAN Line 1800, the initial withdrawal basins within the experiments were focussed within the Abenaki Graben. As initial loading caused salt mobilization, sediments downbuilt into the subbasin as salt extruded onto the high. The downbuilding sediments created depocentres within the Abenaki Graben referred to Sw1 and Sw2a (Figure 5.6) within Experiment 1, and Sw1a and Sw1b within Experiment 2 (Figure 5.12).

Extensional zone over high

Although Experiment 1 is defined by a prominent rollover structure (Er2a; Figure 5.6) over the high with vertical beds instead of several slightly rotated listric faulted blocks as observed in Experiment 2 (Figure 5.12) and NovaSPAN Line 1800, all are representative of structures defining high extension and thinner salt over the high. The change in structures is attributed to Experiment 1 having slightly more silicone over the high, which favoured the expulsion rollover structure. In both the experiments, as with what is expected with nature, these structures indicate high translation of sediments occurred as they were deposited within the Middle and Late Jurassic.

Distal salt diapirs and associated depocentres

Both Experiment 1 and 2 display salt diapirs within the simulated Sable Subbasin as observed in NovaSPAN Line 1800. In the central sections of both experiments, the diapirs are referred to as D2. These diapirs evolved passively in the mid stages of experiment evolution through differential loading as prograding sediments translated

basinward. Extension was accommodated as the ridges of the diapirs broadened, focusing sediments to deposit along the diapir flanks (Sw3b; Figure 5.6 and; Sw3a, Sw3b; Figure 5.12). Within Line 1800, several diapirs exist in this area as the process repeated while sediments began to prograde out into the Sable Subbasin from the Late Jurassic to Early Cretaceous.

Distal expulsion rollover system and associated depocentres

Experiments 1 and 2 both include expulsion rollover systems that sole out onto the silicone tongue canopy feeders as observed in NovaSPAN Line 1800. In Experiment 1 this is identified as Er4, and in Experiment 2 as Er3. These rollover systems evolved as silicone evacuated from the basin and inflated over the basin step until flowing onto the surface as large silicone tongues.

As the sediments rotated into the feeders, silicone withdrawal basins were created in the experiments as observed in Line 1800. In Experiment 1, the withdrawal basin is referred to as Sw4 (Figure 5.6), while in Experiment 2 it is associated with Sw3 (Figure 5.12). As in nature, the rotating and subsiding basins created depositional lows leading to increased accommodation space for prograding sediments and thus continuing the evolution of the expulsion rollover system.

Silicone tongue canopy system (ST)

A prominent feature in the study area is the extensive allochthonous salt tongue-canopy system located throughout the modern day slope with an associated feeder located above the basin step. This salt tongue-canopy system played a significant role in the late stage basin development, as deformation became focused in the slope area. Both

Experiments 1 and 2 produced large silicone tongue-canopy systems in the distal basin with feeders associated with the basin step area. The basin step in both experiments confined silicone inflation to just before the step while pelagic sediments also pinned the inflated silicone until reduced sedimentation rates allowed the silicone to reach the surface and flow onto the experiment surface as silicone tongue complexes. In both the experiments, and as observed in the seismic transect, the reduced rate sedimentation predominately occurred during the Early Cretaceous Logan Canyon Formation.

5.8.2 Differences between the experiments and nature

Expulsion rollover system (Er2a/KG)

As explained in Section 5.9.1, although both the experiments indicate high extension occurred over the North Sable High, Experiment 1 evolved slightly differently with a large expulsion rollover system (Er2a; Figure 5.6). This difference is attributed to high having less original salt in place then originally interpreted. With the adjustment from 1 cm to 0.5 cm original silicone in place, Experiment 2 yielded results more reflective of the basinward-dipping listric fault system observed in NovaSPAN Line 1800.

Extent of the salt tongue-canopy system

Both Experiment 1 and 2 succeeded in producing tongue-canopy systems as observed in NovaSPAN Line 1800. The major difference between the experimental and natural system appears to be the respective extents of the tongues. While NovaSPAN Line 1800 shows a tongue approximately 80 km long, the extent of the tongues in both experiments are closer to 15 – 20 cm, or 15 – 20 km in nature (Figure 5.6; Figure 5.12). These

differences may be attributed more sediment loading occurring over the tongues to allow faster and further spreading in nature, or simply the presence of a more basinward feeder outside of section that resulted in a more basinward tongue coalescing with the tongue fed by the feeder system observed in Line 1800.

5.9 Relation to the evolution of the Abenaki and central Sable Subbasin from experiment results

Although modest differences do occur between the experiments and nature, both experiments have resulted in replicating very similar structures to those observed along the NocaSPAN Line 1800 transect across the Abenaki Graben and central Sable Subbasin. These experiments can therefore provide insight into the basin evolution of the area using the DIC data from both experiments summed up over the main formation intervals through their evolution. Through summation, the data provides insights regarding deformation that occurred throughout each formation's deposition and burial history and hence a better understanding of the evolution of the Abenaki Graben and central Sable Subbasin region.

5.9.1 Scatarie Member and Mohican Formation (Early – Mid Jurassic)

As the experiments simulated the Early to Middle Jurassic early post-rift stage (Mohican Formation; Figure 5.18), subsidence began in the proximal wedge/Abenaki Graben with early sedimentation and subsequent minor, broad inflation occurring over the North Sable High (Vz-Mohican Formation; Figure 5.18). The horizontal displacement overlay indicates basinward translation of sediments across the Abenaki Graben and onto the high. Buckle folding occurs within the inflated silicone over the high as thinning over the high hinders basinward flow of extruding silicone from the Abenaki Graben.

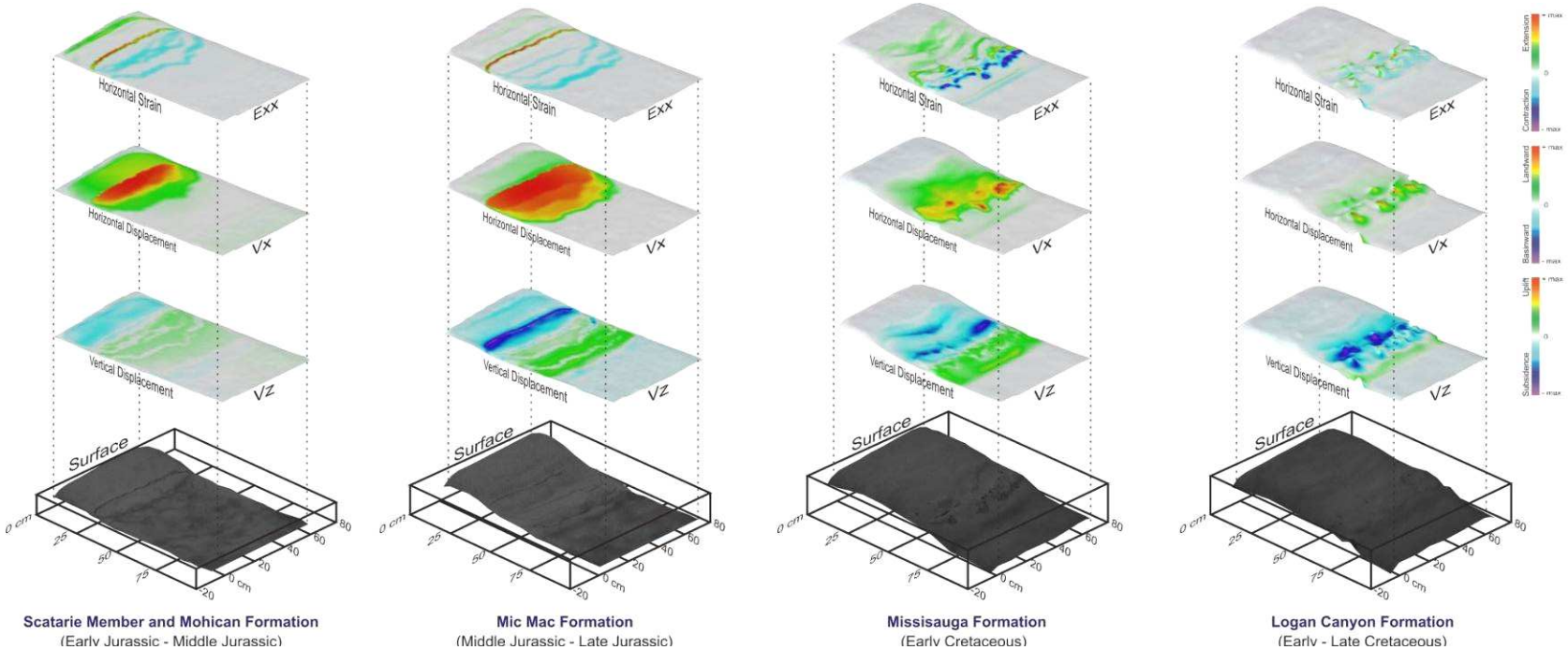

Figure 5.18 Temporal evolution of the Experiment 1 simulating the salt basin evolution of the Abenaki Graben and central Sable Subbasin for formation intervals. The 3D surface intervals include overlays of horizontal strain (Exx), horizontal displacement (Vx), vertical displacement data (Vz). Incremental strain and displacement components obtained by 3D DIC monitoring are summarized for each formation and overlain on the model surface to visualize deformation trends for each interval.

5.9.2 Mic Mac Formation (Mid – Late Jurassic)

From the Mid to Late Jurassic, high subsidence occurred within the basinward portion of the Abenaki Graben as sediments from the Mic Mac Formation were deposited (Figure 5.18). Broad inflation occurred within the mid Sable Subbasin in front of the high as silicone flowed from the high. Across the high, very little vertical displacement occurs as silicone, extruding from the Abenaki Graben, is kept in balance with silicone flowing from the high to the Sable Subbasin. As the silicone flowed across the high, basin-directed strong translation of sediments occurred. Buckle folding is observed with the horizontal strain data, and occurs within the inflated silicone in the Sable Subbasin.

5.9.3 Missisauga Formation (Early Cretaceous)

During the Early Cretaceous, progradation of sediments into the Sable Subbasin effectively evacuated silicone and trapped the remaining silicone within the Abenaki Graben and the landward portion of the North Sable High. This essentially shut down the salt system in that area (Figure 5.18). Silicone inflation translated basinward to above the basin step as subsidence occurred within the landward portion of the Sable Subbasin. As the system's landward portion shutdown, deformation focused mainly within the Sable Subbasin with active keystone grabens and passive diapirs developed and created localized topographic highs and depocentres.

5.9.4 Logan Canyon Formation (Early – Late Cretaceous)

From the Early to Late Cretaceous, the deformation focused on the evolution of the allochthonous silicone tongue-canopy system as the rest of the system welded-out and shut down within the Sable Subbasin (Figure 5.18). Basinward translation took place as the passive diapirs began to flow onto the surface as large silicone tongues. Localized depocentres continued to develop as subsidence landward of the silicone tongue feeders continued.

CHAPTER 6: Evolution of the Abenaki Graben and the central Sable Subbasin

The cross-sections of the completed experiments reveal comparable structural and depositional characteristics to those of the regional seismic data across the Abenaki Graben and central Sable Subbasin (Figure 6.1). The comparable end-member results displayed by the experiments reflect similar tectono-stratigraphic evolutions to the observed natural prototype. Using the realistic parameters described in Chapter 5, the experiment sections reproduced similar structures to those easily observable in the preliminary seismic interpretation, thus reflecting similar tectono-stratigraphic evolutions to the observed natural system. Therefore, results and kinematic concepts can be used to support interpretation of the deeper and less-well imaged parts of the section. Time-series data from the experiments provides valuable insights into the underlying geological processes and guide the investigation of the main control factors of post-rift basin evolution in this segment of the Scotian margin.

The experiments provide insights into the dynamics of key salt and fault structures and related depositional systems of the central Sable Subbasin. This includes a zone of normal faulting over the North Sable High (NSH), trapped salt within the distal part of the subbasin, and an extensive allochthonous tongue-canopy system as discussed in Chapter 5. As for the similarities of key depositional features, a significant correlation between the relative timing of depocentre migration and major silicone mobilization within the experiments can be observed in relation to the stratigraphic time constraints deduced from the regional seismic interpretation. Thus, the experiment results provide valuable insight into the basin history and kinematic evolution of the Abenaki Graben and central Sable Subbasin and their governing salt tectonic processes. The following chapter

focuses on the application and synthesis of the experiment and seismic interpretation results to gain insight into the tectono-stratigraphic and salt tectonic evolution of the Abenaki Graben and central Sable Subbasin and their relation to the regional basin history of the north-central Scotian margin.

6.1 Kinematic segmentation of the Abenaki graben and central Sable Subbasin

The kinematic domains between the experiments and seismic data display close similarities (Figure 6.1) and therefore can be used to discuss and compare the salt and silicone structures and related depositional structures. Both the experiments and seismic data indicate four main kinematic salt tectonic domains from the shelf to the deepwater basin:

1. Salt weld and pillow domain
2. Normal fault and reactive diapir domain
3. Passive diapir and expulsion rollover domain
4. Contractional salt and allochthonous salt tongue-canopy domain

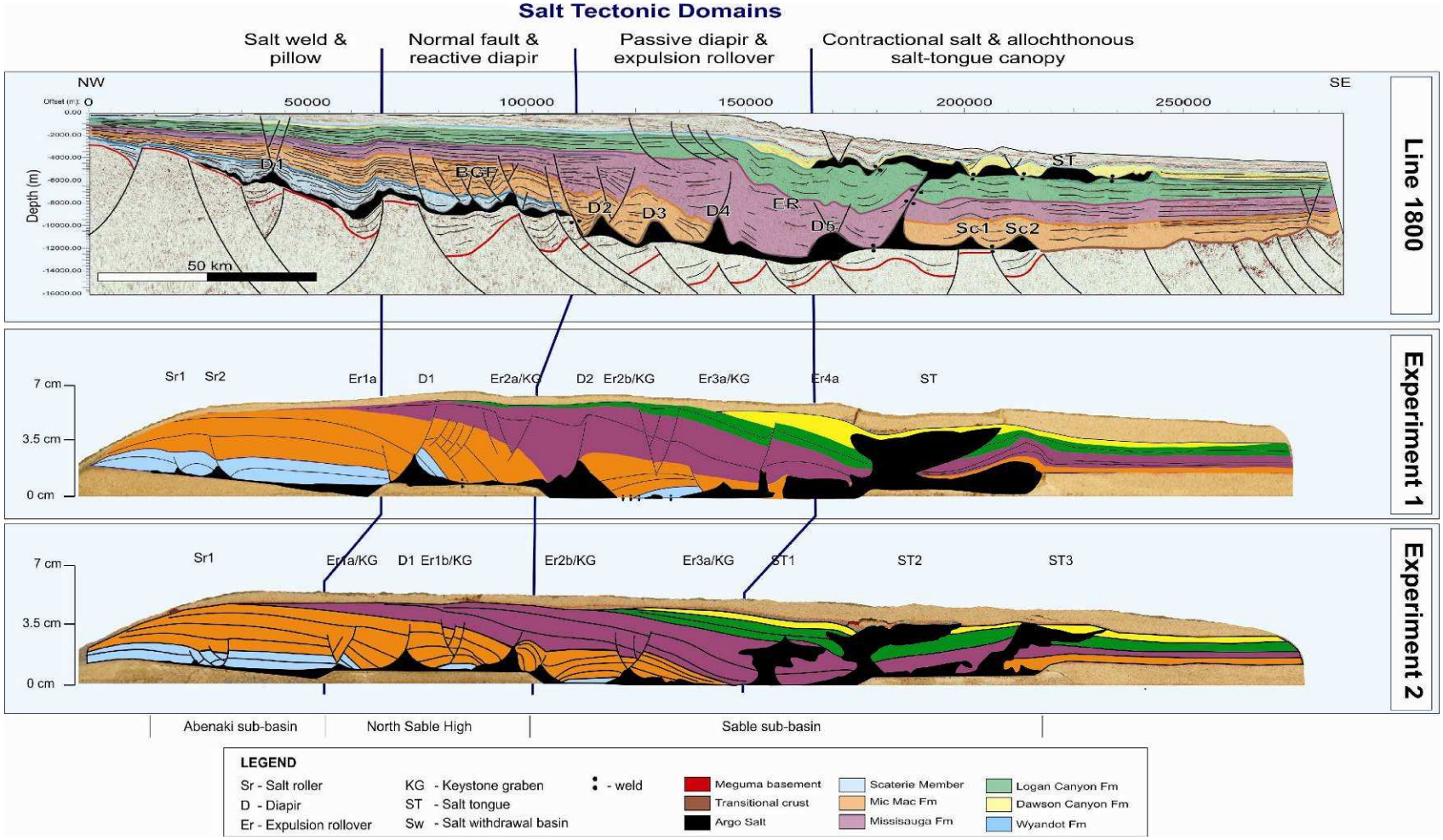

Figure 6.1 Comparison of NovaSPAN Line 1800 with center sections from Experiments 1 and 2. The area has been segmented into four kinematic domains: 1) Salt weld and pillow domain; 2) Normal fault and reactive diapir domain; 3) Passive diapir and expulsion rollover domain; and 4) Contractional salt & allochthonous salt-tongue canopy domain. Features indicated on sections are detailed in the text.

6.1.1 Salt weld and pillow domain

In the seismic data, the *salt weld and pillow domain* extends approximately 50 km from the hinge zone to the basinward limit of the Abenaki Graben. The domain is characterized by small salt pillows and remnant salt trapped within the graben. Major deformation of Early – Middle Jurassic sediment packages above the salt structures indicates the structures of this domain developed in the early post-rift stage of the basin evolution as sediment was downbuilding and seaward-directed salt withdrawal occurred.

In the analog experiments, this domain extends 20 cm across the simulated Abenaki Graben in experiment 1, and 15 cm across in Experiment 2. Within the experiments, the domain consists of trapped remnant silicone within the landward tapering wedge (Abenaki Graben). The *salt weld and pillow domain* developed from 0 – 96 hr as early post-rift sediment input along the basin margin. This led to sediment downbuilding and subsidence as silicone extruded seaward onto the high and later into the central Sable Subbasin. Eventually, deformation ceased within the domain by 96 hr as sediments welded to the basin floor following silicone evacuation and left trapped salt/silicone in the form of silicone pillows and small diapirs.

6.1.2 Normal fault and reactive diapir domain

The *normal fault and reactive diapir domain* observed in the seismic data occurs above the NSH and separates the Abenaki Graben and Sable Subbasin and associated salt structures. It is characterized by triangular reactive salt diapirs trapped in the footwalls of basinward-dipping normal faults across the 50 km NW-SE extent of the NSH. The salt structures in this domain primarily developed during the Middle to Late Jurassic (Mic

Mac Formation) with minor deformation occurring early in the Lower Cretaceous as sedimentation over the NSH waned.

In the analog experiments, this domain also extends across the simulated North Sable High (NSH) and consists of trapped silicone, welded sediments and rotated fault blocks over the high (NSH). Experiment time-series strain data indicate this domain developed from 96 – 156 hr in experiment time. The *normal fault and reactive diapir domain* developed as sediments prograded and downbuilt across the thinner silicone over the high causing shear flow in the silicone layer with high mechanical coupling and high extension within the overburden. This resulted in normal faulting in the overburden over the high, as silicone was further evacuated into the Sable Subbasin. Eventually, in the early Cretaceous, welding of overburden fault blocks occurred, leaving trapped salt/silicone in the form of salt/silicone pillows and small diapirs.

6.1.3 Passive diapir and expulsion rollover domain

The diapir and rollover domain extends 75 km from the landward limit of the Sable Subbasin to the step of the basin floor in the central part of the subbasin (Figure 6.1). The domain consists of several extensional diapirs and a long-lived expulsion rollover system within the subbasin. The diapirs (D2 – D5) range from 2 – 4 km in height and from 10 – 15 km in width at their base separated by depocentres that welded to the basin floor. Both experiments also developed the same domain extending 30 cm from the landward portion of the simulated Sable Subbasin to its basinward step with the creation of extensional diapirs there; e.g. D2 and D3 within Experiment 1 and ST1 within Experiment 2.

Theses diapirs formed passively from the Mid Jurassic to Early Cretaceous as prograding sediments translated basinward due to differential loading. Extension was accommodated in the diapir axes creating wide diapir ridges. Because the diapirs formed dynamic topographic highs, sediment deposition was channelled along their flanks and in the subsiding lows of the adjacent withdrawal basins between them. As sediments continued to prograde into the Sable Subbasin, they were deposited along the landward limit of the inflated massif (D2, D3, and D4 in Figure 6.1). The prograding sediments formed a broad basinward-dipping expulsion rollover (Er in Figure 6.1) system as salt extrusion allowed sediments to downbuild and rotate into the basinward flank of the salt feeder system.

6.1.4 Contractional salt and allochthonous salt tongue-canopy domain

In NovaSPAN Line 1800, the *contractional salt and allochthonous Late Cretaceous salt tongue-canopy domain* is approximately 80 km wide and extends more than 25 km seaward of the original salt basin (ST in Figure 6.1). Sediments deposited on top of the salt tongue canopy system lead to the Late Cretaceous formation of mini-basins and turtle structures as salt extruded along the seafloor. In the experiments, the silicone tongue-canopy systems also formed as individual tongues and spread as much as 20 cm along the surface in seaward direction (Figure 6.1).

The salt tongue-canopy system developed initially in the Late Cretaceous as sediments prograded on the inflated salt massif that formed above the basin step in the central Sable Subbasin. The basin step acted as a buttress confining early salt inflation to the central basin instead allowing further extrusion towards the seaward basin margin. This mid-basin inflation favoured the deposition of deepwater sediments seaward of the

inflated salt massif in the distal Sable basin and out onto the top of the transitional oceanic crust. These pelagic sediments further buttressed the salt from extruding basinward as the diapirs and inflated salt translated basinward from the Early Cretaceous. Later landward uplift of the margin in the Tertiary caused contraction of the overburden sediments resulting in vertical welding of salt feeders and the development of the salt cored folds in the deep basin (Sc1, Sc2 in Figure 6.1). As sea level rose, a reduction of sediment deposition allowed salt within the diapirs in the deep basin to extrude and spread along the seafloor as large salt tongues while sediments continued to downbuild into the basin. Eventually, these salt tongues coalesced to form extensive salt tongue-canopies.

6.2 Improvement of preliminary seismic interpretation of NovaSPAN Line 1800 using experiment results

Kinematic concepts and depocentre patterns derived from the Experiments 1 and 2 were used to improve understanding of the tectono-stratigraphic evolution of the Abenaki Graben and central Sable Subbasin. These concepts were used to better constrain the seismic interpretation in the poorly imaged areas of NovaSPAN Line 1800. The main areas with significant imaging problems include the salt basin floor and deep salt structures located beneath the modern day slope as discussed in Chapter 4 (see Figure 6.1).

6.2.1 Geometry of the salt basin floor

The original salt basin geometry for Experiment 1 implemented concepts discussed in Chapter 5 from previous work by Campbell (2007) and MacDonald (2007) in regards to salt thickness over the North Sable High (NSH). In the seismic section, the

large amount of extension in the overburden accommodated by the basinward dipping growth faults over the NSH indicates a thin original salt layer over the high (approximately ≤ 1 km). The structural evolution above the high in Experiment 1 instead consisted of an extensive expulsion rollover system (ER) that is generally caused by thicker (~1.5 km) salt in place (Krezsek et al. 2007). The resulting structural style indicated that early silicone extrusion from the landward subbasin and subsequent inflation over the high prior to sediment progradation was sufficient to create a slightly thicker salt layer. Consequently, in Experiment 1, when sediments prograded on top of the inflated silicone layer over the high, the thicker salt favoured the evolution of an ER instead of the BGF.

To consider the effect of early silicon inflation over the basement, the original thickness of silicone layer over the high was reduced to 0.5 cm for Experiment 2. Even with further inflation of this thin silicone layer, this resulted in high mechanical coupling and fault-controlled extension as sediments prograded over the inflated salt above the high. This structural style was more closely related to the observations in NovaSPAN Line 1800 and strongly support the interpretation that approximately ≤0.5 km of salt was initially in place over the NSH.

6.2.2 Primary salt structures in the deep basin

Salt structures located in the deeper levels of the section beneath the slope are difficult to interpret on NovaSPAN line 1800. Preliminary seismic interpretation including dip domain analysis of coherent reflectors (Figure 4.10) indicates the presence of deep salt structures. Due to the similar seismic velocities of salt and sediments at this depth, imaging and mapping of their size and dimensions was difficult. With the

application of structural patterns and kinematic concepts derived from Experiments 1 and 2, additional constraints and templates can be used to identify the salt structures and to map their geometries in the deeper part of the Sable Subbasin.

Experiment results support the presence of passive diapirs (D2, D3, D4, and D5) within the deep Sable Subbasin (Figure 6.1). These diapirs have a typical triangular shape (in the dip direction) and formed through extension of the sedimentary wedge. Salt flow in the diapirs created localised depocentres between the passive diapirs. With sedimentation progradation and continued silicone withdrawal, these depocentres developed into salt-withdrawal basins and expulsion rollovers were subsequently were translated basinward. The diapirs eventually shutdown as the intervening salt-withdrawal basins welded to the basin floor.

Insights from the experiments and dip domains taken from sparse coherent seismic horizons indicate similar geometries of salt structures in the deep Sable Subbasin. As both experiments and the natural prototype show similar features, structural pattern and sediment distribution features observed in the experiment can be reasonably transferred to the natural example. This then provides a realistic tectono-stratigraphic concept and kinematic model for the interpretation of the seismic section particular in areas with poor imaging.

6.2.3 Seaward translation of depocentres

An important result deduced from the evolution of Experiments 1 and 2 is the significant basinward translation of early post-rift rafted sediment packages over the high into the Sable Subbasin (see Chapter 5). In the experiments, extension of the early post-rift sediment wedge resulted in the formation of passive silicone diapirs that divided the

landward basins into separate depocentres. These depocentres subsided and translated basinward, and developed into silicone withdrawal basins. It is important to note however that this extensive early translation of sediments within the experiments is partially amplified by the density ratio of the analogue materials causing slightly higher strain rates than expected in the natural prototype (Chapter 5.2). This difference is attributed to a higher density contrast between the silicone polymer and silica sand than compared to halite and clastic sediments. Despite the slightly higher strain rates in the experiment the translation of sediment packages during the early post-rift stage of basin evolution may have occurred within the Abenaki and central Sable Subbasin portion of the Scotian margin on the same or slightly smaller scale.

Interpretation of the areal extent of the Middle Jurassic Mohican Formation and Scatarie Member and their deepwater equivalents in NovaSPAN Line 1800 becomes difficult seaward of the NSH due to discontinuous seismic horizon markers caused by faulting and salt deformation. Results from the experiments indicate that translation of rafted sediments due to extension over the high may have lead to Scatarie/Mohican sediments translating across the high into the Sable Subbasin (Figure 6.1).

6.3 Post-rift evolution of the Abenaki graben and central Sable Subbasin

The interpretation of NovaSPAN Line 1800 and constraints from the physical experiments demonstrate that the tectono-stratigraphic evolution of the Abenaki Graben and central Sable Subbasin has been directly influenced by three main controlling factors: the variable morphology of the salt basin floor, original salt thickness with up to 2 km of salt in place, and the variable sediment input from the Jurassic to Cretaceous time.

The experiment results indicate the following 1st order parameters in the evolution of the area:

1. High rates of sedimentation (Late Jurassic – Early Cretaceous) followed by low rates (Early – Late Cretaceous)
2. A variable basin morphology consisting of a landward tapering wedge, mid-basin high, and symmetrical salt basin with basement step (A, Figure 6.2a).

Combining results from the seismic interpretation discussed in Chapter 4 with the detailed experiment results presented in Chapter 5 (i.e. balanced cross-sections and time series data) enables a conceptual reconstruction of the tectono-stratigraphic evolution for the study area (Figure 6.2a and 6.2b).

6.3.1 Early post-rift salt mobilization and depocentre formation (Early – Middle Jurassic) – B, Figure 6.2a

Deposition of the Early to Middle Jurassic Scatarie Member and Mohican Formation in the Abenaki Graben initiated salt mobilisation with downbuilding and subsidence (B, Figure 6.2a). Seaward-directed salt withdrawal caused salt extrusion and inflation onto the high and into the Sable Subbasin.

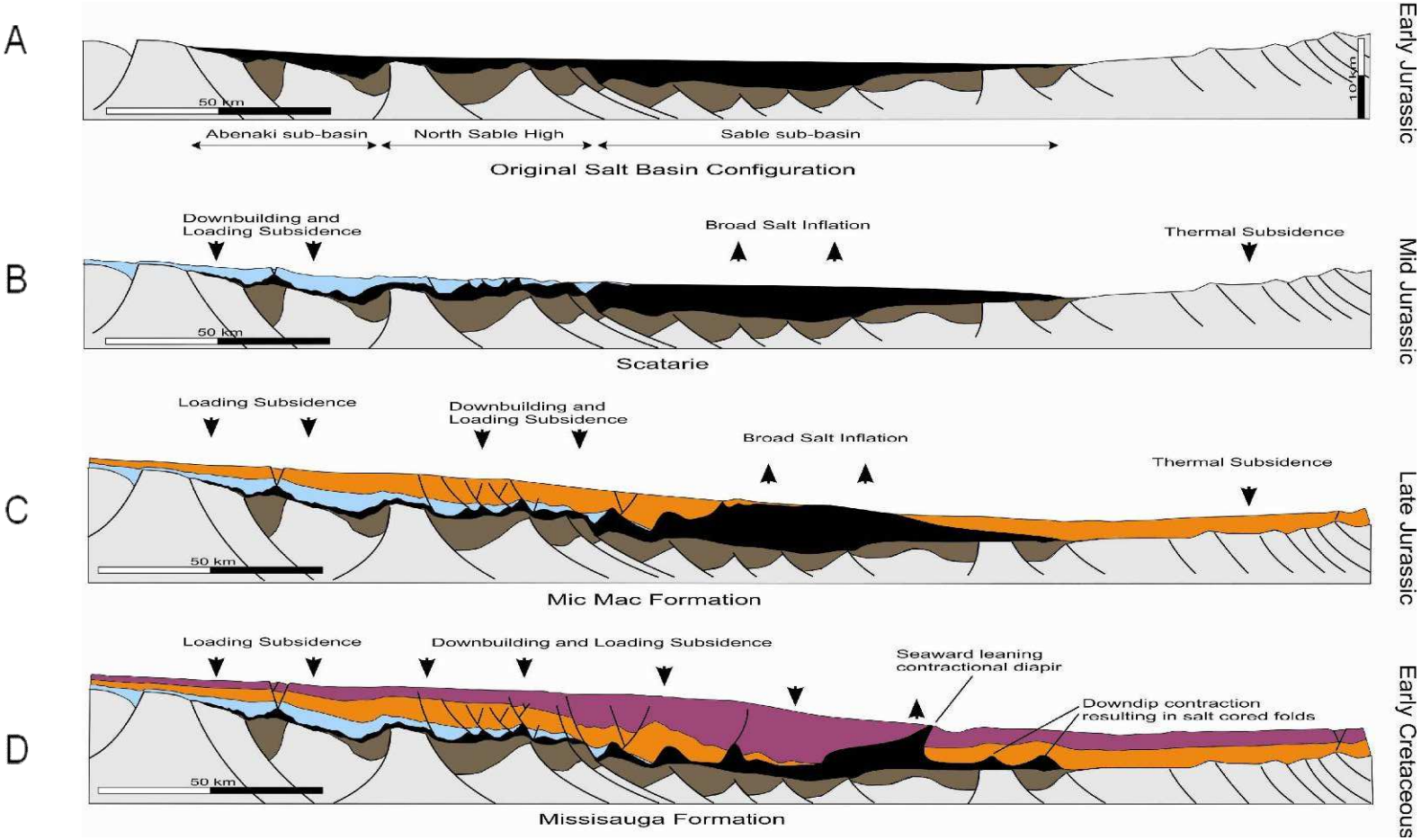

Figure 6.2a Conceptual reconstruction of the structural evolution of the Abenaki Graben and central Sable Subbbasin based on NovaSPAN Line 1800 from the Early Jurassic to the Early Cretaceous. The reconstruction includes: A) Simplified Early Jurassic salt basin configuration of a landward-tapering wedge, intermediate high and symmetric basin with step. B) Middle Jurassic sedimentation of the Mohican Formation and Scatarie Member and deepwater equivalents downbuilding while causing broad seaward salt inflation. C) Late Jurassic sedimentation of the thick Mic Mac Formation and deepwater equivalents downbuilding while salt inflates over the step. D) Early Cretaceous Mississauga Formation sediments and deepwater equivalents driving salt seaward as welding occurs within the proximal basin.

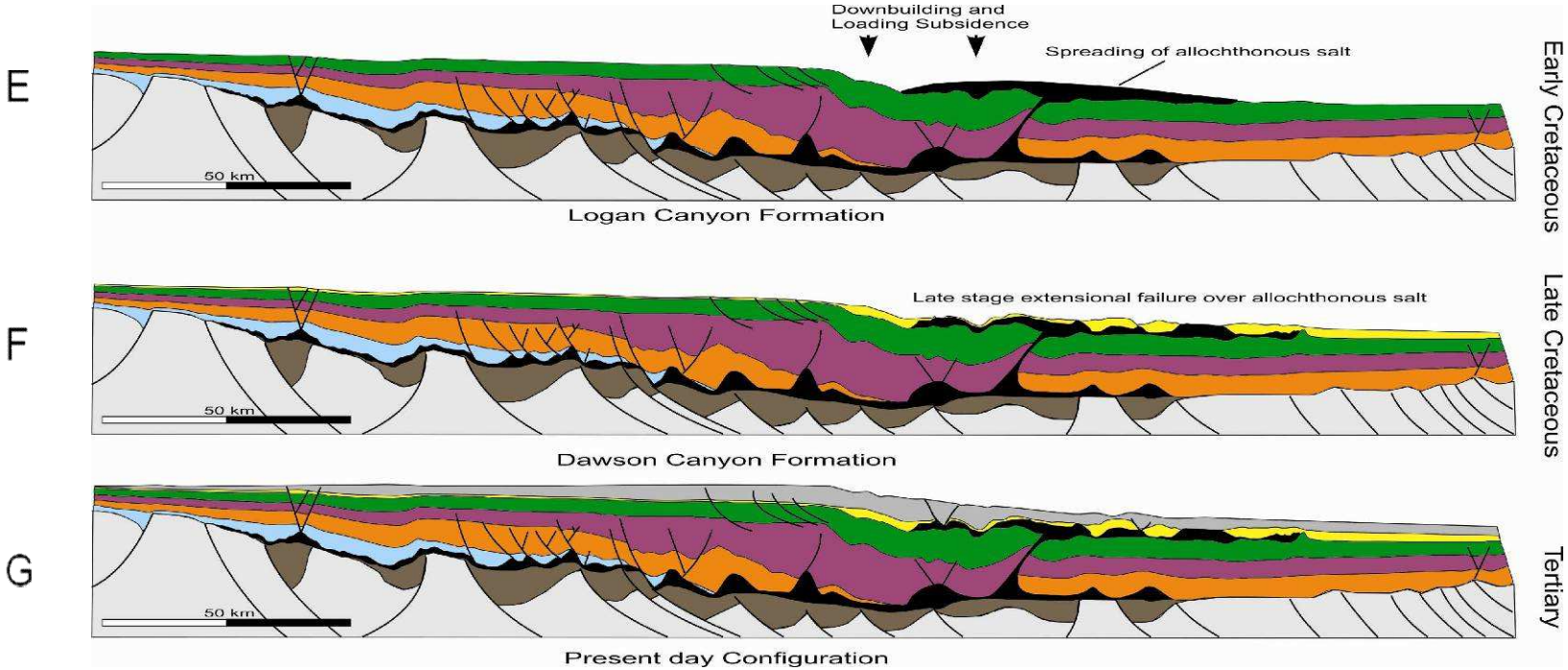

Figure 6.2b Conceptual reconstruction of the structural evolution of the Abneaki Graben and central Sable Subbbasin based on NovaSPAN Line 1800 from the Early Cretaceous to the present day. The reconstruction includes: E) Late Cretaceous reduction in sedimentation of the Logan Canyon Formation and deepwater equivalents allowing salt to extrude onto the surface as large salt tongues. F) Continued reduction of sedimentation of the Late Cretaceous Dawson Canyon Formation allowing for salt tongues to coalesce as large salt tongue-canopies. G) Present day configuration of the eastern Scotian margin as interpreted from NovaSPAN Line 1800.

6.3.2 Continued downbuilding and salt inflation in the Sable basin (Middle – Late Jurassic) – C, Figure 6.2a

From the Middle to Late Jurassic, sediments prograded into the Sable-Subbasin, while in the Abenaki Graben and on the North Sable High (NSH), sediment downbuilding continued (C, Figure 6.2a). Extension caused by a series of basinward-dipping growth faults affected the sediments above the NSH as consequence of the thin underlying salt layer with dominant shear flow. Salt inflation in the central Sable Subbasin took place mainly mid-basin because the basement step hindered the flow of salt (C, Figure 6.2a). In the distal Sable Subbasin, deepwater sediments were deposited seaward of the inflated salt effectively hindering seaward salt extrusion and nappe formation.

6.3.3 Shallow and mid basin welding and evolution of distal rollover system (Late Jurassic - Early Cretaceous) – D, Figure 6.2a

From the Late Jurassic to Early Cretaceous, sediments within the Abenaki Graben began to weld to the basin floor trapping remnant salt (D, Figure 6.2a). At this time, salt tectonics was confined to the Sable Subbasin. Prograding sediments were trapped in the landward flank of the inflated salt massif forming a long-lived expulsion rollover. As a result of the continuous sediment down-building, the expulsion rollover translated basinward and caused further salt inflation over the basin step (D, Figure 6.2a).

6.3.4 Onset of allochthonous salt tongue system (Early – Late Cretaceous) – D,E, Figure 6.2a and 6.2b

From the Early to Late Cretaceous sediment input decreased due to sea level rise that trapped most deltaic sediments on the flooded shelf areas (D, Figure 6.2b; E, Figure 6.2b). Hemi-pelagic and pelagic clay-dominated sediments were deposited far out into the distal basin. The expulsion rollover system still developed and caused further salt

inflation. With diapir growth and inflation rates eventually exceeding distal sediment accumulation rates in the Late Cretaceous, salt extruded on the seafloor forming a large salt tongue system (E, Figure 6.2b).

6.3.5 Evolution of the allochthonous salt tongue-canopy system (Late Cretaceous) – F, Figure 6.2b

Following Cretaceous regional welding of the major Sable Subbasin salt-withdrawal basins, salt tectonics and mini-basin formation during the Late Cretaceous was restricted to the allochthonous canopy level (F, Figure 6.2b). In the slope, deposition was strongly controlled by the dynamic topography of the spreading salt tongues.

6.4 Conceptual paleogeographic and salt structural evolution of the north-central Scotian margin

The results from this study, as well as incorporating results with its co-projects provide new insights into the first-order control factors that govern the dramatic change of salt deformation styles from the salt nappe development and roho-style salt detachment (Banquereau Syn-kinematic Wedge (BSW)) of salt Subprovinces IV and V observed in Line 2000 and AGC Line 89-1 to the extensive salt tongue-canopy system of salt Subprovince III observed in NovaSPAN lines 1600 and 1800 (refer to Chapter 2).

Results from seismic interpretation and 4D analogue experiments from this study area (as discussed earlier in Chapters 4 & 5 and previous at the beginning of this chapter) combined with the results from its co-projects, (MacDonald 2009; Cribb 2009), demonstrate that the salt Subprovinces III, IV, and V of the Sable and Laurentian subbasins developed as a linked salt tectonic system along-strike of the north-central Scotian Basin despite each area showing different end member structural results (Figure

6.3). To illustrate the evolution of the Scotian margin, a series of paleogeographic maps have been produced that incorporate the results of regional seismic interpretation and time-series data of the analogue experiments (Figure 6.6 – Figure 6.10).

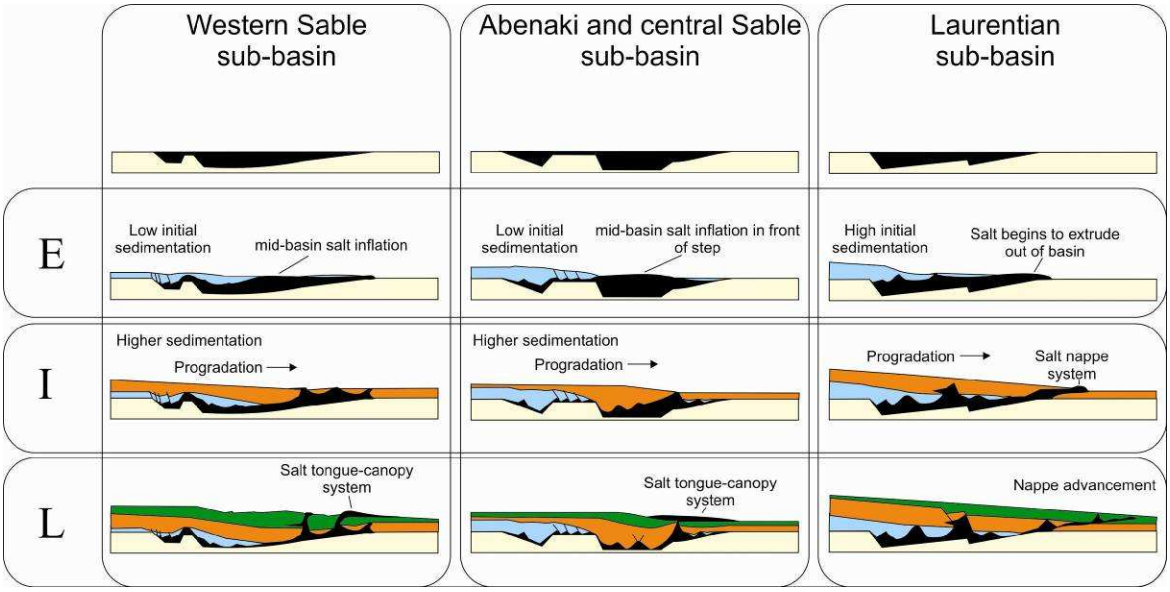

Figure 6.3 Early (E), Intermediate (I) and Late (L) stage evolutions for the Western Sable Subbasin (Line 1600), Abenaki and central Sable Subbasin (Line 1800) and the Laurentian Subbasin (Line 2000).

Paleogeographic maps incorporate:

1. Paleogeographic data of inferred deltas and major trends of sediment transport (Atlantic Geoscience Center 1991)
2. Results deduced from the regional ION-GXT NovaSPAN dataset and experiments including:
    a. Extent of the initial salt basin
    b. Depocentre distribution during different time intervals
    c. Temporal and spatial distribution of major salt structures from the Early Jurassic to Late Cretaceous.

6.4.1 Change in salt basin geometry along strike of North-Central Scotian Margin

The early post-rift salt basin of the north-central Scotian margin covered most of the rift basins from the hinge zone to the seaward limit of continental basement transitional continental crust (Figure 6.4). Thus, the morphology of the syn-rift salt basin is strongly dependent on the variable crustal structure along the margin and strongly controlled the salt thickness in the basin. Post-rift loading and crustal flexure have amplified the morphology of the overall original salt basin as observed on seismic profiles, but still reflect the general syn- and post-rift geometries of the basin floor.

Many similarities exist between the salt basin geometries of salt sub-province IV, e.g. GSC line 89-1, and sub-province V, e.g. NovaSPAN Line 2000 (Cribb 2009). Both seismic sections indicate salt basin geometries with an asymmetric basinward tapering wedge with a basin floor consisting of rift half grabens on rotated basement blocks and syn-rift sediments (Laurentian Subbasin, Figure 6.3). The hinge zone (rift shoulder) in these areas is very prominent with the basin floor dropping approximately 3 km. Further evidence of this basin shape is provided by the depth converted crustal profiles of SMART Line 1 which indicates an approximately 115 km wide seaward tapering basin wedge.

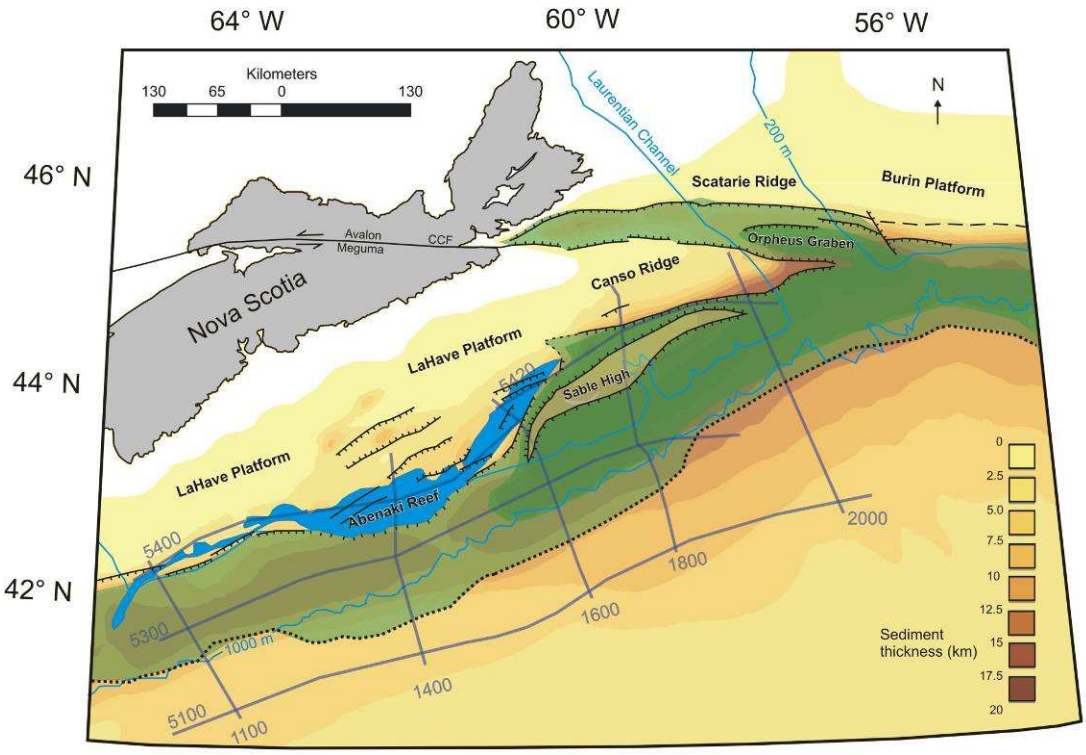

Figure 6.4 Estimated original Early Jurassic salt basin of the Scotian margin based off interpretation of regional seismic profiles (NovaSPAN, GSC).

In the central Sable Subbasin that incorporates the Salt Subprovince III, the salt basin geometry differs greatly from salt sub-province IV and V. The NovaSPAN 1800 transect indicates the salt basin was separated by the North Sable High in the Abenaki Graben and the main Sable Subbasin (Abenaki and central Sable Subbasin, Figure 6.3; Figure 6.4). Like the salt basins of Subprovinces IV and V, the salt basin floor consists of a series of rotated basement blocks and syn-rift fill. However, in Subprovince III, the salt basin does not consist of an overall seaward-tapering wedge geometry. Seaward of the NSH, the main Sable salt basin is a more symmetric basin with an intermediate basement step (Abenaki and central Sable Subbasin, Figure 6.3). Differing from the tapering wedge geometries of Subprovince III and IV, the deepest portion of the salt basin in Subprovince

III occurs within the distal Sable Subbasin and not directly seaward of the hinge zone close to the rift shoulder as observed in the Laurentian Subbasin (Figures 6.3; Figure 6.4).

Results of this study and co-projects adjust the basinward limit of early post-rift autochthonous salt (Figure 6.4) in comparison to previous studies (e.g., Shimeld 2004). Seismic interpretation of NovaSPAN Line 1800 from this study as well as Line 1600 from MacDonald (2009), show the seaward extent of the autochthonous salt basin within Salt Subprovince III is approximately 20 km beyond that observed from the previous interpretation (Figure 3.5; Shimeld 2004). Work done by Cribb (2009) also observes an adjustment seaward to the limits of the original salt basin within Salt Subprovince IV.

6.4.2 Variation of depositional systems

Results of this study and co-projects give insights into the paleogeographic evolution and salt tectonics history of the north-central Scotian margin and define how variable sedimentation and depocentre migration across the basin have affected salt mobilization and the post-rift evolution of the margin. The overall northeast to southwest migration of depocentres demonstrates significant salt mobilisation oblique or parallel to the strike of the margin rather than primarily margin-normal sediment progradation from the shelf to deepwater basin (Figure 6.5). This causes major variations in the timing and pattern of salt structures and related depositional systems along the margin from the original Laurentian delta in the east to the Sable delta in the west over time.

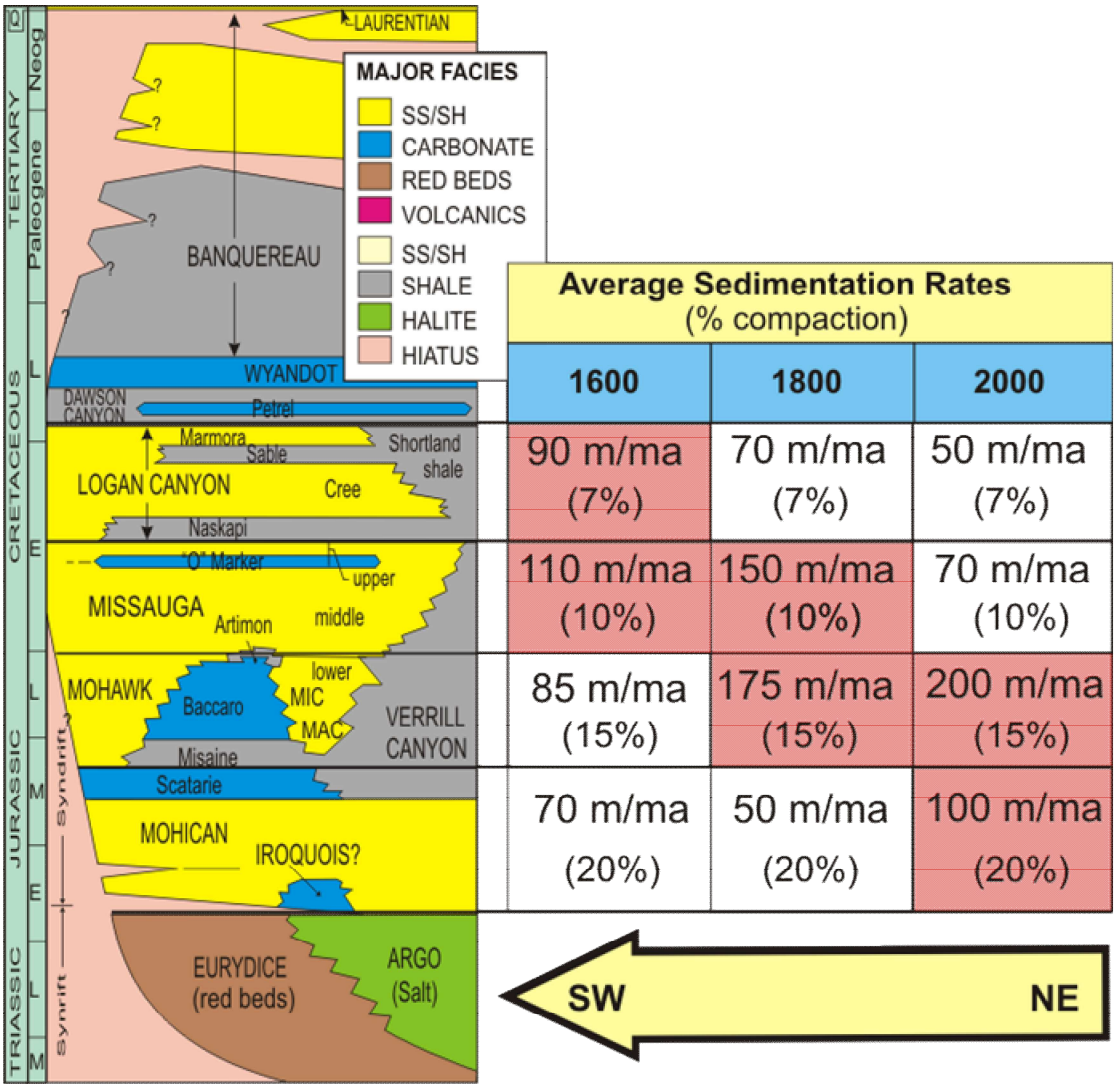

Figure 6.5 Generalized stratigraphy of the Scotian Margin including approximate sedimentation rates from NovaSPAN seismic profiles 1600 (western Sable Subbasin), 1800 (Abenaki and central Sable Subbasin and 2000 (Laurentian Subbasin). Note the NE to SW trend in major sedimentation pulses across the north-central Scotian margin which suggests it was a main factor behind the apparent southwest younging of major salt structures across the north central margin.

Early – Mid Jurassic (Mohican Formation)

During the Early – Mid Jurassic, the main sediment input and subsidence occurred in the northeast portion of the margin in the Laurentian Subbasin (E: Laurentian Subbasin, Figure 6.3; Figure 6.6). In this region (Salt Subprovince IV and V), the gently seaward-climbing basin basement morphology coupled with high early post-rift

sedimentation facilitated very efficient early salt mobilization and massif formation in the distal autochthonous salt basin. The North Sable High acted as a sediment bypass zone that forced transport further out into the basin and initiated salt inflation at the seaward limit of the basin (E: Abenaki and central Sable Subbasins, Figure 6.3). In the Abenaki Graben, limited deltaic sediment input caused subsidence and salt withdrawal and focused sediment deposition southwest along the trend of the Abenaki Graben and NSH.

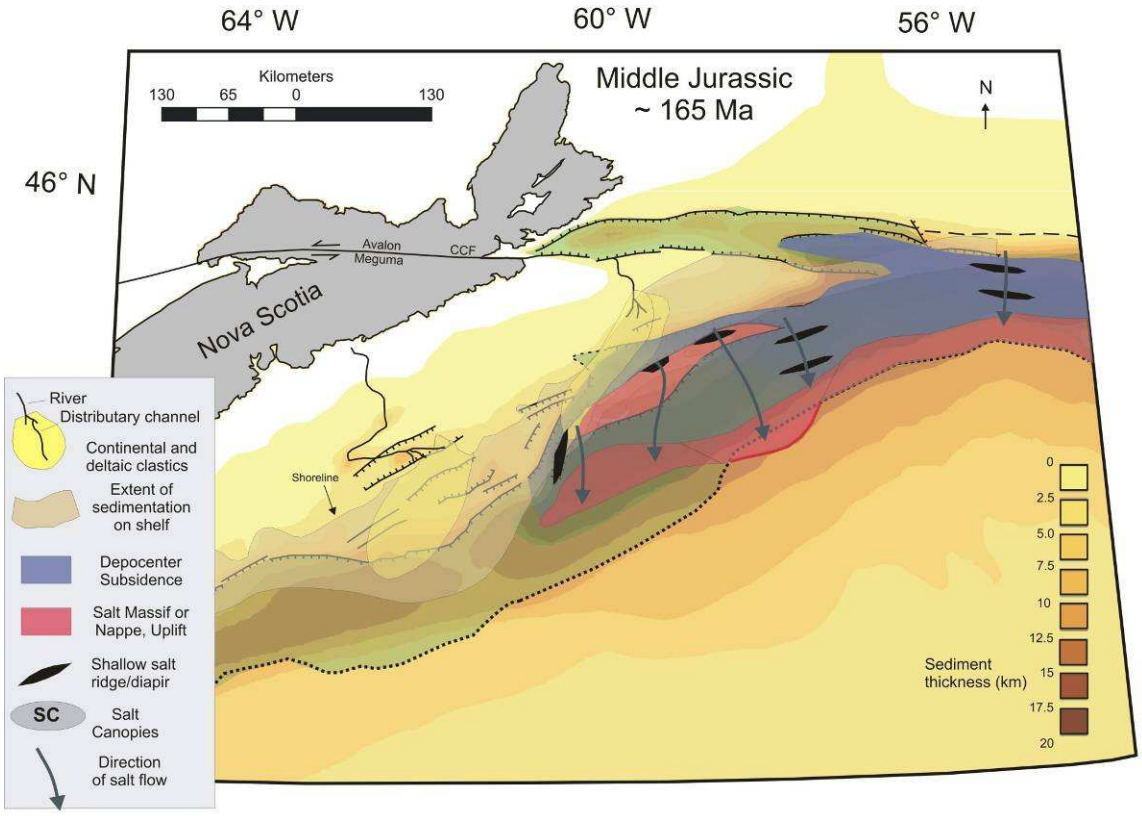

Figure 6.6 Paleogeography and sedimentation patterns of the Middle Jurassic modified from Wade and MacLean (1991) and including results from interpretation of the NovaSPAN dataset. Salt evolution derived from interpretation of NovaSPAN Line 1800 as well as lines 1600 (MacDonald, 2009) and 2000 (Cribb, 2009).

Mid – Late Jurassic (Mic Mac Formation)

During the deposition of the Mic Mac Formation from the Mid-Late Jurassic, the Laurentian delta was the major sediment source in the north-eastern portion of the margin with deposition focused in the Laurentian Subbasin (I: Laurentian Subbasin, Figure 6.3; Figure 6.7). With basinward sediment progradation on the inflated salt massif, salt was extruded out of the autochthonous salt basin into an extensive salt nappe system. By the end of the Late Jurassic, basin-scale salt tectonics ceased in the central portion of Subprovince IV when salt-withdrawal basins welded regionally to the basin floor and remnant salt became trapped.

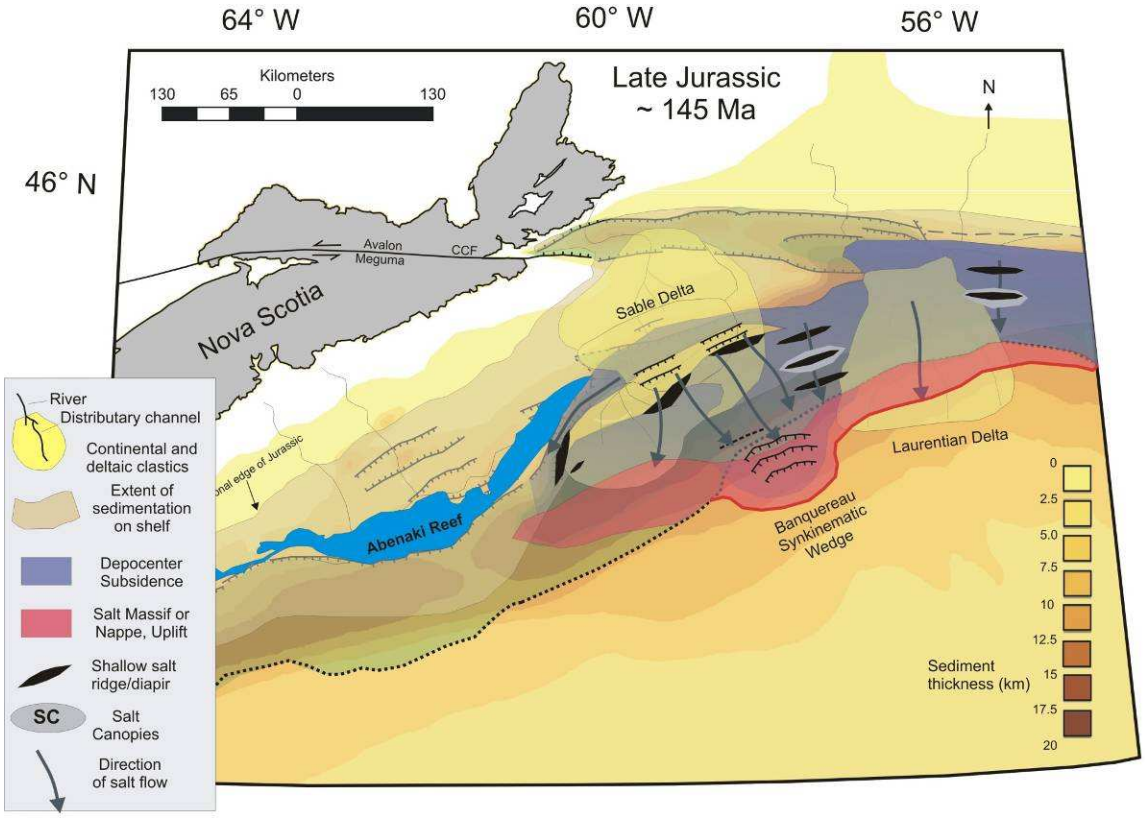

Figure 6.7 Paleogeography and sedimentation patterns of the Late Jurassic modified from Wade and MacLean (1991) and including results from interpretation of the NovaSPAN dataset. Salt evolution derived from interpretation of NovaSPAN Line 1800, as well as lines 1600 (MacDonald, 2009) and 2000 (2009).

In the Abenaki Graben, only small diapirs developed and the bulk of sediments prograded over the NSH into the Sable Subbasin creating a major depocentre in the landward flank of the salt massif (I: Abenaki and central Sable Subbasin, Figure 6.3). At this time, salt began to evacuate out of this location to the southeast as a large salt nappe system. Deformation of sediments over the inflated salt created a basinward dipping listric fault system referred to as the Banquereau Syn-Kinematic Wedge (BSW, Figure 6.7)). In the more central portion of the Sable Subbasin, broad mid-basin inflation occurred at the same time (I: Abenaki and central Sable Subbasins, Figure 6.7).

Early Cretaceous (Missisauga Formation)

In the Early Cretaceous, the major depocentres were located in the central and western portions of the Sable Subbasin as salt was almost completely evacuated out of the Laurentian Subbasin and Abenaki Graben (Figure 6.8). Sediments of the Sable delta (Missisauga Formation) prograded into the central and western Sable Subbasin on the inflated salt massif, triggering the formation of major passive diapirs. Depocentres evolved along diapir flanks that downbuilt into the very thick inflated salt layer (over 3 km). The salt inflated, translated and built-over the basin-stepped and -ramped geometries of the Sable Subbasin. It was hindered from easily translating to the seaward extent of the salt basin by general basin shallowing (I: Western Sable Subbasin, Abenaki and central Sable Subbasins, Figure 6.3).

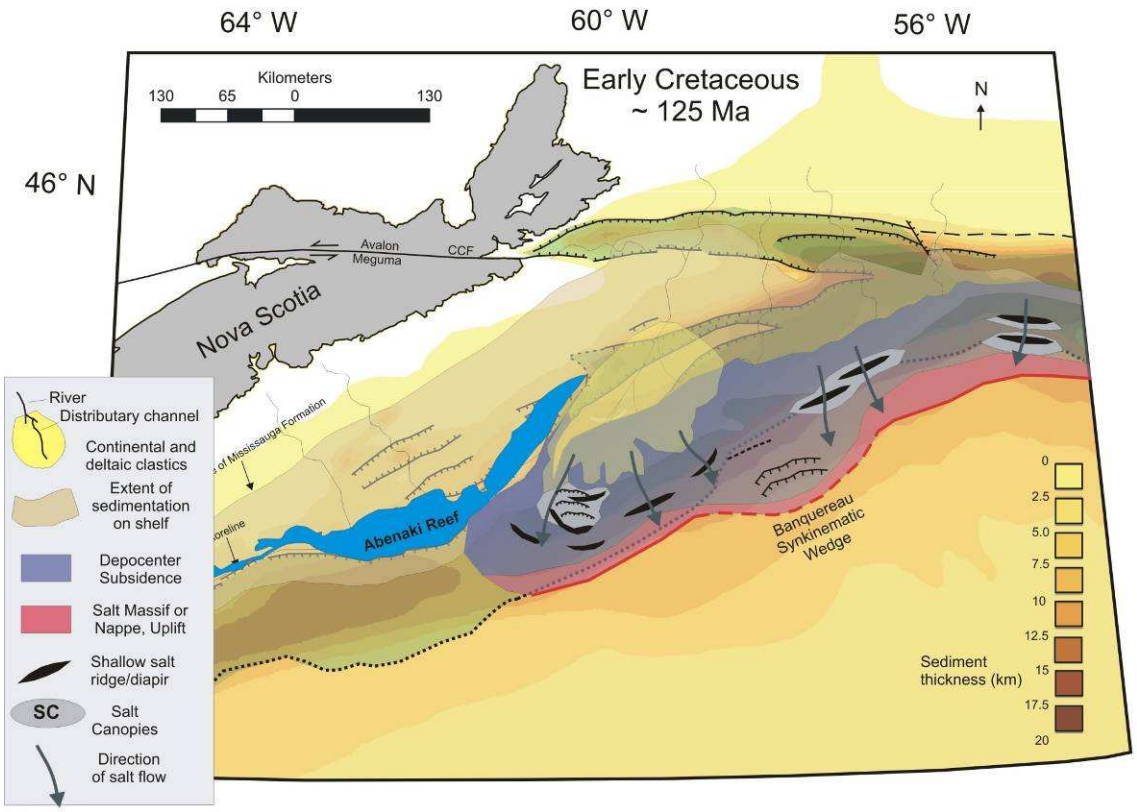

Figure 6.8 Paleogeography and sedimentation patterns of the Early Cretaceous modified from Wade and MacLean (1991) and including results from interpretation of the NovaSPAN dataset. Salt evolution derived from interpretation of NovaSPAN Line 1800 as well as lines 1600 (MacDonald, 2009) and 2000 (Cribb, 2009).

Early – Late Cretaceous (Logan Canyon)

The Early-Late Cretaceous marked a rise in sea level with less sediment input into the slope and deepwater region (Figure 6.9). During this time, major salt deformation was confined to the central and western Sable Subbasin (L: Western Sable Subbasin, Abenaki and central Sable Subbasins, Figure 6.3). Pelagic sediments were deposited in the distal basin as the rollover system continued to evolve with salt inflation over the high. The inflated salt broke through to the surface in the Late Cretaceous and flowed out both landward and seaward as a large salt tongue system. Passive diapirs in the deep portions of the basin continued to grow as sediments downbuilt. Sediments above the

diapirs started to shed and eventually salt reached the surface. Reduced sedimentation allowed salt from the passive diapirs to spread slowly onto the seafloor creating a large salt tongue canopy system with canopies as long as 80 km.

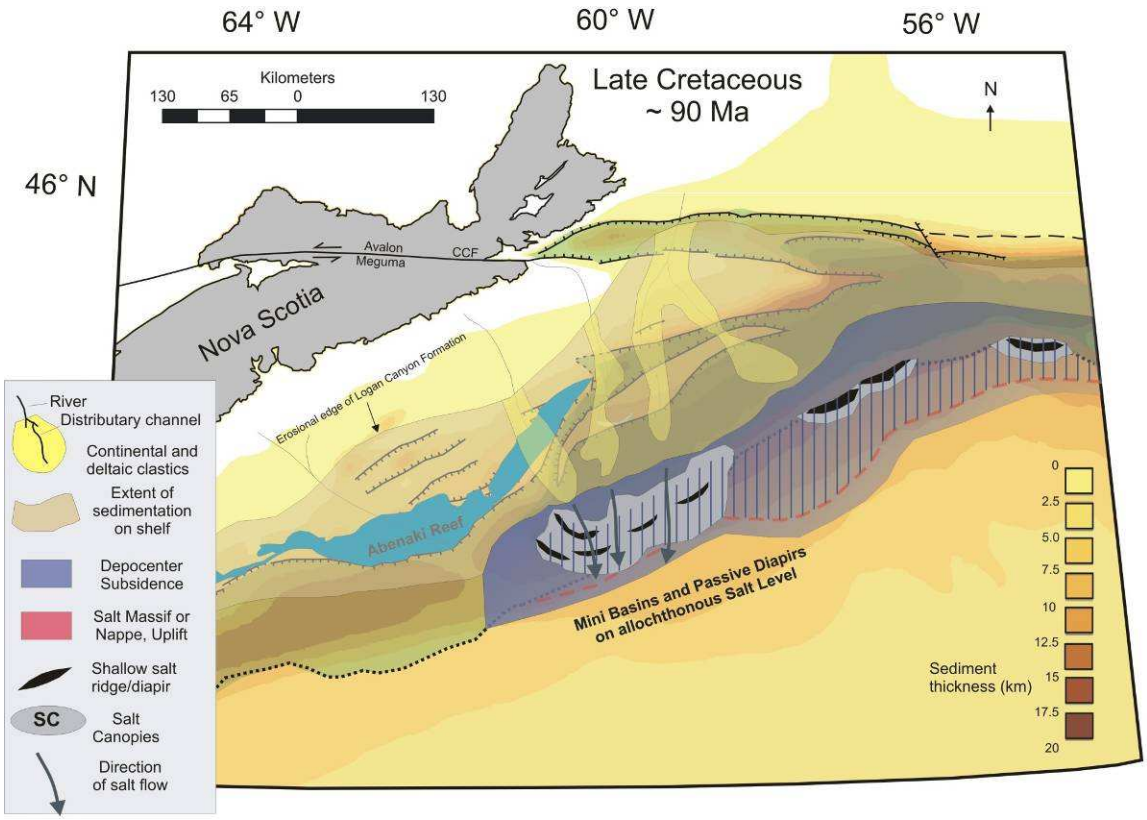

Figure 6.9 Paleogeography and sedimentation patterns of the Late Cretaceous modified from Wade and MacLean (1991) and including results from interpretation of the NovaSPAN dataset. Salt evolution derived from interpretation of NovaSPAN Line 1800 as well as lines 1600 (MacDonald, 2009) and 2000 (Cribb, 2009).

Late Cretaceous (Dawson Canyon and Wyandot Formations)

The intensity of salt tectonics in the north-central margin decreased drastically during the Late Cretaceous. Continued low sedimentation rates during the deposition of the Dawson Canyon Formation sustained spreading of the salt tongue-canopies and deposition of sediments into smaller mini-basins on the secondary salt level. As major deformation had slowed by this time, the main depocentres of the Dawson Canyon

Formation were locally focused between the salt-tongue canopies as deepwater canyon-fill systems.

Tertiary (Banquereau Formation)

In general, only minor salt-related deformation occurred throughout the Tertiary. Late contractional reactivation of diapirs from the late Paleogene / Early Neogene has been interpreted in the north-central Scotian Basin by Shimeld (2004) suggesting landward uplift as the cause. This resulted in pull up of overlying strata, folding over the crests of diapirs and vertical welding of allochthonous salt tongue feeders.

CHAPTER 7: Conclusions

The following chapter presents new concepts and insights into the post-rift evolution of the Abenaki Graben and central Sable Subbasin derived from the integrated seismic interpretation and analogue experiment study. Results from this project provide new constraints to the salt tectonic evolution of the Abenaki Graben and central Sable Subbasin, and implications to the regional tectono-stratigraphic evolution of the north-central Scotian margin. Specifically, this chapter discusses:

1. Advances in regional seismic interpretation of the Abenaki Graben and central Sable Subbasin area deduced from experiments.
2. Insights for future petroleum exploration activities.

7.1 Advances in regional seismic interpretation of the Abenaki Graben and central Sable Subbasin area deduced from experiments

Interpretation of the well imaged regional NovaSPAN Line 1800, aided by well data and derived analogue experiments, generates new insights into understanding the basin architecture and provides mechanical concepts for the interpretation of the deeper parts of the basin buried beneath the continental slope and extensive salt canopies that have limited image quality. Specifically, the study provides new insights and concepts into the:

1. Salt basin morphology.
2. Salt structures.
3. Sedimentation patterns and depositional systems.

7.1.1 Salt basin morphology

From the shelf to the deepwater basin, the salt basin morphology of NovaSPAN Lline 1800 reveals a 45 km wide landward tapering wedge (Abenaki Graben), a 60 km wide intermediate basement high (North Sable High), and a 95 km wide symmetric basin with a basement step (Sable Subbasin). The late syn-rift basin morphology is controlled by the basement rift structure and Eurydice Formation red-bed, syn-rift fill sediments. Thickest accumulations of original salt seem to have occurred within the deep Sable Subbasin (~2 km) just basinward of the North Sable High, with salt thickness decreased to less than 0.5 km over the adjacent High.

Seismic interpretation and results from physical experiments indicate that specific structural and stratigraphic features occur in the study area and have controlled by the salt basin morphology:

1. The landward-tapering wedge within the Abenaki Graben resulted in passive downbuilding and rotation of sediments into the salt basin. This is in contrast to the prominent growth faults forming over the hinge zone (rift shoulder; very thick salt in the landward rift basin) as observed in other portions of the margin (i.e. Laurentian Subbasin, western Sable Subbasin).

2. 4D experiments support a salt basin configuration of two asymmetric salt depocentres consisting of a landward-tapering wedge (Abenaki Graben), intermediate high (North Sable High; NSH), and a symmetric basin with a mid-basin basement step (central Sable Subbasin). The salt basin floor

consists of rotated basement blocks and basement rift half grabens that were partly leveled by syn-rift fill.

3. Thick salt (~2 km) within the Sable Subbasin effectively reduced the mechanical coupling between the salt and brittle sediments. This process favored passive downbuilding of sediments and expulsion rollover into the inflated salt massif.

4. The abrupt rise of the basin floor step in the Sable Subbasin restricted initial salt inflation to before this feature. The step effectively buttressed the inflated salt massif from migrating to the seaward edge of the Sable Subbasin and extruding as a nappe out of the basin.

7.1.2 Salt Structures

Salt structures observed in ION-GXT Line 1800 indicate a complex salt tectonic evolution that was strongly influenced by the variable salt basin morphology and varying sedimentation rates. Salt structures across the seismic transect chronologically young in a basinward direction as the basin evolved. To better understand the basin-scale salt tectonic processes, the observed salt structures have been divided into four kinematic domains (Figure 6.1) as discussed in Chapter 6 comprising, from shelf to the deepwater basin:

1. Salt weld and pillow domain
2. Normal fault and reactive diapir domain
3. Passive diapir and expulsion rollover domain

4. Contractional salt and allochthonous salt tongue-canopy domain

Salt weld and pillow domain

The *salt weld and pillow domain* beneath the modern shelf is characterised by small salt pillows and remnant salt within the Abenaki Graben. This kinematic domain developed as early post-rift sediment input (Early – Mid Jurassic; B, Figure 6.2a) in the landward salt basin led to sediment down-building and subsidence in the graben. Salt extruded from the Abenaki area onto the high and later into the central Sable Subbasin. Welding of this early salt-withdrawal basin occurred when the original salt layer was depleted with remnant salt was trapped in the form of salt pillows and small diapirs.

Normal fault and reactive diapir domain

The *normal fault and pillow domain* over the North Sable High (NSH) is characterised by a series of extensive basinward-dipping normal faults and remnant salt trapped in salt rollers. This kinematic domain developed as salt evacuated from the Abenaki Graben and across the high during the Mid – Late Jurassic (B – C, Figure 6.2a). Early prograding sediments accommodated extension induced by the shear flow of salt through a series of basinward-propagating normal faults. As sediments prograded basinward, fault blocks subsided and welded to the basin floor over the NSH.

Diapir and rollover domain

The *diapir and rollover domain* is located in the Sable Subbasin and characterised by several extensional diapirs (D2 – D5) that were later overrun by a broad expulsion rollover system within the basin (D, Figure 6.2a; E, Figure 6.2b). Diapirs within this

kinematic domain formed passively due to differential loading and gravity-spreading from the Mid Jurassic to Early Cretaceous as prograding sediments translated basinward. Extension was accommodated by the widening diapirs and sedimentation was focused along their flanks. As sediments continued to prograde into the Sable Subbasin, the diapirs eventually were buried and shutdown as the sediments blanketed the system and salt extruded basinward. The prograding sediments created the broad basinward-dipping expulsion rollover system through salt extrusion. This allowed sediments to rotate into the basinward flank of the inflated salt massif as sediment downbuilding occurred. This system was a major mechanism for seaward salt extrusion of the salt massif.

Allochthonous salt tongue-canopy domain

The *allochthonous salt tongue-canopy domain* is characterised by an extensive, approximately 80 km long, salt tongue-canopy system that extends past the original limits of the Abenaki Graben. Induced by mid-basin salt inflation and a late-stage reduction of sediment deposition, the salt reached the seafloor surface and efficiently spread along the seafloor as large salt tongues. These eventually coalesced to form salt tongue-canopies late in the Early Cretaceous (E, Figure 6.2b). Sediments deposited on top of the salt tongue canopy system facilitated the initiation of mini-basins that were later deformed into expulsion rollovers and turtle structures as the salt extruded along the seafloor surface.

7.1.3 Sedimentation patterns and depositional systems

Observations from seismic data and experiment results indicate that the interplay between sediment input and salt mobilization greatly affected the depositional systems of

the Abenaki Graben and central Sable Subbasin areas. Important results deduced from the scaled experiments regarding salt mobilization and related sedimentation patterns and depositional systems are:

1. An initial Early to Middle Jurassic aggradational phase induced early salt mobilization and evacuation from the Abenaki Graben, creating a major depocentre within the subbasin as accommodation was generated. The low sedimentation input into the Abenaki represented a widespread aggradational phase that differed from the higher rates observed in the northern Salt Subprovince IV and V at this time. As mobilization started, salt inflation over the North Sable High (NSH) also restricted major sedimentation to the Abenaki Graben.

2. Through the Late Jurassic, sedimentation increased as sediments began to prograde out over the high into the Sable Subbasin, and succeeded in extruding salt from the Abenaki Graben and NSH into the Sable Subbasin. Inflation of salt over the basin step restricted sedimentation to the basinward and landward flanks as it formed a topographic high. This progradational phase continued into the Early Cretaceous, as Missisauga Formation deltaic sediments were deposited into the Sable Subbasin. Associated downbuilding and rolling occurred along the flanks of the inflated salt that generated more accommodation space for sediments.

3. In the Early Cretaceous, salt inflation in front of the Sable Subbasin mid-basin basement step controlled sediment deposition, restricting it to the flanks of this topographic high.

4. Reduced sedimentation in the Late Cretaceous permitted salt to extrude onto the seafloor surface as a large salt tongue-canopy system. As the canopy system evolved, it to controlled depositional patterns as sediments were funneled and deposited along the flanks of the coalescing tongues that formed topographic highs.

5. Late Cretaceous sedimentation on the secondary salt layer has been greatly controlled by the large salt tongue-canopies that would have funneled deepwater channel systems to the flanks of the salt structures.

7.2 Insights for future petroleum exploration activities

From the application of results derived from this study, key insights have been developed for aiding in future petroleum exploration activities that may significantly reduce exploration risk:

1. Due to the thin original salt layer over the North Sable High, high extension accommodated by a basinward-dipping growth fault system was generated by sediment progradation and dominate shear flow within the salt layer. Thus, Late Jurassic reservoirs in this area may be more compartmentalized and seals may be leaky. However, the throws of normal faults within the Early

Cretaceous sediments are much less, thus indicating potential reservoirs and seals may be less compromised at this stratigraphic interval.

2. Beneath the modern day slope, major Late Jurassic and Early Cretaceous reservoir targets are located at uneconomical drilling depths (approximately 9 to 13 km) as the strata has subsided into the thick original salt layer of the deep Sable Subbasin. Future petroleum exploration should focus on Early Cretaceous (Logan Canyon Formation) channel systems and growth structures along diapir and canopy flanks.

3. As the major faults within the basin appear to be growth faults, hanging walls throughout the post-rift evolution of the basin represented topographic lows. These lows may have funneled and trapped channel sands and turbidite deposits creating potential reservoir accumulations.

4. Despite excellent trapping potential of the seaward salt tongue over deep basin sediments, inflated salt and diapirs, which created the feeder systems of the tongues, likely remained topographic highs throughout their passive stages and confined most sands to their landward flanks. Potential may exist beneath landward salt tongue overhangs which trapped potential reservoir sands from the Early Cretaceous Logan Canyon Formation sands as observed in ION-GXT NovaSPAN Line 1800.

5. Observations from the dip-domain interpretation of NovaSPAN Line 1800 and results from experiments suggest anti-formal structures have very little reservoir potential as, for the most part, they represent topographic highs during syn-depositional deformation. However, as the flanks of these structures subsided, evacuated salt left topographic lows which would have trapped and funneled potential reservoir sands as the expulsion rollovers developed. Though as mentioned earlier, most of these potential structures are very deep or at uneconomical depths in this region (9 km to 13 km). Potential may however exist within deformed strata over the salt tongue-canopy system where true anti-formal turtle structures exist if reservoir sands are present in these areas.

REFERENCES

Adam, J., Krezsek, C., MacDonald, C., Campbell, C., Cribb, J., Nedimovic, M., Louden, K., and Grujic, D. 2008. Basin-Scale Salt Tectonic Processes and Sediment Progradation in the Slope and Deepwater Basin of the North-Central Scotian Margin, *In* Central Atlantic Conjugate Margins Conference, Halifax, Nova Scotia, Canada., Extended Abstracts, CD-Rom.

Adam, J. Urai, J.L., Wieneke, B,. Oncken, O., Pfeiffer, K., Kukowski, N., Lohrmann, J., Hoth, S., van der Zee, W., and Schmatz, J., 2005. Shear localization and strain distribution during tectonic faulting--new insights from granular-flow experiments and high-resolution optical image correlation techniques. Journal of Structural Geology **27**: 283–301.

Anderson, J.E., Cartwright, J., Drysdall, S.J., and Vivian, N., 2000. Controls on turbidite sand deposition during gravity-driven extension of a passive margin: examples from Miocene sediments in Block 4, Angola. Marine and Petroleum Geology, **17**: 1165-1203.

Ascoli, P., 1976. Formaniferal and ostracod biostratigraphy of the Mesozoic-Cenozoic, Scotian Shelf, Atlantic Canada. Maritime Sediments, Special Publication No. 1: 653-771.

Atlantic Geoscience Center, 1991. East Coast Basin Atlas Series: Scotian Shelf. Geological Survey of Cxanada, 150 p.

Barss, M.S., Bujak, J.P., and Williams, G.L., 1979. Palynological zonation and correlation of sixty-seven wells, eastern Canada. Geological Survey of Canada, Paper 78-24: 118.

BASIN database. Available from http://basin.gsca.nrcan.gc.ca/index_e.php [cited 20 September 2009].

Bates, R.L., and Jackson, J.A., 1987, Glossary of Geology, 3rd ed.: Alexandria, Virginia, American Geological Institute: 788 p.

Brace and Kohlshedt, 1980. Limits on lithospheric stress imposed by laboratory experiments. Journal of Geophysical Research, **85**: 6248-6252.

Brun, J.P., and Fort, X., 2004. Compressional salt tectonics (Angolan margin). Tectonophysics, **328**: 129-150.

Brun, J.P., and Mauduit, T. P.-O., 2009. Salt rollers: Structures and kinematics from analogue modelling. Marine and Petroleum Geology, **26**: 249-258.

Campbell, C., 2007. Physical Modeling of the Salt Tectonics of Allochthonous Canopy and Nappe Systems at Deepwater Continental Margins: Applications to the Abenaki and Sable Sub-Basins, Scotian Margin. B.Sc. Thesis, Dalhousie University, Halifax, N.S.

Costa, E. and B.C., Vendeville, 2002. Experimental insights on the geometry and kinematics of fold-and thrust belts above weak, viscous evaporitic decollement. Journal of Structural Geology **24**: 1729-1739.

Cribb, J., 2009. Salt Tectonics of the Laurentian Subbasin: Insights from 4D Physical Experiments and Regional Seismic Interpretation. M.Sc. Thesis, Dalhousie University, Halifax, N.S.

Cummings, D.I., and Arnott, R.W.C., and Hart, B.S., 2006. Tidal signatures in a shelf-margin delta. Geology, **34** (4): 249-252.

Davies, E.H. 1986. The correlation and geohistory of the Hibernia Field. *In*, Program and abstracts for the Canadian Society of Petroleum Geologists 1986 Convention, Calgary.

Deptuck, M.E., K. Kendell, and B. Smith, 2009. Complex deepwater fold-belts in the SW Sable Subbasin, offshore Nova Scotia. *In* Frontiers + Innovation – 2009 CSPG CSEG CWLS Convention, Calgary, Alberta, Canada, Program & Abstracts, CD-Rom.

Doeven, P.H., 1983. Cretaceous nannofossil stratigraphy and paleoecology of the Canadian Atlantic Margin. Geological Survey of Canada, Bulletin **356**: 70.

Ebinger, C.J., and B.E. Tucholke, 1988. Marine Geology of Sohm Basin, Canadian Atlantic Margin. The American Association of Petroleum Geologists Bulletin, **72** (12): 1450-1468.

Eliuk, L.S., 1978. The Abenaki Formation, Nova Scotia Shelf, Canada – a depostional and diagenetic model for the Mesozoic carbonate platform. Bulletin of Canadian Petroleum Geology, **26**: 424-514.

Fort, X., Brun, J.P., and Chauvel, F., 2004. Salt tectonics on the Angolan margin, synsedimentary deformation processes. American Association of Petroleum Geologsists Buletin, **88**: 1523-1544.

Funck, T., H. R. Jackson, K.E. Louden, S.A. Herler, and Y. Wu., 2004. Crustal structure of the northern Nova Scotia rifted continental margin (eastern Canada). Geophysical Journal International, **166** (2): 878-906.

Ge, H., Jackson, M.P.A., and Vendeville, B.C., 1997. Kinematics and dynamics of salt tectonics driven by progradation. The American Association of Petroleum Geologists Bulletin, **81** (3), 398-423.

Gemmer, L., Ings, S.J., Medvedev S., and Beaumont, C., 2005. Salt tectonic driven by differential sediment loading: stability analysis and finite-element experiments. Basin Research, **17**: 382-402.

Gemmer, L., Beaumont, C. and Ings, S.J. 2005. Dynamic modelling of passive margin salt tectonics: effects of water loading, sediment properties and sedimentation patterns, Basin Research, **17**, 383–402.

Gradmann, S., Beaumont, C., and Albertz, M., 2009. Factors controlling the evolution of the Perdido Fold Belt, northwestern Gulf of Mexico, determined from numerical models. Tectonics, **28**, TC2002, doi:10.1029/2008TC002326.

Huismans, R.S., and Beaumont, C., 2008. Complex rifted continental margins explained by dynamical models of depth-dependent lithospheric extension. Geology, **36** (2): 163-166.

Ings, S.J., and Shimeld, J.W., 2006. A new conceptual model for the structural evolution of a regional salt detachment on the northeast Scotian margin, offshore eastern Canada. American Association of Petroleum Geologists Bulletin, **90** (9): 1407-1423.

Jackson, M. P. A. and Talbot, C. J. 1994. Advances in salt tectonics *In* P.L. Hancock, ed., Continental deformation: Oxford, U.K., Pergamon Press and International Union of Geological Sciences, 159-180.

Jackson, M. P. A. and Talbot, C. J. 1991. A glossary of salt tectonics: The University of Texas at Austin, Bureau of Economic Geology Geological Circular 91–4, 44 p.

Jackson, M. P. A. and Talbot, C. J. 1989. Anatomy of mushroom shaped diapirs. Journal of Structural Geology, **11**, 211-230.

Jackson, M.P.A. and Talbot, C.J. 1986. Stepwise centrifuge modeling of the effects of differential sediment loading on the formation of salt structures. *In* Lerche, I. & O'Brien, J. J. (eds.), Dynamical Geology of Salt and Related Structures. Academic Press, Orlando, Florida, 163-259.

Jackson, M.P.A., and Vendeville, B.C., 1994. Regional extension as a geologic trigger for diapirism. Geological Society of America Bulletin, **106**: 57-73.

Jackson, M. P. A., and Vendeville, B. C. 1994. Initiation of salt diapirism by regional extension: global setting, structural style, and mechanical models: The University of Texas at Austin, Bureau of Economic Geology Report of Investigations No. 215, 39 p.

Jansa, L.F., Bujak, J.P., and Williams, 1980. Upper Triassic salt deposits of the western North Atlantic. Canadian Journal of Earth Sciences, **17**: 547-559.

Jansa, L.F., and Wade, J.A., 1975. Geology of the continental margin off Nova Scotia and Newfoundland. *In* Offshore geology of Eastern Canada, **2**, Regional geology. *Edited by* W.J.M. van der Linden, J.A. Wade. Geological Survey of Canada: 74-30, 51-106.

Keen, C.E. and Potter, D.P. 1995. The transition from a volcanic to a nonvolcanic rifted margin off eastern Canada: Tectonics, **14**, 359–371.

Keen, C.E., MacLean, B.C., and Kay, W.A. 1991. A deep seismic reflection profile across the Nova Scotia continental margin, offshore eastern Canada. Canadian Journal of Earth Science, **28**, 1112-1120.

Keen, C.E., and C. Beaumont, 1990. Geodynamics of rifted continental margins. *In* Volume I-1 of Decade of North America Geology. *Edited by* M.J. Keen and G.L. Williams. Publication of Geological Survey of Canada and Geological Society of America: 393-472.

Kent, D.V., Olsen, P.E., and Witte, W.K. 1995. Late Triassic-Early Jurassic geomagnetic polarity sequence and paleolatitudes from drill cores in the Newark rift basin, eastern North America. J. Geophys. Res., **100** (B8), 14965–14998.

Kidston, A.G., Brown, D.E., Smith, B.M. and Altheim, B., 2002. Hydrocarbon Potential of the Deep-Water Scotian Slope. Canada-Nova Scotia Offshore Petroleum Board, Halifax, 111 p. Cd-Rom and www.cnsopb.ns.ca/resources/assessment.html.

Kidston, A.G., Smith, B.M., Brown, D.E., Makrides, C., and Altheim, B., 2007. Hydrocarbon Potential of the Deep-water Scotian Slope, Canada-Nova Scotia Offshore Petroleum Board, Open File Report, 111 p.

Kligfield, R., Rowan, M.G., and Ratliff, R. 1989. Applications of computer-aided section construction, restoration, and balancing models to the petroleum industry. *In* Society of Exploration Geophysicists, 59th annual international meeting, Dallas, TX, United States, **59**, 589 p.

Koyi, H., Talbot, C.J. and Torudbakken, B.O. 1995. Analogue models of salt diapirs and seismic interpretation in the Nordkapp Basin, Norway. Petroleum Geoscience, **1**, no. 2, 185-192.

Krezsek, C., Adam, J., and Grujic, D., 2007. Mechanics of fault and expulsion rollover systems developed on passive margins detached on salt: insights from analogue modeling and optical strain monitoring. Structurally Complex Reservoirs, Geological Society, London, Special Publications **292**:103-121.

Lallemand, S.E., Schnuerle, P., Malavieille, J., 1994. Coulomb theory applied to accretionary and nonaccretionary wedges; possible causes for tectonic erosion and/or frontal accretion. Journal of Geophysical Research B, Solid Earth and Planets **99** (6): 12,033–12,055.

Lehner, F.K., 2000. Approximate theory of substratum creep and associated overburden deformation in salt basins and del- tas. In: Aspects of Tectonic Faulting. *Edited by* y F.K. Lehner & J.L. Urai. Springer-Verlag, Berlin: 21- 47.

Lohrmann. J., N. Kukowsky, J. Adam, and O. Oncken, 2003. The impact of analogue material properties on the geometry, kinematics, and dynamics of convergent sand wedges. Journal of Structural Geology, **25**: 1691-1711.

Louden, K.E, Tucholke, B.E., and Oakey, G.N., 2004. Regional anomalies of sediment thickness, basement depth and isostatic crustal thickness in the North Atlantic Ocean. Earth and Planetary Science Letters, **224**: 193 – 211.

Louden, K., 2002. Tectonic evolution of the east coast of Canada. CSEG Recorder, **27**, 37-49.

MacDonald, C. 2009. Salt Tectonics of the Western Sable Subbasin: Insights from 4D Physical Experiments and Regional Sesimic Interpretation. M.Sc. Thesis, Dalhousie University, Halifax, N.S.

MacDonald, C. 2007. Analogue modeling of the salt tectonics system, offshore Nova Scotia: insights into initial salt mobilization and autochthonous salt structures, B.Sc. Thesis, Dalhousie University, Halifax, N.S.

MacLean, B.C. and Wade, J.A. 1993. East Coast Basin Atlas Series: Seismic markers and stratigraphic picks in Scotian Basin wells. Atlantic Geoscience Centre, Geological Survey of Canada, 276 p.

MacLean, B.C. and Wade, J.A. 1992. Petroleum geology of the continental margin south of the islands of St Pierre and Miquelon, offshore eastern Canada. Bulletin of Canadian Petroleum Geology, **40**, 222–253.

Mauduit, T. P-O., Gaullier, V., Brun, J.P., and Lecanu, H., 1997. Raft tectonics: The effects of basal slope value and sedimentation rate on progressive extension. Journal of Structural Geology, **19**: 1219-1230

Mauduit T. P-O., and Brun, J.P., 1998. Growth-fault/rollover systems: birth, growth, and decay. Journal of Geophysical Research, **103/B8**: 18119-18136.
McIver, N.L., 1972. Mesozoic and Cenozoic stratigraphy of the Nova Scotia Shelf. Canadian Journal of Earth Sciences, **9**: 54-70.

MIRAGE – Map Image Rendering database forGEoscience. Available from http://apps1.gdr.nrcan.gc.ca/mirage/db_search_e.php [cited 20 September 2009].

Nelson, T.H., 1991. Salt tectonics and listric-normal faulting, *in* Salvador, ed., The Gulf of Mexico Basin. Geological Society of America, The Geology of North America, **J**: 73-89.

Oakey, G.N., and Stark, A., 1995. A digital compilation of depth to basement and sediment thickness for the North Atlantic and adjacent coastal land mass, Geological Survey of Canada, Open File # 3039.

Olsen, P.E., 1997. Stratigraphic record of the early Mesozoic breakup of pangea in the Laurasia-Gondwana rift system. Annual Review of Earth and Planetary Sciences, **25:** 337-401.

Poliakov, A. N. B., van Balen, R., Podladchikov, Yu., Daudre, B, Cloetingh, S., and Talbot, C. 1993. Numerical Analysis of How Sedimentation and Redistribution of Surficial Sediments Affects Salt Diapirism. Tectonophysics , **226**, 199–216.

Piper, D.J.W., Pe-Piper, G., and Ingram, S.I., 2004. Early Cretaceous sediment failure in the southwestern Sable Subbasin, offshore Nova Scotia. American Association of Petroleum Geologists Bulletin, **88** (7): 991-1006.

Ramberg, H., 1981, Gravity, Deformation and the Earth's Crust: Academic Press, London, 2nd ed., 452 p.

Rowan, M.G., 2008. Practical Salt Tectonics: A 2-day Short Course Emphasizing the Geometry and Evolution of Salt Structures. *In* Proceedings of the Central Atlantic Conjugate Margins Conference, Halifax, N.S., Canada.

Rowan, M. G., Peel, F. J., and Vendeville, B. C. 2004. Gravity-driven fold belts on passive margins, *In* K. R. McClay (ed.),Thrust tectonics and hydrocarbon systems: AAPG Memoir 82, 157-182.

Sandwell, D.T., and Smith, W.H.F., 1997. Marine gravity anomaly from Geosat and ERS 1 satellite altimetry. Journal of Geophysical Research, **102**: 10039-10054.

Shimeld, J.W., 2004. A comparison of salt tectonic sub-provinces beneath the Scotian Slope and Laurentian Fan, :24th Annual GCSSEPM Foundation Bob F. Perkins Research Conference, Exended Abstract CD: 502-515.

Sibson, R.H., 1974. Frictional constraints on thrust, wrench and normal faults. Nature, **249**: 542-544.

Spiers, C.J., Urai, J.L., Lister, G.S., Boland, J.N., and Zwart, H.J., 1986. The influence of fluid-rock interaction on the rheology of salt rock. Commission of the European Communities, Nuclear Science and Technology, Final Report, EUR 10399 EN: 131.

Ter Heege, J.H., De Bresser, J.H.P. and Spiers, C.J., 2005. Rheological behaviour of synthetic rocksalt: The interplay between water, dynamic recrystallization and deformation mechanisms. Journal of Structural Geology, **27:** 948-963.

Truscheim, F., 1960. Mechanism of salt mobilization in northern Germany. American Association of Petroleum Geologists Bulletin, **44**: 1519-1540.

Urai, J.L., Spiers, C.J., Zwart, H.J., and Lister, G.S., 1986. Weakening of rock salt by water during long-term creep. Nature, **324**: 554-557.

van Keken, P. E., Spiers, C.J., van den Berg, A.P., and Muyzert, E.J., 1993. The effective viscosity of rocksalt: Implementation of steady-state creep laws in numerical models of salt diapirism, Tectonophysics, **225** (4): 457–476.

Vendeville, B.C. 2005. Salt tectonics driven by sediment progradation: Part I, Mechanics and kinematics. AAPG Bulletin, **89**, 1071–1079.

Vendeville, B. C., Jackson, M. P. A., and Weijermars, R. 1993. Rates of salt flow in passive diapirs and their source layers, *In* Armentrout, J. M., Bloch, Roger, Olson, H. C., and Perkins, B. F., (eds.), Rates of geologic processes: tectonics, sedimentation, eustasy and climate: implications for hydrocarbon exploration: Gulf Coast Section, Society of Economic Paleontologists and Mineralogists Foundation, Fourteenth Annual Research Conference. Program with Papers, 269–276.

Vendeville, B.C. and Jackson, M.P.A., 1992a. The fall of diapirs during thin-skinned extension. Marine and Petroleum Geology, **9** (4): 354-371.

Vendeville, B.C. and Jackson, M.P.A. 1992b. The rise of diapirs during thin-skinned extension. Marine and Petroleum Geology, **9** (4): 331-353.

Vendeville, B.C. and Jackson, M.P.A. 1990. Physical modeling of the growth of extentional and contractional salt tongues on continental slopes. AAPG Bulletin, **74**, 784 p.

Wade, J.A and MacLean, B.C., 1990. The geology of the southeastern margin: aspects of the geology of the Scotian Basin from recent seismic and well data. *In* Geology of the Continental Margin Eastern Canada. *Edited by* M.J Keen and G.L. Williams. Geological Survey of Canada, Geology of Canada, 2: 167–238.

Wade, J.A., MacLean, B.C., and Williams, G.L., 1995. Mesozoic and Cenozoic stratigraphy, eastern Scotian Shelf: new interpretations. Canadian Journal of Earth Sciences, **32 (**9): 1462-1473.

Weijermars, R., 1986. Flow behavior and physical chemistry of bouncing putties and related polymers in view of tectonic laboratory applications. Tectonophysics, **124**: 325-358.

Weijermars, R., M.P.A., Jackson, & B.C., Vendeville, 1993. Rheological and tectonic modeling of salt provinces. Tectonophysics **217**, (1-2): 143-174.

Weijermars, R., and Schmeling, H., 1986. Scaling of Newtonian and non-Newtonian fluid dynamics without inertia for quantitative modelling of rock flow due to gravity (including concept of rheological similarity). Physics of the Earth and Planetary Interiors, **986**: 316-330.

Williams, G.L., Ascoli, P., Barss, M.S., Bujak, J.P., Davies, E.H., Fensome, R.A., and Williamson, M.A., 1990. Biostratigraphy and related studies. *In* Geology of the continental margin off eastern Canada. *Edited by* M.J. Keen and G.L. Williams. Geological Survey of Canada, Geology of Canada, 2: 87-137.

Wu, Y., K.E. Louden, T. Funck, H.R. Jackson, and S.A. Dehler, 2006. Crustal structure of the central Nova Scotia margin off Eastern Canada. Geophysical Journal International, **166**: 878-906.

Zheng, Y. and Arkani-Hamed, J. 2002. The elastic properties of the lithosphere beneath Scotian basin, Tectonophysics, **344:** 137-156.

Appendix A:

Salt Tectonics Structures and Terminology

Salt structures

Diapirs – Salt diapirs comprise a mass of salt that has moved in a ductile manner and appears to have discordantly pierced or intruded the sedimentary overburden (Jackson and Talbot 1994). This appearance of piercing led to the idea that density contrast alone was responsible for the initiation of diapirs (Rowan 2005). Newer concepts interpret the formation of diapirs through passive emplacement by downbuilding of sediments or by faulting of the pre-kinematic sedimentary overburden (Jackson and Talbot 1994). Diapirs may be initiated during extension as the overburden is stretched and thinned (Appendix A-1) or by contraction as shortening occurs and the overburden is uplifted in growing detachment folds, faulted and eroded enough for salt to pierce (Appendix A-2; Rowan 2005).

In the extensional setting there are three stages in the evolution of a diapir which are the reactive, active and passive stages.

1. Reactive diapirs occur as overburden becomes thinned by faults causing graben formation in the brittle overburden and an *inverse graben* where the salt meets the overburden (Rowan 2005). Through differential pressure, the salt will react by infilling the space created by the inverse graben creating a triangular, reactive diapir (Rowan 2005).
2. Active diapirism occurs after the diapir is tall enough and overburden is thin enough that the diapir can pierce through the overburden due to buoyancy forces
3. Passive diapirs finally have reached the surface.

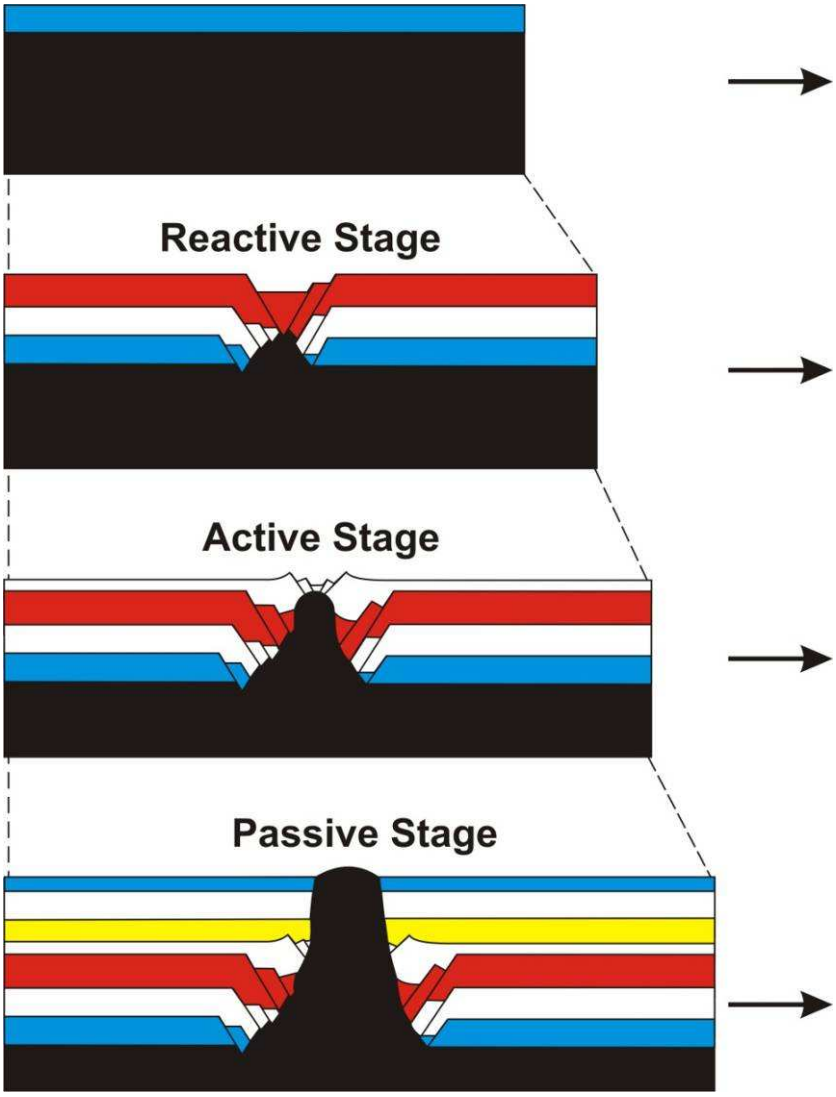

Appendix A-1 Evolution of a diapir in extensional setting. In the reactive stage extension leads to faulting and the formation of a symmetric graben. This causes a pressure differential above the grabens where salt will rise to reach equilibrium. During the active stage salt, driven by buoyancy forces, becomes close enough to the surface to pierce the overburden.. During the passive stage salt reaches the surface and may flow out onto surface (Modified from Jackson and Vendeville 1992).

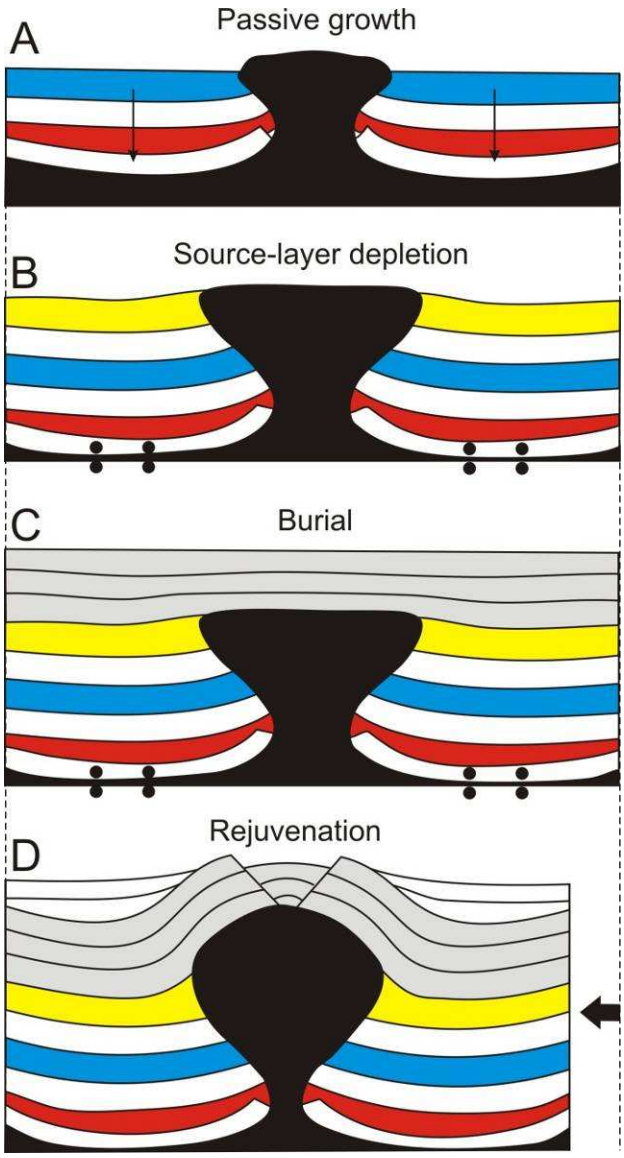

Appendix A-2 Temporal evolution of a diapir through contraction. Contraction allows a buried diapir to be rejuvenated as it is squeezed by the folding and faulting of overlying sediments until salt is forced up to fill accommodation space (Modified from Jackson and Vendeville 1994).

Salt rollers – Salt rollers are low-amplitude, asymmetric salt structures (reactive diapirs) in the footwall of listric normal faults. They comprise a gently dipping flank in conformable stratigraphic contact with the overburden and a more steeply dipping flank in normal-faulted contact with the overburden (Appendix A-3; Jackson and Talbot 1994;

Bally 1981). The presence of salt rollers in a system indicates thin-skinned extension perpendicular to the strike of the rollers.

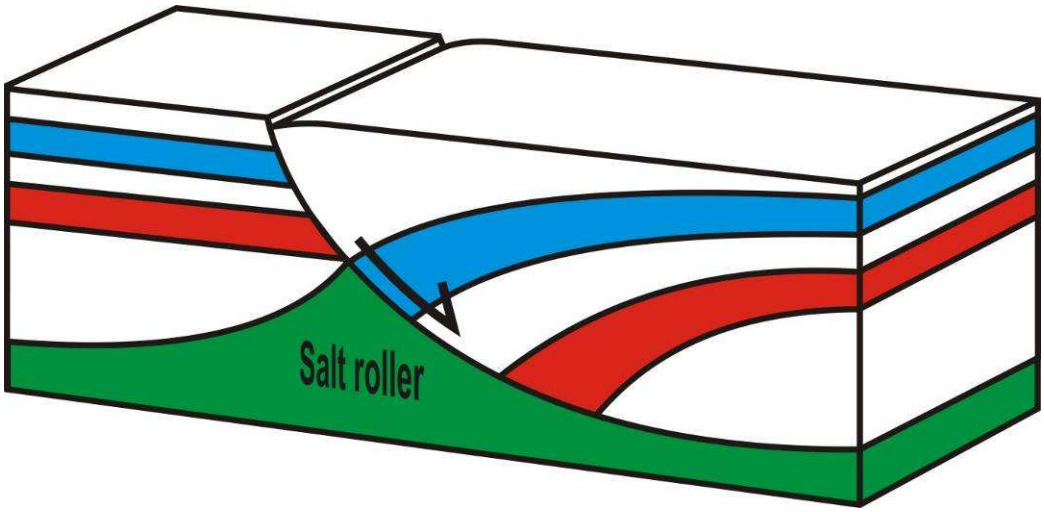

Appendix A-3 Schematic of a salt roller. Salt rollers are essentially low-amplitude, asymmetric reactive diapirs and indicate thin-skinned extension perpendicular to the strike of the rollers.

Salt welds – Salt welds occur when salt is completely withdrawn from its source layer causing the overburden and sub-salt strata to come in contact where the salt was previously emplaced (Appendix A-4; Rowan 2005). Primary welds occur in the autochthonous basin as salt withdrawal causes the overburden and sub-salt strata to come in contact. Secondary welds are vertical to near vertical welds that occur along salt structures such as diapirs and stocks. Tertiary welds are similar to primary welds but occur as welding takes place on secondary allochthonous salt levels such as tongues or nappes.

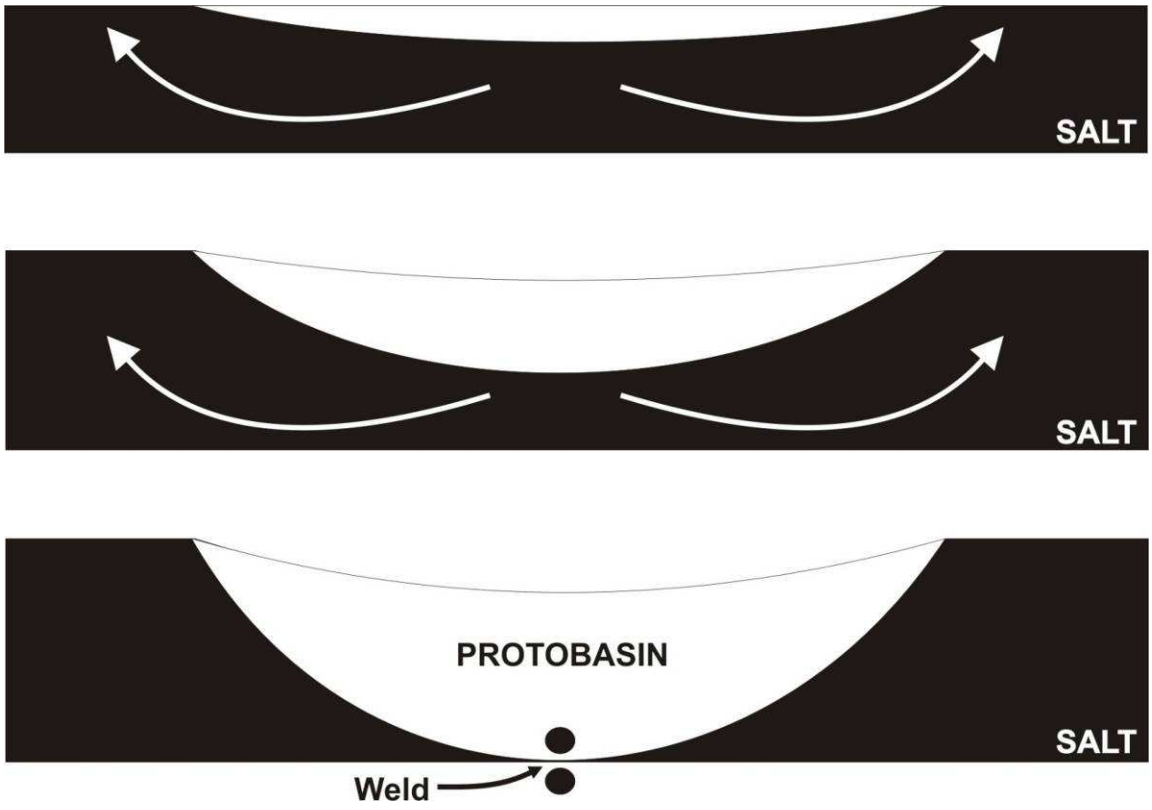

Appendix A-4 Evolution of a salt withdrawal basin. Eventual welding occurrs as salt is expelled away from the main depocentre until it is completely evacuated.

Expulsion rollovers – Expulsion rollovers occur as a result of salt withdrawal (Krezsek et al. 2007). Lateral salt removal forces the progressive sinking, or "rolling" of the overburden below the regional level (Appendix A-5a; e.g. Ge et al. 1997; Krezsek et al. 2007). Important to note is that expulsion rollovers do not accommodate any overburden extension as the evacuating salt localizes the strain (Ge et al. 1997; Krezsek et al. 2007). Expulsion rollovers typically cause depocentre migration as the most of the accommodation space is created close to the evacuating salt body.

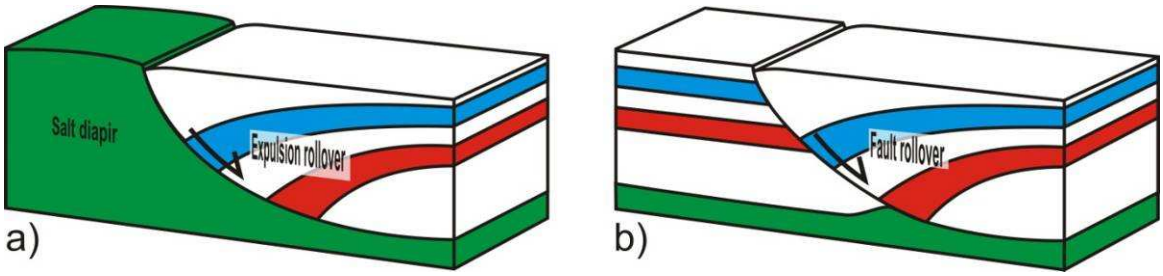

Appendix A-5 Schematic of both an expulsion rollover and growth-fault rollover. A) With expulsion rollovers lateral salt removal forces the progressive sinking, or "rolling" of the overburden below the initial regional level. B) Growth-fault rollover systems are similar to expulsion rollovers but develop due to geometric and space compatibility problems caused by extensional displacement along a listric growth-fault (Modified from Krezsek et al. 2007).

Allochthonous salt – Allochthonous salt refers to sheet like bodies of salt that have migrated to stratigraphic levels above the autochthonous, or original layer in which it was deposited (Jackson and Talbot 1994). Allochthonous salt lies on top of younger strata and underlying strata are usually truncated by the base of salt while the overlying strata are generally parallel or migrated laterally out of the original salt basin (Rowan 2005).

Salt canopies - Salt canopies are diapiric structures formed by the partial or complete coalescence of diapir overhangs or salt sheets (Appendix A-6; Jackson et al. 1987). Salt canopies are allochthonous salt bodies classified by the coalescence of structures such as salt-stock canopies (Appendix A-6a), salt-wall canopies (Appendix A-6b), and salt-tongue canopies (Appendix A-6c; Jackson and Talbot 1994). Salt stocks refer to finger-like diapiric structures (Appendix A-6a). Salt walls refer to elongated upwellings of diapiric salt that form sinuous, parallel rows (Appendix A-6b). Salt tongues refer to passive diapirs that extrude onto the seafloor and flow like a glacier (Appendix A-6c).

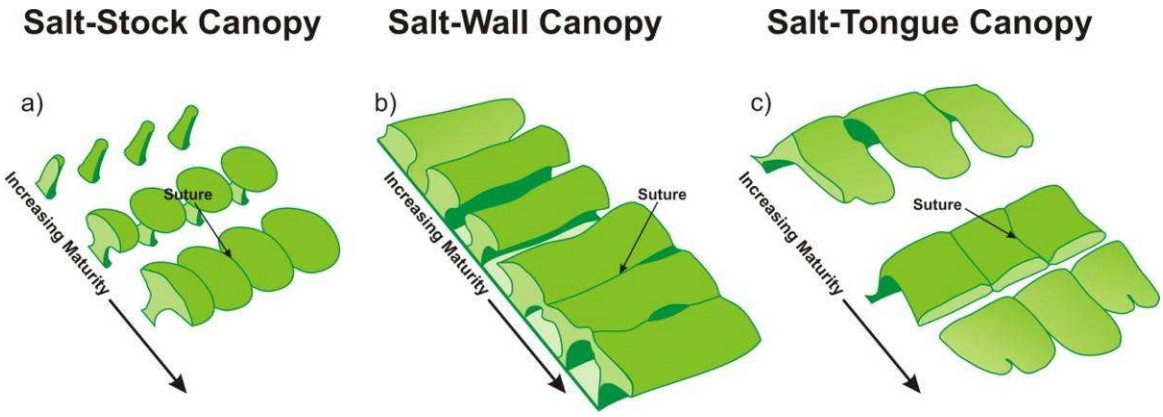

Appendix A-6 Temporal evolution of canopy systems as individual a) salt stocks, b) salt walls or c) salt tongues coalesce (Modified from Rowan 2008).

Salt nappes – salt nappes are similar to salt canopies however they are distinguished by a lack of local feeders (Appendix A-7; Rowan 2005). Salt nappes are also larger than individual salt tongues or stocks (Rowan 2005). Salt nappe emplacement is driven by three overlapping processes including: 1) depositional loading of deep, landward sources; 2) basinward translation of the overburden on the source layer; and 3) depositional loading and translation of the older, landward portions of the nappe.

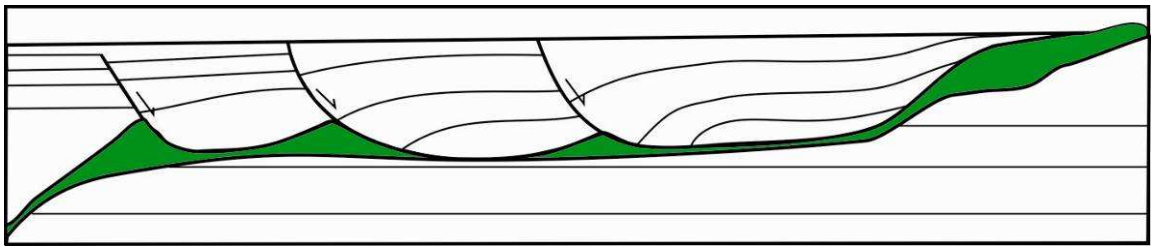

Appendix A-7 Schematic cross-section of a salt nappe. Note the characteristic step-wise shape resulting from the salt climbing synchronically with sediments being deposited.

Salt related fault structures

Growth-fault rollover systems – Growth-fault rollover systems are similar to expulsion rollovers but develop due to geometric and space compatibility problems caused by extensional displacement along a listric growth-fault (Appendix A-5b; Krezsek et al. 2007). This results in the subsequent down-bending of the hanging wall strata (Krezsek et al. 2007).

Keystone grabens – Keystone grabens refer to extensional fault structures that form due to the bending of the brittle overburden in rollovers or over the crests of diapirs. This bending results in a succession of faulting creating grabens with fault steps at the surface (Appendix A-8). The succession of faulting associated with a keystone graben gets younger to the center of the structure.

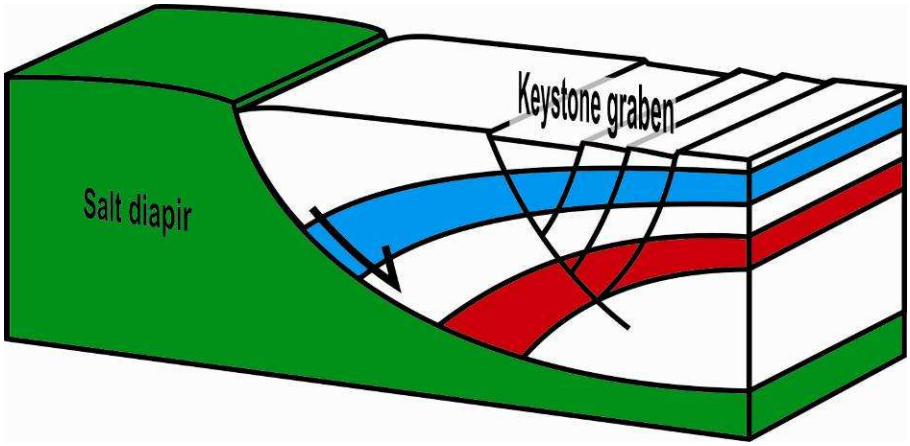

Appendix A-8 Schematic of a keystone graben resulting from extension and thinning of the sedimentary overburden. A succession of faulting creates grabens with fault steps at the surface.

Roho systems – Roho systems refer to of growth-fault rollovers that can drive salt nappe emplacement (Appendix A-9; Rowan 2005). The rollovers accommodate the basinward

translation of the overburden as salt is extruded basinward (Rowan 2005). In these systems the rollovers decrease in age moving basinward.

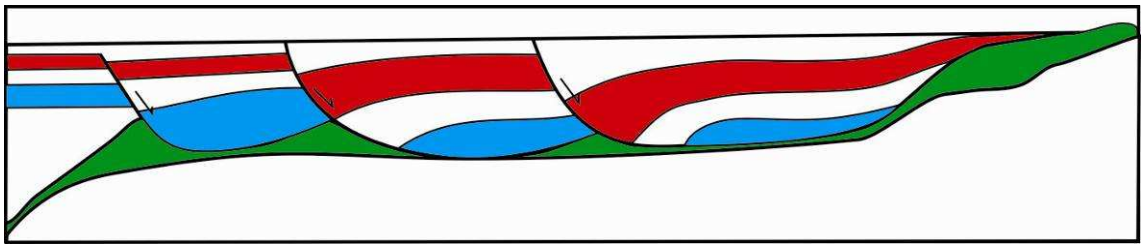

Appendix A-9 Schematic of a roho system created by a succession of growth-fault rollovers driving salt nappe emplacement.

Appendix B:

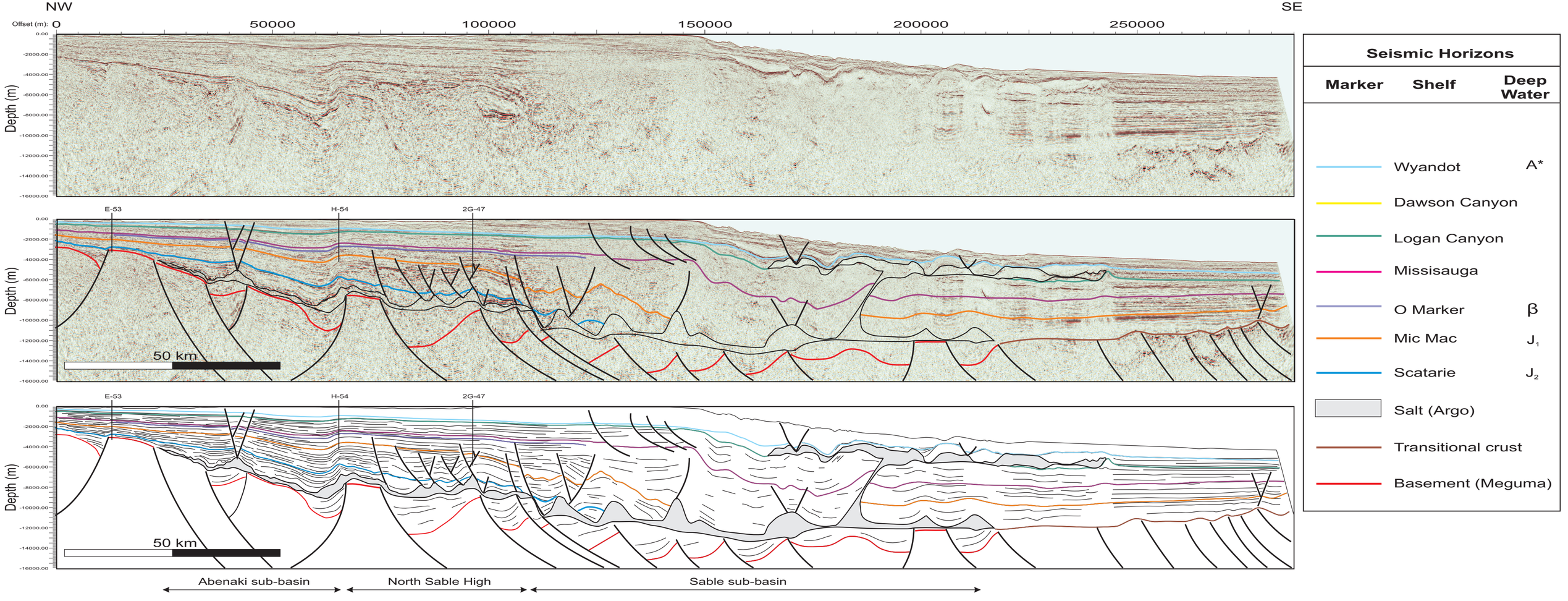
NW
SE
Offset (m): 0
50000
100000
150000
200000
250000
Depth (m)
0.00
-2000.00
-4000.00
-6000.00
-8000.00
-10000.00
-12000.00
-14000.00
-16000.00
E-53
H-54
2G-47
50 km
Abenaki sub-basin
North Sable High
Sable sub-basin
Seismic Horizons
Marker
Shelf
Deep Water
Wyandot
A*
Dawson Canyon
Logan Canyon
Missisauga
O Marker
β
Mic Mac
J1
Scatarie
J2
Salt (Argo)
Transitional crust
Basement (Meguma)

Appendix C:

Public Seismic Reflection Profiles – Shell 8624-S006-032E

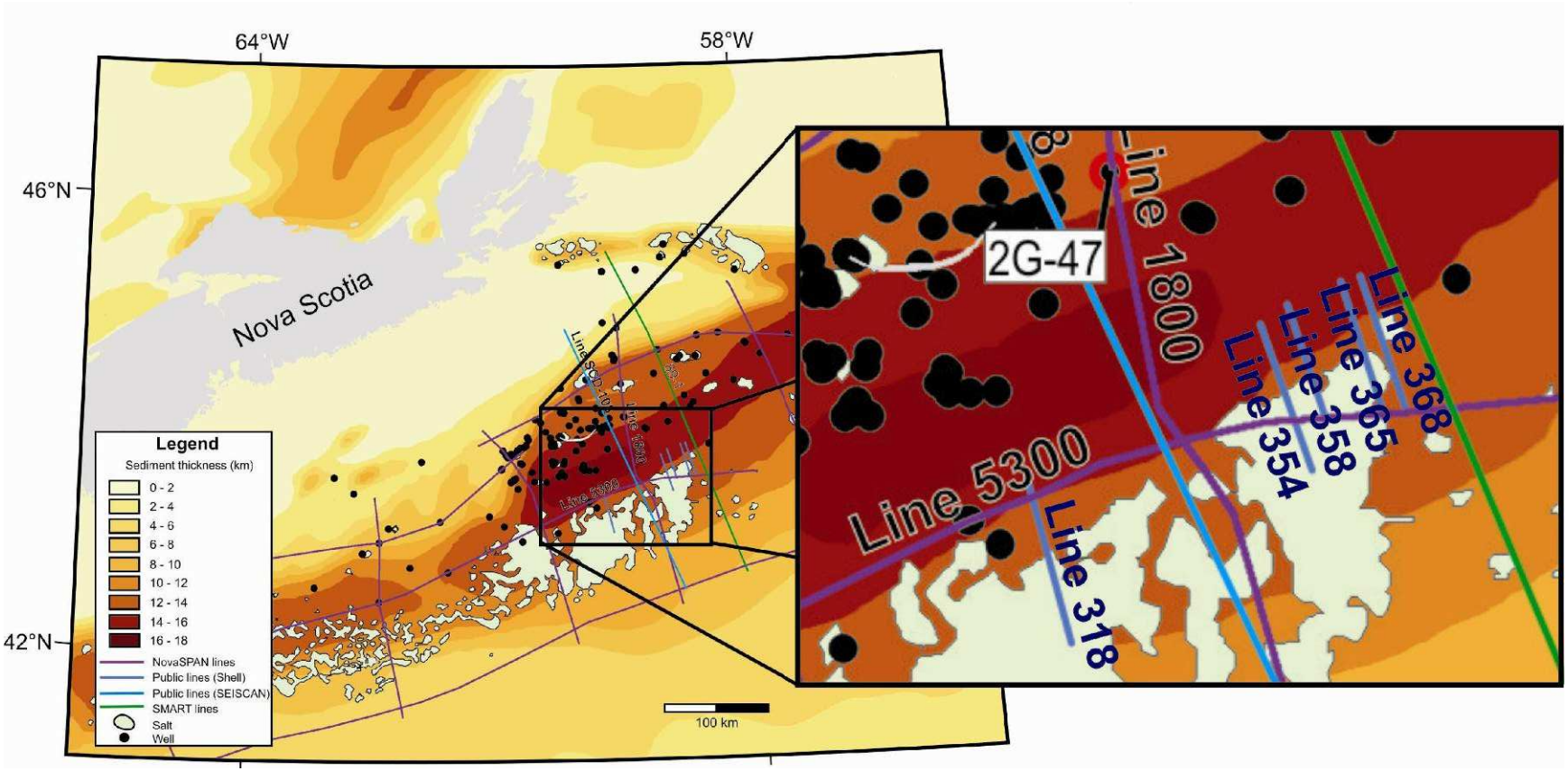

Appendix C-1 Map of sediment thickness, present-day shallow salt bodies and public seismic transects by Shell Canada.

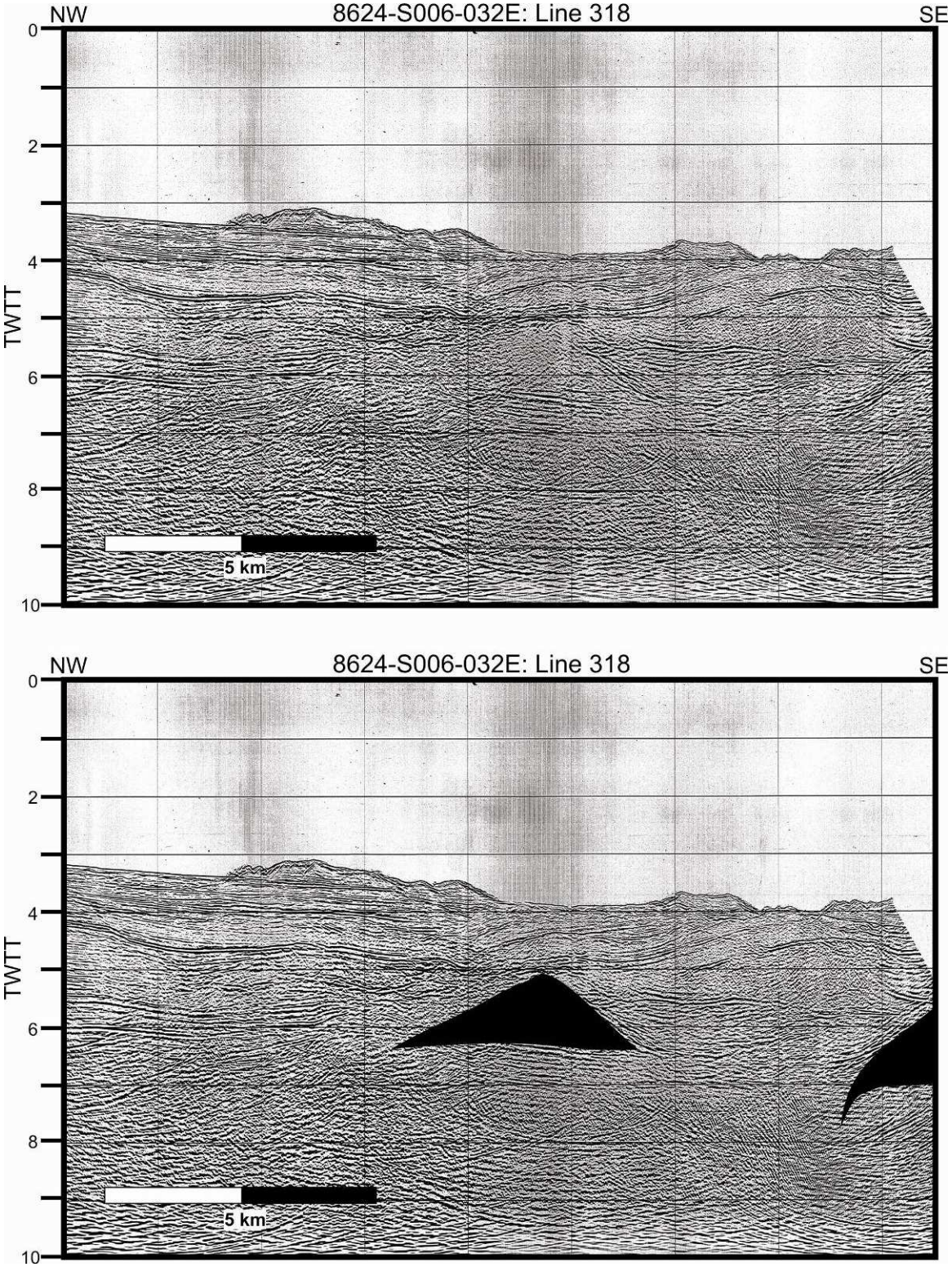

Appendix C-2 Publicly available time-domain seismic reflection profile Shell 8624-S006-032E: Line 318.

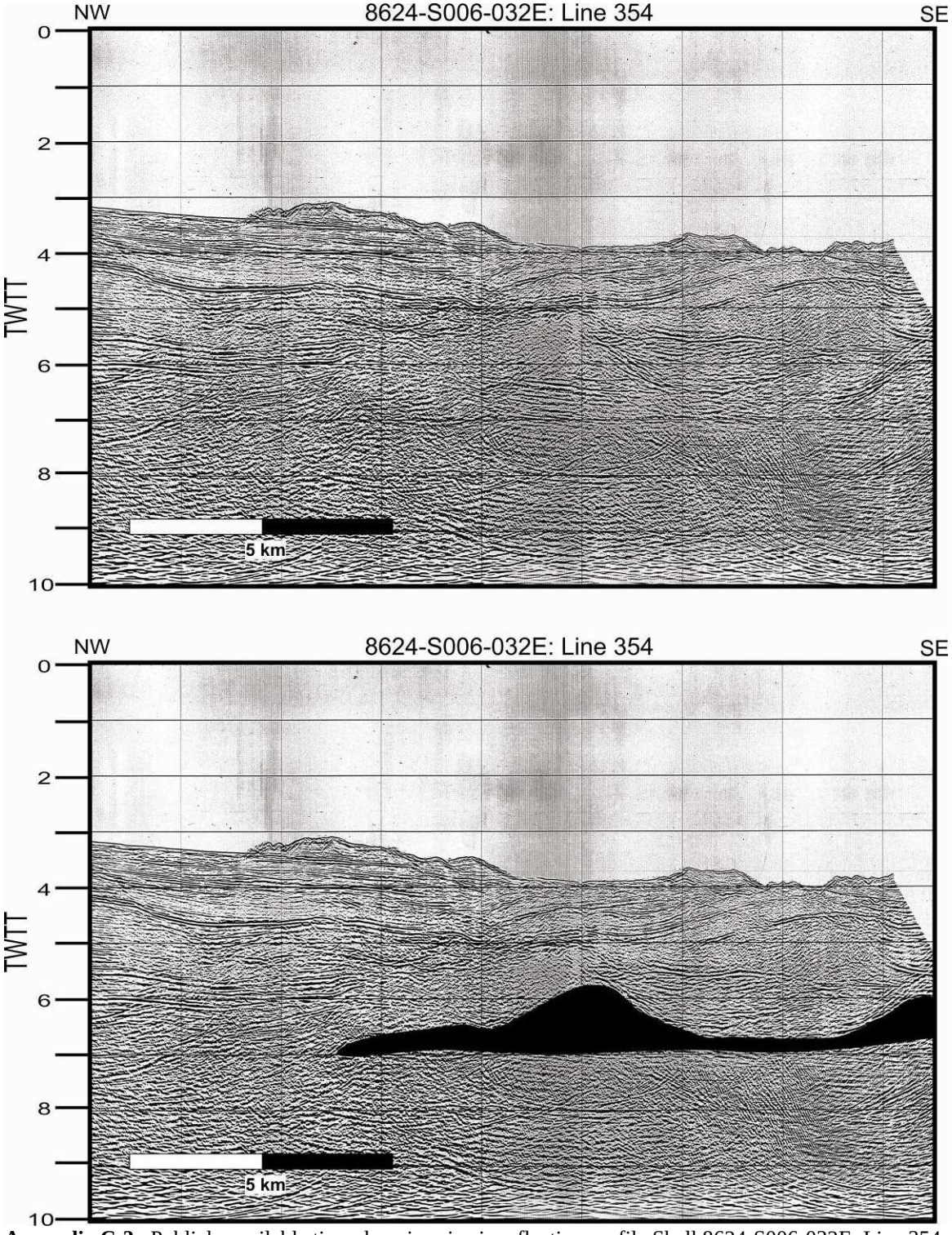

Appendix C-3 Publicly available time-domain seismic reflection profile Shell 8624-S006-032E: Line 354.

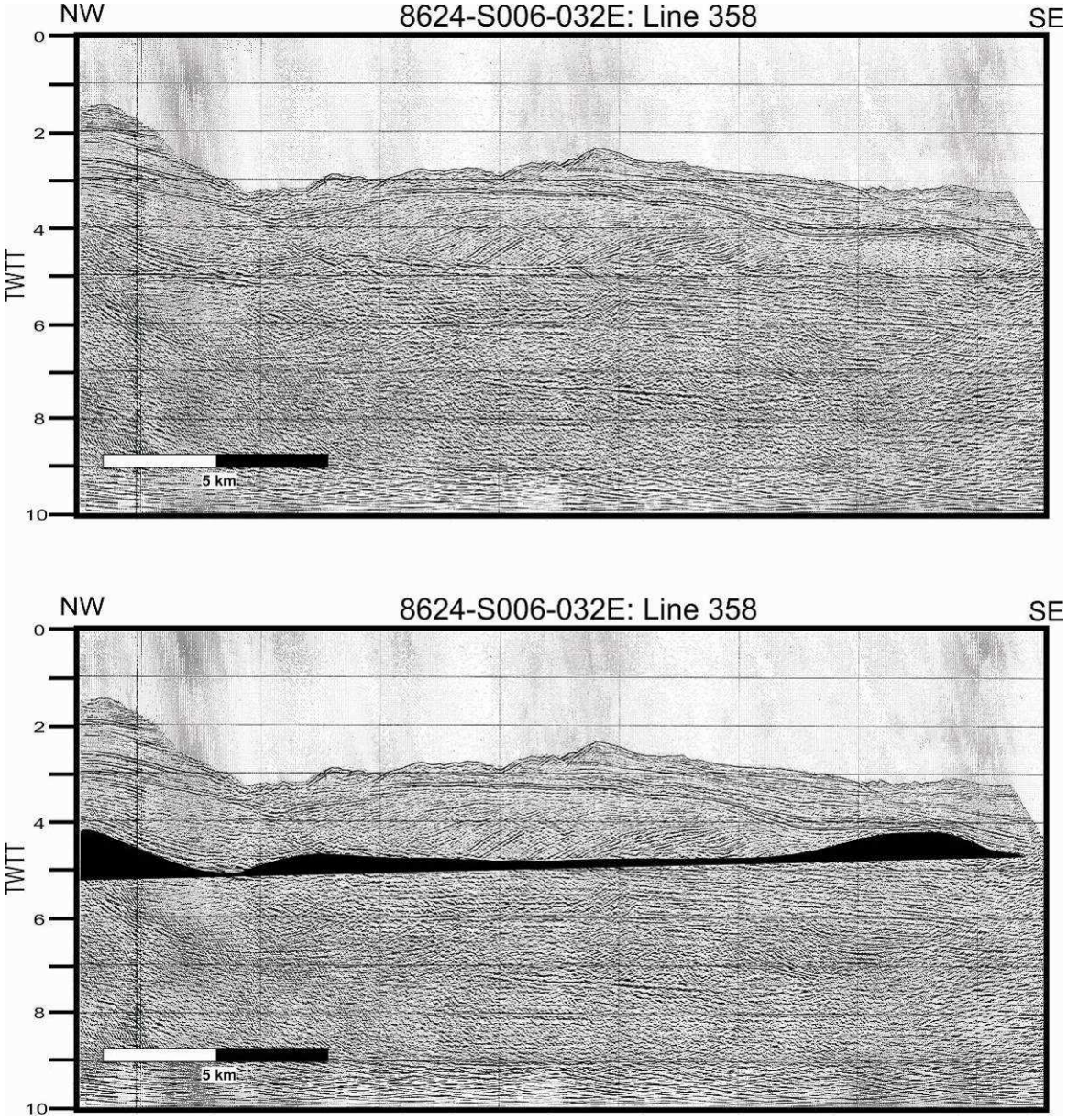

Appendix C-4 Publicly available time-domain seismic reflection profile Shell 8624-S006-032E: Line 358.

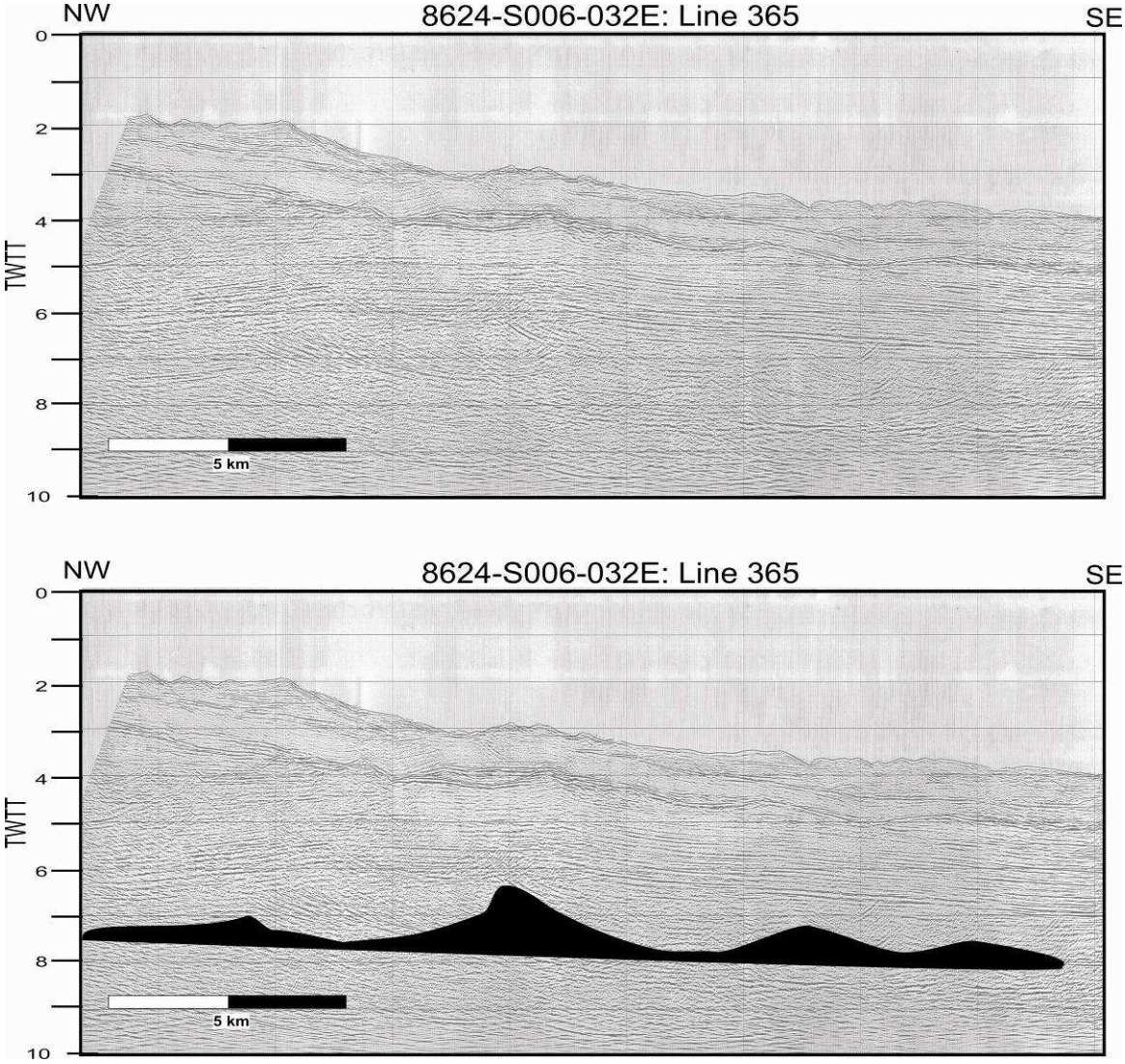

Appendix C-5 Publicly available time-domain seismic reflection profile Shell 8624-S006-032E: Line 365.

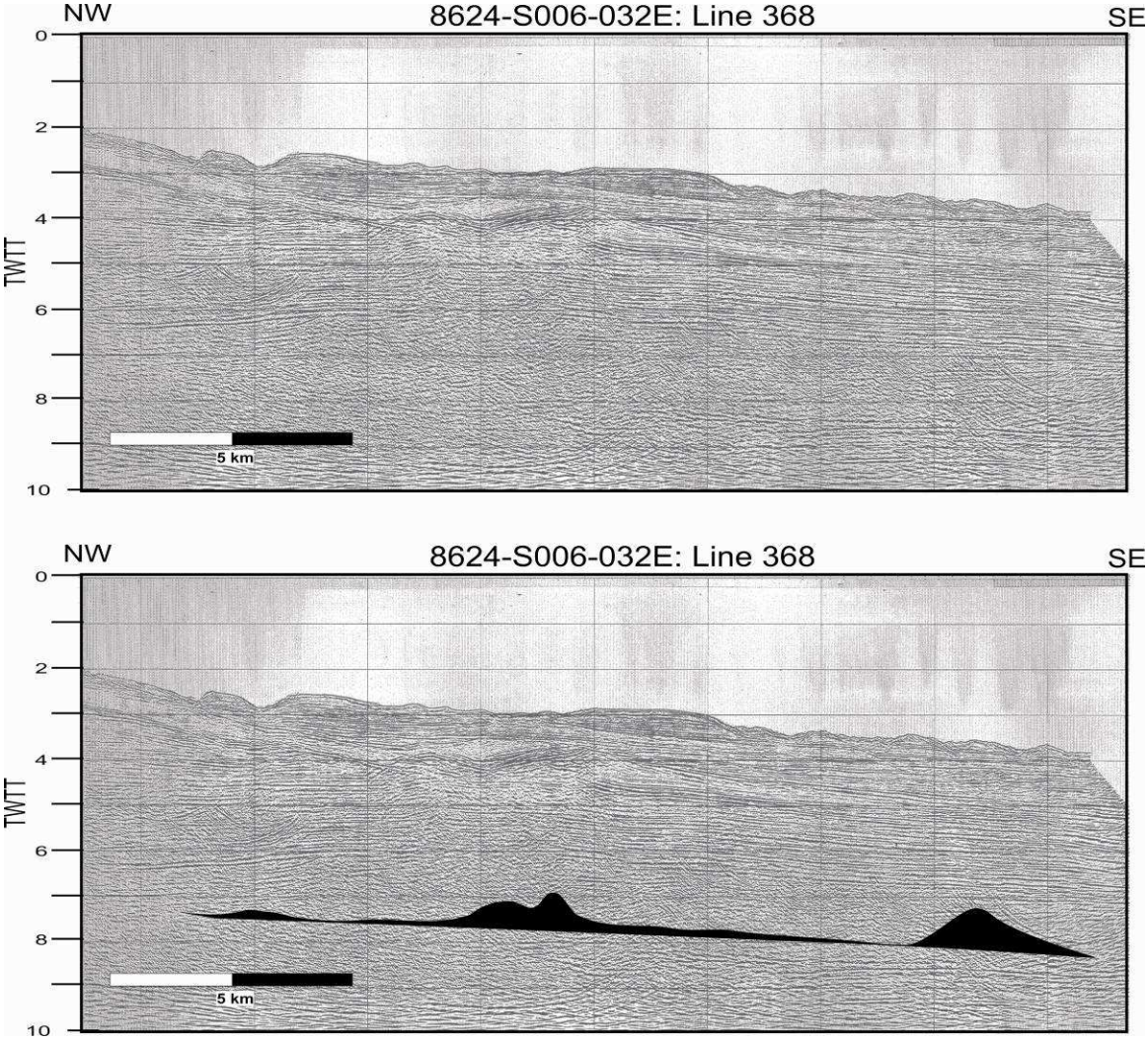

Appendix C-6 Publicly available time-domain seismic reflection profile Shell 8624-S006-032E: Line 368.

Appendix D:

GIS Database Maps

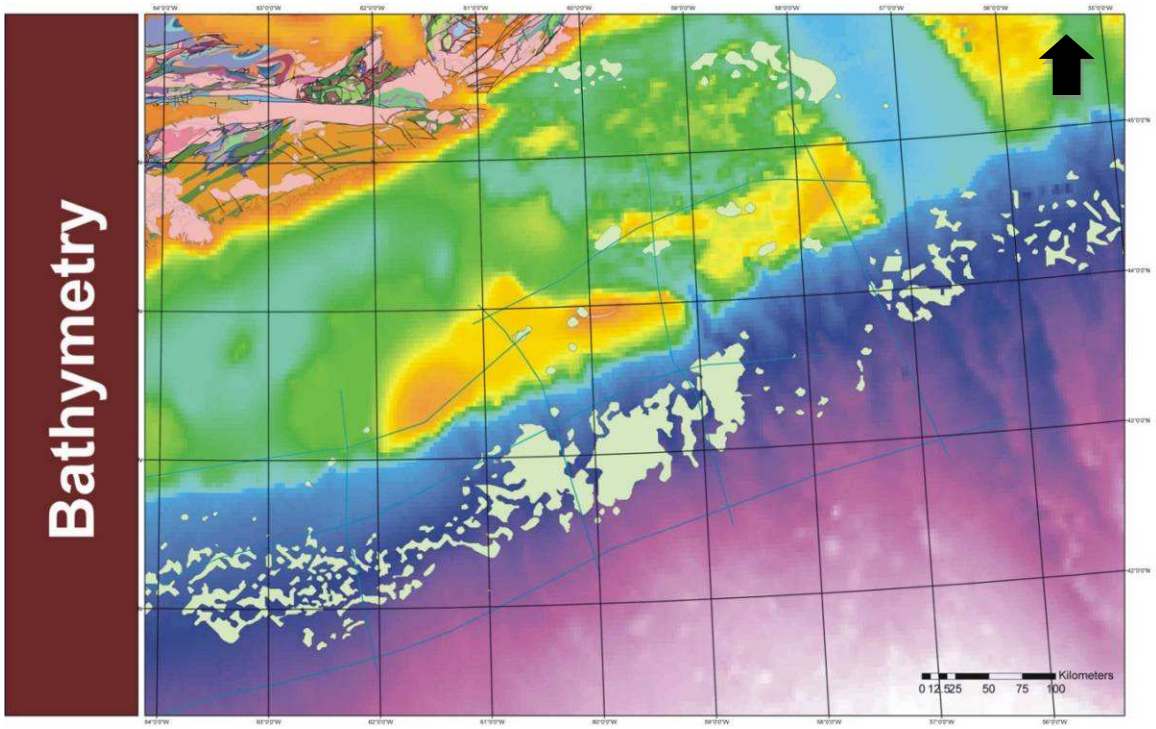

Appendix D-1 Bathymetry map of the Scotian Margin (GSC).

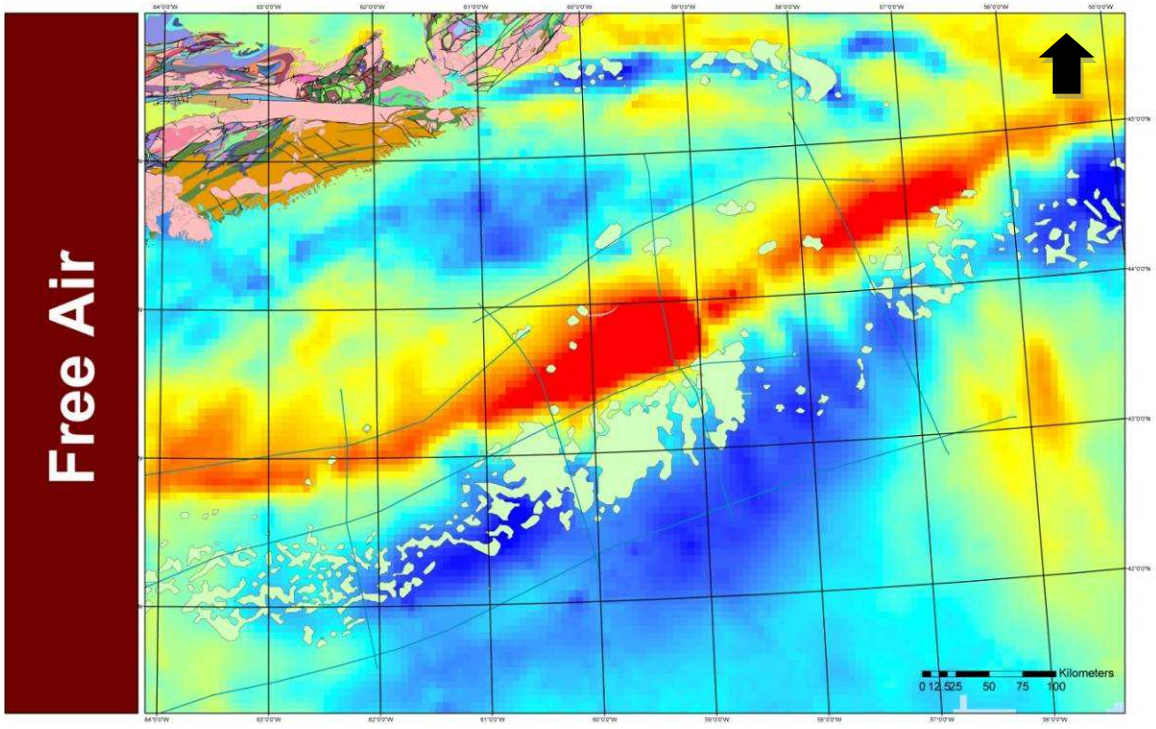

Appendix D-2 Free-air anomaly map for the Scotian margin (GSC).

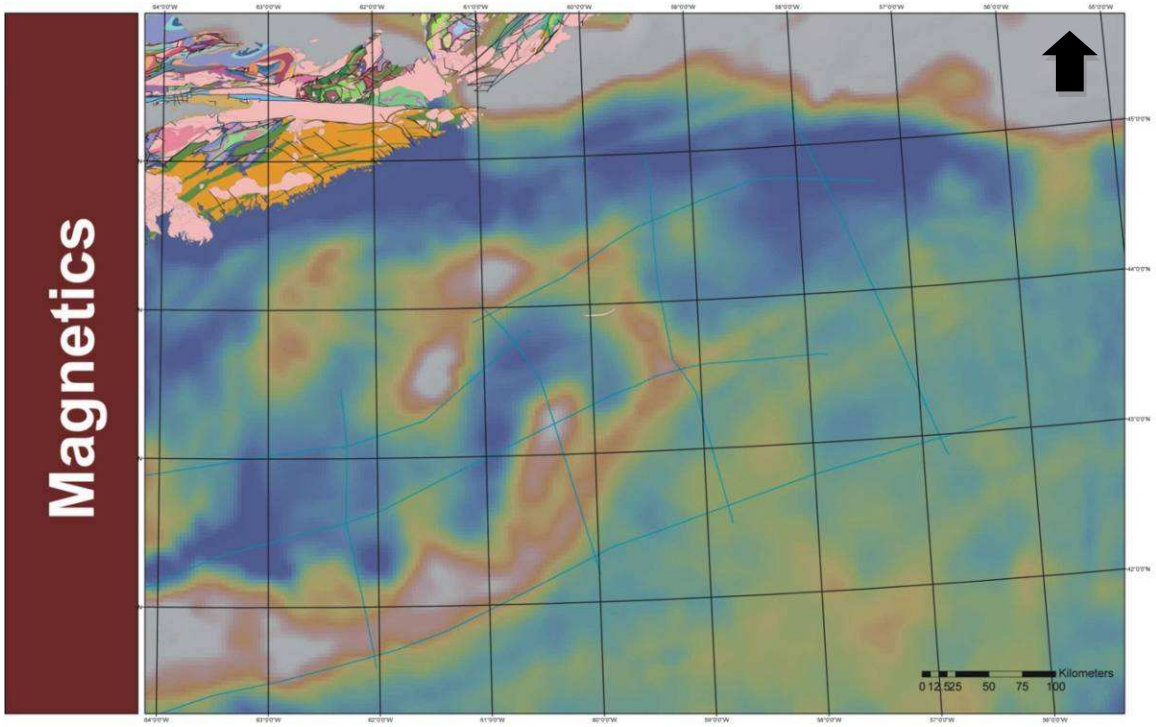

Appendix D-3 Magnetic anomaly map of the Scotian margin (GSC).

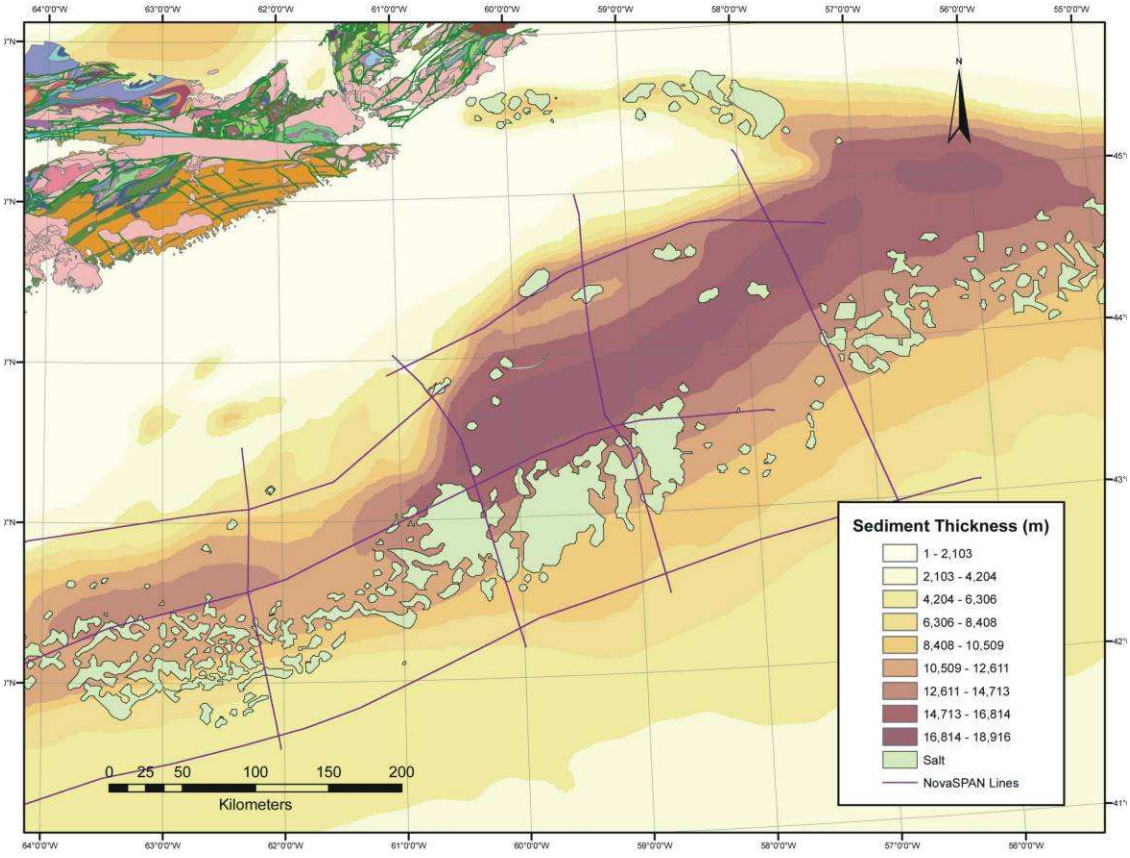

Appendix D-4 Sediment thickness map of the Scotian margin (GSC).

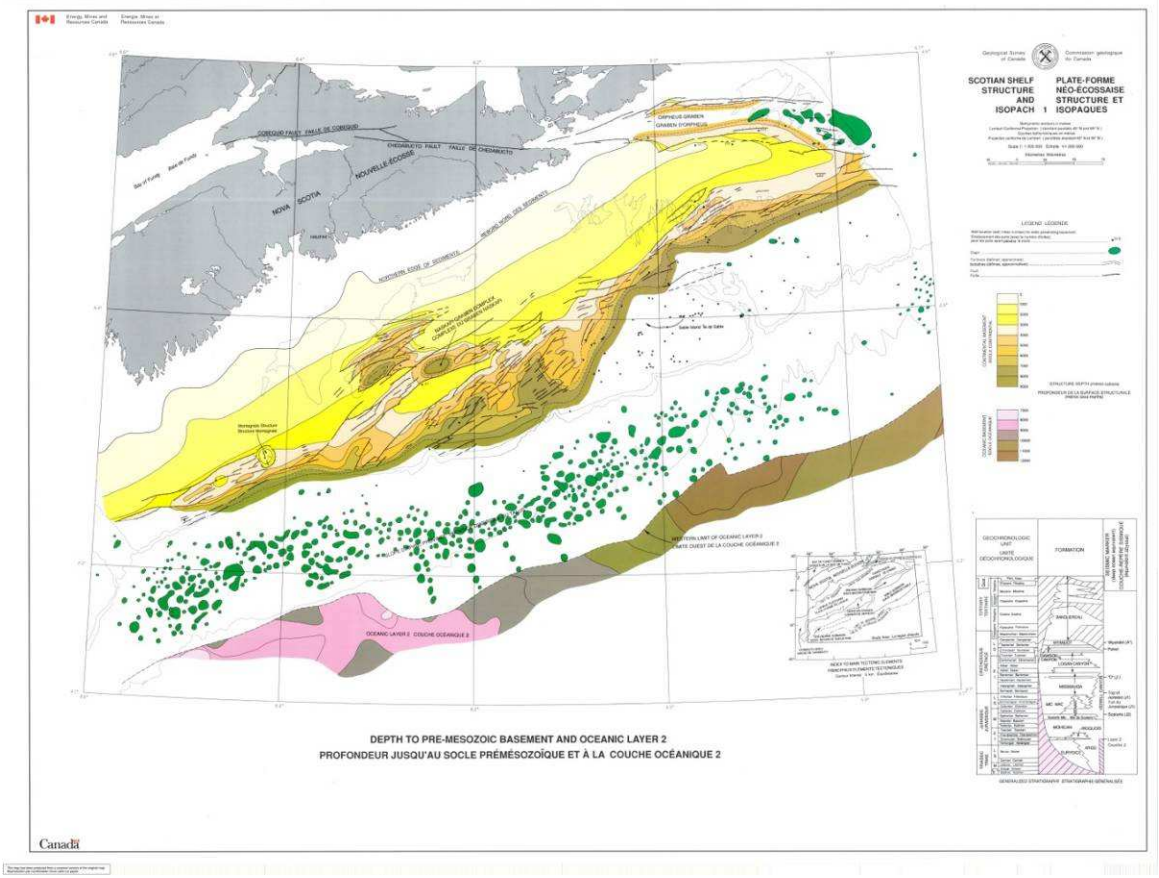

Appendix D-5 Basement map of the Scotian margin (Atlantic Geoscience Center 1991).

Appendix E:

Experiment 1: Abenaki and Central Sable Sub-basin

DALHOUSIE UNIVERSITY
Inspiring Minds

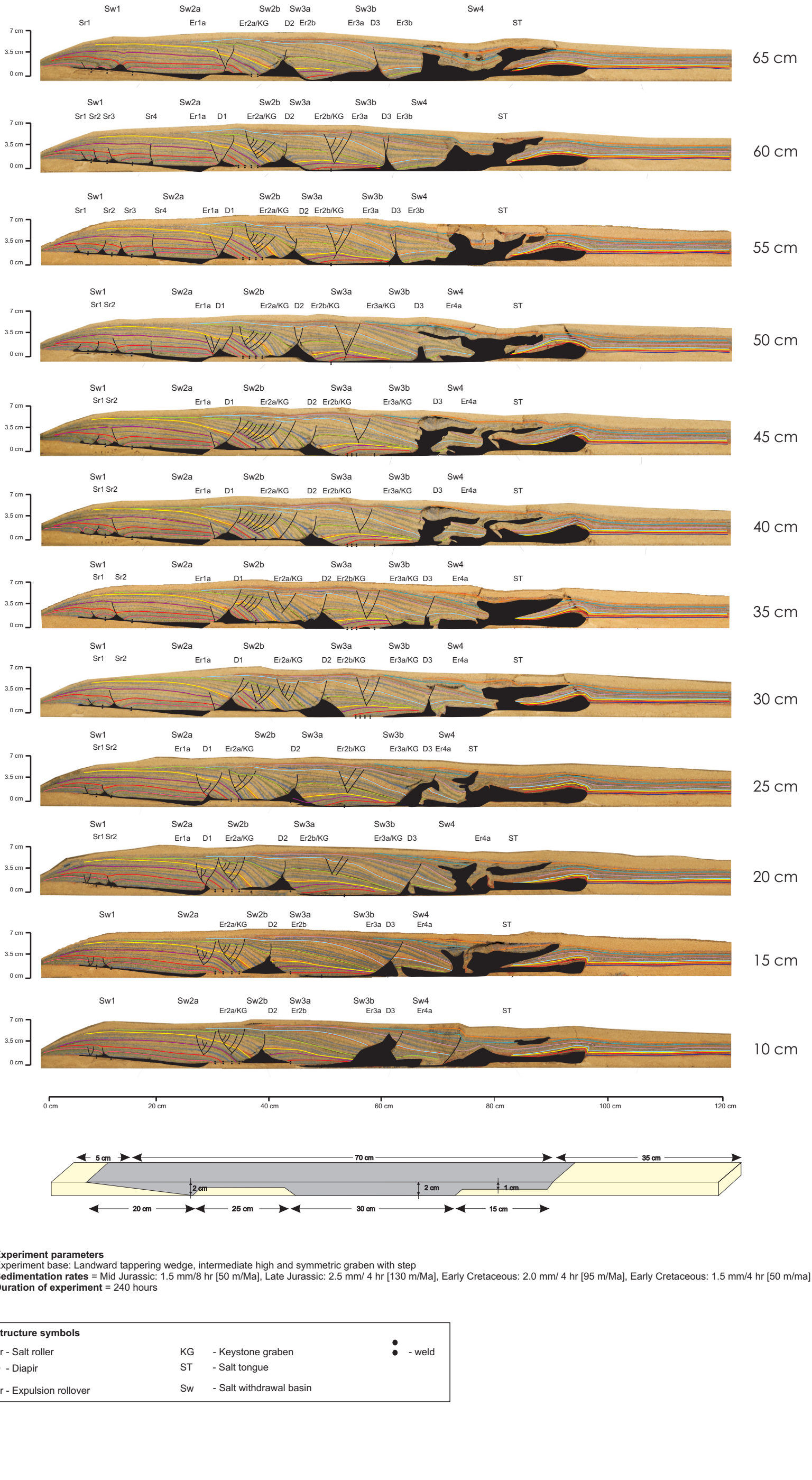

Experiment parameters
Experiment base: Landward tappering wedge, intermediate high and symmetric graben with step
Sedimentation rates = Mid Jurassic: 1.5 mm/8 hr [50 m/Ma], Late Jurassic: 2.5 mm/ 4 hr [130 m/Ma], Early Cretaceous: 2.0 mm/ 4 hr [95 m/Ma], Early Cretaceous: 1.5 mm/4 hr [50 m/ma]
Duration of experiment = 240 hours

Structure symbols

Sr - Salt roller	KG	- Keystone graben	● ● - weld
D - Diapir	ST	- Salt tongue	
Er - Expulsion rollover	Sw	- Salt withdrawal basin	

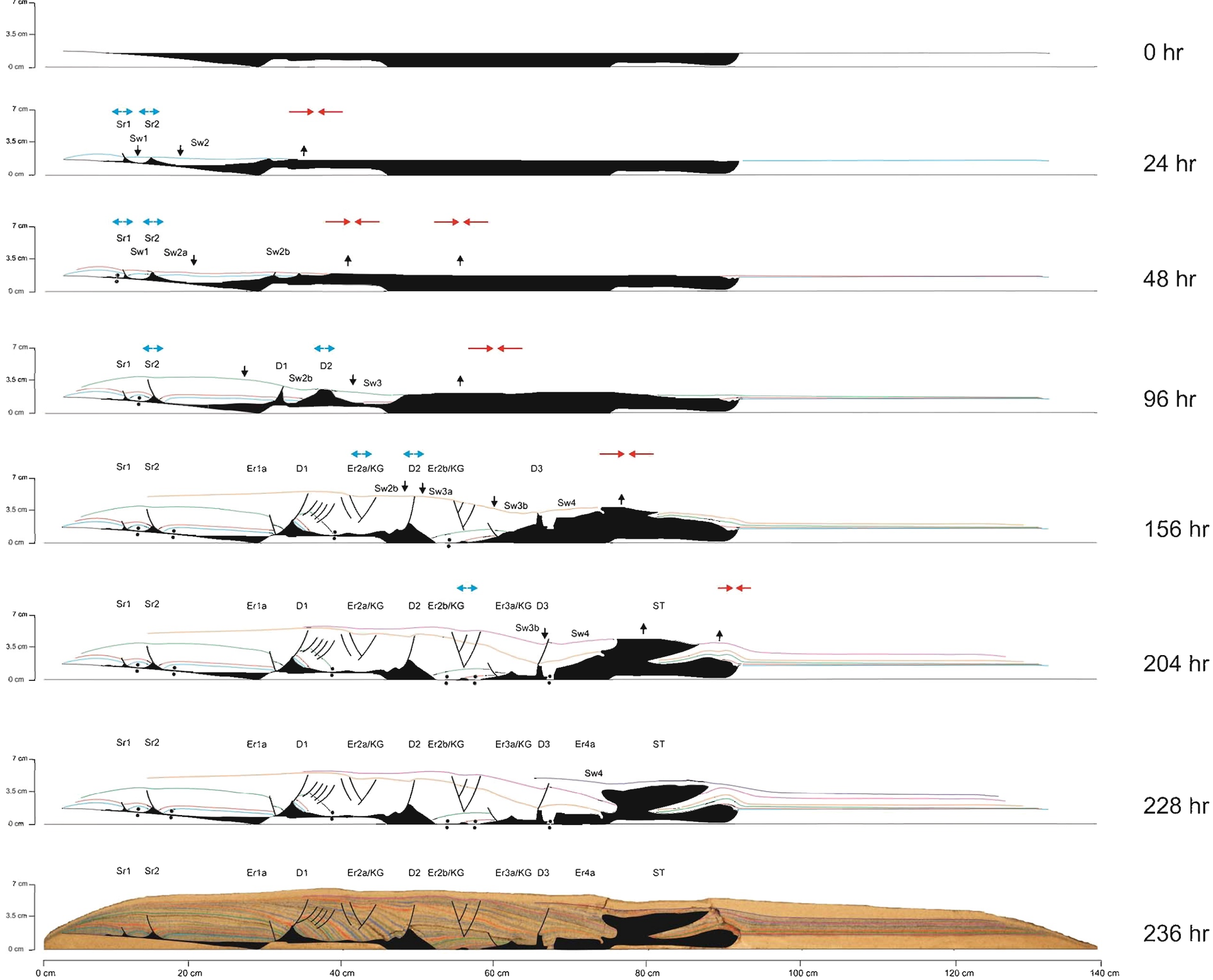
0 hr
24 hr
48 hr
96 hr
156 hr
204 hr
228 hr
236 hr
7 cm
3.5 cm
0 cm
Sr1
Sr2
Sw1
Sw2
Sw2a
Sw2b
D1
D2
Sw3
Er1a
Er2a/KG
Er2b/KG
Sw3a
Sw3b
Sw4
D3
Er3a/KG
Er4a
ST
0 cm
20 cm
40 cm
60 cm
80 cm
100 cm
120 cm
140 cm
←Shelf→ ←Abenaki sub-basin→ ←North Sable High→ ←Sable sub-basin→
Structure symbols
Sr - Salt roller
D - Diapir
Er - Expulsion rollover
KG - Keystone graben
ST - Salt tongue
Sw - Salt withdrawal basin
: - weld
- Contraction
- Extension
- Uplift
- Subsidence

Experiment 2: Abenaki and Central Sable Sub-basin

DALHOUSIE UNIVERSITY
Inspiring Minds

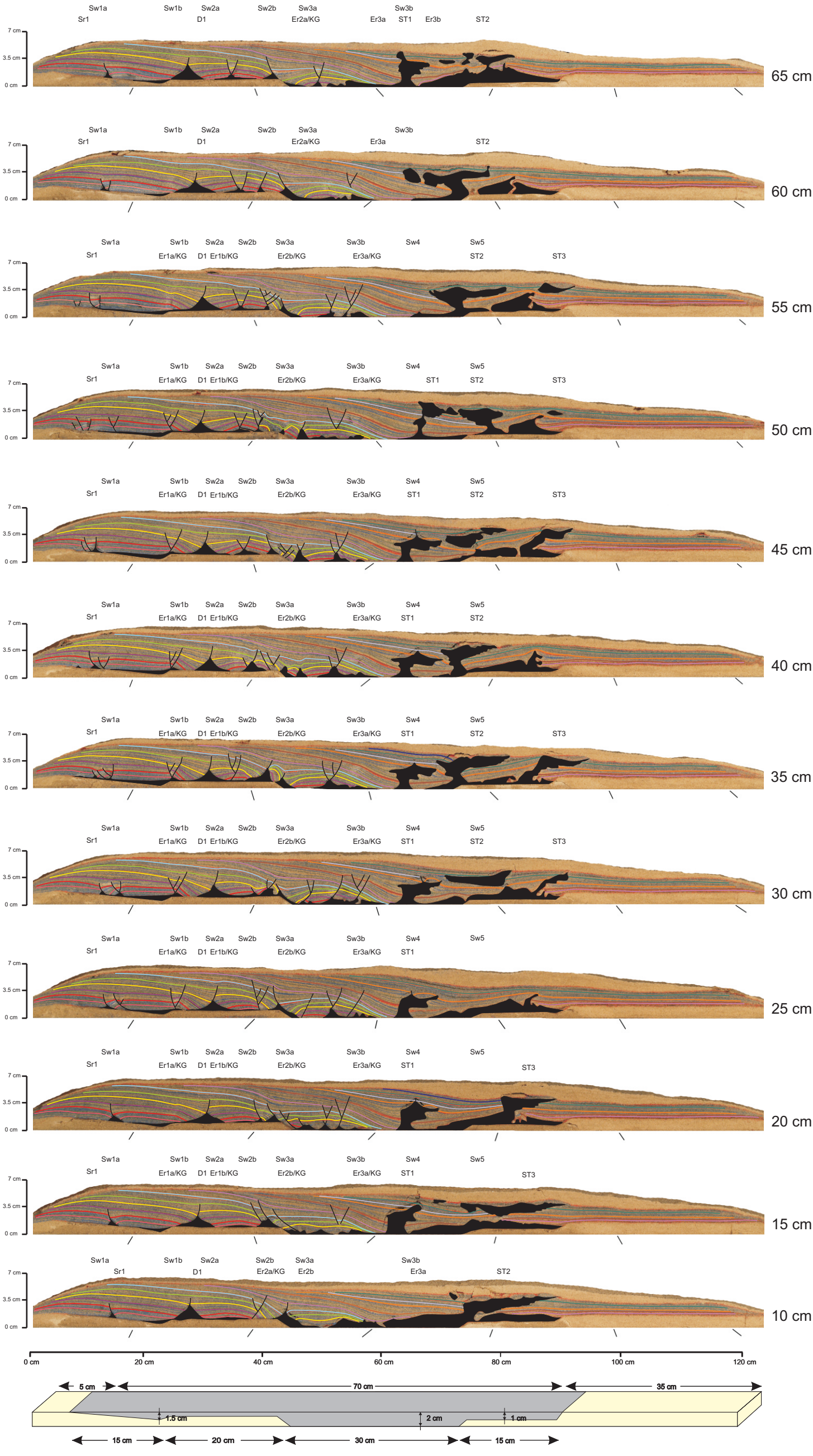

Experiment parameters
Experiment base: Landward tapering wedge, intermediate high and symmetric graben with step
Sedimentation rates = Mid Jurassic: 1.5 mm/8 hr [50 m/Ma], Late Jurassic: 2.5 mm/ 4 hr [130 m/Ma], Early Cretaceous: 2.0 mm/ 4 hr [95 m/Ma], Early Cretaceous: 1.5 mm/4 hr [50 m/ma]
Duration of experiment = 304 hours

Structure symbols

Sr - Salt roller	KG	- Keystone graben	● ● - weld
D - Diapir	ST	- Salt tongue	
Er - Expulsion rollover	Sw	- Salt withdrawal basin	

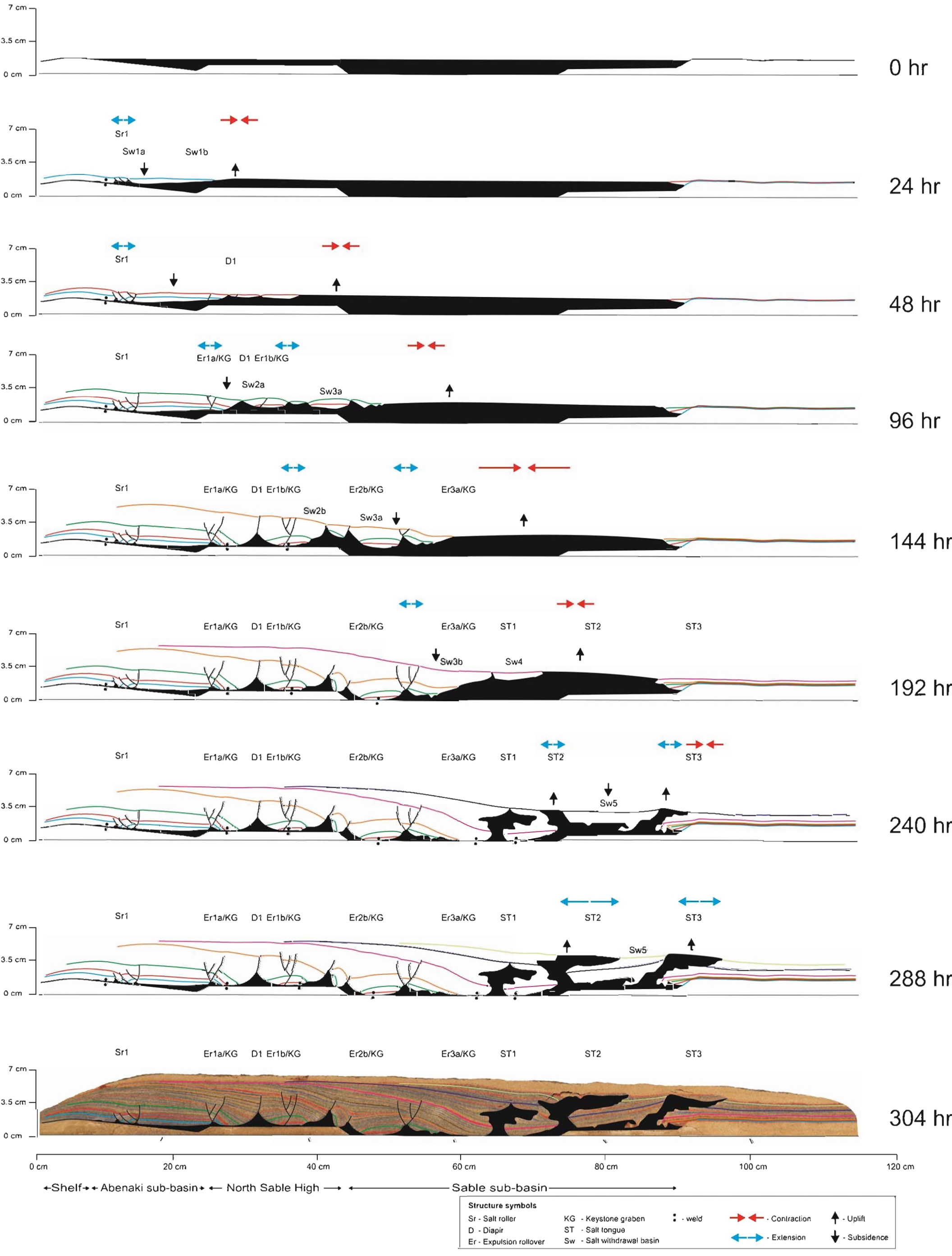
7 cm
3.5 cm
0 cm
0 hr
Sr1
Sw1a
Sw1b
24 hr
D1
48 hr
Er1a/KG
D1 Er1b/KG
Sw2a
Sw3a
96 hr
Er2b/KG
Er3a/KG
Sw2b
144 hr
ST1
ST2
ST3
Sw3b
Sw4
192 hr
Sw5
240 hr
288 hr
304 hr
0 cm
20 cm
40 cm
60 cm
80 cm
100 cm
120 cm
Shelf
Abenaki sub-basin
North Sable High
Sable sub-basin
Structure symbols
Sr - Salt roller
D - Diapir
Er - Expulsion rollover
KG - Keystone graben
ST - Salt tongue
Sw - Salt withdrawal basin
- weld
- Contraction
- Extension
- Uplift
- Subsidence